John Jay College
City University of New York

Final Report

NIH/NIDA Challenge Grant
1RC1DA028476-01/02

IDU Network Topologies and HIV Stabilization Dynamics

Authors:
Bilal Khan
Kirk Dombrowski
Mohamed Saad
Katherine Mclean
Evan Misshula
Ric Curtis
Travis Wendel
William Jett

Version:
3.0 Draft

b

September 1, 2011

This project was supported by NIH/NIDA Challenge Grant 1RC1DA028476-01/02 awarded to the CUNY Research Foundation and John Jay College, CUNY. The opinions, findings, and conclusions or recommendations expressed in this publication are those of the authors and do not necessarily reflect those of the National Institute of Health/National Institute on Drug Abuse. For further information, please contact Project PIs Bilal Khan (bkhan@jjay.cuny.edu) or Kirk Dombrowski (kdombrowski@jjay.cuny.edu). The analyses discussed in this paper were carried out at the labs of the New York City Social Networks Research Group (www.snrg-nyc.org). Special thanks to Dean Karen Terry, Jacob Marini and Susy Mendes in the John Jay Office for the Advancement of Research, and Colleen Syron, Emily Channell, Robert Riggs, David Marshall, Nathaniel Dombrowski, and the other members of the SNRG team. We would like to acknowledge that initial funding for a pilot version of this project was provided by the NSF Office of Behavioral, Social, and Economic Sciences, Anthropology Program Grant BCS-0752680.

Executive Summary

This report presents research findings of the **IDU Network Topologies and HIV Stabilization Dynamics Project**—NIH/NIDA Challenge Grant 1RC1DA028476-01/02 (2009-2011). This research represents an exploration of well-known but until now unaccounted for HIV-1 infection patterns among injecting populations. This research models the interaction of actors within a risk network, an evolving approach in HIV research. Because IDU communities remain reservoirs of HIV, and present the potential for infecting the larger communities in which they live and with whom they continue to interact, understanding the short and long term dynamics of infection transmission represents an important public health priority for both the IDU community itself, and the general population that surrounds it.

The key findings and conclusions of the experiments undertaken here include:

1. **Stabilization.** Simulation trials modeled on the SFHR network resulted in HIV rate sub-saturation stabilization at a level similar to that observed for injecting drug user networks in New York City in the early stages of the HIV epidemic (see p. 99).
2. **Hypothesis 1.** In a majority of cases, and for a range of parameter settings, nodes with mature (i.e. low infectiousness) HIV+ status demonstrated a "firewall effect", dividing the network into clusters of uninfected nodes which remained relatively stable over time. These nodes play an important role in the non-spreading of HIV in the network despite the presence of high numbers of uninfected nodes and the ongoing reappearance of new, high infectiousness nodes (see p. 116 and p. 135-180).
3. **Hypothesis 2.** Local level social network structures within the overall risk network contribute to the non-spreading of HIV in injecting drug user networks despite continuing turnover in network participants, high turnover in network connections, and continuing very high numbers of risk events (see p. 103).
4. **Hypothesis 3.** Injecting drug user networks with stable, sub-saturation levels of HIV-1 infection continue to produce new infections over the

course of time which, while they fail to propagate full throughout the network, never the less represent reservoirs of high infectiousness that can spread to surrounding populations (see p. 102).

5. **Scale.** While networks of size 5,000 through 25,000 behaved within a narrow (and therefore predictable) range of overall characteristics, networks of 1000 nodes showed high variability in their network wide behavior. As a result, known outcomes of interventions in small scale networks may not serve as good indicators of likely outcomes of the same intervention in other small networks, nor in the same networks at a different time. In each case, the effects of random events may render the most successful interventions moot, or the most ill-adapted interventions successful—this without a change in the underlying set of network attributes or dynamics (see p. 103,116,129).

6. **Risk.** In simulations where the overall rate of actor risk was set intentionally high, the firewall effect was pronounced, while in cases where risk rates were low, stochastic variations from one trial to the next seem to dominate an overall infection rates the firewall effect were difficult to predict (see p. 138).

7. **Virus Transmissibility.** Varying rates of virus transmissibility showed high variability in the spread of the virus, including ranges where overall infection rates failed to stabilize, even in very long simulation runs of 40-50 years. From this, it would appear that for set levels of risk, the sub-saturation stabilization phenomenon is specific to a level of infectiousness. It remains possible that changes in the likelihood of infection (for a given risk event) can have serious effects on overall network infection levels unpredicted by historical data. On the other hand, in simulations where stabilization was achieved, increased virus transmissibility did **not** produce a greater proportion of new infections through time, showing that topological effects preventing virus transmission were, in mature networks, robust against large increases in virus transmissibility (see p. 144).

8. **Transient Members of the Network.** Transient participants in an IDU network can have a serious impact on the overall HIV rate. While overall network stabilization remains, even low numbers of transient participants engaging in risk behaviors with long-term network

members increases HIV to levels approaching saturation, enlarging the "reservoir" of HIV infection within injecting drug user networks (see 150).

9. **Network Participation Duration** Stable networks, created by the long-term participation of network members, yield highly stable rates of infection, despite the fact that individuals within the network continue to "churn" their connections to one another. Conversely, high turn over of network participants, even where new participants enter the network in an uninfected state, necessarily produces both higher and continuously rising HIV rates. These dynamics significantly affect the emergence of network structures that mitigate HIV infection. In particular, a high turn over rate of network participants significantly diminishes the firewall effect, while stable networks show consistent effective structural barriers to disease spreading (see 156).

10. **Churn** Variations in the rate at which network participants changed risked partners seemed to have little effect on HIV rates within the network, while increasing the firewall effect. This is caused by the breakup of clusters of mature, low infectiousness nodes whose new connections to uninfected parts of the network increases the isolation of uninfected actors from periodic sweeps of new infection (see 163).

Contents

List of Figures

List of Tables

Chapter 1

Introduction

This report presents research findings of the **IDU Network Topologies and HIV Stabilization Dynamics** project[1], an exploration of well-known but until now unaccounted for HIV-1 infection patterns among injecting populations.

This research models the interaction of actors within a risk network, an evolving approach in HIV research (Bell, Montoya, Atkinson, & Yang, 2002; Goodreau, 2006a). Because intravenous drug user (IDU) communities remain reservoirs of potential HIV infection to the larger communities in which they live and with whom they continue to interact, understanding the short and long term dynamics of infection transmission represents an important public health priority for both the IDU community itself, and the general population that surrounds them.

For the purposes of this report, IDU networks of concern consist of "risk networks"—social connections of varying duration that involve behaviors commonly associated with a risk of infection (regardless of the infection status of either party). For IDU communities, this includes mainly those social relationships which result in drug or injection equipment sharing, or sexual relationships in the course of drug use. Risk networks are now widely

[1]NIH/NIDA Challenge Grant 1RC1DA028476-01/02 (2009-2011).

recognized as critical factors in understanding the infection patterns of IDU communities (Friedman et al., 1997; Bachanas et al., 2002), forming the natural environment in which risk behaviors take place and through which the propagation of infection proceeds.

Social Network research among IDU communities has by now produced considerable data on HIV-1 infection profiles, and equally detailed data on the broad demographic and behavioral profiles of these injecting communities and their risk behaviors. However, prior research has not—and for reasons of cost often cannot—produce long-term, dynamic data on these same populations. Instead, most prior research provides detailed and important snapshots of social processes within risk networks that are otherwise known to be in a state of flux. The simulation of these networks offers an opportunity to understand the long-term behavior of IDU networks themselves—beyond the behavior of individuals that comprise the networks—and to demonstrate (1) how the specific patterns of risk-bearing relationships between injectors came to be the way they are, (2) how infections move (and do not move) across these topologies, (3) where IDU networks and the infections they contain are going in the future, and (4) what the impacts of various interventions might be.

This research presented here shifts our view of risk away from individual risk behaviors to collective, social bodies as the carriers and transmitters of infections. The value of this project is that it can make the dynamic structures of risk networks visible, and help further a change in perspective to one that sees collectivities (and their respective forms and dynamics) as health actors with specific and identifiable structures of risk.

Practical considerations also argue for more simulation of these (and similar) processes. For reasons of cost, most social network studies are relatively small in scale compared to the size of the overall networks they study. Even large-scale IDU network studies like the Social Factors for HIV Risk (SFHR—in Brooklyn, New York, in the early 1990s—upon which significant portions of our model are constructed, and which involved interviews with several hundred people (Friedman, 1999), managed to interview only a small portion of the larger Brooklyn IDU risk network, estimated at the time to be between 30,000 and 80,000 persons. Here too, simulation allows researchers to operate at the scale of the phenomenon of interest. While simulation is necessarily

far from perfect and no substitute for direct research, when based on detailed data and constructed to conform closely to known, short-term social dynamics, it can potentially provide suggestions and even tentative conclusions about critical health phenomenon at a time depth and social scale not possible in direct empirical research.

1.1 Challenges and Impact

The challenge taken up by this proposal is the ongoing public health risk associated with well documented but, as yet, not well-understood HIV-1 dynamics in IDU communities. We have sought to understand the topological principles that lead to stable rates of HIV-1 infection in IDU communities, particularly where stabilization appears to takes place at levels below saturation despite the ongoing presence of new infections and high levels of ongoing risk behaviors. These dynamics have been documented for a large number of IDU communities (Friedman et al., 2000). In the course of this research report, we provide evidence of network structures that explain the occurrence of this phenomenon within networks that are modeled as dynamic systems.

The reported network structures can potentially be influenced by policy seeking to minimize the risk of spreading HIV-1 from seropositive IDUs both to other injectors, as well as to the wider society. A data-driven sense of how best to effect this change is possible only once we understand the dynamic nature of the risk networks, and the spread of HIV-1 across them, over time. A dynamic, agent-based model of IDU networks and their infection dynamics has proven to be a critical and effective step in developing this understanding.

Our simulation draws on a wealth of data produced by synchronic and sequential studies of IDU communities and their infection profiles. Temporal statistical profiles of HIV-1 infection among IDU communities are by now well researched, as are many of the individual factors associated with risk behaviors and HIV-1 transmission (Khan, Awan, Qureshi, Razaque, & Zafar, 2009; Solomon et al., 2010; Kolari, Stajduhar, Gajnik, Rukavina, & Wiessing, 2010; Des Jarlais, Arasteh, & Friedman, 2011; Frajzyngier, Neaigus, Gyarmathy, Miller, & Friedman, 2007; Friedman et al., 2003; Fernando,

Schilling, Fontdevila, & El-Bassel, 2003) Information generated by the CDCs National HIV-1 Behavioral Surveillance System (NHBS; see)10.1371/journal.pone.0017502 has tracked an 80% drop in overall infection rates in the US. A recent retrospective analysis notes that HIV-1 rates among IDUs in New York City stabilized at roughly 50% of the injecting population in the mid 1990s, and declined to roughly 20% among those sampled in a local detoxification center by 2002, dropping further to 13% by 2004 (Des Jarlais, Arasteh, et al., 2007). Detailed recent studies for sub-populations (women (Gore-Felton et al., 2003), African Americans (Kellerman, Begley, Boyett, Clark, & Schulden, 2004b) young people and new injectors (Fennema, Van Ameijden, Van Den Hoek, & Coutinho, 1997) are now available, as are more general studies of IDU communities in Argentina (Weissenbacher et al., 2003), Russia (Rhodes et al., 2002), Ireland (Smyth, O'Connor, Barry, & Keenan, 2003), Spain (Muga, Sanvisens, Egea, Tor, & Rey-Joly, 2003), Brazil (Hacker et al., 2005), Canada (Remis, 2002), China (Kretzschmar et al., 2008), and India (Solomon et al., 2010), This data allows for the simulation to incorporate in-network dynamics like clustering, and more complex models of HIV transmission within those networks Des Jarlais, Arasteh, McKnight, et al. (2011), including sexual transmission, which has assumed increasing importance within drug using contexts.

In addition, many of the interactions between socio-behavioral and social network factors of individual actors (as they affect HIV-1 transmission) have been explored. Egocentric studies of injection partner networks from Baltimore, Maryland to Chennai, India, have considered the dissemination of both high- and low-risk injection practices through social networks of IDUs (Khan et al., 2009; Latkin, Kuramoto, Davey-Rothwell, & Tobin, 2010). Other community-level studies of IDUs have postulated that the practice of serosorting, or making decisions about equipment sharing based upon a knowledge of ones own or anothers HIV status, may explain a stable prevalence of HIV within injector populations reporting high levels of equipment sharing (Burt et al., 2007; Des Jarlais et al., 2004). Egocentric studies of sex partner networks have also been undertaken with a number of different populations, finding regional and community-level variations in network topologies of sexual mixing and concurrency (Adimora, Schoenbach, & Doherty, 2006; Doherty, Padian, Marlow, & Aral, 2005; Morris & Kretzschmar, 1997). Additionally, recent discussion has centered on whether overall network topologies favor the conservation of "disease reservoirs" despite intervention efforts and

overall success (Liljeros, Edling, Amaral, Stanley, & Aberg, 2001; Newman, 2002; Liljeros, Edling, & Nunes Amaral, 2003; Schneeberger et al., 2004). Much of this debate has hinged on the applicable time-scales involved, and on the finer points of statistical model fitting (Jones & Handcock, 2003; Handcock & Jones, 2004), but what remains clear is that improved data on sexual mixing and HIV transmission has allowed network theorists to rethink the social dynamics associated with epidemic thresholds.

Such improved data can be combined with an emerging understanding of the course of HIV-1 infection (and thus individual infectiousness) in a single body. Baeten and Overbaugh (2003) provides a recent summary of research on the course of infectiousness, including potential importance of "virus burden" in HIV-1 positive individuals—a factor which figures significantly in questions of sub-saturation stabilization in IDU networks (Friedman et al., 2000). While viral burden has been shown to play a critical role in infectiousness for sexual contact and mother-infant transmission, equivalent data are mostly missing for transmission among injecting drug users, and are likely to remain so (though see contributors to Philipson, 1995). On the other hand, the impact of high viral burden during the early/primary acute infection period of 4 to 8 weeks—in contrast to lower levels found during a chronic phase that can last for many years (Cates, Chesney, & Cohen, 1997; Kahn & Walker, 1998; Lyles et al., 2007)—has been well established, demonstrating that periods of peak infectiousness appear within 1-2 weeks of initial infection and last for 2-3 months before diminishing significantly. This has led many to postulate that the changing levels of individual infectiousness over the life course of an individual infection is a critical feature of the virus, and a promoter of primary infection epidemics. Previous models/simulations have estimated the chances of seroconversion to be as much as 20 or even 50 times higher in the first three months than compared to those for the chronic phase (for sexual transmission), returning to early levels only at a very advanced stage and the onset of AIDS. Mathematical models of the infectiousness curve have seen this early infection period as a critical factor in epidemic spreading of HIV-1 among IDUs in its early years (Ahlgren, Gorny, & Stein, 1990; Jacquez, Koopman, Simon, & Longini, 1994; J. S. Koopman et al., 1997). Similar infectiousness curves have figured significantly in past simulations (Kretzschmar & Wiessing, 1998), and will also play an important role in our simulations here.

A number of studies have sought to bring these components together—uniting topological studies of IDU communities with both risk behavioral data and epidemiological data on HIV-1 infection/transmission. The goal of these studies has been to understand the ways in which HIV-1 inhabits and move through IDU networks (Brown & Needle, 1994). The Colorado Springs study (Klovdahl et al., 1994) and SFHR (Friedman, 1999) established both the breadth and depth necessary to understand the transmission of sexually transmitted infections among IDUs. These studies provide the foundation necessary for simulations at long timescales. The combination of model-driven surveys, and long-term ethnographic observation in these same communities (see Curtis et al., 1995) has helped focus our attention on a range of factors, including: cohort risk behaviors (Neaigus et al., 1996), network roles (Friedman et al., 1998), individual perceptions of risk (Amadora-Nolasco, Alburo, Aguilar, & Trevathan, 2002), peer context (Hammett et al., 2006), bridge populations (Morris, 1997), and core-user structures (Friedman et al., 2007).

Still, important dynamics related to the ability of IDU networks to function as reservoirs of HIV-1 infection are widely recognized but remain unexplained. Among them is the fact that HIV-1 rates in injecting communities tend to stabilize below saturation, and below what would be expected given the high infectiousness during the primary or "acute" infection period. Moreover, this remains true, in spite of the ongoing presence of risk behaviors, high levels of risk concurrency, the near continuous presence of new infections in the network, and the demonstrable presence of highly interconnected network "cores" (Des Jarlais et al., 1998, 2005; Friedman et al., 2000). Epidemiological models based on the "small world" nature of IDU networks and the rapid spread of new HIV-1 infections would predict the opposite—namely, that HIV-1 rates among highly concurrent injecting communities practicing a high level of risk behaviors would rapidly achieve saturation (Cates et al., 1997; Baeten & Overbaugh, 2003). Recent studies have attempted to explain the paradox of declining HIV incidence in the face of continuing risk behaviors by referencing social practices such as serosorting (Burt et al., 2007), the ecology of HIV in low prevalence regions (Kretzschmar & Wiessing, 2008; Nasir et al., 2011) high IDU mortality, in combination with a dearth of young IDUs (Duan et al., 2010), and IDU mobility out of highly-policed communities (Duan et al., 2010); the network-topological hypotheses in the vein of Friedman et al. (2000) remain in need of further investigation.

1.2 Research questions

In general, injecting drug users continue to be at high risk of becoming infected with HIV and other blood borne pathogens through sharing injecting equipment, or by engaging in unprotected sex with HIV+ persons. In 2006, IDUs accounted for 13% of AIDS cases reported in the United States, with an additional 3% of cases among the heterosexual sex partners of IDUs. The IDU community thus represents a large proportion of the HIV/AIDS epidemic in the United States. Recent studies in New York City have also shown that HIV prevalence levels among non-IDU risk partners of IDUs are now nearly identical to prevalence levels among IDUs themselves, between 14-18% according to Des Jarlais, Hagan, et al. (2007). Through sexual contact with others who do not use drugs, IDUs/non-IDUs provide a major vector for HIV transmission to the general public. Studies of individuals have repeatedly shown that network-level factors are important in understanding the dynamics of HIV transmission. Previous studies and methods have struggled, however, in attempts to gather risk network data over more than a single period, raising obstacles to our understanding of the dynamic nature of disease transmission for HIV and related viruses. The research presented here offers an innovative solution to this problem, and the promise of a more full understanding of the role of social network structure in HIV transmission, potentially leading to effective interventions that might end, or at the very least control, the HIV epidemic.

Following Friedman et al. (2000), we suspect that factors related infectiousness rates over the life of individual infections, interact with local-level network and global-level network structural dynamics to produce network "firewalls". Key individuals are posited be HIV-1 seropositive risk network members whose infection status (HIV-1 positive but low levels of infectiousness) and network position (those highly responsible for network connectivity within a given topology), together, keeps them from transmitting the virus between newly infected individuals and uninfected regions of the same network. To date, the preence of structural configurations that would allow such

"firewall" individuals—having the ability to prevent new infections from being transmitted to as yet un-infected portions of the network—are largely unconfirmed. This brings us to:

> **Hypothesis 1**: Firewall phenomenon will consist of individual agents with mature infections which partition the overall risk network into a series of clusters, in which uninfected clusters remain relatively stable (over simulation time). Frequently, we shall refer to this as the *Firewall Hypothesis*.

Hypotheses about network structures that might contribute to the firewall phenomenon have remained largely conjectural, and the particular network dynamics responsible for producing such configurations have not been discovered. Indeed, given that empirical discovery would necessarily require a constant monitoring of the infection status and risk interactions of all the members of an IDU network over a period of many years, it is unlikely that they could be confirmed by direct research. As such, we explore this question through computer simulations that can act at the scale and time-depth that such hypotheses require. This brings us to:

> **Hypothesis 2**: Local (neighborhood-level) social network structures within IDU networks will combine with varying rates of individual HIV-1 infectiousness over the course of time to stabilize infection rates—contributing to the proposed firewall effect that allows IDU communities to remain at relatively stable infection levels below saturation.

Should this hypothesis prove true, a clear understanding of the exact nature and variety of these dynamics is critical for public health, since IDU communities exist in many areas throughout the U.S. (and the world), and members of all IDU communities continue to interact with non-IDU community members in ways that promote the spread of infections. Given this, the stabilization dynamics described above represent a critical concern. This is because stabilization does not indicate a lack of new infections, but rather a containment of new infections by, we hypothesize, particular aspects of

network topology. As such, IDU communities serve as reservoirs of new infection. We have arrived at:

> **Hypothesis 3**: IDU networks with stable, sub-saturation levels of HIV-1 infection, will continue to produce new infections over the course of time that fail to propagate fully throughout the network, but will instead function as reservoir of overall network infectiousness.

Suggestions like this one have been the source of considerable debate in regard to general sexual networks and non-IDU communities, as discussed above. Given, however, that IDU risk interactions differ considerably from sexual networks, a clear understanding of these networks apart from debates about purely sexual transmission is critical. All three of these hypotheses are tested in this research. All bear on important questions of public health, within and beyond the IDU community.

1.3 Current Approaches

Recently, Kretzschmar and Wiessing have revisited their original work on modeling IDU networks (Kretzschmar & Wiessing, 2008). Their review begins with their own early models (Kretzschmar & Wiessing, 1998) and that of Blower and colleagues (Blower, Hartel, Dowlatabadi, Anderson, & May, 1991), and traces the evolution of mathematical modeling techniques through their impact on our understanding of differentiated infection scenarios (Hendriks et al., 1998; Brenner et al., 2007) and differential risk behaviors (Mathei et al., 2006), to the design of interventions (Van Den Berg, Smit, Van Brussel, Coutinho, & Prins, 2007) and beyond. When discussing the future of these efforts, however, they point out the need for what Snijders et all refer to as "stochastic actor-based models for network dynamics" (Snijders, Bunt, & Steglich, 2010). As Snijders describes it, networks gain their dynamism as actors come and go from the network, and when they change their mutual connections due to:

> the structural positions of the actors within the network e.g., when friends of friends become friends , characteristics of the actors (actor covariates), characteristics of pairs of actors (dyadic covariates), and residual random influences representing unexplained influences. (Snijders et al., 2010, , p. 44).

Unfortunately, this sort of network dynamism has yet to impact mathematical modeling for IDU networks.

By way of contrast, the simulation of HIV and other transmitted infections has grown remarkably in the past two decades, prompted in part by dissatisfaction with prior, overly static modeling approaches. As Goudreau has recently pointed out, past approaches (mainly based on using ordinary differential equations (ODE) to simulate population group dynamics through time) failed to incorporate important features of both the populations they were meant to model and of the dynamics of infection (Goodreau, 2011). Beginning in 2000, however, network simulation of disease transmission began to be seen as a viable alternative in the simulation of disease transmissions by ODE methods, including especially the simulation of HIV and other sexually transmitted infections (Ghani & Garnett, 2000; Morris & Kretzschmar, 2000; J. Koopman, 2004; Danon et al., 2011). Where earlier percolation-type models had focused on the dynamics of infection probabilities and mixing probabilities to calculate the thresholding properties (Jacquez et al., 1994; Iannelli, Milner, Pugliese, & Gonzo, 1997; Blower et al., 1991; Bell et al., 2002), much of this work remained tied random mixing algorithms when calculating transmission probabilities among sub-groups within the network (Peterson, Willard, Altmann, Gatewood, & Davidson, 1990).

As discussed above, simulations of disease transmissions based on Exponential Random Graph Modeling (ERGM) took a different approach. Given that their main concern is with isolating network factors related to some known distribution (in this case, the mixing patterns of different classes of network members, or the prevalence of particular network substructures), ERGM simulation approache proceed by producing logit-type regression analyses of both topological and individual behavioral elements of network actors, which can then be used as predictors of the "causes" discovered network distribution. (Goodreau, 2006b; Snijders, Pattison, Robins, & Handcock, 2006a; Morris,

Handcock, & Hunter, 2008; Morris, Kurth, Hamilton, Moody, & Wakefield, 2009; Goodreau, 2006b) As described by Goodreau, such studies use existing network data to create dynamic networks (networks where the connections between node actors are periodically reassigned according to a given distribution of pair-wise likelihoods) (Goodreau, 2011), which go well beyond inferences drawn from static networks and other random mixing scenarios.

Yet where ERGM techniques have been used to simulate dynamic networks, the method has shown flexibility in its ability to produce dynamic networks which, while changing their overall number of nodes and specific edge distributions, never the less stay consistent with a known network topology. In these applications, network dynamism provided by the random selection of node pairs whose probability of attachment (or edge deletion if they are already linked) is derived from the difference that the absence or presence of this link would make in the overall likelihood of the graph (according the guiding ERGM model) (Goodreau, 2006b). ERGM methods do have their limits, however. Unlike agent based models, the nodes in an ERGM simulation lack individual dynamism—such as the ability to decide individually when and how often they "'churn"' their links, or how long their participation in the simulation will last, or what their preferred number of connections will be, Rather, in ERGM simulation, network dynamism is established at the level of the entire network, rather than at the level of individual nodes.

A second, proposed platform for dynamic simulation has been put forward by McCulloh, Lospinoso and Carley, referred to as the Link Probability Model (LPM). Like the ERGM-based Sienna Platform, LPM takes as it starting point two discreet observations of the same network to generate a model of network change/consistency over time. Unlike ERGM, however, LPM uses these two observations to establish a frequency of interaction matrix between all pairs of nodes. Network dynamism is then produced by simply taking "'snapshots"' of the network at sequential times, where at each time interaval the existence of a connection between two nodes is determined by random chance, which is weighted by the perviously known frequency of interaction between that pair. Like ERGM, LPM has limits that make it unsuitable for our purposes. For one, it works with a fixed set of nodes whose pair-wise edge likelihood is known before hand, and which remains static throughout the simulation. Further, network dynamism in LPM is indifferent to local topology, the main strength of the ERGM methodology, and one which seems

essential if we wish to simulate networks with large numbers of not perviously known actors who will come and go from the network.

Taken together, all of these approaches offer important insights into aspects of network dynamism which seem important to simulation design. The simulation model proposed here, while incoporating ERGM techniques for the selection of weighting of relative link likelihoods, does not use the ERGM platform for simulation.

Several features of the current simulation framework can be distinguished from the various techniques discussed above:

- like agent-based models, we wanted to maintain an actor-based environment, where actions which determined network dynamism originated in characteristics of the nodes themselves. Such actor-based dynamism should include risk behaviors, length of network participation, and when and how to establish new network connections or get rid of prior ones.

- like ERGM-base simulations, we wanted link creation to obey the sorts of node-specific properties (such as gender, age, ethnicity/race) and local structural tendencies (such as network transitivity), so that our dynamic network remained "'real-world"' viable over long simulation times, even while individual nodes/actors came and went from the network.

- like agent-based models, we wanted our actors to draw their individual behaviors (beyond their node-specific characteristics such as age, or gender) from a distribution of possibilities, and to allow for different modalities of participation (such as one might see from two very different classes of network actors—otherwise indistinguishable by node characteristics).

- like ERGM-based models, we wanted to be able to control for network level factors affecting overall network dynamism, such as network stability or adherance to a network-wide degree distribution.

  And finally,

- like agent based models, we wanted to be able to simulate large networks, to determine whether factors of scale affected network dynamics and the dynamic HIV infection over simulation time, and to see simulation results on a scale of the phenomena of interest.

Chapter 2

Modeling risk networks

Our objective in this chapter is to develop and describe a mathematical framework that is capable of producing stochastic actor-based models of real-world risk networks. Generated models should capture heterogeneity, in terms of types of individuals, types of linking relationships between them, and types of pathogens flowing across the link fabric. In addition, they should capture temporal dynamism, at the level of node arrivals and departures, restructuring of relationships, and changes to the pathogen over its lifetime. Whenever possible, this dynamism should be modeled through constraint and specification of *local agency* at the scale of individuals, relationships, and infections, rather than by aggregate systemic constraints. We do not require that the models generated be analytically solvable—indeed it is unlikely that any framework that covers such a vast range of potential systems would be. As much as possible, parameters in the model should map to recognizable forces on local agency, and ideally ones that can be quantified through systematic sampling of real-world networks.

To start, in Section 2.1, we begin be formalizing the notion of an m-property, l-layer, p-pathogen model. Such a (m, l, p) model defines a distribution over the space of all networks in which each node has m categorical attributes, relationships between nodes fall into one of l types, and there are p distinct types of pathogens at large distributed throughout the network's nodes. Then, in Section 2.2.1, we extend the framework to support pathogen dynam-

ics, enabling each of the p distinct infection types to flow between individuals, with the l different types of risk relationships serving as conduits for transmission. Finally, in Section 2.2.2, we incorporate network dynamism—in terms of arrivals and departures of individuals from the risk network, incremental changes to risk relationship structures, and aging. Gradually widening the scope of the framework in three discrete steps is a deliberate strategic choice motivated by efficacy in exposition. The real modeling framework we intend to use, is the one we shall arrive at by the end of this chapter, a qualitative summary of which appears in Section 2.3, p. 67.

2.1 Structural models of static risk networks

In this section, we develop the mathematical edifice for the following process:

1. Building a risk network from a population survey; this is treated in Subsection 2.1.1.
2. Determining which node attributes have the greatest influence on the formation of risk partnerships; this is treated in Subsection 2.1.2.
3. Extracting a structural model from a risk network; this is treated in Subsection 2.1.3.
4. Generating new (static) risk networks from a structural model; this is treated in Subsection 2.1.4.
5. Validating generated risk networks against the original surveyed network from which the structural model was extracted; this is treated in Subsection 2.1.5.

Throughout, some recurring conventions will appear. Sets will be denoted by capital letters, A, B, C, etc., and will be indexed by integer variables i, j, k, etc. Elements within sets will be written in lower case Roman letters, a, b, c, etc. Distributions will usually be expressed as α, β, γ, etc. Types or proper names will be represented in script $\mathscr{A}, \mathscr{B}, \mathscr{C}$, etc. In an exposition

where a set or function, (e.g. V, or I) must be considered time-dependent, the temporal index will appear as a *superscript*, (causing us to write V^t and I^t). In situations where a set or function (e.g. N or f) is being seen as particular to a choice of layer, attribute, or pathogen type, this dependency will be made clear in the *subscript* of the variable, i.e. N_j, or I_k. A function f whose domain is D and range is R will be declared so by the statement $f : D \to R$. Set differences are indicated using the $\setminus$ operator. Finally, as a last resort, the reader might find the index at the end of this report useful; it contains, among other things, a list of all mathematical symbols used in this exposition.

2.1.1 Building a network from a population survey

We view a risk network as an l-layer combinatorial fabric, weaving together a set of individuals, each of whom has m properties, and hosts up to p distinct types of pathogens. Here we make this notion formally precise, and provide an outline of how such a formal object is instantiated in the course of a population survey.

In a complete survey of a population V, each of its constituent individuals v is interrogated regarding a fixed set of m attributes $X = \{x_1, \ldots x_m\}$. For example, x_1 could be gender, while x_2 might be age, etc. We assume that each variable x_i (for $i = 1, \ldots, m$) is categorical, taking values from a finite set U_i that is known in advance. So, (continuing the example), U_1 could be $\{\text{Male}, \text{Female}\}$, while U_2 might be $\{\text{21AndUnder}, \text{Over21}\}$. Each node attribute x_i $(i = 1, \ldots, m)$ is seen as a function $x_i : V \to U_i$.

Network surveys go beyond individual attributes, collecting data on the risk relationships between them. The relationships of interest might be of several concrete types $\mathscr{T}_1, \mathscr{T}_2, \ldots, \mathscr{T}_l$. For example, $\mathscr{T}_1$ might be the relationship of "sharing drugs with", while $\mathscr{T}_2$ relationships could embody "sexual partnership", etc. In practice, during the survey, each individual v from V is questioned about their risk relationships for each type $\mathscr{T}_j$ (for $j = 1, \ldots, l$), and is asked to provide sufficient information with which to identify the individuals $N_j(v) \subseteq V$ with whom v enjoys a type $\mathscr{T}_j$ relationship. The data

thus collected is used to define a degree $d_j(v) \stackrel{\text{def}}{=} |N_j(v)|$ for each individual v; the value of this quantity is the number of type $\mathscr{T}_j$ relationships that v has. The set of all relationships, at each of the $j = 1, \ldots, l$ network layers, is then expressible as

$$E_j = \bigcup_{v \in V} N_j(v).$$

In mapping out risk networks, it is important that surveyed individuals be asked about their relationships within a well-defined temporal frame. For example, in a study designating relationship type $\mathscr{T}_1$ to be "social drug co-use", the survey instrument must be designed to ask subjects to identify individuals with whom they engaged in social drug co-use behaviors *over a specific time period*, e.g. "in the last 30 days". The value $|d_1(v)|$ could then be taken to represent the number of mutual drug use partners of v within a one month period. For each risk network j, we shall denote the temporal frame with respect to which relationships are defined as Θ_j (months).

Pathogens of interest manifest in several distinct forms $\mathscr{P}_1, \mathscr{P}_2, \ldots, \mathscr{P}_p$. Specifying the instantaneous state of a risk network thus requires a collection of p concrete sets of individuals

$$A_1, A_2, \ldots, A_p \subseteq V$$

where A_k is the set of individuals afflicted by pathogen $\mathscr{P}_k$ $(k = 1, 2, \ldots, p)$. For example, if a study designated pathogen type $\mathscr{P}_1$ as HIV, then study subjects could be administered an HIV test as part of the survey process. The subset $A_1 \subseteq V$ would then represent the HIV positive individuals.

Our formal definition of an (m, l, p) **risk network** is the $(m + 2l + p + 1)$ tuple:

$$\mathcal{D} \stackrel{\text{def}}{=} (x_i, V, E_j, A_k, d_j)_{i=1,\ldots,m; j=1,\ldots,l; k=1,\ldots,p}.$$

There is typically a complex interplay between the structure of the network's l layers, the p pathogen types, and each individual's k attributes. In most real-world settings, each of the many types of pathogens can be transmitted via many different types of risk activity, are sensitive to the properties of host individuals, and affected by the presence of other pathogens.

2.1.2 Selecting influential node attributes

In modeling a risk network $\mathcal{D}$, the question arises as to the contents of the model, and particularly, which m attributes $X = \{x_1, \ldots x_m\}$ to consider. In retrospect, patterns of social and risk bearing connectivity in injecting drug user risk networks have been a consistent concern among researchers in their attempts to understand disease transmission, both within IDU networks, and between IDU networks and surrounding communities. Until recently, however, statistical modeling of network connectivity has posed considerable difficulty. The reasons for this are straightforward: ordinary statistical modeling techniques involve linear regression and other forms of tests-against-randomness to determine the relative importance of model factors as they influence the likelihood of particular data samples, and such tests against randomness are not feasible when considering patterns of connectivity in networks, even with recent gains in computational power.

For this reason, past analyses of IDU and other social network data have had to be content with insights derived from the cross-tabulation of connection data (how many men, for example, connect to other men, versus how many men connect to women). While insightful, and capable of answering questions of the dependence and independence of network variables, such statistics do not provide measures of certainty or error, nor the relative weights of variables vis-a-vis one another; nor can they can they tell us how likely the observed patterns of network connectivity are to be the product of random assortment (rather than the result of actual connection preferences among network members).

Questions of determinate variables (and their relative importance), are of paramount importance to our modeling process. In particular, we needed to determine which individual attributes were important to the formation of the network, and to know how these attributes ranked, both relative to one another, and relative to structural determinants produced by the network itself–an example of the latter being network transitivity, which turned out to be an important consideration in determining network dynamics which had not been analyzed in the past.

The means for the discovery of these sorts of modeling parameters were not

available to the authors of either of the network studies (SFHR and P90) on which the current modeling and simulation research is based. Recently, however, the statistical analysis of network data has been advanced considerably by the introduction of Exponential Random Graph Modeling (ERGM). ERGM provides an alternative to the simple cross-tabulation of network link data. Described in more detail below, ERGM techniques can provide likelihood-based estimates of how factors—e.g. gender, age, race/ethnicity, injection history, or network position vis-a-vis the network configuration of one's neighbors—influence overall network connection tendencies. To begin the process of parameterizing the models at the center of the simulation, we applied ERGM analysis to the SFHR and P90 data sets, a step which had never been undertaken previously.

The strategy for this consisted of three steps. In the first step, we isolated each potential individual and structural variable of potential interest, tested its influence on the formation of network connections exhibited in each of the networks (given the total size and density of each network), and examined the level of each categorical value possible for each variable. Drawing on the conclusions of the studies' original authors, the variables we tested were homophily with regard to ethnicity, gender, age, and number of injection partners. In addition, we tested for the influence of various disease categories, marital status, income, injection history, years injecting, education level, work as a prostitute, transitive closure and cycle lengths of 4 and 5. The analysis produced a table for each of the two studies, in which each individual variable, and each of it's possible categorical values, is assigned an exponent, together with an error score and significance level. This table provides the necessary data on the extent to which each variable, taken in isolation, appears to influence the pattern of connectivity in each network analyzed. Of the variables we tested, we found that ethnicity, gender, age, number of injection partners and transitive closure were the most influential (and statistically significant) in predicting the observed network topologies of SFHR and P90.

The second stage of the analysis involved examining the effects of different average personal network size on the results of step 1, to eliminate the possibility that what appeared as network homophily was actually a result of network degree. And finally, the third stage of the analysis was to test a general model for each network to determine the relative importance of the

list of network variables, as a means to select the relevant set of m attributes $X = \{x_1, \ldots x_m\}$. to consider. In Chapter 3, prior to conducting simulation experiments on HIV risk networks, the results of this three-step process are described at length, and their influence on the modeling are discussed.

For completeness, the next section of this chapter provides a brief overview of ERGM, it's general assumptions, and the manner by which it determines the relative importance of variables. It appears here because it played a crucial role in the development of the static model, and in the transition from static characteristics to network dynamics. Readers who are familiar with ERGM may skip the exposition and proceed to Section 2.1.3 on p. 44 with the knowledge that the influential m attributes $X = \{x_1, \ldots x_m\}$ have been selected from the survey using the ERGM analysis. We again note that our simulation does not conform directly to classical simulations based on ERGM models. Rather, we used ERGM for the crucial step of filtering the attributes collected during the survey, so that only those attributes which were seen to exert sufficient influence on the formation of connections are retained. This filtering process is recommended and assumed by the model framework we present here, but it is not part of the framework's basic functioning.

Exponential random graph modeling

ERGM is a statistical technique aimed at determining the extent to which the likelihood of network linkages appears to be biased towards (or against) the creation of specified network substructures, above and beyond what is expected by chance occurrence. Such substructures can be a simple as the tendency of "like" nodes to be connected (at a greater rate than expected by a random distribution of connections), or as complex as specific structures of connection between several individuals (Bearman, Moody, & Stovel, 2004). The theoretical basis for ERGM analysis was laid down by Holland and Leinhardt (1981) and Frank and Strauss (1986), with estimation questions finally settled only recently (Snijders, Pattison, Robins, & Handcock, 2006b).

Like ordinary statistical regression analysis, ERGM modeling aims to determine the probability, as a linear function, of one or more predictors for the distribution of a set of observations (in this case, the observed set of con-

nections in the network under consideration). In this paper, we follow the analytical lead of Goodreau, Kitts, and Morris (2009), in using ERGM to ascertain the importance of both specific network substructures (triads) and node-based homophily (the tendency of association between "like" nodes). The same analysis is carried out over two separate and well-known IDU/-sexual risk networks. The theoretical basis for this analysis is as follows:

According to Kolaczyk (2010, p.180-1), an exponential family random graph takes the following form: given a random graph $G = (V, E)$ with binary random variable $Y = [Y_{ij}]$ that expresses the presence or absence of an network connection $e \in E$ from i to j, the probability of a set of ties Y is expressed as

$$P_\theta(Y = y) \;=\; \frac{1}{\kappa} exp\left\{\sum_H \theta_H g_H(y)\right\}. \tag{2.1}$$

where H is a possible set of edges in G. Here $g_H(y)$ is an indicator variable, taken to be 1 if H actually occurs in y, and 0 if it does not; θ_H is non-zero where Y_{ij} are dependent for all pairs $\{i, j\}$ in H. The normalizing constant $\kappa = \kappa(\theta)$ is defined as

$$\kappa(\theta) \;=\; \sum_y exp\left\{\sum_H \theta_H g_H(y)\right\}. \tag{2.2}$$

As with ordinary statistical regression analysis, here $g_H(y)$ can stand for a series of model covariates that may be deemed important to network formation, and which may be calculated with respect to y: $g_1, g_2, g_3, \ldots, g_h$. The coefficients of $(\theta_1, \theta_2, \theta_3, \ldots, \theta_h)$ then stand for the weights of their respective covariates, and are estimated by the ERGM process.

Following Goodreau (2007), equation (2.1) can be re-expressed in logit form, as the conditional log odds of individual ties:

$$logit\left(P(Y_{ij} = 1 \mid n \text{ actors }, Y_{ij}^c)\right) \;=\; \sum_{h=1}^{H} \theta_h \delta z_h(y) \tag{2.3}$$

where $Y^c_{i,j}$ are all dyads other than Y_{ij} and $\delta z_h(y)$ is the amount by which the covariate $g_h(y)$ changes when Y_{ij} is changed from $0 \to 1$, or from $1 \to 0$. Here Y^c_{ij} ensures the mutual dependence of ties in the conditional, and obviously a single tie may affect multiple covariates.

The interpretation of θ in the expression above is that, where the addition of a tie $i \to j$ increases z_h by 1, then the log odds of that tie forming increases by θ_h. According to Goodreau et al. (2009), this interpretation requires three assumptions.

The first assumption is that the ties in the network are **homogeneous**, such that the change measured in the z statistic (say, when counting the number of such connections in the network between "like nodes", or the number of ties which complete a triad) with the toggling of $i \to j$ would treat all other examples of such ties present in the network as equally probable.

Second, when modeling the effect of node-based attributes (such as gender or age) on the presence or absence of ties between nodes, the model assumes that the importance of a given attribute on a dyad pair will be determined based only on the presence or absence of that attribute, and not on the value of other ties in the network. That is, where a node attribute is considered for its importance in tie formation, the effects of this attribute are assumed to function **independent** of the effects of other attributes.

And finally, as Goodreau et al Goodreau et al. (2009, p.109-110) point out, the determination of θ which provides the maximum likelihood of the known graph is problematic, given that the normalizing constant $\kappa(\theta)$ is incalculable for all but the smallest networks. However, the estimation of $\kappa(\theta)$ can be undertaken using Markov Chain Monte Carlo methods (Snijders et al., 2006a, 2006b; Hunter, Handcock, Butts, Goodreau, & Morris, 2008; Morris et al., 2008; Robins, Snijders, Wang, Handcock, & Pattison, 2007). As Goodreau et al (Goodreau et al., 2009, p.110-111) discuss, such procedures can be used to simulate network dynamics (Goodreau, 2006b), and to test for model degeneracy as well. Such a system can also make use of any number of ordinary network measures as variables (e.g. "centrality measures" or "constraint", the number of ties incident to a specific attribute class, or network-structure-based characteristics like the tendency to "transitive closure"), each of which is then assigned a separate θ coefficient.

2.1.3 Extracting a structural model from a network

Given a risk network $\mathcal{D} = (x_i, V, E_j, A_k, d_j)_{i=1,\ldots,m;j=1,\ldots,l;k=1,\ldots,p}$, one may extract from each of the network's attributes x_i $(i = 1, \ldots, m)$, a set of m univariate distributions $\alpha_i : U_i \to [0, 1]$ for $i = 1, 2, \ldots, m$, wherein for each $u \in U_i$,

$$\alpha_i(u) \stackrel{\text{def}}{=} \frac{1}{|V|}|x_i^{-1}(u)|.$$

We call α_i, the **univariate distribution** of property x_i.

Additionally, each set of type $\mathscr{T}_j$ relationships E_j within the network (for $j = 1, 2, \ldots, l$) give rise to m bivariate frequency distributions $\beta_{i,j} : U_i \times U_i \to [0, 1]$ for $i = 1, 2, \ldots, m$, that can be extracted by taking

$$\beta_{i,j}(u_1, u_2) \stackrel{\text{def}}{=} \frac{1}{|E_j|}|(x_i^{-1}(u_1) \times x_i^{-1}(u_2)) \cap E_j|$$

for each $u_1, u_2 \in U_i$. We call $\beta_{i,j}$, the **bivariate distribution** of property x_i across network layer j.

Each set of type $\mathscr{T}_j$ relationships E_j (for $j = 1, 2, \ldots, l$) also yields a **univariate degree distribution** χ_j. In practice, we will represent this distribution by defining $\chi_j : \mathbb{Z} \times \mathbb{Z} \to \mathbb{R}$ and taking for every pair of integers a, b

$$\chi_j(a, b) \stackrel{\text{def}}{=} \frac{|\{v \in V \mid a \leqslant d_j(v) < b\}}{|V|}.$$

In addition, we may obtain a **bivariate degree distribution** $\bar{\bar{\chi}}_j$. We will define this distribution $\bar{\bar{\chi}}_j : (\mathbb{Z} \times \mathbb{Z})^2 \to \mathbb{R}$ by taking, for every 4-tuple of integers a, b, a', b'

$$\bar{\bar{\chi}}_j(a, b, a', b') \stackrel{\text{def}}{=} \frac{|\{e \in E_j \mid e = (u, v); a \leqslant d_j(u) < b; a' \leqslant d_j(v) < b'\}}{|E_j|}.$$

The network $\mathcal{D}$ provides us with a population size $n \stackrel{\text{def}}{=} |V|$. In addition, for each of the P pathogen types $\mathscr{P}_k$ $(k = 1, 2, \ldots, p)$, we can compute the

pathogen prevalence within the population:

$$p_k \stackrel{\text{def}}{=} |A_k|/|V|.$$

The formal definition of a (m, l, p) **structural model** is $(2m + ml + 2l + p)$-tuple

$$\mathcal{M}(\mathcal{D}) \stackrel{\text{def}}{=} (\alpha_i, \beta_{i,j}, \chi_j, \bar{\bar{\chi}}_j, p_k)_{i=1,\ldots,m;j=1,\ldots,l;k=1,\ldots,p}.$$

In what follows, we will assume that the univariate distributions (resp. bivariate distributions) are pairwise independent. In practice, if α_i and α_j (resp. β_i and β_j) do not comply with this independence assumption for some $i \neq j$ (e.g. as determined by the Pearson χ-squared test at a given significance level), then one may choose to coalesce variable x_i and x_j into a single variable $x' : V \to U_i \times U_j$.

2.1.4 Generating networks from a structural model

Given a structural model $\mathcal{M}$, the three-phase procedure **MakeNetwork** (see Listing 1) instantiates a new network of size n using the provided model as a statistical guideline. In the first phase (line 1), procedure **MakePopulation** is called to create individuals, assign each of them their attributes x_i using the univariate distributions α_i, as well as ideal ego network sizes d_j within each of the network layers $j = 1, \ldots, l$ using degree distributions χ_j. In the second phase (line 2), procedure **MakePathogens** is called to distribute each of $k = 1, \ldots, p$ types of pathogens among the population V, reflecting the specified prevalence levels p_k of each. In the third phase (line 3), a call to procedure **MakeRelations** connects individuals via each of the l types of pairwise relationships, reflecting each individual's ideal ego network size d_j in layer j of the network. Relationships are chosen in a manner that takes into consideration the specified bivariate attribute distributions $\beta_{i,j}$ and bivariate degree distributions $\bar{\bar{\chi}}_j$. The network is constructed in the time interval $[0, 1)$.

The **MakePopulation** procedure (see Listing 2) creates n individuals, as-

Listing 1: Procedure **MakeNetwork**

Input: structural model $(\alpha_i, \beta_{i,j}, \chi_j, \bar{\bar{\chi}}_j, p_k)_{i=1,\ldots,m;j=1,\ldots,l;k=1,\ldots,p}$; and desired population size n.

Output: risk network $(x_i, V, E_j, A_k, d_j)_{i=1,\ldots,m;j=1,\ldots,l;k=1,\ldots,p}$.

1 $(\{x_i\}, \{d_j\}, V) \leftarrow$ **MakePopulation**$(n, \{\alpha_i\}, \{\chi_j\})_{i=1..m;j=1..l}$
2 $\{A_k\} \leftarrow$ **MakePathogens**$(V, \{p_k\})_{k=1..p}$
3 $E \leftarrow$ **MakeRelations**$(\{\beta_{i,j}\}, \{\bar{\bar{\chi}}_j\}, \{x_i\}, \{d_j\}, V)_{i=1..m;j=1..l}$
4 **return** $(x_i, V, E_j, A_k, d_j)_{i=1,\ldots,m;j=1,\ldots,l;k=1,\ldots,p}$.

signing each of their m properties independently at random, using the univariate distributions $\alpha_1, \ldots, \alpha_m$ (see lines 4,5). Then (see lines 7,8) we use the degree distributions χ_j to assign each individual an idea ego network size, or *ideal degree*, $d_j(v)$ within each of the layers $j = 1, \ldots, l$.

Listing 2: Procedure **MakePopulation**

Input: pop. size n, attribute distributions $\{\alpha_i\}_{i=1..m}$, degree distributions $\{\chi_j\}_{j=1..l}$.

Output: $(\{x_i\}, \{d_j\}, V)_{i=1..m;j=1..l}$.

1 $V = \{v_1, v_2, \ldots, v_n\}$.
2 **foreach** v_k *in* V **do**
3 // Set the properties of individual v_k.
4 **foreach** i *in* $1 \ldots m$ **do**
5 $x_i(v_k) :=$ an element of U_i randomly selected via α_i.
6 // Set individual v_k's ideal ego net size at each layer.
7 **foreach** j *in* $1 \ldots l$ **do**
8 $d_j(v_k) :=$ an integer randomly chosen via pdf χ_j.
9 **return** $(\{x_i\}, \{d_j\}, V)_{i=1..m;j=1..l}$.

Once the population has been instantiated, the **MakePathogens** procedure (see Listing 3) distributes each of the p types of pathogens (line 2) to the each of the individuals in V (line 3), in a manner that reflects the specified prevalence levels for the particular pathogen type (lines 4,5).

Listing 3: Procedure **MakePathogens**

Input: population V, pathogen prevalences $\{p_k\}_{k=1..p}$
Output: $\{A_k\}_{k=1..p}$

```
1 A_1 = A_2 = ... = A_p = ∅
2 foreach k in 1...p do
3     foreach v_i in V do
4         if Random(0,1) < p_k then
5             A_k := A_k ∪ {v_i}
6 return {A_k}_{k=1..p}
```

Once population has been instantiated and initial pathogens distributed, the **MakeRelations** procedure creates risk relationships between individuals (see Listing 4). To do this, it initialized the layer j (line 3) neighbors of each node v_i (line 2) to be the empty set (line 4), and then schedules execution of **MakeEdge** for each node v_i and each layer j to take place at time $1/i$ (line 5).

Listing 4: Procedure **MakeRelations**

Input: bivariate attribute distributions $\{\beta_{i,j}\}_{i=1..m;j=1..l}$, bivariate degree distributions $\{\bar{\bar{\chi}}_j\}_{j=1..l}$, individual attributes $\{x_i\}_{i=1..m}$ and ideal degrees $\{d_j\}_{j=1..l}$, the population V
Output: E

```
1 E = ∅.
2 foreach i in 1...|V| do
3     foreach j = 1...l do
4         N_j(v_i) := ∅.
5         Schedule MakeEdge(v_i) to take place at time 1/i.
6 Wait until time 1.
7 E := ⋃_{i=1}^{|V|} ⋃_{w∈N(v_i)} {(v, w)}
8 return E
```

Each execution of **MakeEdge** takes place in the context of a given vertex v, layer j and time T (see Listing 5). The procedure first computes the layer j edge deficit for vertex v (line 2), that is the difference between v's ideal degree and actual degree (at time T) in network layer j:

$$\delta_j(v) \stackrel{\text{def}}{=} d_j(v) - |N_j(v)|.$$

If v has a positive deficit (line 3) we find a new neighbor w for v and add the edge (v, w). The individual w is selected from among a set C of candidates who also have a positive deficit, but are not already neighbors of v (line 5). The likelihood of selecting a particular candidate c is biased by (i) the current degrees of v and c (line 8)[1], the joint attributes of v and c (line 9), and the scaled magnitude of c's edge deficit (line 10)[2]. These factors are used to construct a probability distribution over the set of candidates C (lines 11,12), using which one of the candidates w is selected from C (line 13). The edge (v, w) is then added (lines 15,16) by augmenting the neighbor sets of v and w. Finally, **MakeEdge** reschedules itself to be called for vertex v layer j, at a time halfway between T (now) and time 1 (see line 17). Thus, in a manner reminiscient of Zeno's paradox, each individual v approaches fulfillment of itsideal degree over time. Fortunately, since all ideal degrees are finite, by time < 1 the edge building process of all nodes necessarily terminates. The calling procedure **MakeRelations** need only wait until time 1 before aggregating the set of all edges (see lines 6,7 of Listing 4).

[1]In practice, particularly when using models that are derived from surveyed risk networks, the influence of the degrees of v and c must be arrived at by "binning" the appropriate x_i attribute which captures the degree. Binning is necessary to avoid assigning probability 0 to large regions in the space of joint degrees in which the survey did not discover any edge. In this description of **MakeEdge**, a uniform bin width of 2ϵ is being used. In general, the binning of degrees need not be uniform; it is part of the network generation process, but will not be addressed in detail here.

[2]In practice, the influence of the candidate c's edge deficit $\delta_j(c)$ is weighted by composing it with a C^∞ monotonic function $\sigma(x)$ which approaches 1 as $x \to \infty$ and is identically 0 when $x \leqslant 0$. We chose the function

$$\sigma(x) \quad = \quad \begin{cases} e^{\frac{-1}{x}} & x \geqslant 0 \\ 0 & x < 0. \end{cases}$$

Listing 5: Procedure **MakeEdge**

Input: individual v, layer j, time T

// Compute the edge deficit of v in layer j

$\delta_j(v) := d_j(v) - |N_j(v)|$.

// Determine if v has not yet reached its ideal degree

if $\delta_j(v) > 0$ **then**

  // Determine candidate new neighbors for v.

  $C(v) := \{u \in V \mid \delta_j(u) > 0\} \backslash (N_j(v) \cup \{v\})$.

  if $|C(v)| > 0$ **then**

    foreach c *in* $C(v)$ **do**

      Compute the degree-based affinity of v and c using the bivariate degree distribution $\bar{\bar{\chi}}_j$:

$$a_\chi(v,c) := \bar{\bar{\chi}}_j(|N_j(v)| - \epsilon, |N_j(v)| + \epsilon, |N_j(c)| - \epsilon, |N_j(c)| + \epsilon).$$

      Compute the attribute-based affinity of v and c using the bivariate attribute distributions $\beta_{i,j}$:

$$a_\alpha(c) := \prod_{i=1}^{m} \beta_{i,j}(x_i(v), x_i(c)).$$

      Compute the affinity due to c's edge deficit:

$$a_\delta(c) := \sigma(\delta_j(c)).$$

      Use the 3 affinities to compute propensity of edge (v, c):

$$\omega(c) := a_\delta(c) \cdot a_\chi(c) \cdot a_\alpha(c).$$

      Normalize propensity to obtain a distribution over $C(v)$:

$$p(c) := \frac{\omega(c)}{\sum_{c' \in C(v)} \omega(c')}.$$

    $w :=$ choose from $C(v)$ randomly according to distribution p.

    // Add the edge connecting v to w.

    $N(v) := N(v) \cup \{(v, w)\}$

    $N(w) := N(w) \cup \{(w, v)\}$

    Schedule **MakeEdge**(v_i) to be called at time $(1 + T)/2$.

2.1.5 A framework for validating generated networks

So we see that from a network survey, we can derive a risk network $\mathcal{D}$ (see Section 2.1.1), and from a risk network we can derive a structural model $\mathcal{M}$ (see Section 2.1.3), and from a structural model we can generate new risk networks $\mathcal{D}'_1, \mathcal{D}'_2, \mathcal{D}'_3$, etc. (see Section 2.1.4). In this section, we shall develop techniques to quantify the difference between the original $\mathcal{D}$ and a particular generated network $\mathcal{D}'$. These techniques shall be particularly relevant to assessing the possible **degeneracy** of a model $\mathcal{M}$, by which me mean its potential inability to generate networks that are "similar" to $\mathcal{D}$.

We begin by considering the problem of quantifying the similarity or difference between two models. Clearly, not all (m, l, p) models are directly comparable. Let us say that two (m, l, p) models

$$\begin{aligned} \mathcal{M}_1 &= (\alpha_i, \beta_{i,j}, \chi_j, \bar{\bar{\chi}}_j, p_k)_{i=1,\ldots,m;j=1,\ldots,l;k=1,\ldots,p} \\ \mathcal{M}_2 &= (\alpha'_i, \beta'_{i,j}, \chi'_j, \bar{\bar{\chi}}'_j, p'_k)_{i=1,\ldots,m;j=1,\ldots,l;k=1,\ldots,p} \end{aligned}$$

"belong to the same **family** of models" if the domains of corresponding distributions agree

$$\begin{aligned} Domain(\alpha_i) &= Domain(\alpha'_i) \\ Domain(\beta_{i,j}) &= Domain(\beta'_{i,j}) \end{aligned}$$

for all $i = 1, \ldots, m; j = 1, \ldots, l$. Given two models belonging to the same family, how might we quantify their similarity or difference?

Since models are tuples of distributions[3], we begin by considering how one may assess the similarity between two probability distributions f, f' over the same set X. Many approaches exist, including histogram intersection (Barla, Odone, & Verri, 2003), Chi-square statistic (Read, 1993), quadratic form

[3]The pathogen prevalence numbers p_k (for $k = 1, \ldots p$) can be seen as parameters in in Bernoulli distribution on a random variable describing whether a randomly chosen v is afflicted with pathogen $\mathscr{P}_k$. The distribution of the random variable can be expressed as

$$\rho_k \begin{cases} \text{true} & \text{with prob. } p_k \\ \text{false} & \text{with prob. } 1 - p_k \end{cases}$$

distance, match distance, Kolmogorov-Smirnov distance (Stephens, 1974), earth mover's distance, Kullback-Leibler divergence—sometimes now called information divergence, information gain, relative entropy—see Kullback and Leibler (1951), and Jensen-Shannon divergence—also known as information radius, *IRad*, or total divergence to the average —see Lin (1991).

In this work, we choose to measure the difference between two probability distributions as

$$\Delta(f, f') \stackrel{\text{def}}{=} \sqrt{IRad(f, f')}$$

because this choice provides us with a true metric on the space of all probability distributions on an underlying set (Endres & Schindelin, 2003; sterreicher & Vajda, 2003). The *IRad* of two distributions is defined to be their mean Kullback-Leibler divergence from the average (as distributions). Applying this to the constituent distributions in the two models, we get

$$\begin{aligned}
\Delta(\alpha_i, \alpha'_i) &= \sqrt{\sum_{x \in U_i} \alpha_i(x) \log \frac{\alpha_i(x)}{\bar{\alpha}_i(x)} + \alpha'_i(x) \log \frac{\alpha'_i(x)}{\bar{\alpha}_i(x)}} \\
\Delta(\beta_{i,j}, \beta'_{i,j}) &= \sqrt{\sum_{(x,y) \in U_i \times U_i} \beta_{i,j}(x,y) \log \frac{\beta_{i,j}(x,y)}{\bar{\beta}_{i,j}(x,y)} + \beta'_{i,j}(x,y) \log \frac{\beta'_{i,j}(x,y)}{\bar{\beta}_{i,j}(x,y)}}
\end{aligned}$$

where $\bar{\alpha}_i$ is the average of α_i and α'_i (a distribution over U_i), and $\bar{\beta}_{i,j}$ is the average of $\beta_{i,j}$ and $\beta'_{i,j}$ (a distribution over $U_i \times U_i$). Analogous distance measures (omitted here) may be defined between the two models' corresponding univariate degree distributions χ_j, bivariate degree distributions $\bar{\bar{\chi}}_j$, and pathogen prevalences p_k (interpreted as Bernoulli distribution parameters).

Having defined the distance between corresponding distributions in the two models, we use the L_∞ norm to extend to a definition of distance Δ between two models:

$$\begin{aligned}
\Delta(\mathcal{M}_1, \mathcal{M}_2) = \max \Big(& \max_{i=1}^{m} \Delta(\alpha_i, \alpha'_i), \quad \max_{j=1}^{l} \max_{i=1}^{m} \Delta(\beta_{i,j}, \beta'_{i,j}), \\
& \max_{j=1}^{l} \Delta(\chi_j, \chi'_j), \quad \max_{j=1}^{l} \Delta(\bar{\bar{\chi}}_j, \bar{\bar{\chi}}'_j), \\
& \max_{k=1}^{p} \Delta(\rho_k, \rho'_k) \Big)
\end{aligned}$$

Now the distance between two networks $\mathcal{D}$ and $\mathcal{D}'$ may be taken to be the distance between their respective structural models:

$$\Delta(\mathcal{D}, \mathcal{D}') \stackrel{\text{def}}{=} \Delta(\mathcal{M}(\mathcal{D}), \mathcal{M}(\mathcal{D}')).$$

We have thus endowed each family of networks (and the space of associated structural models) with a metric structure based on the similarities of their constituent distributions. The metric Δ will be useful in two ways:

1. When we generate new networks from a structural model that was extracted from a surveyed risk network (see the procedure described in Section 2.1.4), the metric Δ will enable us to detect outliers, i.e. it will be able to detect when the generated networks $\mathcal{D}'$ are very different from the surveyed network $\mathcal{D}$ from which the generative model was constructed.

While networks generated from a structural (see Section 2.1.4) can be certified to be compatible with the original surveyed network (by determining that Δ is small), because each network is generated independently, one cannot justify considering a sequence of generated networks as having arisen sequentially over time. To overcome this limitation, in the next section of this chapter, we will extend the model framework to include a dynamism model consisting of additional parameters that specify the mechanisms governing a network's evolution over time. Where our original model presented in Section 2.1.3 could be used only to generate isolated instances of networks, the **extended model** which contains both structural and dynamism components, will be used to generate **trajectories**, each of which will be a sequence of networks *over time*. The extension will be carried out in two stages: First, in Section 2.2.1, we shall extend the model to support pathogen dynamics over time. Then, in Section 2.2.2, we shall extend the model still further to support modeling the evolution of network topologies and size over time.

2. Upon extending the model framework to support dynamic evolution of the network (as outlined above), the measure Δ will enable us to measure the drift in network's structure across its trajectory in time. Specifically, it will allow us to measure the divergence between the initial network $\mathcal{D}$ and its evolute, $\mathcal{D}'$.

In both the applications of Δ described above, whenever we discover that $\mathcal{D}$ and $\mathcal{D}'$ are significantly different (i.e. $\Delta(\mathcal{D}, \mathcal{D}')$ exceeds some prescribed threshold), the recursive definition of Δ will permit us to dissect the contributions of the constituent distributions to determine which of them are the most significant contributors to the divergence.

The question naturally arises as to what the threshold value should be. Put another way, if $\mathcal{D}'$ was generated by the model $\mathcal{M}(\mathcal{D})$, then what value must $\Delta(\mathcal{D}, \mathcal{D}')$ exceed before the networks $\mathcal{D}'$ is said to have diverged from $\mathcal{D}$?

To provide the reader with a sense of the scale of suitable thresholds, below is a table of Shannon-Jensen divergences between two distributions. The first distribution F_1 is the uniform distribution on a set of size k. The second distribution F_2 is a small perturbation of this uniform distribution—one where the probability of one of the k elements is increased ρ percent, i.e. from $1/k$ to $\frac{1+\rho}{k}$, and each the remaining $k-1$ elements reduces its probability equally as required, i.e. from $1/k$ to $\frac{1}{k}(1 - \frac{\rho}{k-1})$, so as to renormalize the probability mass to 1. The table on the next page renders the Shannon-Jensen divergence between F_1 and F_1 for different settings of k and ρ.

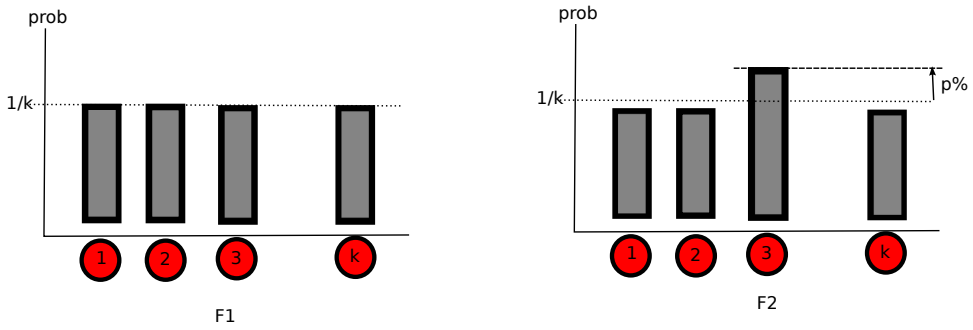

Figure 2.1: (Left) A uniform distribution on a set of size k; (Right) a pointed deviation of ρ percent.

	ρ=2.5%	ρ=5.0%	ρ=7.5%	ρ=10.0%	ρ=12.5%
k=2	$7.81 \cdot 10^{-5}$	$3.12 \cdot 10^{-4}$	$7.04 \cdot 10^{-4}$	$1.25 \cdot 10^{-3}$	$1.96 \cdot 10^{-3}$
k=4	$2.58 \cdot 10^{-5}$	$1.02 \cdot 10^{-4}$	$2.28 \cdot 10^{-4}$	$4.03 \cdot 10^{-4}$	$6.26 \cdot 10^{-4}$
k=6	$1.54 \cdot 10^{-5}$	$6.12 \cdot 10^{-5}$	$1.36 \cdot 10^{-4}$	$2.40 \cdot 10^{-4}$	$3.72 \cdot 10^{-4}$
k=8	$1.10 \cdot 10^{-5}$	$4.37 \cdot 10^{-5}$	$9.73 \cdot 10^{-5}$	$1.71 \cdot 10^{-4}$	$2.65 \cdot 10^{-4}$

Throughout our studies of HIV dynamics, at each point in time, the simulation engine computes the values of the Shannon-Jensen divergence between the initial risk network's univariate/bivariate distributions, and the corresponding distributions from the risk network at the present time. In theory, if *any* of the Shannon-Jensen divergences was found to exceed our set threshold $1.0 \cdot 10^{-4}$, the software was to raise a warning, stop the simulation, and "roll back" the trial all the way to the beginning, so it could try a different (random) evolutionary trajectory. In practice, the Shannon-Jensen divergences for the HIV status variable, the AgeBinned variable (and in some cases, the DegreeBinned variable) were all excluded from the "roll back" criteria, because the distributions of these variables was expected to diverge from the initial distribution. As such, divergences in these distributions could not be interpreted as a degeneracy of the model.

To get a sense of what a threshold of $1.0 \cdot 10^{-4}$ implies, we consult the table above. A uniform distribution over a 2-category variable can be perturbed no more than 3% if it is to stay below the threshold. A uniform distribution over a 4-category variable can be perturbed no more than 6% for it to stay below the threshold. And finally, a uniform distribution over an 8-category variable can be perturbed no more than 9% for it to stay below the threshold.

In practice, we found that roll back was never triggered for networks of any significant size. Initially, when our simulations were of small networks of fewer than 500 nodes, roll back triggers were occasionally observed. In large networks of tens of thousands of nodes, deviations from the sample distributions are small, and rollback criteria are never triggered.

2.2 Dynamism models of evolving risk networks

The model framework developed so far captures (and can be subsequently used to generate) instantaneous snapshots of risk networks. However, in order to support modeling pathogen transmission and evolution of the network structure *over continuous time*, the framework must be extended.

2.2.1 Pathogen dynamics

An individual v's infection status with respect to a pathogen $\mathscr{P}_k$ (for some k in $1, \ldots, p$) may change because v engages in risk behaviors (via relationships in some layer j of the network) with a risk partner w who is afflicted with $\mathscr{P}_k$. We refer to aspects of the framework which speak to such events occur as the *risk process* for pathogen $\mathscr{P}_k$. An exposition of the risk process follows.

The description that follows is from the vantage point of a fixed layer j and time t, but applies to all layers $j = 1, \ldots, l$ at all times $t > 1$. At a given time t, each individual is represented as a node $v \in V^t$ within a network

$$\mathcal{D}^t \stackrel{\text{def}}{=} (x_i^t, V^t, E_j^t, A_k^t, , d_j)_{i=1,\ldots,m;j=1,\ldots,l;k=1,\ldots,p}.$$

The set $N_j^t(v) \subseteq V^t$ represents the potential layer j risk partners for v within the a temporal frame of duration Θ_j, i.e. $N_j^t(v)$ are the potential layer j risk partners of v during the time $[t, t + \Theta_j)$, as known to v at time t.

Each individual v has the propensity to engage in risk acts at layer j of their network, with one of their partners from $N_j^t(v)$. In anticipation of this, when a node v first enters the network, we assign it a propensity for risk activity $t_j^R(v)$. In the current model, this number is assumed to be time-invariant for each individual, and is randomly chosen from the positive reals using a truncated Gaussian (Robert, 1995) with (time-invariant) mean μ_j^R and (time-invariant) standard deviation σ_j^R. This Gaussian distribution was adopted in order to allow for controllable variation (across individuals) in the appetite for risk acts (per network layer j). In the present model, the selection of

$t_j^R(v)$ occurs independently for all individuals v and layers j—however, this need not be the case if data could be obtained on correlations between risk act propensities in different layers of the network.

The quantity $t_j^R(v)/|N_j^t(v)|$ represents the expected time between successive layer j risk impulses *experienced* by v. Statistically speaking, one may say that on average, every $t_j^R(v)$ months, individual v is expected to have engaged in roughly $|N_j^t(v)|$ risk events at layer j. The $2l$ parameters μ_j^R and σ_j^R (for $j = 1, \ldots, l$) are included in the dynamism model.

A risk impulse stream is generated by independent Poisson processes operating at each individual v. To achieve the above characteristics (regarding mean times between impulses) in a memoryless fashion, the time between successive risk impulses follows an exponential distribution with rate $|N_j^t(v)|/t_j^R(v)$. Upon experiencing a layer j risk impulse at time t, node v selects a partner w uniformly at random from its layer j neighbors $N_j^t(v)$, and engages in a mutual layer j risk act.

During a layer j risk act involving v and w, *any* of the pathogens $\mathscr{P}_k$ (for $k = 1, \ldots, p$) may propagate. The likelihood of this is taken to be 0 if both individuals have the same infection status status, i.e. when $v, w \notin A_k^t$ and when $v, w \in A_k^t$. If the individuals are serodiscordant with respect to pathogen $\mathscr{P}_k$, i.e. precisely one of the two individuals is infected then the probability of transmission is modeled using an *infectiousness curve* $I_{j,k}$. For concreteness of exposition, let's assume v is the positive for pathogen $\mathscr{P}_k$. The infectiousness curve $I_{j,k}$ then maps the age of v's infection (with pathogen $\mathscr{P}_k$) to the probability of the pathogen's transmission during a layer j risk act. To support this within the model, it is necessary for the risk network representation to be augmented so as to maintain information about the time when individuals become positive for pathogen $\mathscr{P}_k$. We shall store this information using a set of l functions $t_k^+ : V \to \mathbb{R}$ for ($k = 1, \ldots, p$). This entails an augmentation of the risk network representation (not an augmentation of the structural model).

While it is easy to update t_k^+ during the course of a trajectory, we must also specify the infection times for individuals who are initially created infected, i.e. in the **MakePathogens** procedure (see Listing 3). We do this for each v in V^1 by initializing $t_k^+(v)$ to a value selected uniformly at random from

the interval $[1 - T_k^+, 1]$ of T_k^+ months prior to time 1. The k parameters T_k^+ are included in the dynamism model, as are the lp infectiousness curves $I_{j,k}$ (for $j = 1, \ldots, l$ and $k = 1, \ldots, p$) that capture the time dependencies of transmission risks of pathogen $\mathscr{P}_k$ via layer j risk acts. Typically, the infectiousness curves are stored in parametric form.

The new parameters added to the dynamism model in support of the risk process are summarized in the table below.

Param	Description	Units/Range
μ_j^R	Mean time between inter layer j risk impulses	Months
σ_j^R	Inter layer j risk impulse std. dev.	Months
T_k^+	Age interval for initial $\mathscr{P}_k$ infections.	Months
$I_{j,k}^+$	Infectiousness curve for $\mathscr{P}_k$ via layer j.	Fcn. of age

Consider a $p = 1$ single pathogen scenario in which $\mathscr{P}_1$ is HIV. In the case of HIV, it is well known that HIV infectiousness can be estimated by a function of infection age, decreasing sharply at approximately three months, and remaining at low levels until approximately eight years later (Cates et al., 1997; Kahn & Walker, 1998; Lyles et al., 2007). We use this information to construct a parameterized infectiousness function $I_{j,1}$.

Given that we know the infectiousness drop sharply (for all types $\mathscr{T}_j$ of risk acts) approximately 3 months after the time of initial infection, we approximate the infectiousness curve $I_{j,1}$ by a step function whose value is p_j^H for the 3 month high infectiousness, or "*acute*" phase, and $c_j^{L/H} \cdot p_j^H$ thereafter, in the low infectiousness or "*chronic*" phase. We note here that $c_j^{L/H} \ll 1$. With such a model, if $t - t_1^+(v) \leqslant 3$ then with probability p_j^H individual w acquires HIV from v during the layer j risk act. If, on the other hand, $t - t_1^+(v) > 3$, then the transmission occurs with a much smaller probability $c_j^{L/H} \cdot p_j^H$. In either case, if w acquires HIV during the layer j risk act, then w is added to A_1^t and we set its infection time $t_1^+(w) := t$. To support such a model of HIV pathogen transmission, the $2l$ parameters p_j^H and $c_j^{L/H}$ (for $j = 1, \ldots, l$) are included in the dynamism model.

In practice, the likelihood of infection appears to depend not only on the

age of v's infection, but also on the structural properties of v and w, since agents in the core tend to engage in high risk behaviors more frequently than nodes at the periphery (Curtis et al., 1995; Friedman et al., 2000). This dependency is modeled by the risk intensity parameter which controls how frequently individuals engage in risk acts. The infectiousness curve $I_{j,1}$ captures the probability of transmission *normalized per risk event*.

The new parameters added to the dynamism model in order to capture the various likelihoods of pathogen transmission during a single risk act are summarized in the table below.

Param	Description	Units/Range
p_j^H	Layer j trans. prob. in infectious period	Between 0 and 1
$c_j^{L/H}$	Reduction in trans. prob. post 3 months	Between 0 and 1

2.2.2 Network dynamics

Having developed a dynamism model which supports pathogen dynamics over time, we now turn to the problem of modeling the evolution of network structure over time. To determine how the dynamism model needs to be extended, we must first decide on the types of network dynamism that is to be supported. We have in mind an evolutionary process that is not based purely on global statistical invariants, nor purely on local agency, but rather a combination thereof. Changes in network structure shall be initiated through individual agency, but shall be subject to pressures from global statistical invariants. Below is an initial list of phenomena that we know produce change in the structure of real-world risk networks; these inform our choices subsequently.

1. An individual's risk partnerships may change if and when they decide to abandon an existing risk partner (or when the risk partner decides to abandon them). Social instability due to a significant reduction in

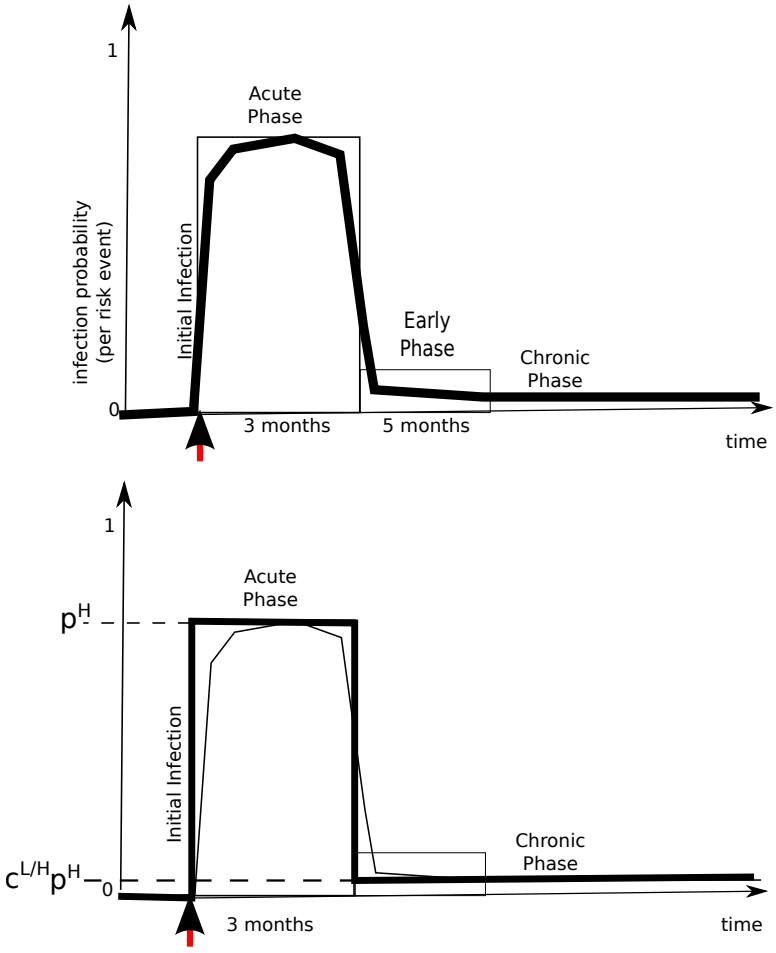

Figure 2.2: (Top) Infectiousness of HIV as a function of age of infection; (Bottom) A two-parameter representation within the model.

the number of risk partners may induce an individual to find new risk partners. We refer to these two events, in conjunction, as comprising the *churn process*; it is the subject of Section 2.2.2.

2. An individual may age over time, and this may alter their risk partner preferences. We refer to this as the *aging process*; it is the subject of Section 2.2.2.

3. The population may change because an individual enters or leaves the risk network. We refer to this as the *population process*; it is the subject of Section 2.2.2.

In what follows, each of the three processes are described. Throughout each of the three sections the narrative is written from the vantage point of a single layer j of the risk network, embodying risk acts of type $\mathscr{T}_j$. However, the reader should bear in mind that the processes described are replicated and operate concurrently at each of the $j = 1, \ldots, l$ layers of the risk network.

The churn process

While the set $N_j^t(v)$ represents the potential layer j risk partners for v at time t, it is possible for individuals to abandon (or be abandoned by) their risk partners over time. Furthermore, social instability due to a loss of layer j risk partners may induce individuals to seek new risk partners to compensate for loss of social context. The central premise of our model concerning partner "churn" is the idea that each individual v has an ideal degree (ego network size in layer j) which remains stable over time.

This premise is reflected in the fact that the ideal degree at layer j is selected using the degree distribution χ_j in line 8 of procedure **MakePopulation** (see Listing 2). Although d_j is permitted to vary over the population, it is assumed to be fixed over time. In effect, we view $d_j(v)$ as the ideal size of v's ego network in layer j, and reflecting v's stable personality. On the other hand, while the ideal degree $d_j(v)$ is assumed fixed over time, the actual membership (and cardinality) of v's layer j risk partners $N_j^t(v)$ is permitted to vary with time.

Each individual v has the propensity to change the membership of $N_j^t(v)$, in an act we refer to as "churn". At creation time, each node v is assigned propensity for churn $t_j^C(v)$. In the current model, this number is assumed to be time-invariant for each individual, and is randomly chosen from the positive reals using a truncated Gaussian (Robert, 1995) with (time invariant) mean μ_j^C and (time invariant) standard deviation σ_j^C. The Gaussian distribution was chosen to model controlled variation (across individuals) in their appetite for churn acts (per network layer j). In the present model, the selection of $t_j^C(v)$ occurs independently, for all individuals v and layers j—however, this need not be the case if data could be obtained on correlations between churn act propensities in different network layers.

The quantity $t_j^C(v)/|N_j^t(v)|$ represents the mean time between successive churn impulses *experienced* by v. Statistically speaking, on average every $t_j^C(v)$ months, individual v is expected to have engaged in $|N_j^t(v)|$ churn events at layer j. The $2l$ parameters μ_j^C and σ_j^C are included in the dynamism model.

The churn impulse stream is generated by independent Poisson processes operating at each individual. To achieve the desired characteristics (regarding mean times between impulses) in a memoryless fashion, the time between successive churn impulses in the Poisson process must follow an exponential distribution with rate $|N_j^t(v)|/t_j^C(v)$. Upon experiencing a layer j churn impulse at time t, node v engages in a Bernoulli trial, responding to the impulse by adding a partner with probability

$$p_{j+}^t(v) \stackrel{\text{def}}{=} \frac{\left(\frac{|N_j^t(v)|+1}{d_j(v)+1}\right)^{w_j^S}}{\left(\frac{|N_j^t(v)|+1}{d_j(v)+1}\right)^{w_j^S}+1}$$

or abandoning an existing partner with probability $p_{j-}^t \stackrel{\text{def}}{=} 1 - p_{j+}^t$. The function $p_{j+}^t(v)$ enjoys the following properties:

- If $|N_j^t(v)| = d_j(v)$, then $p_{j+}^t(v) = p_{j-}^t = 1/2$.
- If $|N_j^t(v)| < d_j(v)$, then $p_{j+}^t(v) > p_{j-}^t$. As the edge deficit $d_j(v) - |N_j^t(v)|$ tends to infinity, $p_{j+}^t(v)$ tends to 1 and p_{j-}^t tends to 0. The rate of this

convergence increases when w_j^S is increased.

- If $|N_j^t(v)| > d_j(v)$, then $p_{j-}^t > p_{j+}^t(v)$. As the surplus $|N_j^t(v)| - d_j(v)|$ tends to infinity, $p_{j+}^t(v)$ tends to 0 and p_{j-}^t tends to 1. The rate of this convergence increases when w_j^S is increased.

The parameter w_j^S is a new addition to the dynamism model. It governs the extent to which individuals are willing to tolerate deviations from their ideal degree at layer j, before feeling compelled to take compensatory action by adding or abandoning partners. If the Bernoulli trial due to a churn impulse at v triggers abandonment of a risk partner, the partner to be abandoned is selected uniformly at random from $N_j^t(v)$. If the Bernoulli trial triggers adding a partner, the new partner is selected by the procedure **AddEdge** (see Listing 6), which is identical to procedure **MakeEdge** except for 3 key differences:

1. The set of candidate new risk partners $C_j^t(v)$ includes *all* individuals who are not already partners of v;

2. The propensity of each candidate c in $C_j^t(v)$ is biased by the deviation between c's ideal and actual degrees, as captured by $p_{j+}^t(c)$, which is precisely c's probability of adding a new edge in response to its own churn events.

3. The propensity of each candidate c in $C_j^t(v)$ is also biased by the number of triangles (at layer j) that would be created by the addition of edge (v, c), weighted by a constant scalar factor $w_j^\Delta - 1$. This introduces a controlled mechanism for the influence of transitivity (i.e. triadic closure).

4. Procedure **AddEdge** does not reschedule itself to be called again, the way that **MakeEdge** does.

The $4l$ parameters added to the dynamism model in support of the churn process are summarized in the table below.

Listing 6: procedure **AddEdge**; compare with Listing 5 p. 49.

Input: individual v, layer j, time t

// Determine candidate new neighbors for v.

$C_j^t(v) := V_j^t \backslash (N_j^t(v) \cup \{v\})$.

if $|C_j^t(v)| > 0$ **then**

  foreach c *in* $C_j^t(v)$ **do**

    Compute the degree-based affinity of v and c using the bivariate degree distribution $\bar{\bar{\chi}}_j^t$:

$$a_\chi^t(v,c) := \bar{\bar{\chi}}_j(|N_j^t(v)| - \epsilon, |N_j^t(v)| + \epsilon, |N_j^t(c)| - \epsilon, |N_j^t(c)| + \epsilon).$$

    Compute the attribute-based affinity of v and c using the bivariate attribute distributions $\beta_{i,j}$:

$$a_\alpha^t(c) := \prod_{i=1}^{m} \beta_{i,j}(x_i(v), x_i(c)).$$

    Compute $\Delta_j^t(v,c)$, the number of layer j triangles which would be formed if (v,c) was added as a layer j edge.

    Compute propensity of edge (v,c) ;

$$\omega_j^t(c) := (w_j^\Delta - 1)\Delta_j^t(v,c) \cdot p_{j+}^t(c) \cdot a_\chi^t(c) \cdot a_\alpha^t(c).$$

    Normalize propensity to obtain a distribution over $C_j^t(v)$:

$$p_j^t(c) := \frac{\omega_j^t(c)}{\sum_{c' \in C_j^t(v)} \omega_j^t(c')}.$$

  $w :=$ choose from $C_j^t(v)$ randomly according to distribution p_j^t.

  // Add the layer j edge connecting v to w.

  $N_j^t(v) := N(_j^t v) \cup \{(v,w)\}$

  $N_j^t(w) := N_j^t(w) \cup \{(w,v)\}$

Param	Description	Units/Range
μ_j^C	Layer j churn interval mean	Months
σ_j^C	Layer j churn interval std. dev.	Months
w_j^S	Layer j degree stability bias	Positive real
w_j^Δ	Layer j triangle bias	Positive real

The population process

The population of the risk network is controlled at both aggregate-level and individual-level processes. We refer to these respectively as macroscopic and microscopic controls; each is treated separately below.

Macroscopic population controls To support population growth/decline over time, we extend the dynamism model to include a new parameter r_p which captures the growth/decline of the population every 10 years (120 months). Taking $r_p = 100$, for example, specifies that the population should doubles every decade. Taking $r_p = -25$, on the other hand, specifies that a quarter of the population is lost every ten years. The parameter r_p is a new addition to the dynamism model.

Suppose the initial population is n_1, and the population at time t is n_t. If $r_p > 0$, the population process operates monthly (by acting at each integer time t months). To cause the creation of

$$V^+ \stackrel{\text{def}}{=} (1 + r_p)^{1/120} n_1 - n_t$$

new individuals in the one month interval $(t, t + 1]$, the population process schedules the creation of $\lfloor V^+ \rfloor$ individuals at times uniformly randomly chosen from $(t, t + 1]$, and then with probability $V^+ - \lfloor V^+ \rfloor$, it schedules the creation of 1 addition individual randomly in that same time interval. In this manner, the expected number of new individuals that are introduced during the interval $(t, t + 1]$ is exactly V^+.

If $r_p < 0$, the population process operates monthly (by acting at each integer

time t months). To cause the removal of

$$V^- \stackrel{\text{def}}{=} n_t - (1 - r_p)^{1/120} n_1$$

existing individuals in the one month interval $(t, t+1]$, the population process schedules the removal of $\lfloor V^- \rfloor$ individuals at times uniformly randomly chosen from $(t, t+1]$, and then with probability $V^- - \lfloor V^- \rfloor$, it schedules the removal of 1 addition individual in that same time interval. In this manner, the expected number of existing individuals that are removed during the interval $(t, t+1]$ is exactly V^-.

Microscopic population controls In addition to the macroscopic trends in population represented by the r_p parameter, we have individual agency of nodes that drives them to leave the network. Each node v has an associated "lifetime" within the risk network, which we denote by $L(v)$ months. The value of $L(v)$ is set when node v is created (enters the risk network). The value is selected by randomly drawing a positive real from a truncated distribution (Robert, 1995) that is the weighted sum of two Gaussians:

$$pdf(L(v) = x) = f_{tr} e^{-\sigma_{tr}(x-\mu_{tr})^2} + (1 - f_{tr}) e^{-\sigma_{st}(x-\mu_{st})^2}$$

In effect, this bimodal distribution is used to model a population consisting of two types of nodes: **transient** nodes, which occur with relative frequency f_{tr}, and **steady** nodes, which occur with relative frequency $1 - f_{tr}$. Transient nodes have lifetimes which are derived from a Gaussian distribution with mean μ_{tr} and standard deviation σ_{tr}, while steady nodes have lifetimes which are derived from a Gaussian distribution with mean μ_{st} and standard deviation σ_{st}. Typically, $\mu_{st} \gg \mu_{tr}$. Each individual v removes themselves from all layers of the network at time $b(v) + L(v)$; they will be replaced if mandated by the macroscopic population process described previously. The parameters $\mu_{tr}, \sigma_{tr}, \mu_{st}, \sigma_{st}$ are assumed to be time-invariant, and are new additions to the dynamism model .

The 6 parameters added to the dynamism model in support of the macroscopic and microscopic aspects of the population process are summarized in the table that follows.

Param	Description	Units/Range
r_p	Population growth rate every 10 years	Percentage (real)
f_{tr}	Fraction that are "transient"	Between 0 and 1
μ_{tr}	Mean duration of transients' lifetimes	Months
σ_{tr}	Std. dev. of transients' lifetimes	Months
μ_{st}	Mean duration of steadies' lifetimes	Months
σ_{st}	Std. dev. of steadies' lifetimes	Months

The aging process

Each individual, when created, is assigned values for attributes x_i (for $i = 1, \ldots, m$) by random sampling from the corresponding distribution α_i. Of these attributes, some may be time dependent. In particular, if one of the x_i variables represents categorical age, then it would be incorrect for the model to assume that an individual remains the same age over the course of the network trajectory. The resulting inaccuracy is of potential consequence, since age plays a role in edge formation when the corresponding bivariate distributions $\beta_{i,j}$ contribute to the propensities of layer j edges being created in the course of a network's evolution. It is therefore important to update age-related x_i attributes over time, so that they accurately change as time passes. A subtle consequence of needing to support the aging process is that the birth time $b(v)$ needs to be maintained for all individuals v. Let us see how this will be achieved.

We explain how aging would be implemented via a concrete example. Suppose x_3 is a time-dependent variable, e.g. AgeBinned, which identifies the 5-year interval in which the individual's age lies. Clearly, each individual's x_3 values must transition into higher bins once roughly every 60 months for the network to remain a faithful to the physical system it purports to represent. How might we achieve this? Recall that when a node was first created, its x_3 attribute (AgeBinned) was selected with reference to model attribute distribution α_3; suppose for instance $x_3(v) = [A, A + 5)$ for some integer A representing age in years. We augment the node creation process so that once x_3 is selected, we select the precise birth time $b(v)$, by choosing uniformly at

random from the interval

$$[t - 12A, t - 12(A + 5)].$$

We must store this information on birth times using a function $b^t : V \to \mathbb{R}$. This entails an augmentation of the risk network representation (not an augmentation of the structural model).

During the simulation trajectory, we implement the aging process by the procedure **Aging** (see Listing 7). This procedure is first scheduled for time $T = 1$, and is then reschedules itself to be executed successively at each integer times $T > 1$. Note that the procedure in Listing 7 is written with the assumption that x_3 is time dependent, and is quantized in 5-year intervals. Of course, if other attributes are time dependent or have different quantization, then analogous update procedures must be instantiated for them as appropriate.

Listing 7: Procedure **Aging**.

```
   Input: current time T
1  foreach v in V do
2      if (t − b(v))/12 ∉ x3(v) then
3          Increment the value of x3(v) to be the next higher age bin.
4  Schedule Aging(vi) to take place again at time T + 1.
```

2.3 The general framework

The result of this chapter is a general framework for network modeling. It takes as inputs a list of important node attributes which are determined externally to the model to have significant effect on the interaction of model actors. It also allows for the specification of intra-node transaction, in this case in the form of the passing of pathogens. With this framework, large numbers of network actors can be produced according distributions of actor attributes drawn from the analysis of real world networks—indeed many more actors can be produced than were actually involved in the the study

upon which the model is built, allowing the simulation to proceed at scales unreachable by direct research.

In the general form of the framework, a variety of "actor types" can be included, whose behavioral profile (like their attribute profile) can be varied from other actor types. Network actors may also draw from a range of behavior distributions to determine their own interaction profile. From this profile they gather and change partners, engage in risk events, and recover their own pattern of connectivity after perturbations caused by the actions of other actors.

Additionally, attributes (like age, or pathogen dynamics) can be made time dependent. The framework supports growing and shrinking networks, and include actor-specific participation regimes/distributions, such that networks are not simply dynamic, but can also feature participants entering and leaving the realm of network participation. This feature is a key element in moving beyond "closed network" assumptions that too often impede network modeling.

All of these features aim to take advantage of the actor-based nature of the framework—allowing maximum agency at the level of network actors while leaving the possible overall network topology to emerge from the aggregate of these behaviors. As discussed above, such a strategy necessarily raises questions of model degeneracy. In maximizing node-level agency, the risk of network-wide variation is inevitable—it can be monitored but not prevented. The framework presented takes step to do just that, by quantifying the extent of risk network variation over time. Within simulations, this permits us to monitor network divergence across their histories, and if needed "roll back" highly divergent networks (to a prior simulation stage) before allowing them to proceed once more. Such conditions are the outcome of choices that favor local-scale constraints over network-scale constraints.

Chapter 3

Models of real HIV risk networks

3.1 The SFHR and P90 surveys

Having developed a general framework for dynamic network modeling, our next step is to implement a particular set of simulation parameters within the framework. Our main concern in this chapter is to specify how the SFHR data was fit to the general framework, including distributions of both actor attributes (the "structural model") and inter-actor dynamics (the "dynamism model"). Secondarily, we discuss the distributions used to model the P90 data as well. We note here, however, that our main concern in the bulk of this report is with producing a dynamic model that fits best with the SFHR data. The reasons for this are several. The first is that the regional-basis of the SFHR data—the greater New York area—contained a well-documented example HIV-rate sub-saturation stabilization, as well as the necessary topological data from which to produce a dynamic network model. Second, and perhaps most importantly, project co-PI Ric Curtis served as lead ethnographer on the SFHR project, allowing us to draw on a wealth of personal experience and professional expertise that was not available for other data sets.

3.1.1 The Social Factors and HIV Risk (SFHR) study

The SFHR study produced a wealth of landmark data on network substructures, and their relationship to HIV/infection transmission (Friedman, Curtis, Neaigus, Jose, & Jarlais, 2010). Conducted between 1990 and 1993, SFHR was a cross-sectional, mixed methods project that asked 767 out-of-treatment IDUs about their risk networks and HIV risk behaviors in the prior 30 days. Interested in both individuals' network composition (namely, the presence of high-risk partners) and sociometric risk position, the SFHR study produced several major findings relevant to risk populations with high HIV prevalence and low secondary incidence (Friedman et al., 1998, 2007; Goldstein et al., 1995; Des Jarlais et al., 1998; Jose et al., 1993; Kottiri, Friedman, Neaigus, Curtis, & Des Jarlais, 2002; Neaigus et al., 1994, 1995). SFHR documented 92 connected components among 767 subjects, including a 105-member 2-core within a large connected component of 230 individuals. With subjects located within the 2-core more likely to be infected with HIV (Friedman et al., 1997), the study emphasized the importance of HIV prevention within densely-connected network components (a point illustrated in the opposite manner by Project 90).

SFHR also characterized the salience of personal network composition with regards to ethnicity. While membership in the 2-core was roughly the same across ethnic groups, SFHR documented significantly higher rates of HIV infection among African-American and Hispanic subjects. Authors ultimately tied elevated HIV prevalence in these groups to homophily in edge formation by ethnicity (Friedman et al., 1997). Writing that HIV spread more rapidly among African American and Hispanic individuals in the earliest stages of the epidemic, SFHR reasoned that the tendency among study subjects to form ethnically homogeneous networks accelerated HIV infection within existing high prevalence groups (Kottiri et al., 2002).

The SFHR study collected baseline information on the demographic traits, risk behaviors, and risk network of 767 subjects, additionally documenting 662 edges within the network. All SFHR subjects and their mutual connections were included in this re-analysis, and the original coding of subject attributes was retained for use as partition data in the ERGM analysis.

3.1.2 The Project 90 study

Conducted between 1988 and 1992 in Colorado Springs, Project 90 was a prospective study of heterosexual subjects who were defined as being at "high-risk" for STI/HIV infection (Potterat et al., 2002, 1994). Eligible subjects reported at least one of the following behaviors in the past 12 months: exchanging sex for money or drugs, sex (paying or non-paying) with a prostitute, injection of illicit drugs, or sex with an injection drug user. Unlike the cross-sectional SFHR, the Project 90 study followed its subjects for up to 5 years, with no requirement for year-to-year continuity; new subjects were additionally recruited each year. 595 enrolled individuals produced 1091 interviews, which named 8,164 network contacts overall. The multitude of papers arising from the Project 90 study linked the low prevalence and incidence of HIV in Colorado Springs to the relative dearth of HIV positive individuals in the densely-connected network core (Klovdahl et al., 1994; Potterat et al., 2002; Potterat, Rothenberg, & Muth, 1999; Potterat et al., 1993; Rothenberg, Potterat, & Woodhouse, 1996; Woodhouse et al., 1995, 1994). While 36 subjects in the cumulative study population (including reported contacts) were HIV positive, only 16 were located within the large connected component of the network linking 7,151 individuals, and they occupied peripheral positions therein; no HIV-positive individuals were found within the 3-core of the largest connected component— the "heart of the risk network" (Potterat et al., 2002, p.103). Although Project 90 revealed a densely-connected network of individuals involved in high-risk behaviors, it simultaneously spoke to the importance of network centrality for infected individuals in predicting the epidemic spread of HIV.

While Project 90 collected similar demographic data to SFHR, we note that all P90 variables were recoded for concordance with SFHR. In addition, not all subjects in the Project 90 data set were included in this analysis. P90 subjects eligible for inclusion in our analysis included those who satisfied the following four conditions: (1) received an HIV test during the original study, (2) completed at least one survey during the study period, (3) reported IDU activity in the past 6 months at the time of the interview, and (4) were linked to at least one other study subject who also met criteria 1-3. Applying these criteria allowed us to extract the "IDU core" from the P90 network. By doing this, we would be comparing the epidemiological properties of two

functionally equivalent risk networks that differed only in the social context in which they were found. In the end, this re-analysis included 569 vertices and 272 edges from the original Project 90 data set. All future references to the "P90 network" should be read as references to this restricted data set.

3.2 Selecting influential node attributes

In the analysis used to determine the relative importance of attribute and structural data to the dynamic model, special attention is paid to homophily and transitive closure. Homophily is the tendency of "like" nodes to connect with one another—in this case as variable that measure the extent to which racial/ethnic, age, or gender "sameness" (or "differentness") affects the likelihood of there being a connection among two randomly chosen nodes (individuals) in the network (above a level expected by simple random mixing). In addition, we also investigate the extent to which network importance—in this case as indicated by self-estimated total number of injection partners-displays homophilous tendencies as well.

Beyond homophily in gender, age, race/ethnicity and number of needle partners, another significant variable traced here is transitive closure, also known as network transitivity (Goodreau et al., 2009). Transitive closure in this sense is the tendency of two nodes (or people) to share a connection with one another given their simultaneous mutual connection to a third node, independent of other considerations (such as homophily of degree or some other attribute). Transitive closure is defined as the tendency for A to form a connection with C, given their mutual connection with B (over and above the likelihood of that connection existing via random mixing).

We begin by using ERGM analysis to determine influential node attributes. The process is carried out in 3 stages. First, we isolate each variable and test its influence on the formation of connections, given the total size and density of the network. Then, we determine the extent to which the various homophilies discovered in step 1 may be due to differences in the average level of connectedness of any one of the subgroups within each attribute class. Finally, a set of composite models are tested to determine the relative

importance of each attribute versus transitive closure, and a full model of all variables is produced to indicate the relative importance of all variables relative to one another.

3.2.1 Isolating variables

In the tables below, a number of models are presented. In the first set of analyses (Table 3.1 & 3.2), ERGM analysis was used to obtain an initial "edges" measure. The value of the "edges" measure represents the log odds that a randomly chose pair of nodes in the network will have a connection between them based only on the total number of connections in the network. Such a statistic provides a base-line measure against which the influence of the other "tested" variables can be determined. In each subsequent model, the edges measure is tested in bi-variate mode with another single variable (age, gender, race/ethnicity, number of partners, and transitive closure) to determine the extent to which homophily variables (for age, race/ethnicity, gender and number of needle partners) and network considerations (transitive closure) influence edge formation over and above that expected when only the density of the graph is considered. In these bivariate cases, the edges variable is expected to diminish in those cases where the additional variable exerts significant influence on the pattern of connectivity. Thus, in each model, one first examines the base line, "edges" value and compares the subsequent variable value θ to determine the relative influence of the identified variable.

Several observations can be made from the above data.

- Both Table 3.1 & 3.2 show transitive closure to be the most significant factor, when taken in isolation, in determining the given patterns of edge formation. Put another way, in comparison with the other variables considered individually, structural features trumped attribute features in determining the patterns of connection seen in both the SFHR and P90 networks.
- For P90, homophily across self-identified number of needle partners proved more important than other forms of homophily. Homophily among self-proclaimed number of injection partners was also significant

(Individual Variable Results for SFHR)

Variable Name	Edges Value	θ	Error	p-value
Edges	-6.343		0.044	***
Transitive closure	-6.257	3.422	0.076	***
Gender homophily (all)	-6.520	0.286	0.092	**
Gender (male)	"	0.257	0.096	**
Gender (female)	"	0.439	0.111	**
Race/Ethnic homophily (all)	-7.044	1.394	0.094	***
R / E (Black)	"	1.043	0.120	***
R / E (Hispanic)	"	1.801	0.122	***
R / E (White)	"	1.513	0.121	***
R / E (Other)	"	-Inf	NA	NA
Age homophily (all)	-6.43338	0.382	0.099	***
Age (15-19)	"	3.794	1.036	***
Age (20-24)	"	0.229	1.002	0.819
Age (25-29)	"	0.306	0.199	0.125
Age (30-34)	"	0.478	0.170	**
Age (35-39)	"	0.341	0.160	*
Age (40-44)	"	0.329	0.196	0.093
Age (45-49)	"	0.904	1.003	0.368
Age (50-54)	"	1.934	1.007	0.055
Age (55-59)	"	-Inf	NA	NA
Age (60+)	"	-Inf	NA	NA
# Needle Partners last 30 days homophily (all)	-6.457	0.418	0.094	***
0 partners	"	1.348	0.504	**
1 partners	"	0.276	0.106	**
2 partners	"	0.731	0.204	***
3 partners	"	1.155	0.321	***
4+ partners	"	2.418	0.508	***

Showing the effects of individual variables on the likelihood of an edge between a randomly chosen pair of vertices, in log odds form.
*** ($p<0.001$) ** ($p<0.01$) * ($p<0.01$)

Table 3.1: ERGM Analysis Step 1 for P90

(Individual Variable Results for P90)

Variable Name	Edges	θ	Error	p-value
Edges	-4.668		0.037	***
Transitive closure	-5.000	1.673	0.036	***
Gender homophily (all)	-4.701	0.082	0.075	0.274
Gender (male)	"	-0.877	0.140	***
Gender (female)	"	0.54091	0.080	***
Race/Ethnic homophily (all)	-4.99091	0.750	0.074	***
R / E (Black / AA)	"	0.585	0.080	***
R / E (Hispanic)	"	1.509	0.122	***
R / E (White)	"	0.909	0.221	***
R / E (Other)	"	1.612	0.590	**
Age homophily (all)	-4.77483	0.582	0.088	***
Age (15-19)	"	1.278	0.509	*
Age (20-24)	"	0.767	0.173	***
Age (25-29)	"	0.671	0.139	***
Age (30-34)	"	0.343	0.156	*
Age (35-39)	"	0.337	0.241	0.161
Age (40-44)	"	1.137	0.340	***
Age (45-49)	"	-Inf	NA	NA
Age (50-54)	"	-Inf	NA	NA
Age (55-59)	"	-Inf	NA	NA
Age (60+)	"	-Inf	NA	NA
Needle Partners last 5 years homophily (all)	-5.066	1.053	0.074	***
0 partners	"	1.070	0.076	***
1 partner	"	0.574	0.322	0.075
2-3 partners	"	0.792	0.284	**
4-6 partners	"	1.162	0.455	*
6 or more partners	"	1.314	0.251	***

Showing the effects of individual variables on the likelihood of an edge between a randomly chosen pair of vertices, in log odds form.
*** ($p<0.001$) ** ($p<0.01$) * ($p<0.01$)

Table 3.2: ERGM Analysis Step 1 for P90

among network members in the SFHR network, though it was of less importance there than race/ethnicity. In both cases, the highest level of homophily in number of needle partners was seen among particular subcategories, i.e. those with higher numbers of partners—3 or more partners in the SFHR network; 4 or more partners in the P90 network. Homophily levels among those with lower numbers of self-identified partners were much lower.

- Gender homophily was not significant in the P90 data, though the overall nature of the measure in the aggregate may have masked an important feature of the network. In the Colorado Springs data, men and women showed robust but opposite trends. Men showed significant ($p < 0.001$) negative homophily (sometimes called heterophily) in their risk relationships—perhaps indicating that, as far as gender is concerned, heterosexual sex was the main risk relationship governing connectivity trends. Women in the same data set, on the other hand, showed a lower but equally robust trend to homophily (also $p < 0.001$). The same was not true in the SFHR network where both genders showed positive trends toward homophily, though here too women showed a stronger trend to mutual association in their risk relationships than men.

- Age homophily was significant in both networks, though in both cases it applied only narrowly across age subcategories. The overall effect, though, was a significant if somewhat less important source of connectivity dynamics than either race or structural considerations.

3.2.2 Adjusting for connectedness

To determine whether the homophily results shown in Tables 3.1 & 3.2 were the result of attribute homophily rather than degree homophily, a further set of analyses were conducted (Tables 3.3 & 3.4). Such tests are necessary where potential differences in average degree across attribute subcategories can appear as tendencies to mutual affiliation. For example, in a network where the average number of network connections of women was twice that of men, a random distribution of edges that followed the degree patterns

would result in many more connections between women than between men, even where the number of men and women were the same, and even where no actual preference for same-gender affiliation was present.

So for purposes of determining whether differences in average degree by sub-category figured importantly in the distribution of connections, ERGM analysis was used to determine the probability of an edge appearing between two randomly selected nodes where either one of the nodes was a member of the sub-category in question. Thus Table 3.3, line 1 shows that the likelihood of a randomly chosen connection will have a node identified as male as one of its end points. In this case the value of $e^{-3.16}$ in line 1 can be compared with the value for women, $e^{-3.20}$ in line 2, to see that gender sub-category has little effect on the likelihood of being incident to a connection. In such a case, the gender homophily for the SFHR network (in the corresponding Table 3.1) can be seen as largely the result of gender assortment preferences, and not the result of markedly different levels of connection between men and women.

Put more generally, similar values for exponents across those same categories do not play a significant role in explaining the homophily scores identified in Tables 3.1 & 3.2. Table 3.3 & 3.4 list the result of such tests for all attributes tested for homophily above, with the exception of self-proclaimed number of needle partners, which is already associated with network degree in both networks.

- The results of these analyses indicate that for the SFHR network (Table 3.3), degree considerations do not play a major role in any of the attribute homophily trends seen in Table 3.1. Large differences in the θ value for attribute subcategories in Table 3.3 are rare, appearing mainly at the lowest and highest age brackets, and accompanied there by relatively large error scores.

- In the P90 network, noticeable differences appear between genders ($\theta = -3.08$ for men; $\theta = -2.52$ for women). Such a score indicates that women are $e^{-2.52-(-3.08)}e^{0.56} = 1.75$ more likely to be part of a dyad because of differences in average degree than are men. Given that this exponent is roughly equivalent to the homophily exponent for

(Degree-based Homophily Comparison Results for SFHR)

Variable Subcategory	θ	Error	p-value
Gender (male)	-3.160	0.030	***
Gender (female)	-3.198	0.054	***
Age (15-19)	-3.469	0.408	***
Age (20-24)	-3.323	0.163	***
Age (25-29)	-3.213	0.067	***
Age (30-34)	-3.039	0.058	***
Age (35-39)	-3.093	0.055	***
Age (40-44)	-3.312	0.070	***
Age (45-49)	-3.308	0.191	***
Age (50-54)	-3.335	0.249	***
Age (55-59)	-3.757	0.577	***
Age (60+)	-3.467	1.001	***
R / E (Black / AA)	-2.848	0.277	***
R / E (Hispanic)	-3.049	0.052	***
R / E (White)	-3.144	0.050	***
R / E (Other)	-3.295	0.047	***

Showing the effects of individual variables on the likelihood of a randomly chosen vertex having at least one edge, in log odds form. Similar values indicate that there is little difference in mean degree of variable sub-categories.
*** ($p<0.001$)

Table 3.3: ERGM Analysis Step 2 for SFHR

(Degree-based Homophily Comparison Results for P90)

Variable Subcategory	θ	Error	p-value
Gender (male)	-3.084	0.043	***
Gender (female)	-2.521	0.031	***
Race/Ethnicity (Black / AA)	-2.780	0.032	***
Race/Ethnicity (Hispanic)	-2.536	0.051	***
Race/Ethnicity (White)	-3.047	0.080	***
Race/Ethnicity (Other)	-2.916	0.146	***
Age (15-19)	-2.756	0.123	***
Age (20-24)	-2.768	0.063	***
Age (25-29)	-2.591	0.049	***
Age (30-34)	-2.810	0.054	***
Age (35-39)	-2.746	0.066	***
Age (40-44)	-3.029	0.111	***
Age (45-49)	-3.470	0.291	***
Age (50-54)	-2.723	0.177	***
Age (55-59)	-3.883	0.503	***
Age (60+)	-2.971	0.282	***

Showing the effects of individual variables on the likelihood of a randomly chosen vertex having at least one edge, in log odds form. Similar values indicate that there is little difference in mean degree of variable sub-categories.
*** ($p<0.001$)

Table 3.4: ERGM Analysis Step 2 for P90

women in the P90 network in Table 3.2, it is likely that a considerable amount of the homophily between women may be due to differences in average degree rather than tendencies for women to engage in risk relationships with one another (at a higher rate than predicted by random assortment, and at a higher rate than their male network counterparts).

- Similar differences exist among a small number of age categories in the P90 data as well. Such differences are difficult to quantify across a large number of subcategories, but a comparison of these subcategories with their exponents given in Table 3.2 indicates that all of the divergent values (Age 45-49, Age 55-59) appear in subcategories whose internal connectedness was too low to compute meaningful homophily scores (as indicated in Table 3.2 by the $-inf$ value of θ).

3.2.3 Composite models

Given the results above, several larger multivariate models were tested to determine the effect of various model parameters on one another, and to get a better understanding of the relative importance of network (transitive closure) versus node-based (homophily across personal attributes) factors in both networks. These results are available in Table 3.5 & 3.6. In both cases, four models were tested. In the first three, transitive closure was tested against the influence of age-based, gender-based, and race/ethnicity-based homophily. In the final model (4), a composite of transitive closure, self-estimated number of needle partners, and the three attributes from models 1-3 was tested.

- As in Tables 3.1 & b, Transitive closure continues to show far greater exponent values than any other variable. This is true for both the SFHR and P90 data sets, with the greater differences seen in the SFHR network. Given that the values given in Tables 3.5 & 3.6 represent log odds, they can be interpreted to indicate that, for example, model 4 in Table 3.5 shows that transitive closure is:
  - $e^{3.592-0.367} = e^{3.225} \approx 25$ times more important than age,

(Multivariate Models for SFHR)

Model	Variables	Edges	θ	Error	p-value
1	Transitive closure	-6.976	4.902	0.076	***
	Age homophily	"	0.821	0.103	***
2	Transitive closure	-6.917	4.306	0.076	***
	Gender homophily	"	0.277	0.096	**
3	Transitive closure	-7.390	3.715	0.000	***
	Race / Ethnicity homophily	"	0.843	0.006	***
4	Transitive closure	-7.583	3.592	0.020	***
	Age homophily	"	0.367	0.115	**
	Gender homophily	"	0.058	0.102	0.566
	Race / Ethnicity homophily	"	1.205	0.098	***
	Needle Partner homophily	"	0.460	0.104	***

*** (p<0.001) ** (p<0.01) * (p<0.01)

Table 3.5: ERGM Analysis Step 3 for SFHR

(Multivariate Models for P90)

Model	Variables	Edges	θ	Error	p-value
1	Transitive closure	-5.517	2.501	0.036	***
	Age homophily	"	-0.101	0.095	0.290
2	Transitive closure	-4.845	1.740	0.037	***
	Gender homophily	"	-0.145	0.083	0.081
3	Transitive closure	-5.170	1.710	0.037	***
	Race / Ethnicity homophily	"	0.659	0.319	***
4	Transitive closure	-5.438	1.375	0.000	***
	Age homophily	"	0.458	0.001	***
	Gender homophily	"	-0.360	0.000	***
	Race / Ethnicity homophily	"	0.614	0.001	***
	Needle Partner homophily	"	0.574	0.000	***

*** ($p<0.001$) ** ($p<0.01$) * ($p<0.01$)

Table 3.6: ERGM Analysis Step 3 for P90

  - $e^{3.592-1.205} = e^{2.387} \approx 11$ times more important than race/ethnicity, and
  - $e^{3.592-0.460} = e^{3.132} \approx 23$ times more important than the number of recent needle partners, in determining the likelihood of individual connection choices.

- Similar, though smaller differences can be seen in Table 3.6, model 4. There, structural features (i.e. transitive closure) are:

  - $e^{1.375-0.458} = e^{0.917} \approx 2.5$ times more important than age,
  - $e^{1.375-0.360} = e^{2.387} \approx 2.8$ times more important than gender,
  - $e^{1.375-0.614} = e^{0.761} \approx 2.1$ times more important than race/ethnicity, and
  - $e^{1.375-0.574} = e^{0.801} \approx 2.2$ times more important than the number of recent needle partners, in determining the likelihood of individual connection choices.

- In the SFHR network, race/ethnicity remained the second most important factor in determining node connection patterns. This was true for the P90 network as well, though here the differences with other attributes were less.

- Interestingly, gender dropped out of significance in the SFHR network (Table 3.5, model 4), indicating that its significance in Table 3.1 was likely masked a more significant co-variation relationship with one of the other attributes. The opposite was true for the P90 network. Here gender was not statistically significant in Table 3.2, but is (at the $p < 0.001$ level) in Table 3.6. As discussed above, this is perhaps due to the greater number of men in the network than women, and possibly due to the fact that the positive homophily shown for women in Table 3.1 was a mask for degree considerations (as indicated in Table 3.4)—a covariation relationship (with needle partners) that was uncovered in the multivariate analysis.

3.3 Structural model of the SFHR network

The data from the SFHR study (Friedman et al., 2010) yielded were $n = |V| = 767$ individuals, with $|E| = 662$ links connecting them. Of the questions asked of each individual ERGM analysis (see Section 3.2, p. 72) showed that only $k = 4$ properties were found to significantly influence edge formation. These were:

x_i : Name	Possible values (U_i)
x_1 : Gender	{Male, Female}
x_2 : Ethnicity	{White, Hispanic, African-American, Other}
x_3 : AgeBinned	{[15-20), [20-25), [25-30), [30-35),[35-40), [40-45), [45-50), [50-55)}
x_4 : DegreeBinned	{[0-2), [2-4), [4-10), [10-20)}

HIV prevalence p_1 was found to be 39%.

3.3.1 Univariate distributions

The tables below provide the univariate distributions of the above four variables derived from the sample ($N = 767$).

The univariate distribution of the Gender variable for the SFHR node set:

	Male	Female
α_1	540/767	227/767

The univariate distribution of the Ethnicity variable for the SFHR node set:

	White	Hispanic	African-American	Other
α_2	243/767	206/767	311/767	7/767

The univariate distribution of the AgeBinned variable for the SFHR node set:

	[15-20)	[20-25)	[25-30)	[30-35)	[35-40)	[40-45)	[45-50)	[50-55)
α_3	6/767	32/767	158/767	172/767	198/767	159/767	23/767	19/767

The univariate degree distribution χ is already treated separately in the model (see p.45), so it does not need to be considered as one of the univariate node attributes x_i. The univariate distribution of the DegreeBinned variable for the SFHR node set was:

	[0-2)	[2-4)	[4-10)	[10-20)
χ	322/767	221/767	161/767	63/767

3.3.2 Bivariate distributions

The tables below provide the univariate distributions of the above four variables derived from the sample ($N = 662$).

The bivariate distribution of the Gender variable for the SFHR edge set:

β_1	Male	Female
Male	94/145	51/145
Female	76/127	51/127

The bivariate distribution of the Ethnicity variable for the SFHR edge set:

β_2	White	Hispanic	African-American	Other
White	115/178	18/178	43/178	2/178
Black	11/157	112/157	31/157	3/157
Hispanic	32/175	25/175	117/175	1/175
Other	2/7	4/7	1/7	0

The bivariate distribution of the AgeBinned variable for the SFHR edge set:

β_3	[15-20)	[20-25)	[25-30)	[30-35)	[35-40)	[40-45)	[45-50)	[50-55)
[15-20)	1/4	1/4	2/4	0	0	0	0	0
[20-25)	1/26	1/26	7/26	6/26	7/26	3/26	1/26	0
[25-30)	1/147	8/147	41/147	45/147	38/147	12/147	2/147	0
[30-35)	0	5/153	33/153	50/153	43/153	16/153	5/153	1/153
[35-40)	0	4/161	20/161	41/161	56/161	29/161	6/161	5/161
[40-45)	0	2/137	14/137	27/137	44/137	40/137	3/137	7/137
[45-50)	0	0	2/20	6/20	6/20	4/20	2/20	0
[50-55)	0	0	0	2/14	6/14	4/14	0	2/14

The bivariate degree distribution $\bar{\bar{\chi}}$ is already treated separately in the model (see p.45), so it does not need to be considered as one of the bivariate node attributes β_i. The bivariate distribution of the DegreeBinned variable for the SFHR edge set:

$\bar{\bar{\chi}}$	[0-2)	[2-4)	[4-10)	[10-20)
[0-2)	77/158	37/158	29/158	15/158
[2-4)	57/203	77/203	40/203	29/203
[4-10)	42/195	50/195	64/195	39/195
[10-20)	15/100	23/100	31/100	31/100

3.4 Structural model of the P90 network

The data from the P90 study (Potterat et al., 2002, 1994) yielded were $n = |V| = 569$ individuals, with $|E| = 272$ links connecting them. Of the questions asked of each individual ERGM analysis (see Section 3.2, p. 72) showed that only $k = 4$ properties were found to significantly influence edge formation. These were:

x_i : Name	Possible values (U_i)
x_1 : Gender	{Male, Female}
x_2 : Ethnicity	{White, Hispanic, African-American, Other}
x_3 : AgeBinned	{[15-20), [20-25), [25-30), [30-35),[35-40), [40-45), [45-50), [50-55)}
x_4 : DegreeBinned	{[0-2), [2-4), [4-10), [10-20)}

HIV prevalence p_1 was found to be 3.5%.

3.4.1 Univariate distributions

The tables below provide the univariate distributions of the above four variables derived from the sample ($N = 569$).

	Male	Female
α_1	257/569	312/569

	White	Hispanic	African-American	Other
α_2	385/569	56/569	107/569	21/569

	[15-20)	[20-25)	[25-30)	[30-35)	[35-40)	[40-45)	[45-50)	[50-55)
α_3	26/569	103/569	137/569	151/569	93/569	48/569	4/569	7/569

The univariate degree distribution χ is already treated separately in the model (see p.45), so it does not need to be considered as one of the univariate node attributes x_i.

	[0-2)	[2-4)	[4-10)	[10-20)
χ	382/569	82/569	69/569	26/569

3.4.2 Bivariate distributions

The tables below provide the univariate distributions of the above four variables derived from the sample ($N = 272$).

β_1	Male	Female
Male	94/145	51/145
Female	76/127	51/127

β_2	White	Hispanic	African-American	Other
White	159/196	10/196	24/196	3/196
Black	12/21	6/21	2/21	1/21
Hispanic	22/49	2/49	24/49	1/29
Other	3/6	1/6	2/6	0/6

β_3	[15-20)	[20-25)	[25-30)	[30-35)	[35-40)	[40-45)	[45-50)	[50-55)
[15-20)	2/12	2/12	4/12	3/12	1/12	0	0	0
[20-25)	5/42	11/42	9/42	14/42	1/42	0	0	2/42
[25-30)	1/52	6/52	15/52	21/52	2/52	3/52	1/52	3/52
[30-35)	2/70	5/70	19/70	30/70	10/70	2/70	0	2/70
[35-40)	2/51	6/51	5/51	19/51	12/51	6/51	0	1/51
[40-45)	1/39	3/39	5/39	8/39	10/39	10/39	1/39	1/39
[45-50)	0	0	2/4	1/4	1/4	0	0	0
[50-55)	0	0	1/2	0	0	0	0	1/2

The bivariate degree distribution $\bar{\bar{\chi}}$ is already treated separately in the model (see p.45), so it does not need to be considered as one of the bivariate node attributes β_i.

$\bar{\bar{\chi}}$	[0-2)	[2-4)	[4-10)	[10-20)
[0-2)	81/131	26/131	20/131	4/131
[2-4)	14	77/43	40/203	29/203
[4-10)	42/195	50/195	64/195	39/195
[10-20)	15/100	23/100	31/100	31/100

3.5 Dynamism model parameters

Param	Description	Values used
μ_R	Inter risk impulse interval mean	1.00 Months
σ_R	Inter risk impulse interval std. dev.	1.00 Months
p_H	Infection probability in infectious period	0.05
$c_{L/H}$	Reduction in infectiousness post 3 months	0.01
T_+	Infection interval for individuals initially HIV+	3 Months
μ_C	Churn interval mean	60 Months
σ_C	Churn interval std. dev.	48 Months
w_S	Degree stability bias	2.9
w_Δ	Triangle bias	3.0
r_P	Population growth rate every 10 years	0.0, +0.20, -0.20
f_{tr}	Fraction of individuals that are "transient"	0.0, 0.001, 0.01, 0.05, 0.10
μ_{tr}	Mean in-network lifetime of transients	0.10 Months
σ_{tr}	Std. dev. of in-network transients lifetime	0.01 Months
μ_{st}	Mean in-network lifetime of steadies	60 Months
σ_{st}	Std. dev. of in-network steadies lifetime	48 Months

μ_R , σ_R **Inter risk impulse interval mean; Inter risk impulse interval std. dev.** These parameter were set in accordance with the SFHR data set. Given that the criteria for connection in the SFHR survey was, primarily, a risk event in the last 30 days (Friedman, 1999) p. 115, the risk parameter μ_R was set such that nodes would draw from a distribution of risk profiles centered at one risk event per month per risk partner. With a mean degree of 3.4, this means, in effect, that the average actor will engage 3-4 risk events in a 30 day period. Further justification for this comes from a description of the 30 day risk

event rate analyses (Friedman, 1999) p. 136-7. There the authors note that the mean number of network injection partners in the previous 30 days varied by years injecting from 1.78 to 2.3, while the mean number of shared syringe uses with a network partner varied from 0.70 to 0.98, and finally the number of network partners who had been sex partners (ever) ranged from 0.76 to 0.99. One notes that the majority of those interviewed fell in the long term user category (9 years or more, n=496/767), where the number of injection partners (2.3) and syringe sharing partners (0.86) were among the highest rates. In addition, 32 % of respondents reported sex with an injector in the last 32 days (Friedman, 1999) p. 123.

Further description points to a wide range of risk behavior rates. SFHR interview subjects reported an average of 112 monthly injections (not all of which, obviously, involved a risk event), with a standard deviation of 139 (Friedman, 1999) p. 120. Taking the latter as our guide, we set the standard deviation for the risk distribution σ_R equal to the mean. This produced a truncated distribution with a near flat distribution between 0 and 2, and long but diminishing tail for rates greater than 2 risk events per number of risk partners per month.

p_H **Infection probability in infectious period:** This parameter was set differently from the others. Where the other settings have real world equivalents that can draw on direct research, this parameter refers to a fictitious entity, the "risk event" which is a composite of very different events, each with very different transmission likelihoods. Further, disaggregation of this phenomenon was not possible, as the various forms of risk had been aggregated at the level of data collection in the studies that formed the basis of the simulations. As a result, this parameter was used to "tune" the simulation, meaning that—once the other parameters had been set according to the SFHR data, a series of trials were done on the simulated data, and the transmission parameter was set such that the simulated HIV rates for the SFHR settings regularly matched those of the SFHR sample (i.e. 40%).

$c_{L/H}$, T_+ **Reduction in infectiousness post 3 months; Infection interval for individuals initially HIV+:** A full discussion of the dynamics of HIV infectiousness is given in Section 2.2.1 above. A factor of 1.0% the max transmission rate was use as an estimate for a wide range of

published measures, from 1/20th to 1/1000th, based on comparisons between periods of high and low infectiousness. Similarly, a period of three weeks was chosen as an approximation for published a range of estimates from 9 to 14 weeks (Daar, Moudgil, Meyer, & Ho, 1991; Kahn & Walker, 1998).

μ_C , σ_C **Churn interval mean; Churn interval std. dev.:** The rate at which network actors changed their current list of risk partners reflects a stable network where risk partners are held as such for an average of 5 years. Justification for this (Friedman, 1999), p. 130 includes the fact that, 53 percent of the network noted that they had known *all* of their network for at least a year, and 43 percent of the network felt "very close" to some or all of their network. Ethnographic reports from the SFHR network (Curtis et al., 1995) note considerable longevity to risk partnerships (see also (Friedman, 1999) chapter 3). Here again, where wide variation in individual characteristics obtained, we chose a standard deviation that ensured that actors chose their individual churn behavior from a distribution that allowed for rapid turn overs of less than 2 years (for their entire personal network) to long-term partnerships (of 8 years or more). As discussed in Chapter 7, wide variations in the churn parameter actually had little overall effect on HIV rate stabilization over the course of many simulations. We note here, however, that adequate diachronic data was not available from the SFHR data set to determine this variable more precisely, and as a resulted we depended on our estimates based on long-term ethnographic experience in the SFHR network (via co-authors Curtis and Wendel).

w_S **Degree stability bias:** As above, this parameter determined how closely individual nodes maintained their degree over the course of their participation in the network. On the whole, the justification for a fixed degree comes from prior work on drug scene "roles" (Friedman et al., 1998; Curtis et al., 1995). While, obviously, no direct parameter settings can be drawn from the data described by Friedman et al and Curtis et al, the function used to determine the effects of the parameter, and the original parameter setting of 2.9 was designed such that variations from initial degree by roughly 30 % were very likely to be corrected. As with network churn, it was later discovered that the overall effects of variation in the degree stability parameter had little effect

on the simulation outcomes as regards HIV rate stabilization and the firewall effect.

w_Δ **Triangle bias:** The derivation of the triangle bias is covered in Chapter 3. While the results there could have argued with a higher setting than the value of 3 chosen here, this would have served to so significantly diminish the value of actor attributes as to render them meaningless. While there is good reason to expect an important role for triadic closure in the SFHR network, a setting that rendered actor attributes meaningless would have flown in the face of well established results from the SFHR study, where actor attributes were found to be a crucial factor in both local and researcher explanations of network dynamics. Tests of higher ranges of triangle bias are discussed in Chapter 7, where the model derived from the ERGM analysis of the next chapter are examined.

r_P **Population growth rate every 10 years:** Given that little is known about the effects of growth or shrinkage on network-level behavior, we decided to simulate the effects of growth and shrinkage at rates of 20% per decade.

f_{tr} **Fraction of individuals that are "transient":** While a number of individuals in the SFHR study had few partners, or would be considered marginal members of the network itself, there is also a wealth of ethnographic reports on very short-term visitors to the network (Friedman et al., 1998; Curtis et al., 1995). As far as we know, no solid estimates of the proportion of these transient participants is given, nor would we expect the number to be uniform across sub-networks in New York City. A "drug market" zone like that studied by the SFHR project is likely to have a greater proportion of transient members than a smaller, let public network. The original setting of 0 transients was meant to serve as a base-line against which (among other things) the effects of variations in the transient participation rate could be measured.

μ_{tr} , σ_{tr} **Mean duration of transients' lifetimes; Std. dev. of transients' lifetimes:** The transient participation rate was set at 0.1 months (with a standard deviation rate of 0.01 months) to ensure rapid entry and exit from the network. More strict control (i.e. a lower standard deviation in proportion to the variable itself, when compared with other model

settings discussed here) was used to effect tighter control over the length of transient participation.

μ_{st} , σ_{st} **Mean duration of steadies' lifetimes; Std. dev. of steadies' lifetimes:** Hear, as with network churn, a dearth of diachronic data meant that we relied heavily for these parameter settings on ethnographic observation and the experience of project co-authors in the SFHR network. While many of the SFHR network members had been injectors for longer than 9 years, this does not mean that their they participated in the same IDU network for that entire time. For this reason, the settings were made identical to the churn settings above, such that participation varied widely from 2-8 years for "steady" participants. Here again, there was wide variation in individual participation times reported by SFHR researchers. We chose a standard deviation that ensured that actors chose their individual duration in network from a distribution that allowed for rapid node turnover of less than 2 years to long-term network participation (of 8 years or more). As discussed in Chapter 7, wide variations in the steady duration parameter actually had significant effect on HIV rate stabilization over the course of many simulations. Because this parameter had to be set by estimation, special attention to the effects of variation deserve attention.

Chapter 4

HIV stabilization dynamics

Having fit the SFHR model to the general simulation framework described above, new artificial networks which follow the SFHR topology can be generated, and these networks then be simulated over long periods of time. Of particular interest in this Chapter is determining the extent to which networks generated by the SFHR model (parameterized as described in the previous chapter) would achieve stabilization that remained "real world viable" when compared with HIV rates in the greater New York City area.

In what follows, we will present the results of a number of such experiments, each performed on random networks generated from the SFHR model (see Section 3.3, p. 84). In each case the model was used to instantiate 10 independently generated networks at each of 4 different sizes: 1k nodes, 5k nodes, 10k nodes, and 25k nodes.

We note that since the mean in-network lifetimes of individuals was taken to be $\mu_{st} = 60$ months (standard deviation $\sigma_{st} = 48$ months), the total number individuals which participated in these network over the in 15 years was closer to $1,000 \times 180/60 = 3,000$, $5,000 \times 180/60 = 15,000$, $10,000 \times 180/60 = 30,000$, and $25,000 \times 180/60 = 75,000$.

In each of the resulting 40 simulation experiments, the following time varying metrics were computed continuously throughout the simulation's execution.

1. **Number of nodes.** This metric in non-constant in simulations where the population process growth parameter $r_p \neq 0$ (see Section 2.2.2, p. 64).

2. **Mean age of individuals.** This metric increases if individuals are always replaced according to the same distribution that the network nodes were created using—the aging process (see Section 2.2.2, p. 66) pushes the age variable up continuously until they are removed because their in-network lifetime expires.

3. **Number of edges.** This metric is non-constant in simulations if there is any churn $\mu_1^C < \infty$ (see Section 2.2.2, p. 60), or if in-network lifetimes are bounded $\mu_{st}, \mu_{tr} < \infty$, or the population growth parameter $r_p \neq 0$ (see Section 2.2.2, p. 64).

4. **Average degree.** The quotient of the above two metrics—it is non-constant, if either of them are non-constant.

5. **Average deviation from ideal degree.** Each vertex v has a constant ideal degree $d_1(v)$ and time varying actual actual degree $|N_1^t(v)|$ at time t. This metric's value is the average deviation of the two values

$$\frac{1}{|V|}\sum_{v\in V} |N_1^t(v)| - d_1(v).$$

   This metric is non-constant if the number of edges is non-constant, or there is any churn $\mu_1^C < \infty$ (see Section 2.2.2, p. 60).

6. **Average magnitude of deviation from ideal degree.** This metric's value is the unsigned average deviation of the actual and ideal degrees

$$\frac{1}{|V|}\sum_{v\in V} \big|\ |N_1^t(v)| - d_1(v)\ \big|.$$

   This metric is non-constant if the number of edges is non-constant, or there is any churn $\mu_1^C < \infty$ (see Section 2.2.2, p. 60).

7. **HIV prevalence (among steady nodes) in the population.** This metric takes a value equal to the number of HIV positive individuals expressed as a fraction of the total population, i.e. p_1^t, which is $|A_1^t|/|V^t|$ (see p. 45 for details).

8. **Number of recent infections (HIV+ individuals in the highly infectious "acute" phase).** This metric takes a value equal to the integer number of HIV positive individuals v for which

$$t - t_1^+(v) \leqslant 3$$

(see Section 2.2.1, p. 45 for details).

9. **Number of components.** This metric takes a value equal to the number of disconnected components in the graph obtained upon deleting all the "old" chronic stage HIV+ individuals, i.e. individuals for which $t - t_1^+(v) > 3$.

10. **Average component size.** This metric takes a value equal to the average size of the components so obtained (see the metric **Number of Components**).

11. **Size of the largest component.** This metric takes a value equal to the size of the largest component so obtained (see the metric **Number of Components**).

Not all the metrics above appear in the remainder of this chapter. As our focus here is limited to understanding evolving HIV prevalence levels over time in network trajectories generated by the SFHR model, only those metrics which help to explain the observed phenomena shall appear. Other metrics, however, will be used in later chapters which are devoted to parallel investigations of firewalling, and to assessing the robustness of our conclusions against variations from the base SFHR model parameters.

4.1 Simulations based on the SFHR model

The graphs that follow depict the 15-year trajectories of ten independently generated 10,000 node networks based on the SFHR model, depicting various metrics over the simulation interval. Each of the 10 trajectories is referred to as a **trial**.

Before considering the simulations, we present a few subtleties that bear mentioning in considering what we mean by a "10,000 node network". Note that the mean in-network lifetimes of individuals was $\mu_{st} = 60$ months (standard deviation $\sigma_{st} = 48$ months). As such, the number of individuals which participated in the network over the in 15 years was closer to $10,000 \times 180/60 = 30,000$. When an individual's lifetime expired, they were remove and replaced by the population process, in order to keep the number of individuals in the network at 10,000.

Similarly, given that 30,000 individual nodes participated in the network, each with an average degree of 3.4 and an average churn rate set to their life expectancy (such that each node would on average churn through his/her entire set of connections completely over the course of their participation in the network), we can estimate that $(30,000 \times 3.4$ initial connections$)$ + $(30,000 \times 3.4$ churned connections$)$=$204,000$ total edge changes took place over the course of the 15 year simulation. Given that, with a risk rate of 1, each of these edges was (on average) subject to a risk event monthly, we can estimate that each simulation trial entailed approximately 37 million risk events across which HIV infection could have taken place.

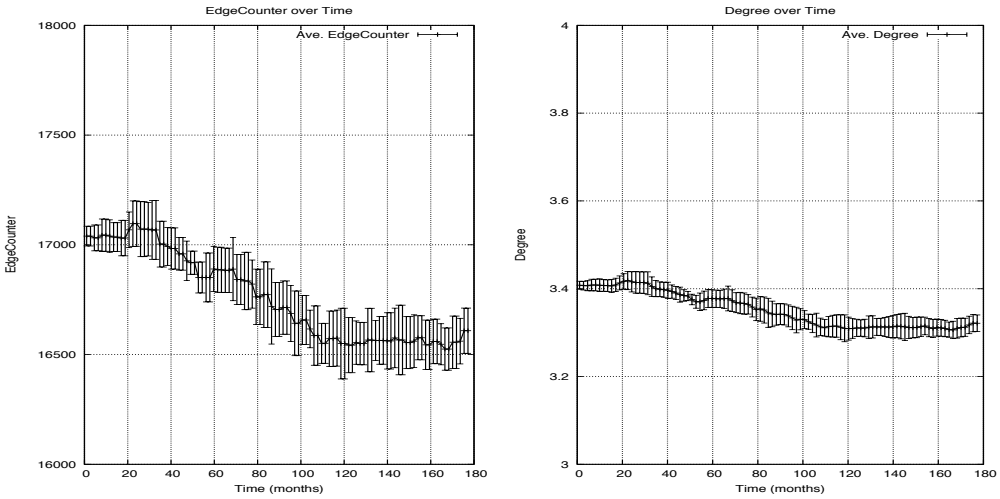

Figure 4.1: Number of edges (left) and mean degree (right) in a SFHR-based risk network.

We see from the left graph in Figure 4.1 that the number of edges remains relatively stable over the course of the simulation, as well as across simulation trials. Fluctuations in edge numbers were due to the fact that new individuals entering the network were assigned new ideal degrees based on the degree distribution χ of the SFHR model. The right graph depicts the average number of risk partnerships over time, which fluctuated in a narrow range slightly below 3.4.

Figure 4.2 shows the HIV prevalence (over time) in 15 year simulations of ten independently generated 1k, 5k, 10k, and 25k node networks based on the SFHR model. These graphs show that from an initial infection rate of 0.5%, HIV spreads throughout the network in 12-18 months (in all but the 1,000 node network), to a prevalence level of roughly 40%. From here, it remains relatively stable, rising to 50% over the next 15 years. These figures are commensurate with HIV levels measured in New York City's IDU networks during the early stages of the HIV epidemic (Des Jarlais, Arasteh, & Friedman, 2011; Des Jarlais et al., 2005, 1998, 1989). We note here as well the effects of scale, whereby the 1,000 node network exhibits higher variance across simulations and different stabilization characteristics than the larger networks. These effects of scale for networks below 1000 nodes remains consistent in the simulation experiments that follow.

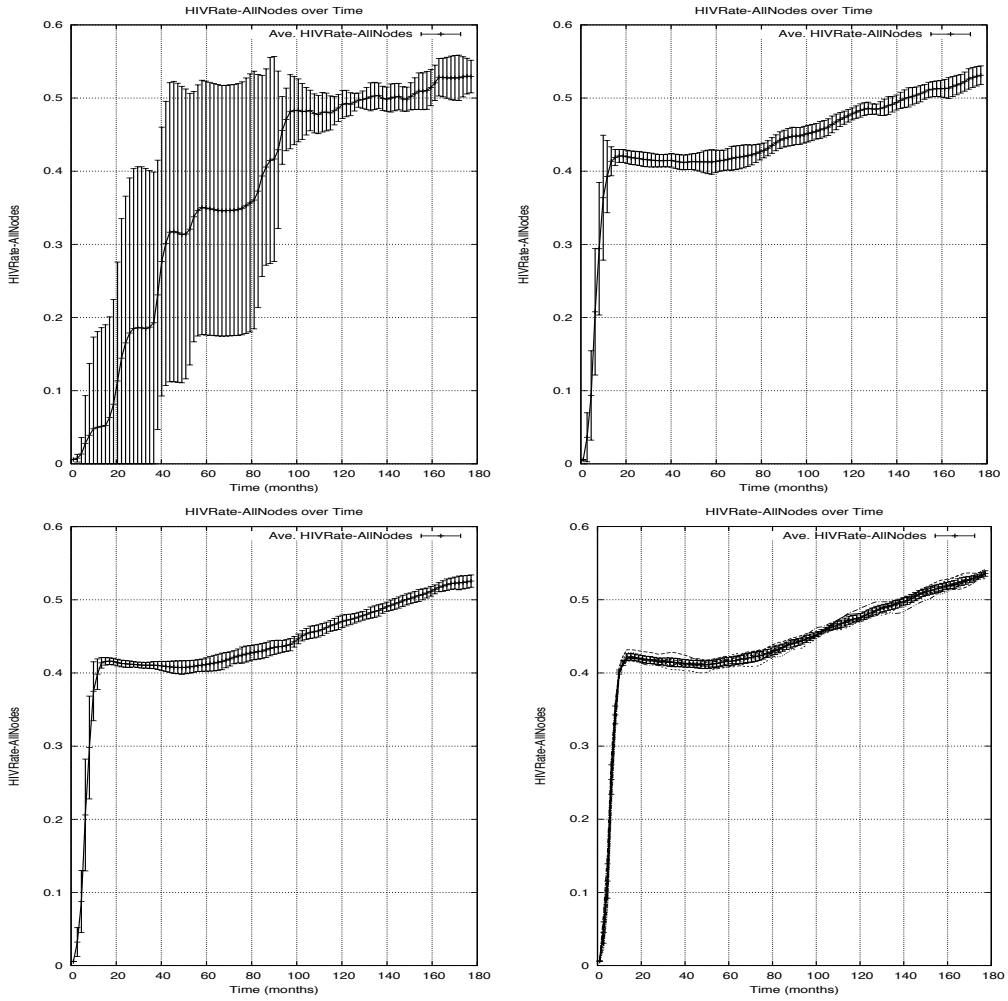

Figure 4.2: HIV prevalence in a SFHR-based risk network of size 1,000 (top left); 5,000 (top right); 10,000 (bottom left); and 25,000 (bottom right).

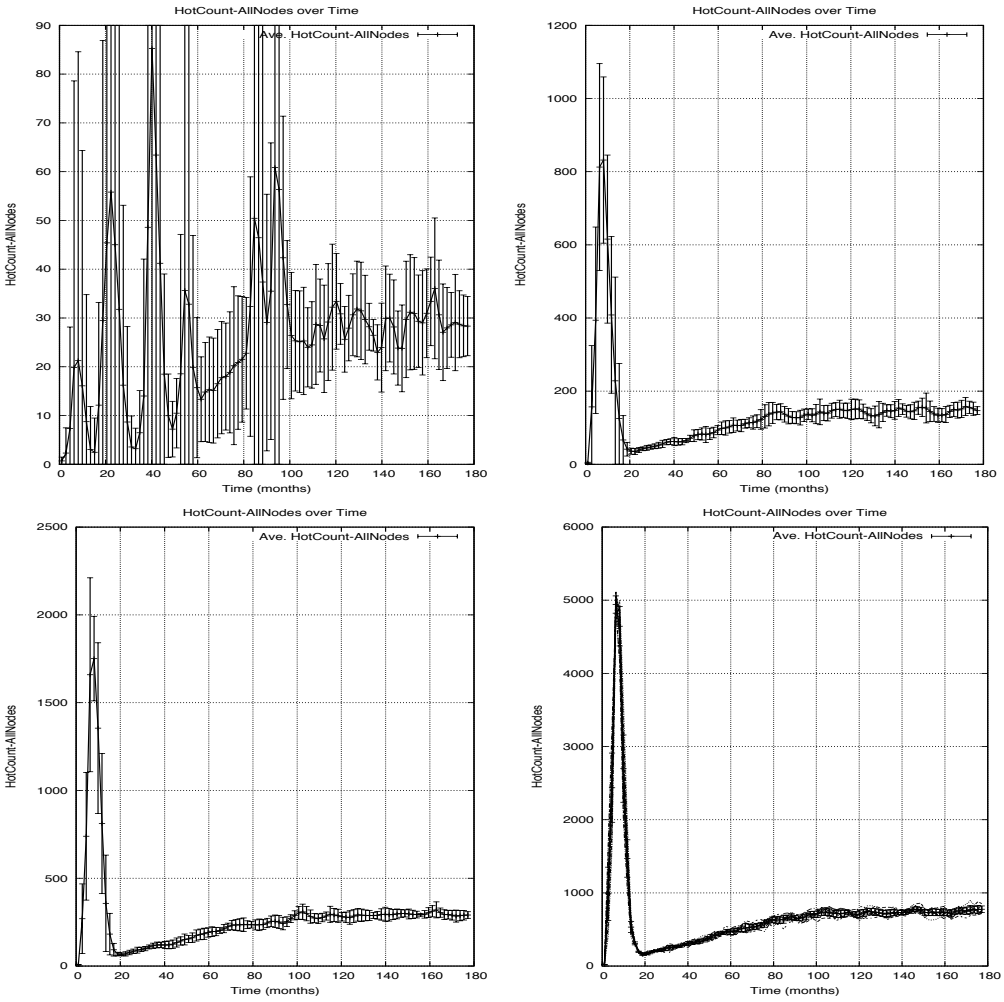

Figure 4.3: Count of highly infectious nodes in a SFHR-based risk network of size 1,000 (top left); 5,000 (top right); 10,000 (bottom left); and 25,000 (bottom right).

Figure 4.3 shows the number of highly infectious nodes (over time) in 15 year simulations of ten independently generated 1k, 5k, 10k, and 25k node networks based on the SFHR model. These graphs show that in the three larger networks, a surge of acute infections appears roughly 10 months into the simulation, encompassing roughly 20% of all individuals. In the 10 months after the spike, the acute infections dissipate, and the network returns to having relatively few acute infections (approximately 3%). This low but steady rate

of new infections over time, together with the stabilization of HIV shown in Figure 4.2 demonstrate that while the network continues to produce new infections over the course of time, they fail to propagate fully throughout the network (Hypothesis 3). At the smallest scale of 1,000 nodes, no such "hot spike" appears. From this we can conclude that the validity of Hypothesis 3 is dependent on factors of scale.

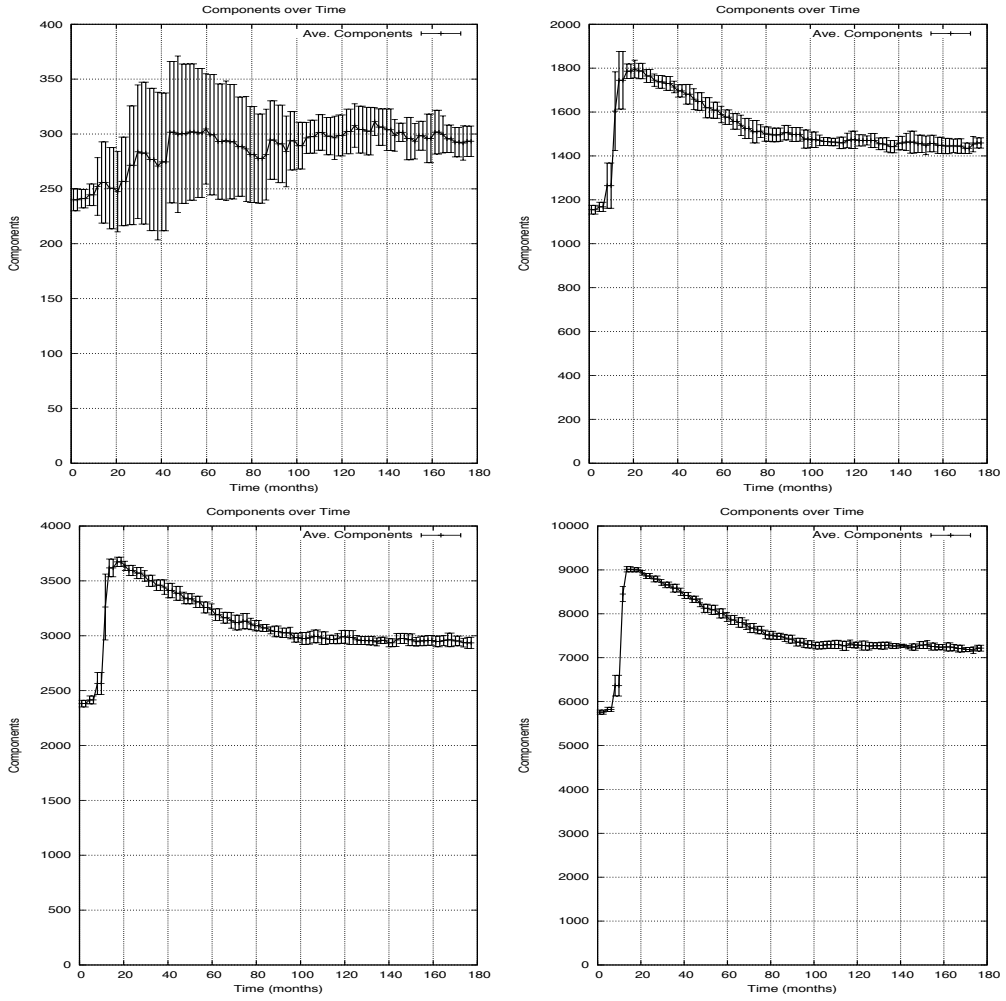

Figure 4.4: Number of components post deletion of old infections (and their incident edges), in a SFHR-based risk network of size 1,000 (top left); 5,000 (top right); 10,000 (bottom left); and 25,000 (bottom right).

Figures 4.4 and 4.5, together, show that for sufficiently large networks (of size greater than 1,000), once we remove the HIV positive nodes whose infections have reached the chronic stage of low infectiousness, the overall network shatters into a large number of components, with each component having on average fewer than 2 members. Thus, even though the network continues to produce new infections, the bridging effect of old infections limits the spread of HIV from highly infectious individuals in the acute phase. These small components are neighborhood-level social network structures; old infections lie at the boundaries of these structures, and serve to limit the potential spread of HIV within the network as a whole. The two together account for a firewalling effect that allows IDU communities to remain at relatively stable infection levels below saturation. This resolves Hypothesis 2.

We note from Figure 4.3, that upward spike in the number of components coincides with the rapid decline in the "hot spike" of acute infections. The rise in the number of components limits the topological transmission range of acute HIV+ individuals, while the rise in the number of acute infections produces a rise in the number of components—albeit delayed by 3 months. We speculate that infections burn quickly through the core of the network, leaving only sparsely connected margins.

At the smallest scale, a network with 1,000 nodes exhibits much higher variance across simulations and has different stabilization characteristics than the larger networks. From this we can conclude that like Hypothesis 3, the validity of Hypothesis 2 is dependent on factors of scale.

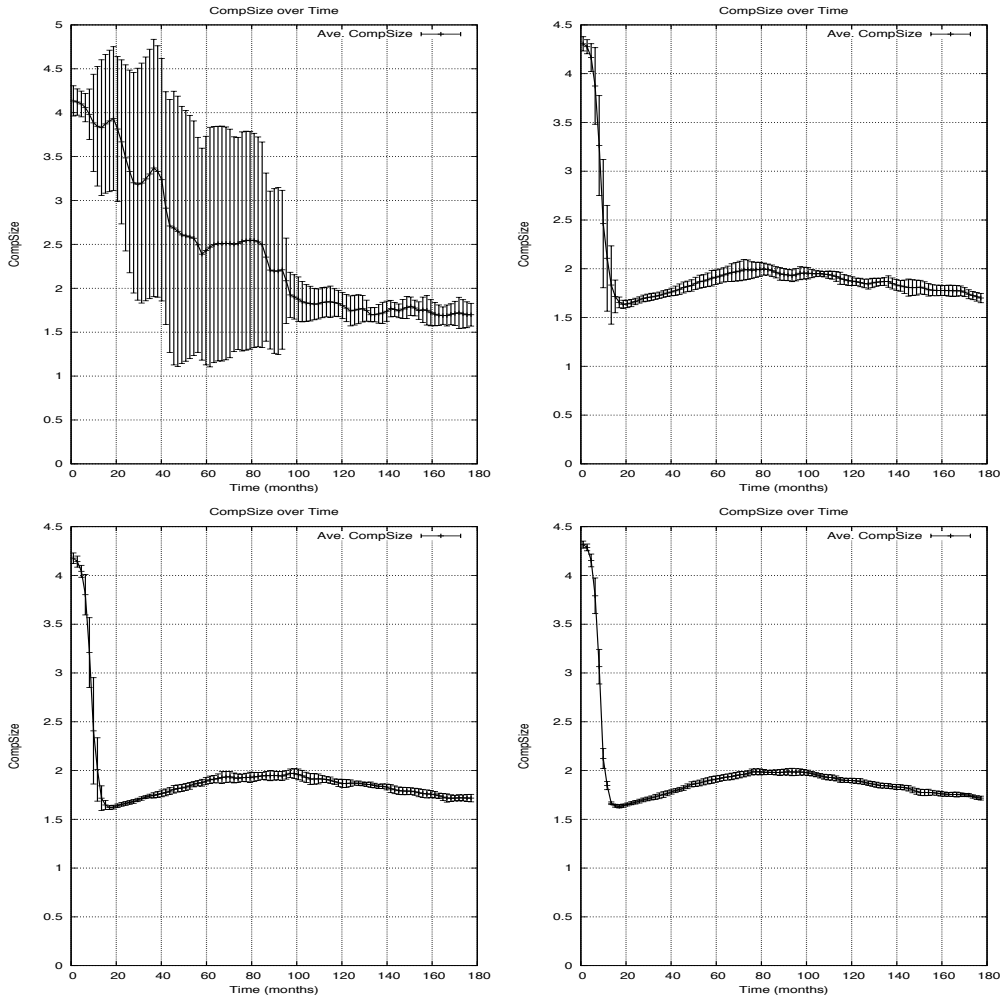

Figure 4.5: Component size post deletion of old infections (and their incident edges), in a SFHR-based risk network of size 1,000 (top left); 5,000 (top right); 10,000 (bottom left); and 25,000 (bottom right).

4.2 Non-constant population size scenarios

Next we consider scenarios in which the population size is not kept constant over time. Figure 4.6 (resp. Figure 4.7) depicts the HIV prevalence in populations that are growing (resp. shrinking) at a rate of 20% per decade.

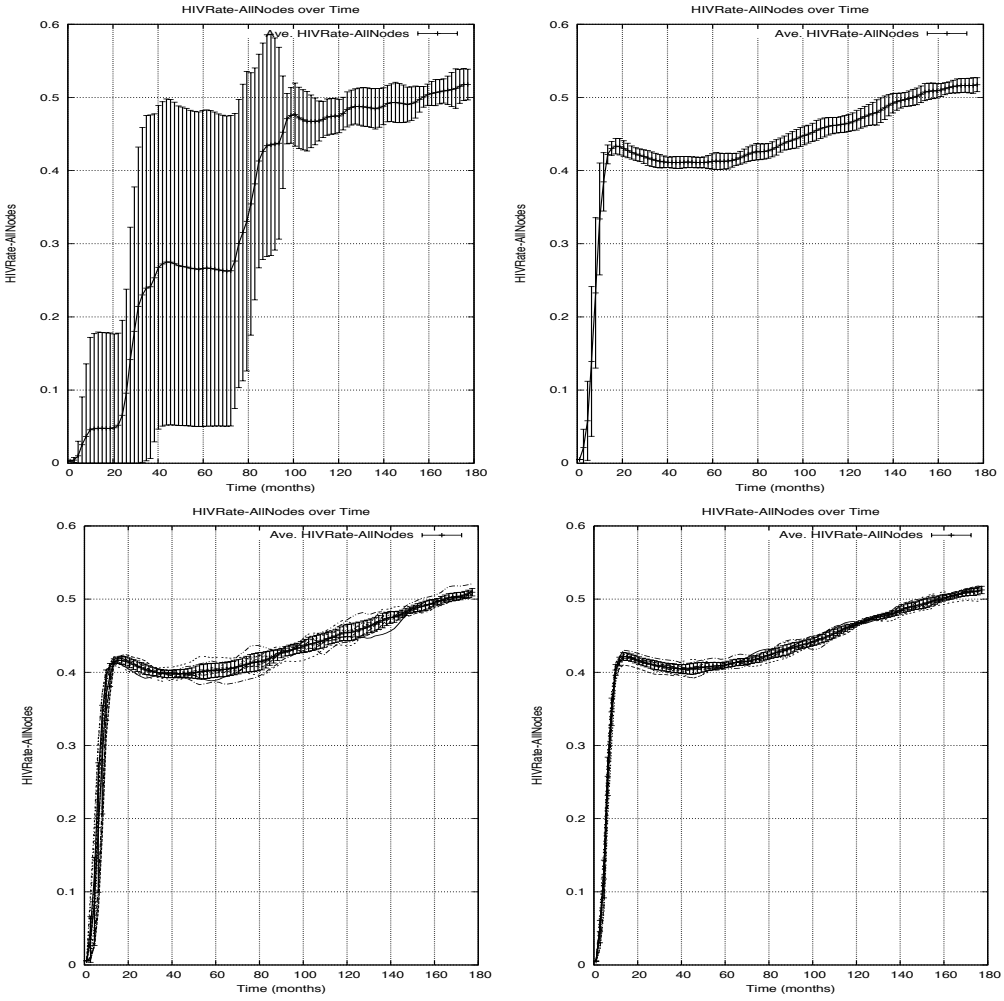

Figure 4.6: HIV prevalence in a growing SFHR-based risk network of size 1,000 (top left); 5,000 (top right); 10,000 (bottom left); and 25,000 (bottom right).

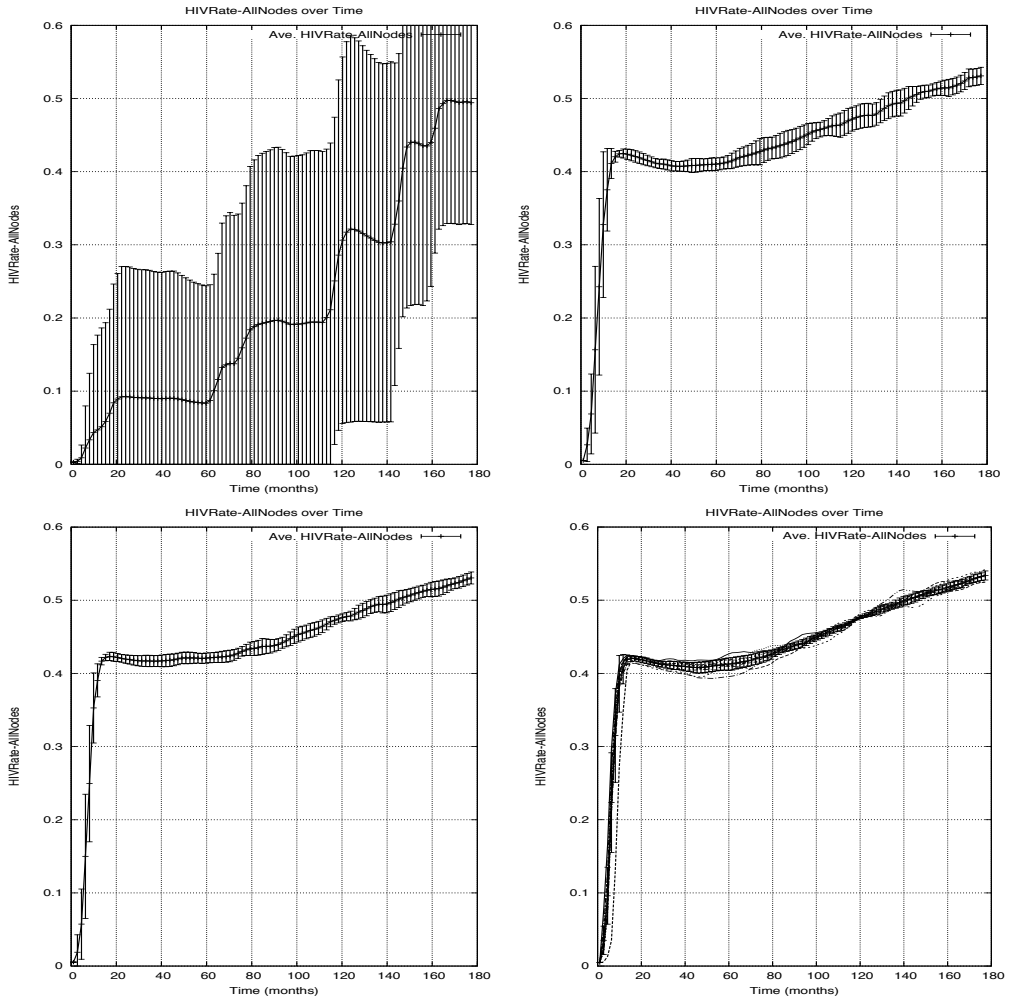

Figure 4.7: HIV prevalence in a shrinking SFHR-based risk network of size 1,000 (top left); 5,000 (top right); 10,000 (bottom left); and 25,000 (bottom right).

As can be seen in Figures 4.6 and 4.7, changes in network size over the course of the simulation had little impact on the stabilization rates, nor for that matter on the overall rates of HIV in the network as a whole. The simulation results demonstrate that HIV prevalence stabilizes in both growing and shrinking populations in much the same way as it does in settings of constant population size (compare Figure 4.2, p. 100). In addition, we note here that the effects of small scale carried over in both growing and

shrinking networks, with the greatest variability between runs shown in the shrinking network. Indeed, the small scale growing network (Figure 4.6, top left) appears to narrow in variability between runs after 10 years, where the network would have achieved a population size of approximately 1200 nodes. In contrast, the shrinking networks of small scale (Figure 4.7, top left) neither stabilizes nor narrows its run-to-run variability.

4.3 Remarks concerning the simulations

Given this first set of experiments, some initial remarks concerning the results of these simulations can be enumerated:

- **Stabilization.** In general, the parameter settings discussed in Chapter 3 resulted in all networks above 1000 nodes to show HIV rate sub-saturation stabilization at a level similar to that observed for IDU networks in New York City in the early stages of the HIV epidemic (Des Jarlais, Arasteh, & Friedman, 2011; Des Jarlais et al., 2005, 1998, 1989).

- **Hypothesis 3.** Evidence for the establishment of Hypothesis 3—that IDU networks with stable, sub-saturation levels of HIV-1 infection will continue to produce new infections over the course of time which fail to propagate full throughout the network—was given in Figure 4.3. As originally proposed by Friedman (Friedman et al., 2000), the presence of highly infectious individuals engaging in risk activities does not, alone, ensure that HIV infection will spread throughout a risk network.

- **Hypothesis 2.** As evidenced in Figure 4.5, there is good reason to suspect that local-level social network structures within the risk network contribute to the non-spreading of HIV (Hypothesis 2), despite the presence of highly infectious individuals engaging in risk activities. We verify that the reduced component size of pockets of uninfected nodes coincides with periods of HIV rate stabilization, and that such configurations are maintained over long periods of simulation time. As above, this phenomenon exists despite continuing turnover in network

participants, high levels of network edge churn, and very high numbers of network risk events.

- **Growing and Shrinking Networks.** All of the above apply to networks whose overall size is changing as well, whether these networks are growing or shrinking. Indeed, changes in overall network size showed little or no effect on the dynamics described here (nor on evidence used to evaluate Hypotheses 2 and 3).

- **Scale.** All of the above is conditioned on factors of scale. Consistently throughout the various simulations and the metrics used to evaluate them, we found that while networks of size 5,000 through 25,000 followed a narrow (and therefore predictable) range of trajectories, smaller networks of 1000 nodes showed high variability in their network wide behavior.

The last of these remarks bears serious consideration for those concerned with interventions aimed at influencing the overall rate of HIV among injecting drug user networks. If smaller networks show high variability in their dynamics—leading to the idea that they are more subject to stochastic events than networks of large size—then understanding where and how particular interventions will succeed or fail becomes very difficult. What such variability indicates is that stochastic factors may outweigh node level dynamics in determining network-wide outcomes through time. Put another way, the outcome of interventions in small scale networks may not serve as good indicators of likely outcomes of the same intervention in large networks, other small networks, nor in the same networks at a different time. In each case, the effects of random events may render the most successful interventions moot, or the most ill-adapted interventions successful—all this without a change in the underlying set of network attributes or dynamics.

Chapter 5

HIV firewalling effects

In this Chapter, we evaluate the extent to which the Firewall Hypothesis holds in networks generated by the SFHR model. Recall, as originally stated on p. 28:

> *Firewall Hypothesis.* Firewall phenomenon will consist of individual agents with mature infections which partition the overall risk network into a series of clusters, in which uninfected clusters remain relatively stable (over simulation time). Originally

To evaluate the validity of this hypothesis, we shall require a mathematical formulation, or more precisely, a computable expression which, when applied to a specific risk network (at a particular instant in time), will produce a value of 1 if the network absolutely satisfies the Firewall Hypothesis, and a value of 0 if the hypothesis absolutely fails therein. In addition, the mathematical formulation should be designed to produce intermediate values between 0 and 1, with magnitude reflecting the "extent" to which the hypothesis holds for the specific network at the particular time.

To better understand the circumstances which leading to firewalling (and by duality, which cause it to fail), we shall consider the structure of the risk network at a resolution that is pertinent to viral propagation dynamics.

Because of the nature of the infectiousness curve for HIV-1, nodes for whom the time since infection exceeds 3 months enter a chronic stage in which they present much lower transmission potential for the virus (see Figure 2.2 on p. 59). In view of this, we will be particularly interested in analyzing the structure of the risk network *minus* the old infections. This is justified by the observation that individuals in the chronic phase play a much smaller role in viral propagation compared to acute infections and HIV- individuals, which represent sources and sinks of HIV, respectively.

The top image in Figure 5.1 below shows a 26 node risk network with three connected pieces comprising 2, 3, and 21 individuals respectively The bottom image shows the risk network once individuals with old chronic-stage infections (and their incident edges) have been deleted. The resulting graph (post deletion process) is seen to have six components. In effect, the top figure is a **human-centric rendering** of the risk network, while the combinatorial object at the bottom of the figure is a **virus-centric rendering** of the same risk network. We note that the virus propagates on the human-centric network, because that is where risk events are transacted. The virus-centric view merely represents an analytic strategy, algorithmically derivable from the human-centric view.

At each instant in time, the virus-centric rendering of risk network may be decomposed into a collection of "connected **components**". The fates of individuals in each connected component are seemingly intertwined by sequences of risk relationships, while individuals lying in different components have more independent destinies with respect to infection outcomes (assuming a static network structure). Each connected component can be assigned a *risk status*, wherein it is deemed to be "**at-risk**" (resp. a "**firewalled**" component), if acute HIV infection(s) are present (resp. absent) from it. In the virus-centric rendering of the risk network shown at the bottom of Figure 5.1, 4 of the 6 components are "at-risk"; the remaining 2 are "firewalled".

In this analysis, the HIV- individuals within each component in the virus-centric view, inherit the risk status of the component in which they lie. Since the 4 components that are "at-risk" have 4, 2, 3, and 1 HIV- individuals in them (respectively), the total number of individuals said to be "at-risk" is 4+2+3+1=10. On the other hand, since the 2 components that are "firewalled" both have 3 HIV- individuals in them, the total number of individu-

als said to be "firewalled" is 3+3=6. From this, we conclude that out of the total 10+6=16 HIV- individuals, a 6/16=0.375 fraction may attribute their present safety and good fortune, to the fact that the virus cannot reach them because of local structures that "partition the overall risk network into a series of clusters". In the example, the validity of the firewall hypothesis would be taken to be 0.375. This is a relatively low value, within the range 0 to 1 of possible values. If simulations of networks generated by some model (e.g. the SFHR model) were to consistently produces risk networks whose trajectories exhibited such low firewall hypothesis validity measures (across the entire duration of the simulation), we might justifiably conclude that the Firewall Hypothesis is largely untrue in the networks that the model generates.

As it turns out, however, the opposite occurs. That is, our simulations of networks generated by the SFHR model are seen to produce risk networks whose trajectories exhibit high values (nearer to 1) for the Firewall Hypothesis validity measure. To illustrate the subtleties underlying this assertion, consider the human-centric view of a risk network shown at the top of Figure 5.2. This 26-node risk network has precisely the same HIV prevalence, and the same number of acute and chronic (old) infections. When viewed purely as combinatorial graphs, the two networks at the top of Figures 5.2 and Figure 5.1 are isomorphic. Furthermore, chronic infections are situated identically in the two networks, and hence the virus-centric views are also isomorphic (as combinatorial graphs). What is different between the two networks, is the placement (but not the number) of acute infections, relative to the constant locations of chronic infections. The virus-centric view of the network in Figure 5.2 has 2 "at-risk" components and 4 "firewalled" components. Of the 16 HIV- individuals, the number of "at-risk" HIV- individuals is 1, while the number of "firewalled" individuals is 15. Thus, sheerly by of the relative placements of the acute and chronic (old) infections, the validity of the firewall hypothesis in this network is 15/16=0.938. This is a relatively high value, in the range of possible value from 0 to 1.

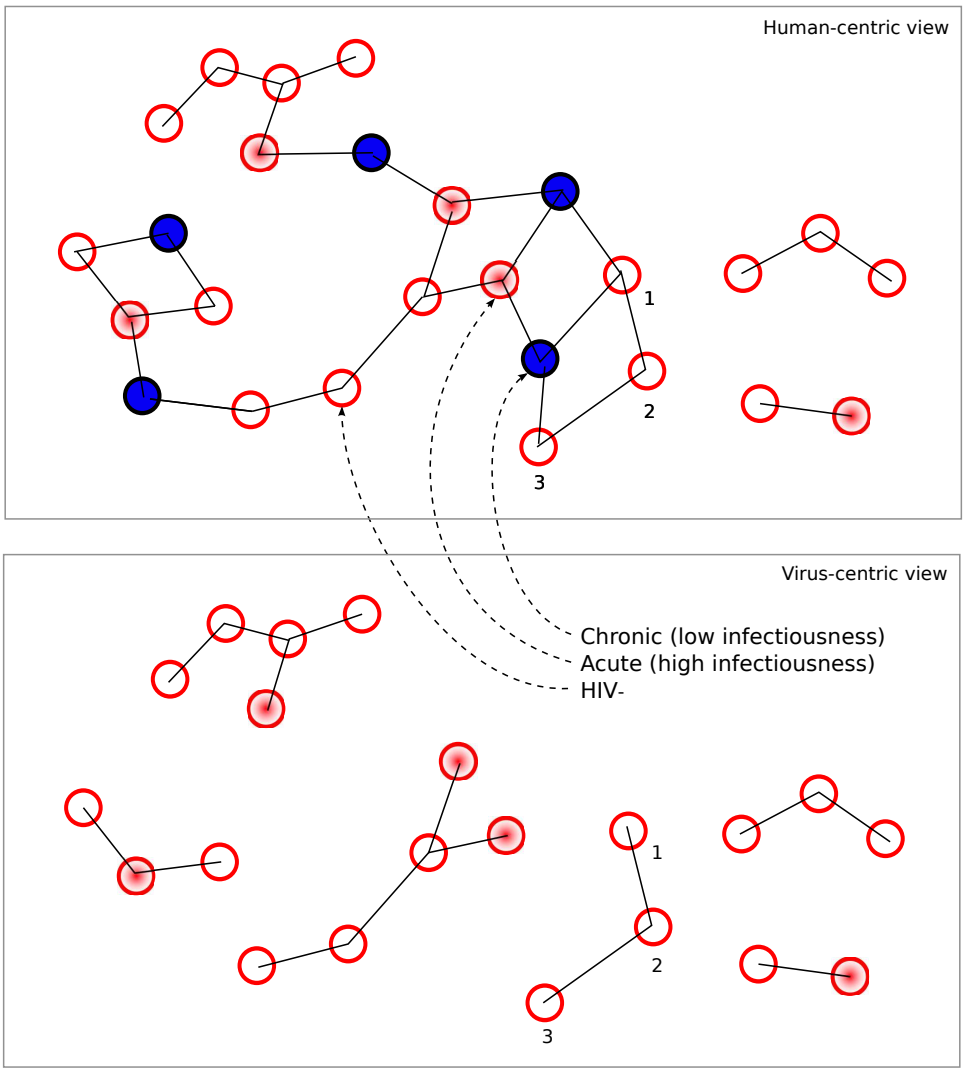

Figure 5.1: (Top) A human-centric view of a 26 node risk network with HIV rate 10/26, 4 of 10 HIV+ individuals have acute infections; (Bottom) The virus-centric view of the same network. The measure of Firewall Hypothesis Validity is 6/16=0.375.

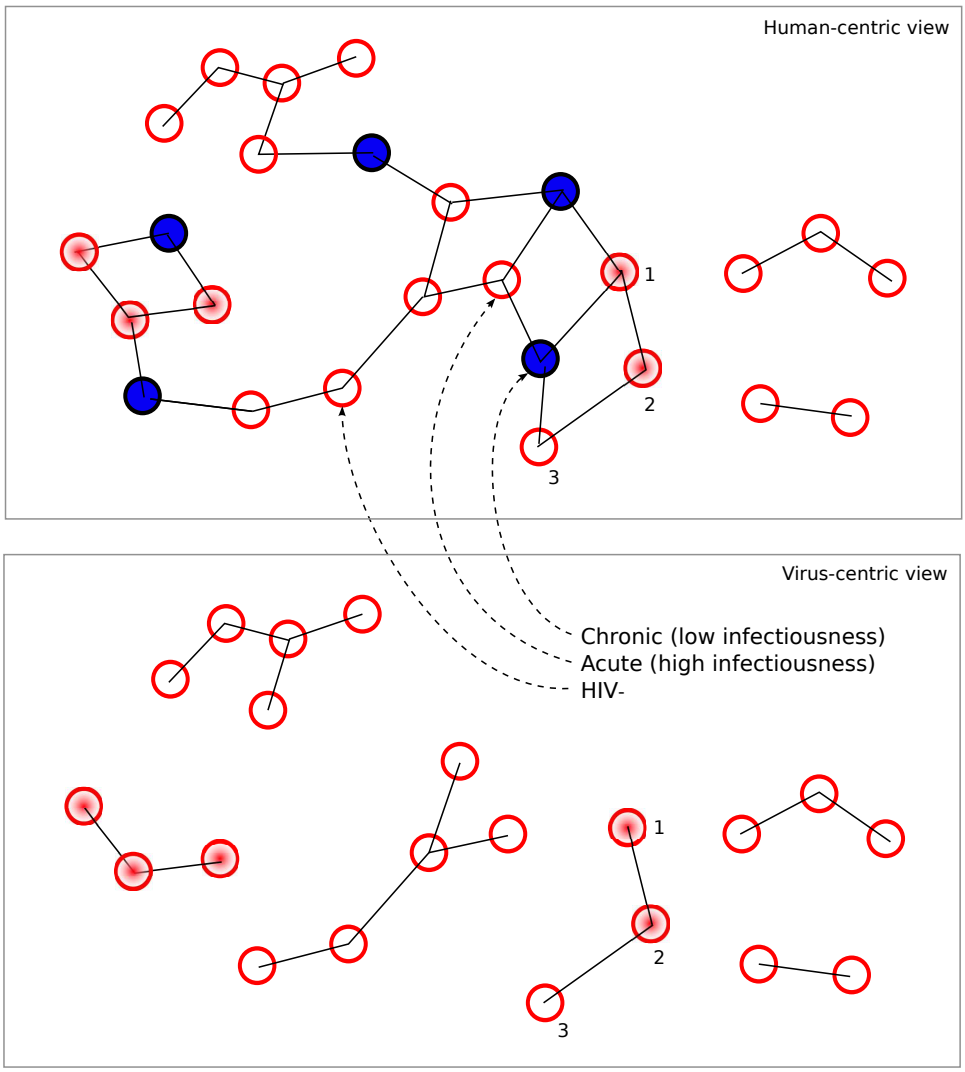

Figure 5.2: (Top) A human-centric view of a 26 node risk network with HIV rate 10/26, and 4 of 10 HIV+ individuals have acute infections; (Bottom) The virus-centric view of the same network. The measure of Firewall Hypothesis Validity is 15/16=0.9375

What these two artificial examples illustrate is that the Firewall Hypothesis validity measure is defined in terms of local structures in the network, as relevant to the virus propagation dynamics. The measure requires computations on the combinatorial structure of the risk network. It is sensitive to the relative placement of acute and chronic infections, and cannot be predicted purely from HIV prevalence, network topology, or the numbers of acute and chronic infections.

In Section 5.2, we shall report on experiments which compute the Firewall Hypothesis measure over long term simulations of networks generated by the SFHR model. Before that, however, it is incumbent on us to carry out our mathematical responsibilities, in providing the reader with a rigorous, graph-theoretic exposition of the measure that has been presented informally above.

5.1 Network obstructions to saturation

In this section, we provide a formal mathematical treatment of the Firewall Hypothesis validity measure. We begin by noting that at each fixed instant in time t, we have a population V^t, of which a subset $A_1^t \subseteq V^t$ are HIV positive[1]. The HIV prevalence at time t is given by the expression

$$p_1(t) \stackrel{\text{def}}{=} |A_1^t|/|V_1^t|$$

The HIV positive individuals can be partitioned $A_1^t = N_1^t \sqcup O_1^t$. The set N_1^t consists of new infections, that is, highly infectious individuals who acquired HIV within the past three months and are presently in the acute phase (Cates et al., 1997; Kahn & Walker, 1998; Lyles et al., 2007). The complement of N_1^t (within the set of HIV+ individuals) is $O_1^t = A_1^t \backslash N_1^t$, the set of older infections. These individuals were infected with HIV at time prior to ($t -$ 3 months), and are now in the chronic significantly less infectious phase.

The individuals V_1^t are inter-connected by a set of pairwise risk relationships[2] $E_1^t \subseteq V^t \times V^t$, allowing the topology of the risk network to be modeled as

[1] In framework formalisms, we have $p = 1$ pathogens, with HIV being type $\mathscr{P}_1$.

[2] In framework formalisms, we have $l = 1$ layers, of which needle-sharing is type $\mathscr{T}_1$.

an undirected graph $G_1^t = (V^t, E_1^t)$ having vertex set V_1^t and edge set E_1^t. In general, G_1^t need not be a "connected" graph, i.e. every pair of individuals might not be related through a chain of risk relationships. The partitioning of G_1^t into disjoint components is one network obstruction to viral propagation. Another, more subtle network obstruction exists because individuals with older infections have low infectiousness, and so serve to limit the extent of viral outbreaks. We seek to formally define a measure which captures the extent to which these two network obstruction phenomena are manifested at any given time.

Towards this, let us take ${G_1^t}'$ to be the graph obtained by deleting from G_1^t all old HIV infected individuals O_1^t (along with all their incident edges). While ${G_1^t}'$ need not be a connected graph, it can be described as a collection of ℓ_t disjoint components,

$$ {G_1^t}' = C_1^t \sqcup C_2^t \sqcup \ldots \sqcup C_{\ell^t}^t. $$

We introduce a function $I^t : V^t \backslash O^t \to \{1, \ldots, \ell^t\}$ that identifies the component in which each individual v from $V_1^t \backslash O_1^t$ is to be found, i.e. I^t is defined such that $v \in C_{I^t(v)}^t$ for all v in $V_1^t \backslash O_1^t$. An HIV negative individual $v \in V_1^t \backslash A_1^t$ is said to be "at high risk" if the v is connected to a highly infectious individual by a chain of risk relationships involving uninfected nodes, i.e. if $C_{I^t(v)}^t \cap N_1^t \neq \emptyset$; otherwise, the individual is said to be "at low risk". We define a Boolean-valued function $\beta^t : V^t \backslash A_1^t \to \{0, 1\}$ by putting

$$ \beta_t(v) = \begin{cases} 1 & C_{I^t(v)}^t \cap N_1^t = \emptyset \\ 0 & \text{otherwise.} \end{cases} $$

Note that $\beta^t(v) = 1$ if and only if v lies in a component of ${G_1^t}'$ that has no highly infectious HIV+ individuals. This can occur in one of two ways:

- v is in a component of G_1^t with no highly infectious HIV+ individuals,
- v is in a component of G_1^t that contains highly infectious HIV+ individual(s), but v is protected by interceding nodes from O_1^t.

It follows that $\beta^t(v) = 1$ precisely when individual v enjoys one of the two

network obstruction phenomena discussed above. Given this fact, we introduce the quantitative measure

$$hyp(t) \stackrel{\text{def}}{=} \frac{\sum_{v \in V^t \setminus A_1^t} \beta^t(v)}{|V^t \setminus A_1^t|}.$$

If $hyp(t) \approx 1$, then it may be asserted that at time t almost all HIV negative individuals experience one of the two network obstruction phenomena.

5.2 Looking for firewall effects

Figure 5.3 depicts the value of $hyp(t)$, plotted as a function of time for 15 year trajectories of ten networks generated by the SFHR model. Four network sizes are considered: 5k, 10k, and 25k nodes. In all but the smallest network scenario, the Firewall Hypothesis validity rises rapidly from 0 to 0.8 during the first 18 months, rebounding briefly to 0.75 in the next 5 years, and then re-stabilizing again back at the 0.8 level. Figure 5.4 shows the results of analogous simulation experiments on growing and shrinking networks whose initial size is 25k nodes. In all cases, the Firewall Validity Hypothesis measure follows a similar arc over the course of the simulation. Given that the Firewall Hypothesis validity measure remains above 0.85 for all but the initial 18 months, we take this as validation of Hypothesis 1 (see p. 28), that being that individual agents with mature infections partition the overall risk network into a series of clusters, in which uninfected clusters remain relatively stable over simulation time. Accordingly, we shall hereafter refer to the Firewall Hypothesis as the **firewall effect**. In smaller networks of 1000 nodes, the extent of the firewall effect varied considerably between trials, showing that stochastic factors outweigh structural/node-based behaviors in the determination of simulation outcomes.

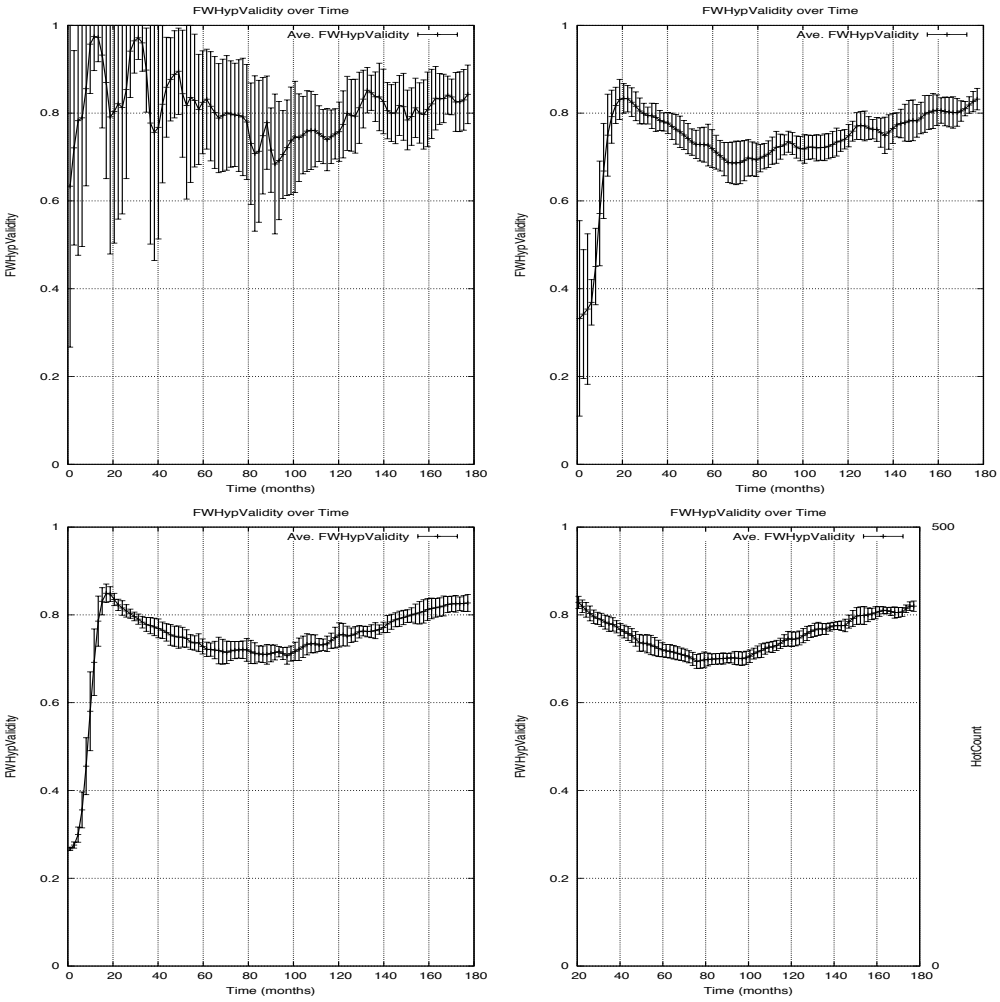

Figure 5.3: Firewall Hypothesis Validity in stable risk networks of 10,000 (top) and 25,000 (bottom) nodes over 10 years.

We now provide a local level structural explication of the phenomena underlying the Firewall Effect. To facilitate the exposition, we divide the simulation period into two stages, which we will refer to as the *emergent* period, and the *steady* period. The emergent period spans roughly the first 18 months, while the steady period will be taken to be remaining 13+ years in the simulation. In what follows, we shall seek to explain the mechanisms underlying the trajectory followed by the Firewall Hypothesis Validity measure. Each of the two periods, emergent and steady, shall be treated in a separate section.

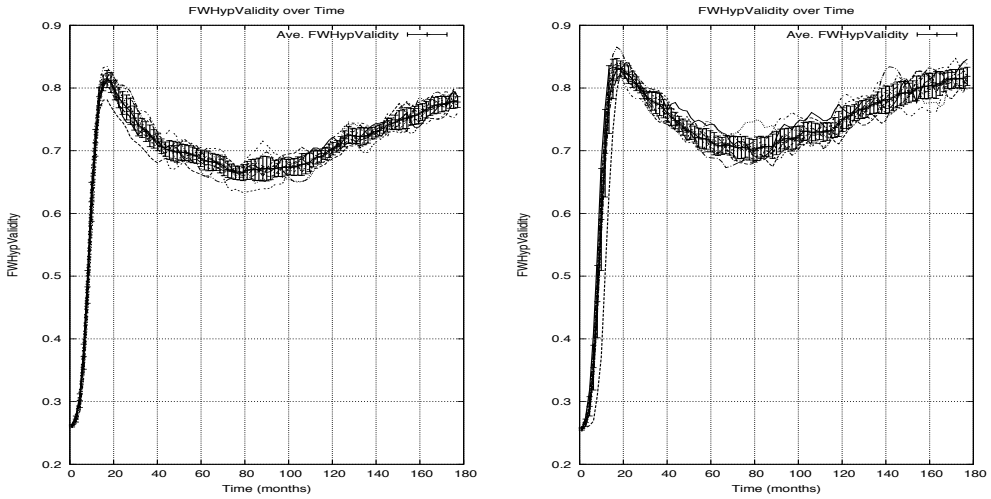

Figure 5.4: Firewall Hypothesis Validity in growing (left) and shrinking (right) risk networks having an initial size of 25k nodes.

5.2.1 Emergent period

To understand why the Firewall Validity Hypothesis measure follows the particular trajectory that it does, we return to the definition of the measure as a quotient of two quantities: the number of firewalled individuals divided by the number of HIV- individuals.

The number of firewalled individuals, which appears in the numerator of the hypothesis validity measure, is depicted over the 18 month emergent period in the left graph in Figure 5.5. We can see from the graph that at the outset, approximately 25% of all individuals are firewalled, but that this number which doubles and plateaus over the 18 months duration of the emergent period.

The number of HIV- individuals, on the other hand—which appears in the denominator of the hypothesis validity measure—can be readily determined from HIV prevalence levels, since the number of HIV- individuals is simply the population size multiplied by 1 minus the HIV prevalence. Recall that in these simulations, the population size is held constant. The right graph of

Figure 5.5 shows that over 18 months, the number of HIV negative individuals falls from its initial value of 99.5% of all individuals, plateauing at a mere 57%, just one year into the simulation.

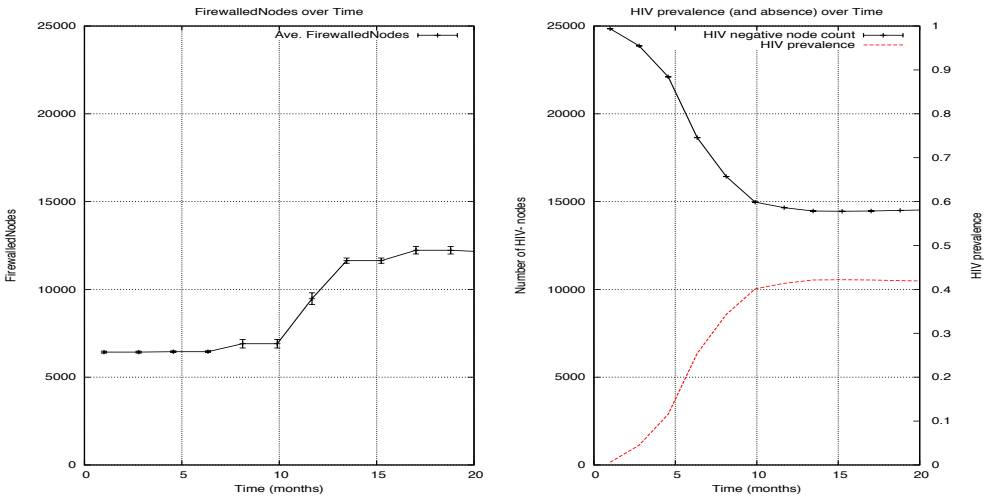

Figure 5.5: The emergent period: firewalled nodes (left); HIV prevalence, number of HIV- individuals (right) in a risk network of 25k nodes

The two quantities discussed above, namely, (a) the number of firewalled nodes (left graph in Figure 5.5), and (b) the number of HIV negative individuals (right graph in Figure 5.5) are the two ingredients which, together, explain the behavior of the Firewall Hypothesis validity measure (see Figure 5.3). To obtain a clearer understanding, however, we must get a sense of "why" these two ingredient quantities behave as they do during the emergent period. Each quantity will be considered in turn. To assist with the exposition, we shall make use of the four graphs in Figure 5.6. Each graph illustrates the dynamic relationship between just two variables, though the reader is advised to bear in mind that all four relationships coexist and operate concurrently.

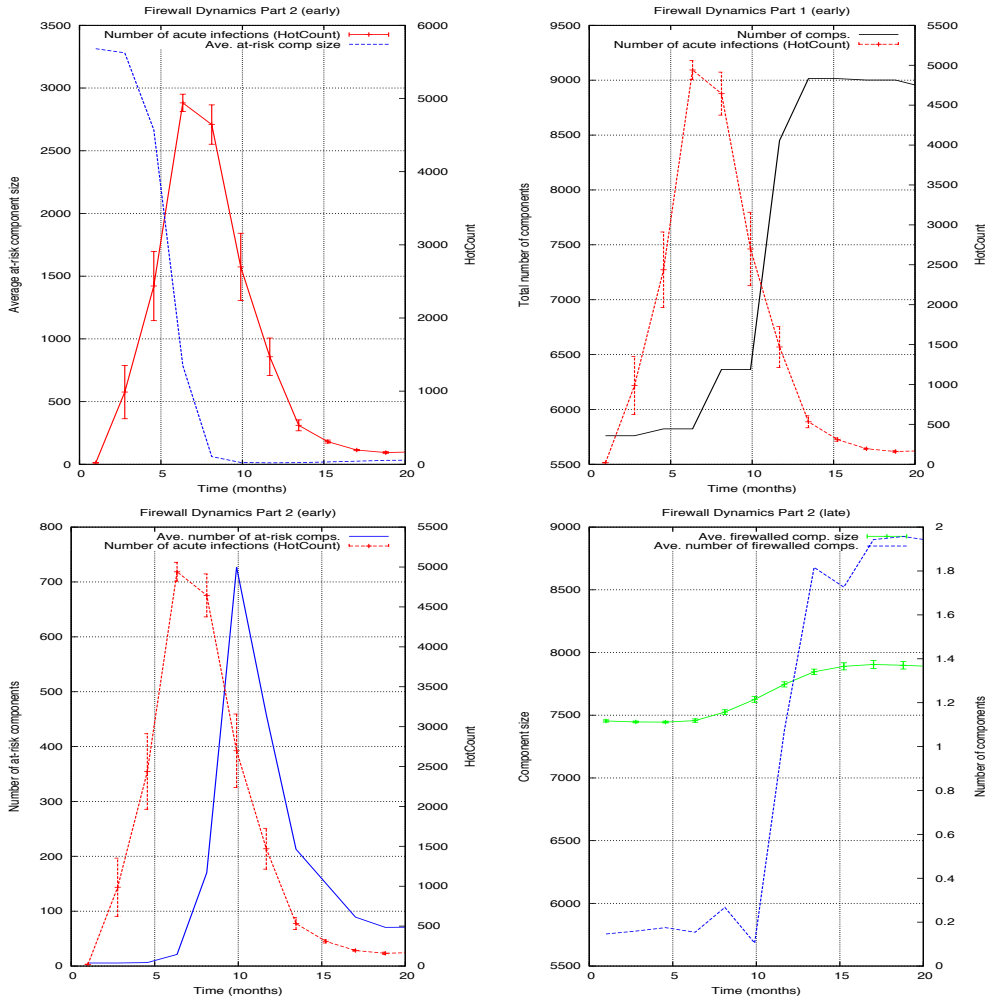

Figure 5.6: The firewall effect during the emergent period.

(a) The number of HIV- individuals. We begin by considering the top left graph in Figure 5.6, which reveals that the number of acute HIV infections (i.e. the "HotCount") rises exponentially from close to 0 to around 5,000 over a brief 6 month initial segment of the emergent period. After rising sharply for 6 months, the number of acute infections begins to decline. To understand why this occurs, we contemplate the second curve in the top left graph, which indicates that the average size of at-risk components decreases sharply from over 3,000 to nearly 1 by month 7 of the emergent period. But to say that the average at-risk component size is small (near 1), is precisely to

say that each acute infection can impact very few HIV negative individuals through transmission. When the ability of acute infections to spread has been mitigated in this way, as it clearly has by month 7, acute infections cease to be able to increase exponentially, and instead begin to decay in number as they transition naturally from acute to chronic phase over time. This explanation is confirmed in the top left graph of Figure 5.6, which indeed shows the decay in the number of acute infections begins at month 7 of the simulation. Note that the number of acute infections does not drop to 0, because even chronic infections have a non-zero probability ($c^{L/H} \cdot p^H > 0$) of transmitting HIV and thereby generating new infections. Thus, we see that the large numbers of chronic infections act as a reservoir of infectiousness, and are responsible for continuing to produce new infections that fail to propagate fully throughout the network (see Hypothesis 3, p. 29). The decline in the number of acute infections immediately explains the trajectory of the number of HIV- individuals (right graph in Figure 5.5).

(b) The number of firewalled nodes. Having described the mechanisms underlying the trajectory of the number of HIV- individuals during the emergent period, we turn our attention to the number of firewalled nodes (left graph in Figure 5.5). To understand the trajectory of this quantity, we begin by considering the top right graph in Figure 5.6. Here we see that three months after the rise in acute HIV infections begins, the number of components (in the virus-centric view of the risk network) begins to rise. The cause for this delayed response is clear: the rise in the number of components begins as acute infections start to transition into the chronic phase, causing individuals to be removed from the virus-centric view and splitting the risk network into components in the process. The increase in number of components (from 5,700 to 9,000) takes longer than the increase in the number acute infections, because not every transition of an HIV+ individual from acute to chronic phase induces a component split in the virus-centric risk network. Indeed, some components succeed in splitting off only when several such transitions have taken place (see e.g. the component containing vertices 1,2,3 in Figures 5.2 and 5.2, which requires two acute infections to transition to chronic before it detaches from the larger component). Regardless, we see that 3,300 new components have arisen, and since each component can always be classified as "firewalled" or "at-risk", it is natural to ask which classification dominates these newly created components. To resolve this, note that since each at-risk component must, by definition, contain at least

one acute HIV infection, a rise and fall in the number of acute HIV infections necessarily precipitates (with a lag of 3 months), a corresponding rise and fall in the number of at-risk components. This reasoned conclusion is confirmed in the bottom left graph of Figure 5.6. Indeed, we see that the number of at-risk components rises and falls, and stabilizes by time 18 months. If the number of at-risk components rises and then falls[3] (bottom left graph), but the total number of components rises (top right graph), then it follows by reasoning alone, that the number of firewalled components must rise. This conclusion is verified by the bottom right graph of Figure 5.6. There we see that the number of firewalled components rises from near 5,700 to near 9,000. In the same time period, the average size of firewalled components stays relatively constant, increasing only slightly from 1.2 to 1.4. Taken together, these last two observations complete the explanation of the trajectory of the number of firewalled nodes (see right graph in Figure 5.5).

5.2.2 Steady period

Next we turn to an exposition of the dynamics of the Firewall Hypothesis validity measure during the steady period, a term we designate for the simulation period post the "hot spike". As before, the hypothesis validity measure is defined as the quotient of (a) the number of firewalled individuals over (b) the number of HIV- individuals. The number of firewalled individuals, which appears in the numerator of the hypothesis validity measure, is seen to decline from 12,000 to 10,000 over the 13+ years of the simulation (see the left graph in Figure 5.7). The number of HIV- individuals, on the other hand, which appears in the denominator of the hypothesis validity measure, is seen to slowly decrease from just under 15,000 to just under 12,000 over the same time period (see the right graph in Figure 5.7).

[3]The fact that the number of at-risk components stabilizes at a higher level than its initial value at time 0 is explained by the fact that there are many more chronic infections at time 18 months than at the outset, and these continue to produce new infections, which while failing to propagate fully throughout the network, do greater numbers of components to be classified as at-risk.

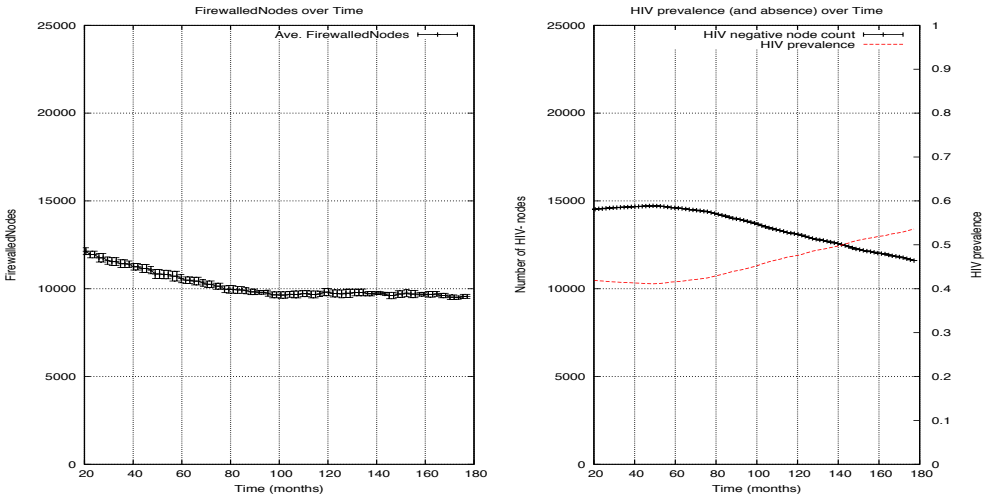

Figure 5.7: The steady period: firewalled nodes (left); HIV prevalence, number of HIV- individuals (right) in a risk network of 25k nodes

To render transparent the mechanisms underlying the trajectories of the number of firewalled individuals and the number of HIV- individuals, we shall make use of the two auxiliary graphs of Figure 5.8, each of which illustrate the dynamic relationship between two variables.

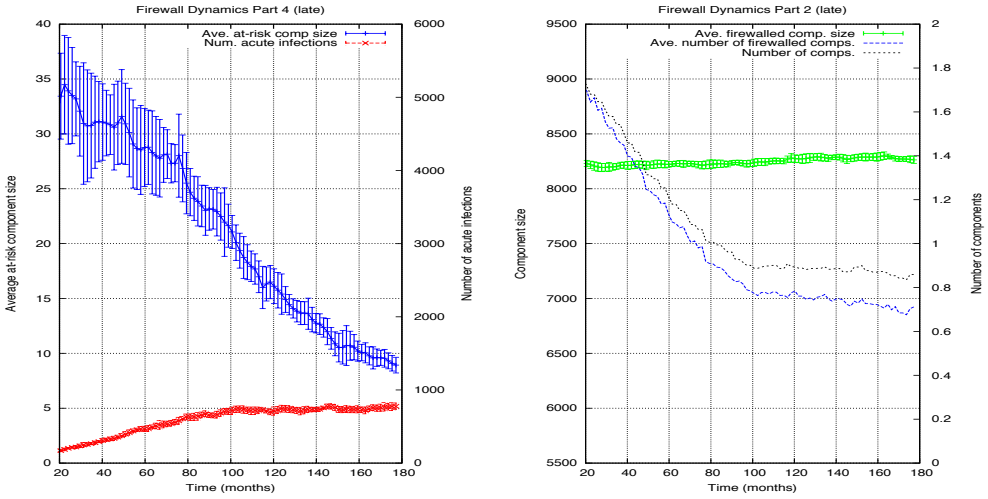

Figure 5.8: The firewall effect in the steady period.

(a) The number of HIV- individuals. The top left graph in Figure 5.8 depicts both the number of acute infections, and the average risk component size over time. The right y-axis of the graph has been made identical to the right y-axis of top left graph in Figure 5.5, so as to provide a sense of the relative scale of number of acute infections across the two periods. As noted earlier, even once the "hot spike" has ended, the the number of acute infections does not drop to 0, because chronic infections have a non-zero probability ($c^{L/H} \cdot p^H > 0$) of transmitting the virus to their HIV- neighbors. In our base SFHR model $c^{L/H} \cdot p^H = 0.05 \times 0.01 = 5 \cdot 10^{-4}$, which while being small is still nonzero, providing a "slow burn" that produces new infections. This slow burn is unable to explode into a "hot spike" precisely because the average risk component size is small (thanks to the previously demonstrated structural side effects of the emergent phase). The slow burn proceeds, driving the mean size of at-risk components lower, which in turn, limits the rate at which acute infections can be generated. The two quantities (number of acute infections and average risk component size) equilibrate over the steady period. Given an understanding of the trajectory of acute infections, we implicitly arrived at an explanation of the trajectory of the number of HIV- individuals, since these two quantities are trivially related (right graph in Figure 5.7): if the number of acute infections stabilizes to a constant non-zero number, then HIV prevalence will increase at a rate proportional to this number.

(b) The number of firewalled nodes. Having described the mechanisms underlying the trajectory of the number of HIV- individuals during the steady period, we turn our attention to the number of firewalled nodes (left graph in Figure 5.7). To understand the trajectory of this quantity, we begin by considering the right graph in Figure 5.8. Here we see that in the first 5 years of the steady period, the total number of components (in the virus-centric view of the risk network) declines from 9,000 components to 7,200, a mere 80% of its starting value. This implies that 1,800 components seemingly vanished, and since each component can always be classified as "firewalled" or "at-risk", it is natural to ask which classification dominates the components which disappeared. The graph shows us that the number of firewalled components experiences a commensurate decline—and hence the components that are destroyed in the first 5 years are in fact almost exclusively firewalled components. How might this happen? The third curve in the graph shows the average size of firewalled components over time. We see that this number

stays fairly steady in the neighborhood of 1.4, implying that a significant of the firewalled components are islets. It is now apparent what is occurring: when firewalled islets become infected by the "slow burn" of adjacent old infections, firewalled components disappear from the virus-centric network.

5.3 Remarks concerning the firewall effect

Given the results of these experiments, some remarks concerning the results of the simulations and the validity of Hypothesis 1 can be enumerated:

- **Hypothesis 1.** The main concern of this project was to determine, in a simulation environment that matched HIV dynamics described for injecting drug user networks in New York City in the early 1980s, whether nodes with mature (i.e. low infectiousness) HIV+ status would divide the network into clusters of uninfected nodes which remained relatively stable over time. As described in this chapter, this appears to be the case for a high percentage of uninfected individuals given the simulation settings derived from the SFHR network. While never 100 percent the case, the "firewall effect" manifests significantly in these cases, and presents an important barrier to HIV infection in risk networks.

- **Scale.** As observed in Chapter 4, small networks (in this case those below 1000 nodes) showed very different network-wide characteristics than what is seen by networks whose size exceeds 1000, where the results appear very uniform across trials. In small networks, the extent of the firewall effect varied considerably between trials, showing again that stochastic factors outweigh structural/node-based behaviors in the determination of simulation outcomes.

- **Time frame.** In considering the mechanics of the firewall effect, we find it helpful to examine the network during two phases of HIV infection: an initial, "emergent" phase of rapid spreading, and a later period of stable HIV rates. Where Chapter 4 noted the enduring presence of new infections that failed to propagate during the stable phase of the

network, we can now see that this is because the structural impact of the emergent phase, during which a significant number of uninfected nodes cluster into small components in the virus-centric view of the network. These small clusters represent margins of the network, and are frequently composed of a few (or even single) individuals. The ability for new infections to spread *across* the network via such an individual is near nil.

Chapter 6

Resilience to variations in the structural model

While the main focus of our analysis concerns the SFHR data set, and models derived thereof, we were concerned that the phenomena of interest—HIV stabilization and the firewall effect—may have been an artifact of the specific network topology of the SFHR data. To test this, we sought out a related but alternative topology, the P90 data produced by the Colorado Springs STI project, also from the early 1990s, and which also centered on the effects of risk events across a network of sex and drug use. Thus, to test the effects of local topology, the experiments of Chapters 4 and 5 were repeated using the demographic and link distribution of the P90 data sets. Those results are presented in this Chapter.

Some important conditions apply to these results however. Because one of the directors of this project served as the ethnographer of the SFHR project (Curtis), we had privileged access and wealth of personal knowledge of the dynamics of the SFHR data set, information that was not as readily available to us for the P90 data. In addition, because one of our concerns was whether an alternative network topology would render similar simulation results (in effect, serving as a test of the resilience of the Firewall and Stabilization conclusions reach for SFHR), we chose to simulate the P90 data using the same network dynamism model that was used in SFHR simulations. This, of

course, renders the results of the P90 simulations discussed here invalid in any direct historical sense. Because the P90 project was more concerned with the risk results of commercial prostitution, and only secondarily with injection use and its risks, the distribution and logic of risk interactions were likely very different from the SFHR data. For this reason, the results presented below should be read as a test of the robustness of the conclusions reached in Chapters 4 and 5 across a related but distinct topology—a topology that none the less is drawn from actual interactions across a risk network—rather than as a representation of the long term trajectory of HIV infection in Colorado Springs. If the latter had been the goal of the P90 simulations, the dynamism parameters would have had to have been completely recalibrated.

The P90 simulations were designed, therefore, to overlap in scale with the SFHR simulations. Simulation runs of 1000, 5k, and 10k nodes were completed in stable, growing, and shrinking environments. In addition, we also ran a series of small network simulations of 500 nodes with the P90 topology, to examine whether the scale-effects shown by the SFHR networks carried over to the P90 network. Scaling effects like these raise serious concerns for the planning of HIV interventions. If small networks exhibit highly unpredictable HIV dynamics, when compared with the narrow distributions of results from networks on the scale of those found in New York City, interventions aimed at smaller cities, such as Colorado Springs, would have to be evaluated on a very different basis than those planned for large urban networks.

The table below summarizes the network sizes at which the SFHR and P90 models were simulated. What follows are the results of P90 simulations in graph form, with the corresponding metric from the SFHR model being indicated as a comparison baseline in red.

network size	SFHR model	P90 model
500		✓
1,000	✓	✓
5,000	✓	✓
10,000	✓	✓
25,000	✓	

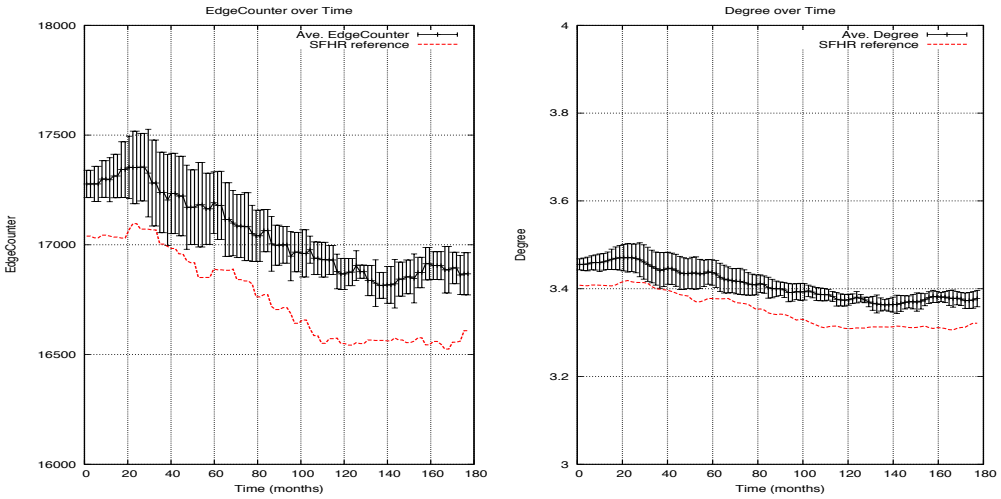

Figure 6.1: Number of edges over time (left) and mean degree (right).

In Figure 6.1, the left graph shows the number of edges in 15-year simulations of ten independently generated 10,000 node networks[1] based on the P90 model. We see that while the P90 degree distribution is shifted higher than it is in the SFHR network, the number of edges remains relatively stable over the course of the simulation. The right graph depicts the average number of risk partnerships per individual over time, a quantity which fluctuates in a narrow band just below 3.4.

6.1 Robustness of stabilization

Figure 6.2 shows the HIV prevalence (over time) in 15-year simulations of ten independently generated 500, 1k, 5k, and 10k, node networks based on the P90 model. We note the effects of scale, whereby the smaller networks (of 1000 or fewer nodes) exhibit much higher variance across simulations and have different stabilization characteristics than the larger networks. Large

[1]Once again, we note that the number of individuals which participate in the network over the in 15 years was closer to $10,000 \times 180/60 = 30,000$, since in-network lifetimes of individuals were on average $\mu_{st} = 60$ months (standard deviation $\sigma_{st} = 48$ months), following the birth/death process is described in detail in Section 2.2.2.

networks (having more than 1000 nodes) whose structural characteristics are governed by the P90 model are seen to exhibit stabilization dynamics that are comparable to SFHR based networks of commensurate size, though small P90-based networks (size 5000 or smaller) tend to stabilize at levels that are about 5% higher than comparable SFHR-based networks.

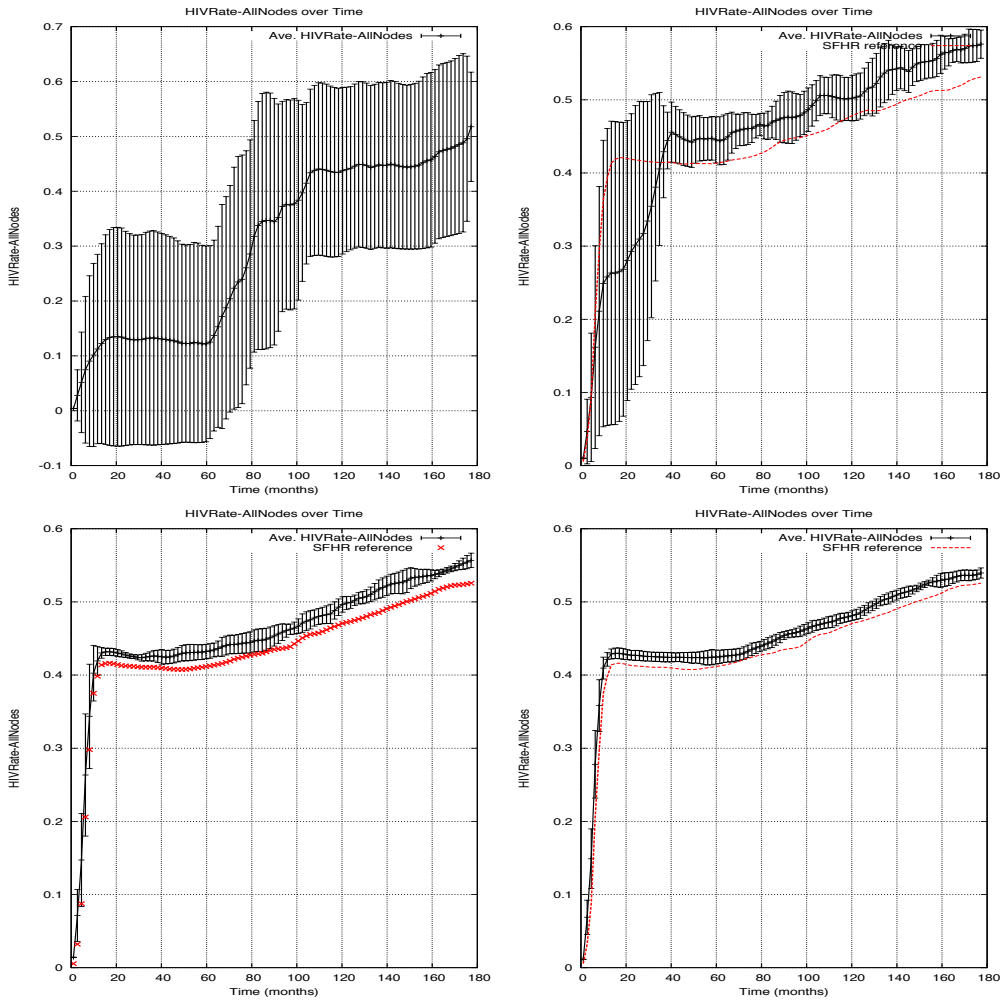

Figure 6.2: HIV prevalence over 15-years, in P90-based risk network of size 500 (top left) 1k (top right) 5k (bottom left) and 10k (bottom right).

While HIV stabilization levels in P90-based networks were comparable (or marginally higher) than those in their SFHR-based analogues, Figure 6.3 below shows that, for small networks (of sizes <10,000), removing HIV positive nodes whose infections have reached the chronic stage of low transmissibility shatters the P90-based network into fewer components than SFHR-based network of comparable size. This implies that the average size of each of these potentially at-risk components is necessarily larger.

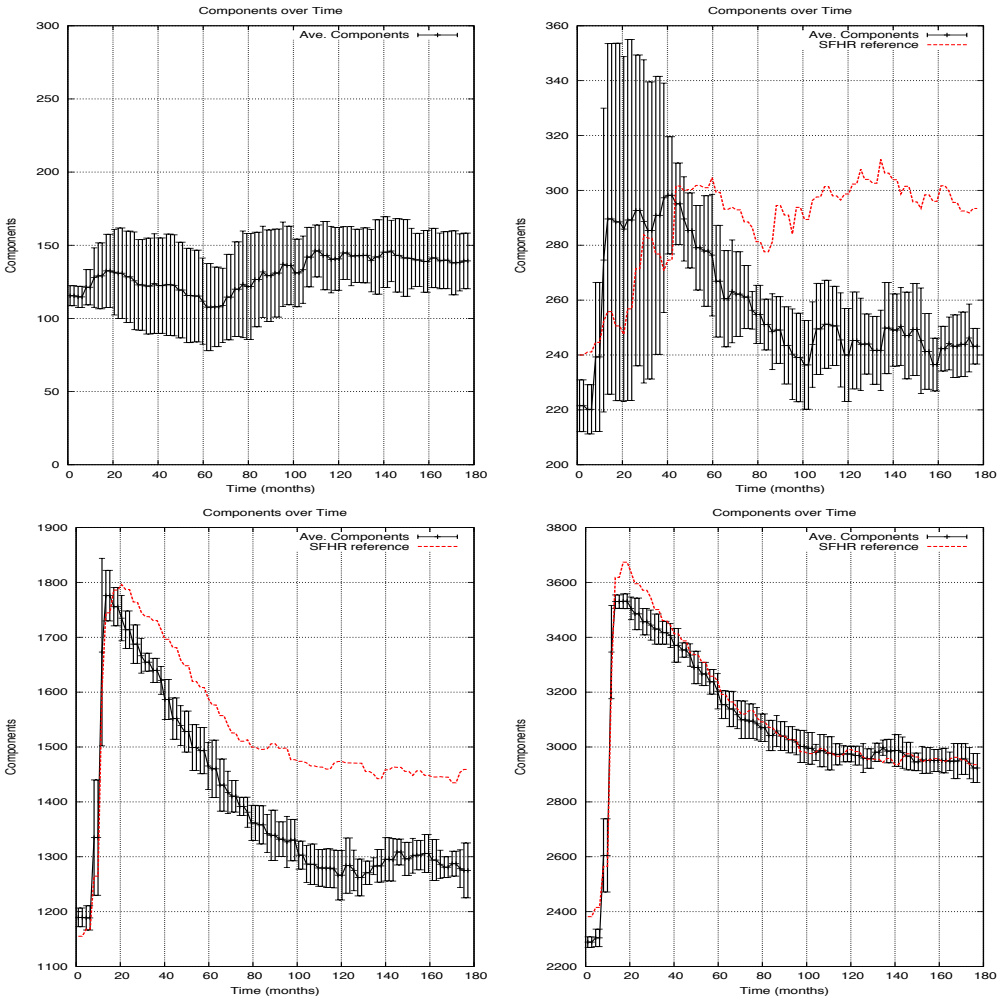

Figure 6.3: Average number of components over 15-years, in a P90-based risk network of size 500 (top left) 1k (top right) 5k (bottom left) and 10k (bottom right).

6.2 Robustness of firewalling

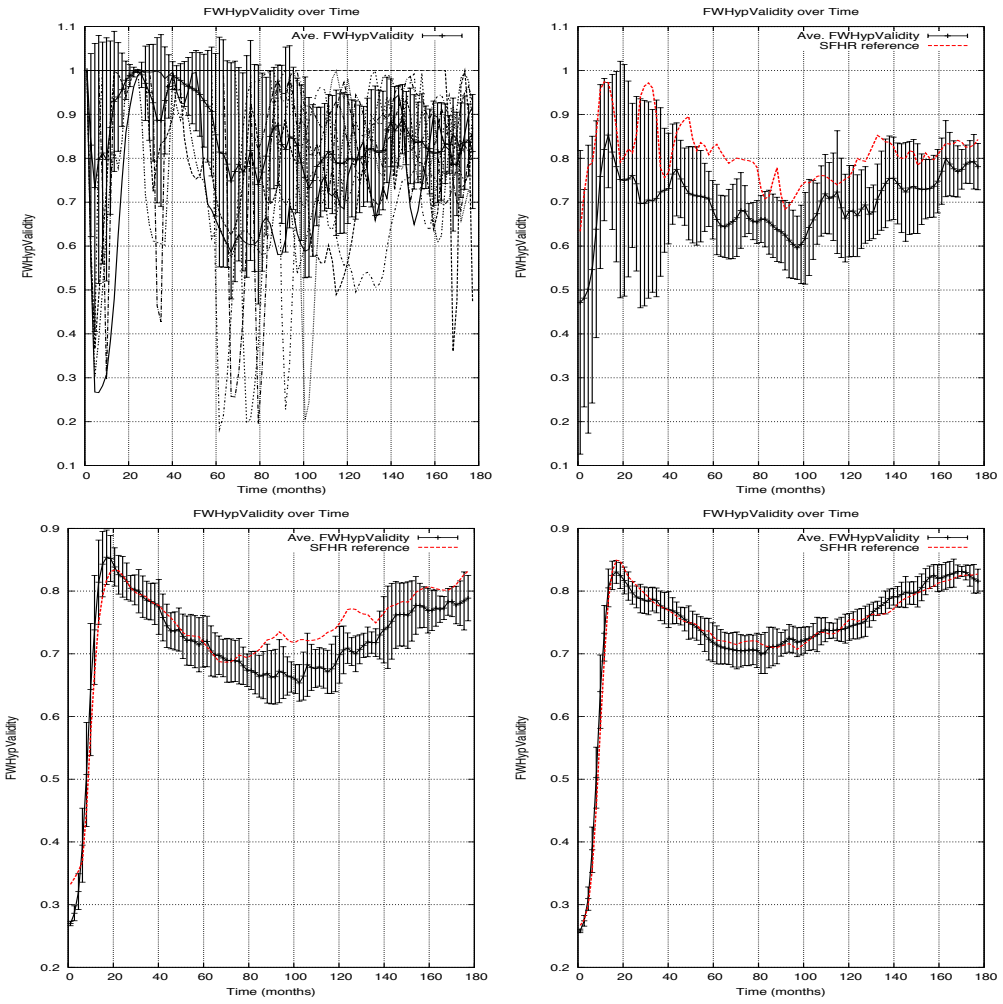

Figure 6.4: Firewall hypothesis validity in P90-based risk networks of size 5k (left) and 10k (right).

Having seen that smaller-scale networks derived from the P90 model tend to converge to structures in which components (post deletion of old infections) are larger than in comparably sized networks based on the SFHR model, virus outbreaks can travel farther in these networks, firewalling effects are necessarily less pronounced, and hence less central to explaining sub-saturation

in these networks. This claim is verified in Figure 6.4, which shows that in small P90 based networks, the variability in Firewall Hypothesis validity is high, and remains below values exhibited by SFHR-based networks (see especially, the top right graph, depicting the metric for simulations of 1000 node networks). We conclude that old infections play a lesser role in the stabilization dynamics of small networks based on P90 networks, making them more vulnerable to outbreaks of the virus than SFHR.

Knowing this, we can answer the question raised at the outset of this chapter: does the specific local topology—the pattern of connections and connection preferences—influence the validity of the conclusions reached in Chapters 4 and 5? The answer would appear to be a qualified yes. From Figures 6.2 and 6.4, it appears that local topology does play a role in the stabilization dynamics and the ability of the firewall effect to account for those dynamics. The impact may be small (a few percentage points) but nonetheless seems to fall regularly outside of the results predicted by multiple runs of the SFHR model used here. This seems particularly true at small network sizes, which we have already seen to be vulnerable to stochastic factors. The results here show that such questions of scale apply across distinct topologies, providing further evidence of the variability of IDU network dynamics as small scales.

Chapter 7

Resilience to variations in the dynamism model

As above, the parameters for the SFHR simulation were set in accordance with both published material on the project, a review of related research results from projects concerned with IDU community dynamics, and extensive conversations with the SFHR researchers and other researchers of drug-using-communities in New York. The parameters chosen for the test runs discussed in Chapters 4 and 5 reflect the results of those settings.

An important concern for the current project, and one of the central virtues of simulation, is the ability to test the limits of the parameter space over which the phenomena of interest—HIV stabilization and the firewall effect—hold. Towards this, we sought to understand how variations in the settings of individual parameters would affect both the firewall effect seen in the multi-scale simulation runs, and the HIV rate stabilization seen in the networks over simulation time.

To determine this, each of the parameters was systematically varied both above and below the standard settings used in Chapters 4 and 5. The results are presented here in graph form, with the standard setting indicated in red as a baseline for comparison. Because the network of 10k nodes exhibited near identical dynamic characteristics as graphs both larger and smaller, and

because network growth or shrinkage seemed to have little effect on graphs of this size, the 10k steady population simulation was chosen as the basis for comparison, and all of the simulation runs depicted in this chapter similarly feature 10k nodes in a non-growth/non-shrinking environment.

The effects of parameter variation are sometimes great, sometimes small. In effect they represent the sensitivity of the HIV stabilization and the firewall effect to singular changes in network dynamism, which, we feel, represent a novel way to strategize future interventions. If, for example, we find that changes in network churn (the rate at which people change risk partners) exerts less of an influence on the ability of the network to stabilize, or raises/lower the overall infection rate less significantly than does, say, the effect of greater/lower infectiousness, then intervention strategies can be crafted that attempt to maximize their own effectiveness by targeting one element of dynamism (infectiousness) rather than another (churn). While the mapping that follows does not test specific interventions, it does intend to produce a view of network dynamism that is itself plastic, and sensitive to changes in what are essentially changeable behavioral or epidemiological factors. A full test of specific interventions is possible in a simulation environment such as this, but awaits future collaboration with those engaged directly in their design and implementation.

7.1 Mapping risk process influence

We begin by considering variations in the risk process and their impact on network dynamics exhibited. The risk process and its parameterization was described at length in Section 2.2.1 (p. 55). We shall focus on the effects of changes in the intensity of the risk process, as well as impacts on pathogen dynamics via changes to the maximum transmission probability (i.e. the probability of transmission during a single risk act in the highly infectious period).

7.1.1 The impact of variations in risk process intensity

The following parameters of the risk process (see Section 2.2.1 on p. 55) are of interest:

- μ_j^R: Mean time between inter layer j risk impulses (in months) normalized by the individual's layer j ego network size.
- σ_j^R: Standard deviation of inter layer j risk impulse times (in months) normalized by the individual's layer j ego network size.
- p_j^H: Layer j transmission probability during infectious period (between 0 and 1). Fixed in these experiments, at 0.05.
- $c_j^{L/H}$: Reduction in transmission probability post infectious period (between 0 and 1). Fixed in these experiments, at 10^{-2}.
- Duration of infectious period was fixed in these experiments, at 3 months.

Since we only consider one layer in our network for these simulations, we will drop the j subscript, taking μ^R, σ^R, p^H, and $c^{L/H}$ as our parameters. Of these, the following parameters were varied in the experiments that follow.

Scenario	μ^R	σ^R
1	0.1	0.1
2	0.5	0.5
standard	1	1
3	2	2
4	5	5

In effect, these experiments amount to varying the rate at which individual nodes engage in risk events with their network neighbors. As above, the

numbers in table above represent the number of months (on average) required for a node to participate in a number of risk events equal to the number of his/her network neighbors. The remaining settings are taken from the base SFHR model (see p. 84) extended by the standard dynamism model parameters (Section 3.5, p. 90). The standard settings for risk is a factor of 1, meaning that on average a node engages in a number of risk events each month equal to his/her degree. Changing the risk parameter to 0.1, for example, would mean that an individual engages in a risk event equal to the number of neighbors he/she has every 0.1 months (or roughly every 3 days, on average). Thus in this case, risk parameter settings lower than 1 indicate simulations of highly active risk behaviors, while those greater than 1 represent networks in which risk events are more rare. In each case, recall that each individual node draws an individual risk rate designated by the mean and standard deviation described by these parameters. Individual node risk rates can thus vary considerably across the population. What we seek to examine here is the effect of varying the mean (and proportional deviations from that mean). In every case, however, considerable (relative) variation between node behaviors occurs.

Not surprisingly, Figure 7.1 shows clearly that the level of mean average risk behavior has a tremendous impact on overall network HIV rates. Where risk rates are 10 times higher than the standard setting (top left), HIV prevalence quickly rises to 70% of the network, and gradually approach 80%. By contrast, in situations where risk rates are 1/5th the rate of the standard model, HIV rates overall remain far lower, approaching 15% only after 10 years of network-based transmission. Perhaps the most interesting are the two graphs closest to the standard settings. Where risk rates are twice the standard rate (top right), HIV rates increase by roughly 60%; where rates are half the standard, HIV rates decline by approximately 40%. We note that in all cases except those involving the lowest risk settings, HIV rates continue to stabilize at sub-saturation levels, though it appears that the level at which it stabilizes bears a strong relationship to the average rate of risk exhibited by network members.

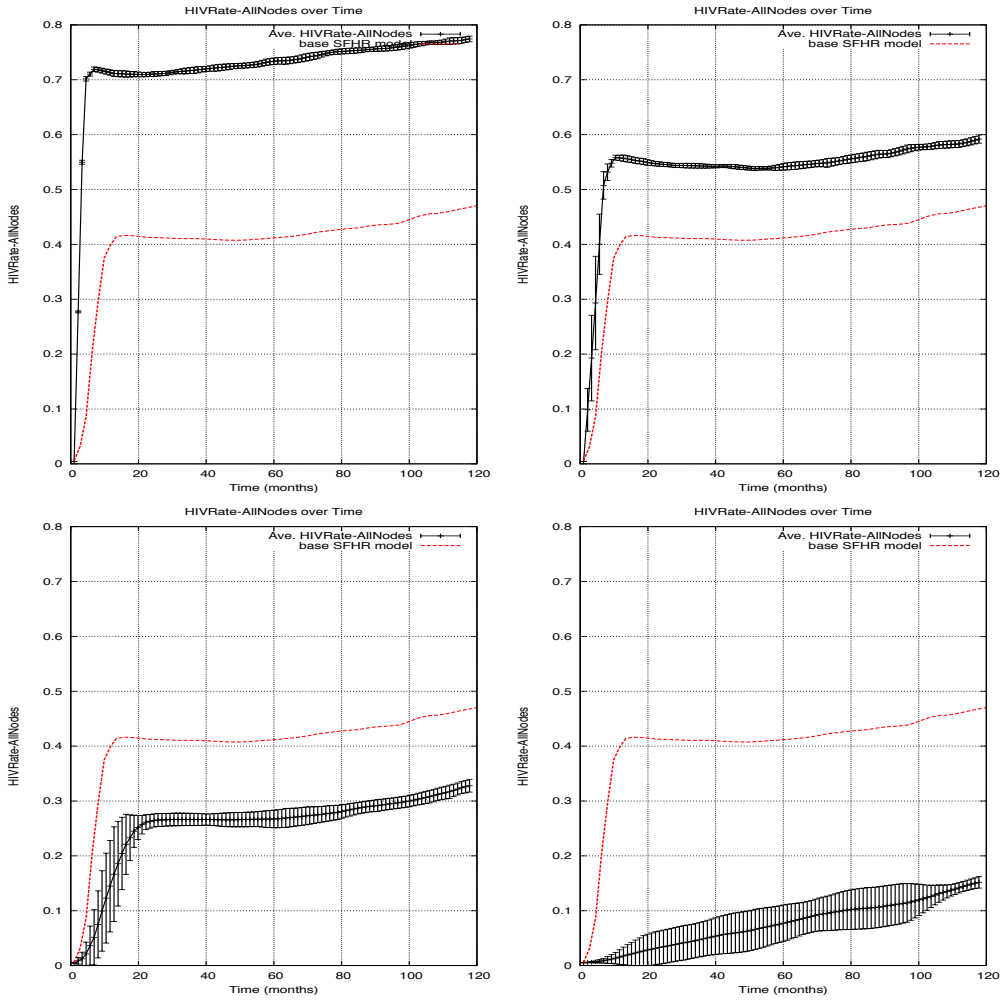

Figure 7.1: HIV prevalence over 10 years, in a risk network of size 10,000 nodes with mean normalized risk interval 0.1 (top left), 0.5 (top right), 2.0 (bottom left), and 5.0 months (bottom right).

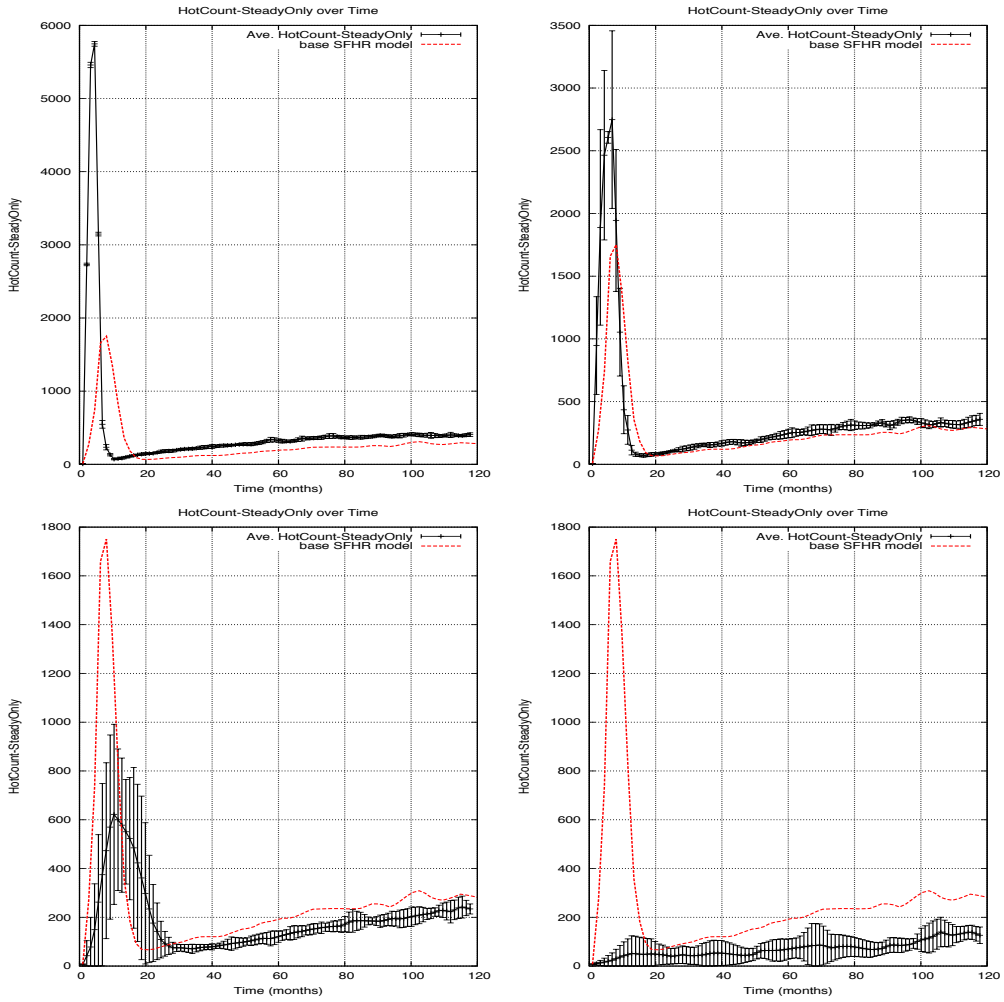

Figure 7.2: Highly infectious steady nodes over 10 years, in a risk network of size 10,000 nodes with mean normalized risk interval 0.1 (top left), 0.5 (top right), 2.0 (bottom left), and 5.0 months (bottom right).

In Figure 7.2 we see the impact of rates of risk, on the number of highly infectious individuals in the network. In particular, we can see the effect of varying risk rates on the "hot spike" which is expected in the emergent phase of the simulation. In essence, one effect of raising or lowering risk rates is a direct impact on the height of the spike, with very low rates of risk resulting in the elimination of the initial emergent period of rapid epidemic spread altogether (bottom right).

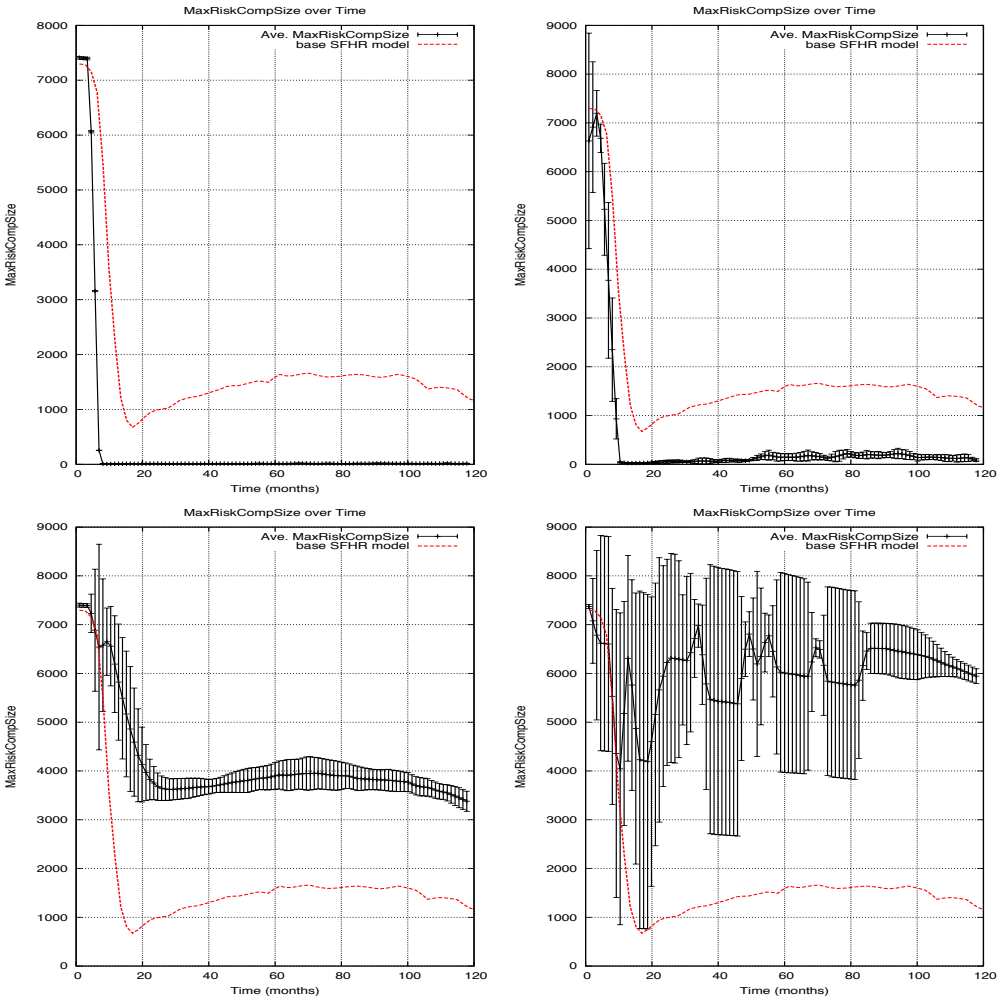

Figure 7.3: Maximum risk component size over 10 years, in a risk network of size 10,000 nodes with mean normalized risk interval 0.1 (top left), 0.5 (top right), 2.0 (bottom left), and 5.0 months (bottom right).

Figure 7.3 shows the size of the largest "at-risk" component—that is, the size of largest cluster of interconnected uninfected nodes that *does* contain a node in a state of high infectiousness. This is, in effect, a measure of how many nodes remain at risk of potential epidemic spreading, should that infection begin to spread (as it is likely to do, give the high state of infectiousness for 3 months). Where risk rates are high (top left), the early onset of the epidemic in the beginning of the simulation means that after a very short

time, few uninfected nodes remain within such a risk component. On the other hand, in both cases where risk was set to rates lower than the standard setting (bottom row), the number of nodes who remain at-risk is very high (somewhere between 40 and 60% of the total number of nodes in the network). Indeed the high variability in the lowest risk rate setting (bottom right), as demonstrated by the long variation bars across most of the simulation, show that high numbers of at-risk nodes creates a situation where stochastic factors can greatly influence overall risk level of the network in very short periods of time.

Figure 7.4 shows the validity of the firewall hypothesis (as discussed in Chapter 5) in scenarios in which the mean rate of risk events per node is varied. At the extreme ends of the parameter space, we see widely varying results. In situations of high rates of overall risk, the firewall hypothesis seems well established, likely as a result of the rapid burn-through of infection caused by the epidemic spreading at the emergent phase of the simulation. In comparison with the standard rate (dotted line), the validity of the hypothesis is considerably higher, meaning that at high rates of risk, a greater number of uninfected nodes will owe their status to the presence of neighbors with older infections who dominate transmission paths from new infections. At the other extreme, in situations of very low risk, we see a situation similar to that discussed for the effect of risk rates on the size of the largest risk component. Here, a low percentage of the network owes its HIV negative status to the effect of older infections blocking possible transmission routes.

Overall, the impact of the firewall effect would seem to be continuous across the range of the parameter space explored here, with higher rates of risk (top right) indicating a greater "firewall effect" and lower rates of risk indicating (lower left) a lower "firewall effect". And finally, as was discussed above, in situations of very low risk activity (bottom right), stochastic variations from one trial to the next seem to dominate. This is indicated in the wide variation bars in the graph. In essence, this phenomenon points to a problematic situation relatively unanticipated in the HIV / IDU literature—that situations of low risk seem to open networks up to stochastic factors, and thus to conditions where contingency makes it difficult to predict the impact of local events on the network as a whole. This, interestingly, is similar to what was found for effects of small scale on network behavior, and overall the susceptibility of small networks to random events.

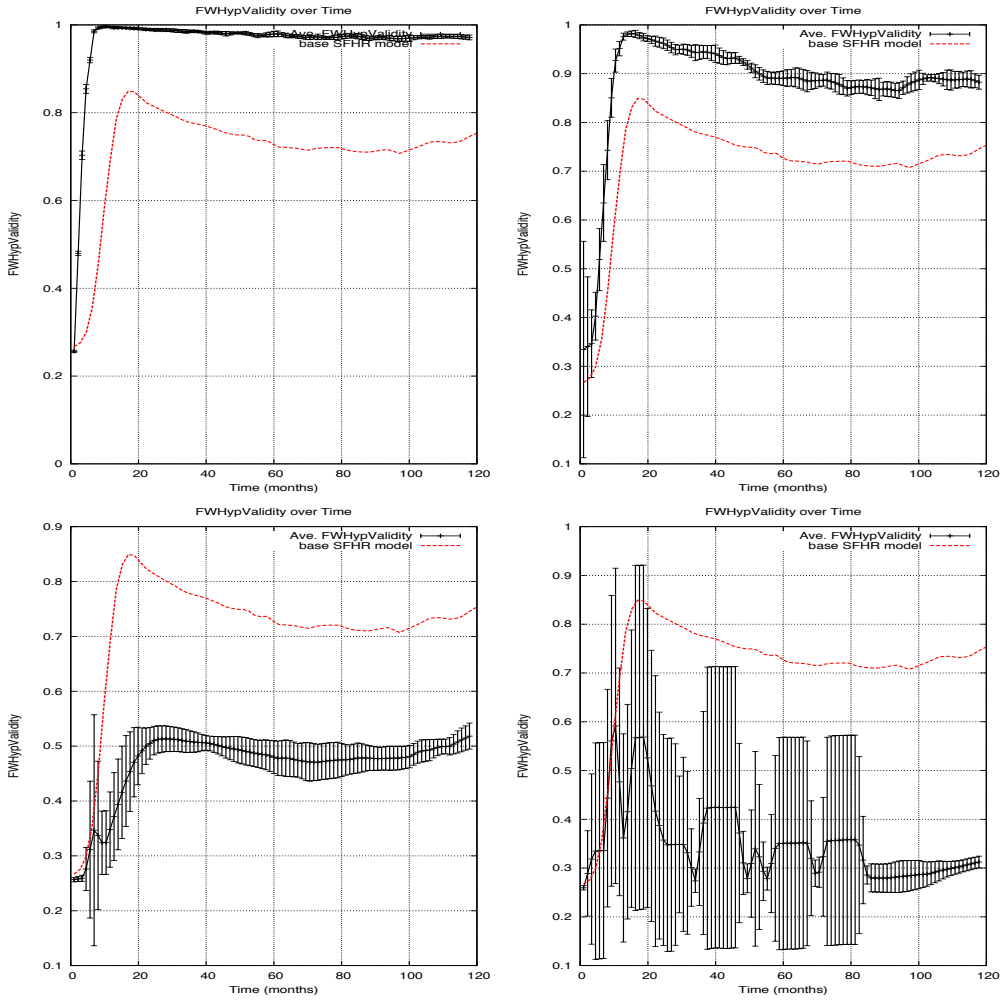

Figure 7.4: Firewall hypothesis validity over 10 years, in a risk network of size 10,000 nodes with mean normalized risk interval 0.1 (top left), 0.5 (top right), 2.0 (bottom left), and 5.0 months (bottom right).

7.1.2 The impact of viral transmission probability

The following parameters of the risk process (see Section 2.2.1 on p. 55) are of interest:

- p_j^H: Layer j transmission probability during infectious period (between 0 and 1).
- $c_j^{L/H}$: Reduction in transmission probability post infectious period (between 0 and 1).
- Duration of infectious period: 3 months.
- μ_j^R: Mean time between inter layer j risk impulses (in months). Fixed in these experiments, at 1 month.
- σ_j^R: Standard deviation of inter layer j risk impulse times (in months). Fixed in these experiments, at 1 moth.

Since we only consider one layer in our network for these simulations, we will drop the j subscript, taking p^H, and $c^{L/H}$, μ^R, σ^R, as our parameters. Of these, the following parameters were varied in the experiments that follow.

Scenario	p^H	$c^{L/H} \cdot p^H$	Initial HIV rate
1	0.001	$0.01 \cdot 10^{-2}$	0.5%
2	0.01	$0.01 \cdot 10^{-2}$	0.5%
3	0.02	$0.02 \cdot 10^{-2}$	0.5%
standard	0.05	$0.05 \cdot 10^{-2}$	0.5%
4	0.10	$0.05 \cdot 10^{-2}$	0.5%

The remaining parameters and distributions were taken from the SFHR structural model (see p. 84) extended by the standard dynamism model parameters (Section 3.5, p. 90). As mentioned in the discussion of the original simulation parameter settings (see p. 84), maximum transmission likelihood is unique among the simulation settings in having no "real world" counterpart from which to derive a standard simulation parameter setting. In short, we have very little way of knowing what the mean likelihood of risk of infection is for an average risk event. Thus, while the other network dynamism settings were based on SFHR project data or related sources, this parameter was set such that the network achieved stabilization at a level approximating that of the SFHR network at the time of the study (roughly 45%), while all other dynamism model parameters were set to "real world" values. For this reason, the sensitivity of the simulation results to variations in the maximum transmission probability were of particular interest.

From the graphs in Figure 7.5 it is clear that varying the rate at which HIV is transmitted during periods of peak infectiousness has important results on both the overall rate of network infection, and on the stabilization potential of the network. At levels well below (1/50th) our standard level of infectiousness, the virus fails to spread at all, even across mulitiple, multi-year simulations; while at a level twice the infectiousness of our standard, the rate stabilizes more quickly and a higher level. Through multiple trials (including many not shown here), infectiousness levels of 0.01 (1/5th of the standard used in Chapters 4 and 5 and shown here at top right), showed high variability in the spread of the virus, here visble in the wide distribution bars seen throughout the 10 years of simulation time. At this setting network infection dynamics related to the spread of the virus are highly unstable. In addition, at this level of infectino risk, the overall network infection rate did not stabilize, even in much longer simulation runs of 40-50 years. From this, we speculate that, for the topology presented by the SFHR network and for a set of given level of overall aggregate risk behavior, the subsaturation stabilization phenomenon is specific to a level of infectiousness. As such, even where stabilization and firewalling are apparent, it remains possible that changes in the likelihood of infection (for a given risk event) can have serious effects on overall network infection levels.

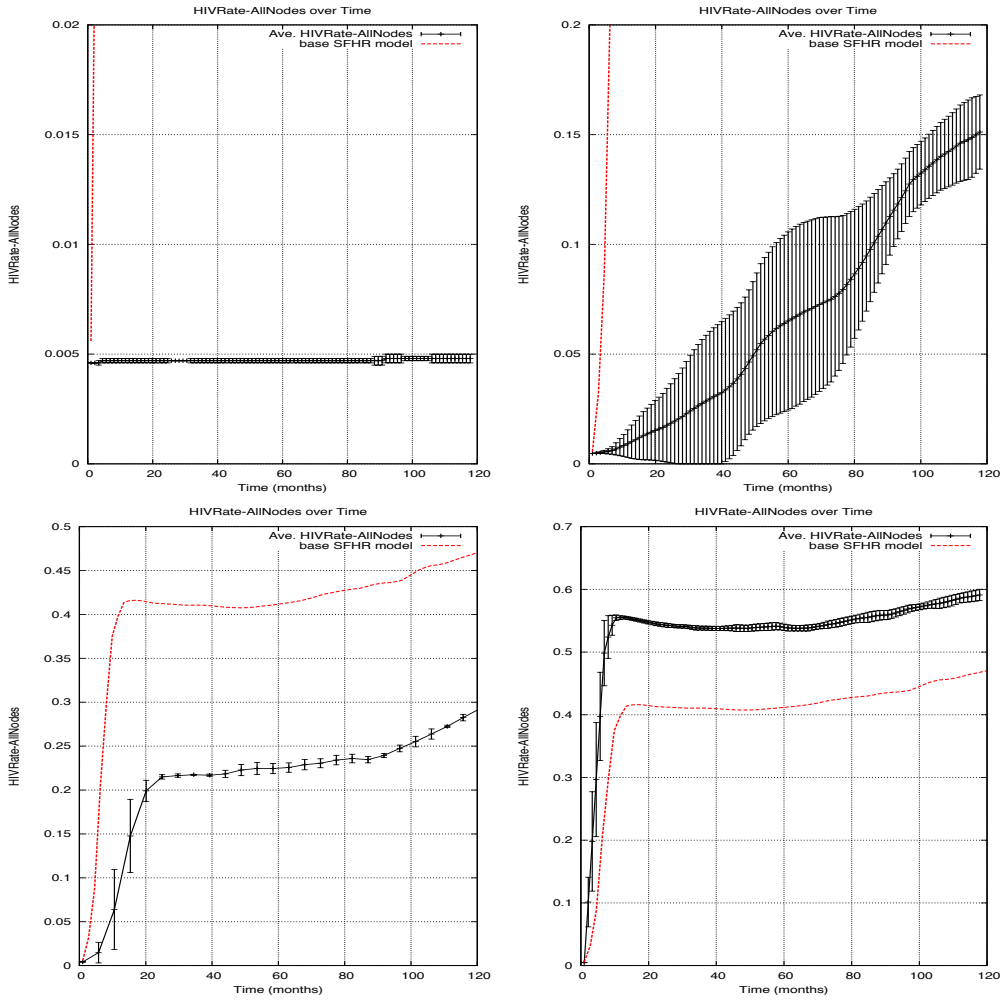

Figure 7.5: HIV prevalence over 10 years, in a risk network of size 10,000 with transmission risk during high infectiousness 0.001 (top left), 0.01 (top right), 0.02 (bottom left), and 0.10 (bottom right).

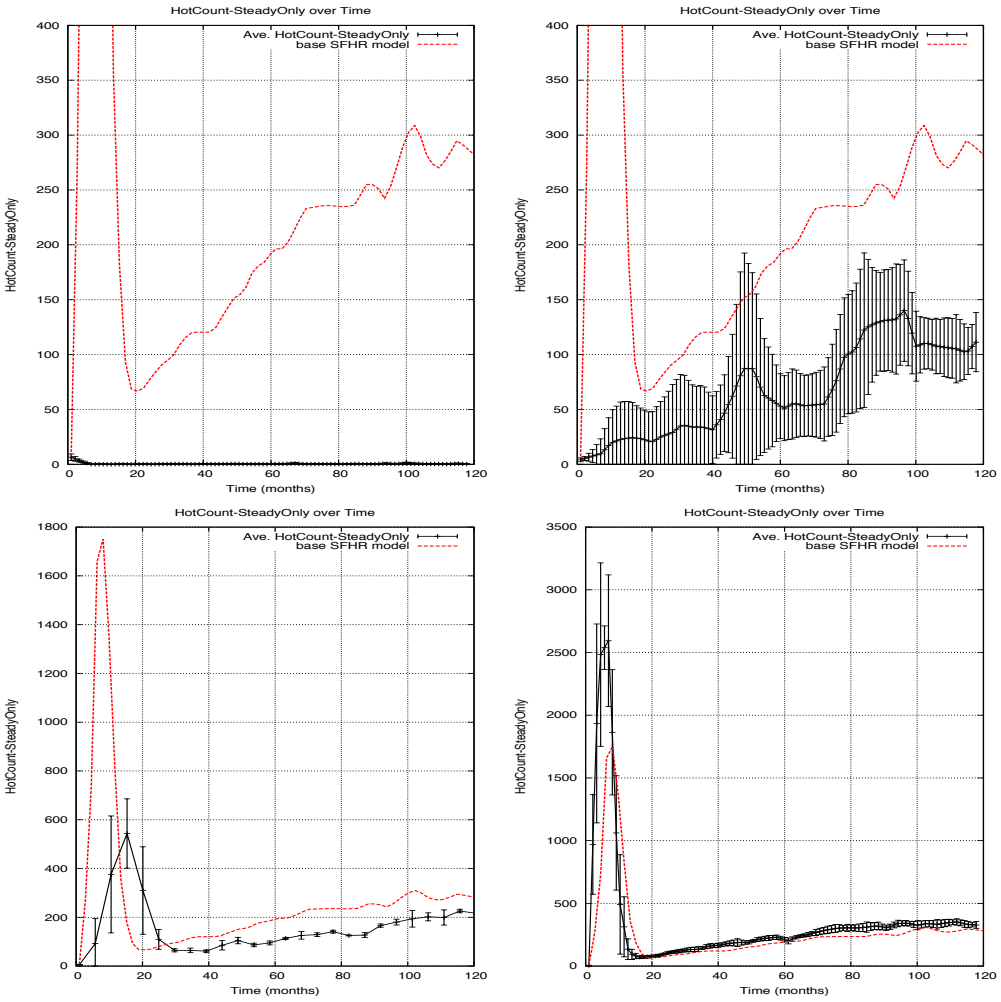

Figure 7.6: The number of highly infectious nodes over 10 years, in a risk network of size 10,000 with transmission risk during high infectiousness 0.001 (top left), 0.01 (top right), 0.02 (bottom left), and 0.10 (bottom right).

While the results in Figure 7.6 are perhaps not, overall, surprising, the dynamics of high levels of infectiousness (bottom right) deserve comment. Where the number of highly infectious individuals is uniformly lower in the other three variations of the standard setting (where all are based on lower levels of infectiousness), the simulation of high infectiousness shows a higher "hot spike", but stabilizes at a number of highly infectious nodes similar to the number in the standard runs (where the infectiousness rate was 1/5th

the level shown here). We note that this stabilization represents long periods in which the rate at which new infections are being generated is relatively constant, here at a level that seems robust to the likelihood of infection of a given risk event, provided that level of risk is above that required for overall network HIV rate stabilization.

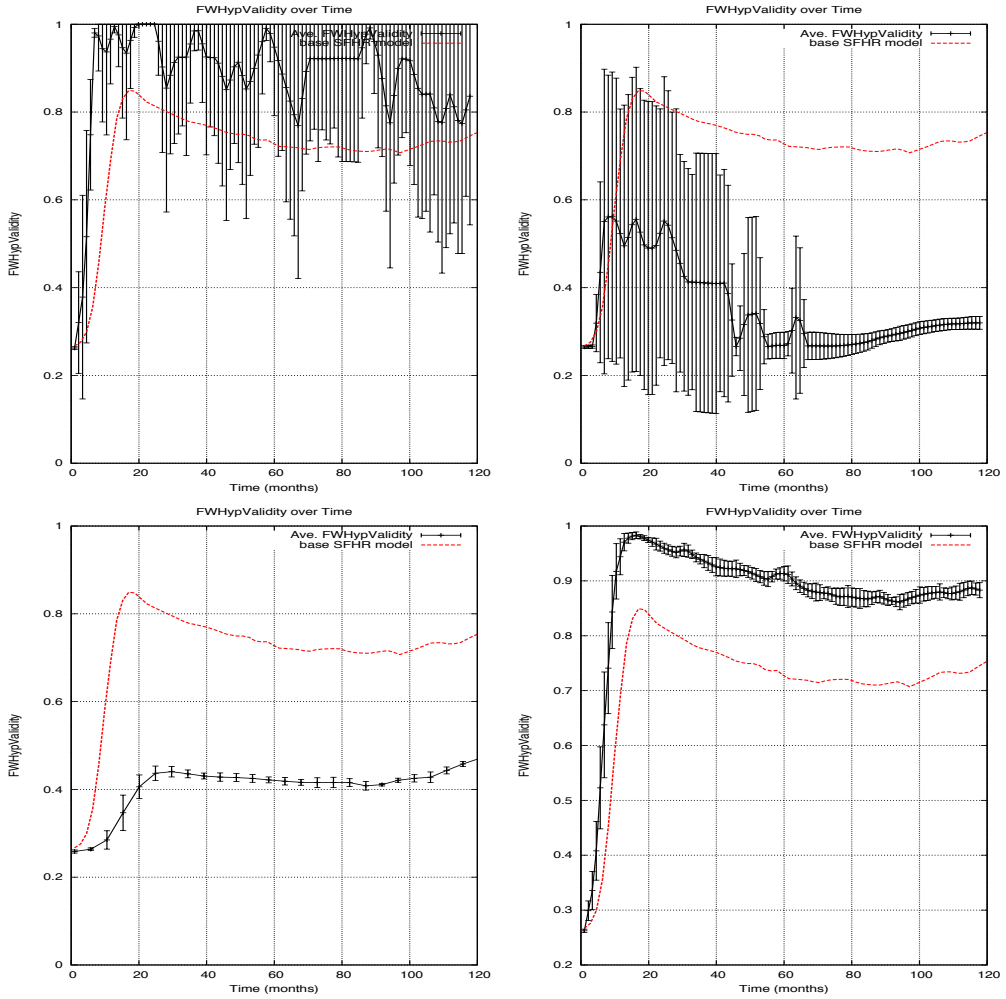

Figure 7.7: Firewall hypothesis validity over 10 years, in a risk network of size 10,000 with transmission risk during high infectiousness 0.001 (top left), 0.01 (top right), 0.02 (bottom left), and 0.10 (bottom right).

In Figure 7.7, a diversity of results are apparent. At very low levels of infection, where extremely few new infections appear, the firewall hypothesis seems highly supported. This, however, is liklye a "red herring": where no infections exist, the network as a whole is, by definition "firewalled". On the other hand, the graphs simulating low infectiousness, show that fewer unifected nodes owe their "status" to the presence of old infections blocking routes of virus spreading from newly infected individuals. On the other hand, in the high infectiousness scenario (bottom right), the firewall hypothesis accounts for a higher percentage of uninfected nodes than it does at the standard level used in Chapter 5.

7.2 Mapping population process influence

We continue by considering variations in the population process and their impact on network dynamics exhibited. The population process and its parameterization was described at length in Section 2.2.2 (p. 64). We shall focus on the effects of changes in two parameters: the extent to which transient individuals are present in the network, and the distribution of individual lifetimes within the risk network.

7.2.1 The impact of the presence of transients

The following parameters of the population process (see Section 2.2.2 on p. 64) are of interest:

- f_{tr}: Fraction of individuals that are "transient" (between 0 and 1).
- μ_{tr}: Mean duration of transients' lifetimes (in months). Fixed in these experiments, at 3 days.
- σ_{tr}: Standard deviation of transients' lifetimes (in months). Fixed in these experiments, at 1/3 day.
- μ_{st}: Mean duration of steadies' lifetimes (in months). Fixed in these experiments, at 5 years.
- σ_{st}: Standard deviation of steadies' lifetimes (in months). Fixed in these experiments, at 6 years.

Of these, the following parameters were varied in the experiments that follow.

Scenario	f_{tr}	Transients %	Steady %
standard	0.0	0%	100%
1	0.001	0.1%	99.9%
3	0.02	1%	99%
4	0.05	5%	95%
5	0.10	10%	90%

The remaining parameters and distributions were taken from the SFHR structural model (see p. 84) extended by the standard dynamism model parameters (Section 3.5, p. 90). In the standard model, no transients were included in the simulation. Our purpose here is to examine the impact of short-term network members/visitors such as might occur in drug-market zones.

From Figure 7.8 it is readily clear that even a low number of transient participants in an IDU network can have a serious impact on the overall HIV rate. While overall network stabilization remains, even low numbers of transient participants engaging in risk behaviors with long-term network members increases HIV to levels approaching saturation. It has long been expected that transient visitors posed a risk of infection from IDU communities to the general public. What seems clear in these graphs, at least in so far as they capture the dynamics of ongoing in drug market areas, is the role transient visitor/users play in increasing rates of HIV infection within these same networks.

Figure 7.9 shows the largest remaining component of the graph absent a newly infected node once those nodes with older infections (and their connections) have been removed. In all but the 1st case (top left, with the lowest percentage of transient participants), the comparison line (dotted) from the standard 10k tests of Chapter 4 and 5 are completely out of scale and not visible on the graph. Here, it is clear that the presence of transients (and the number of infections they generate) shatter the virus-centric view of the network into very small and scattered groups of HIV negative nodes with little or no connections among them.

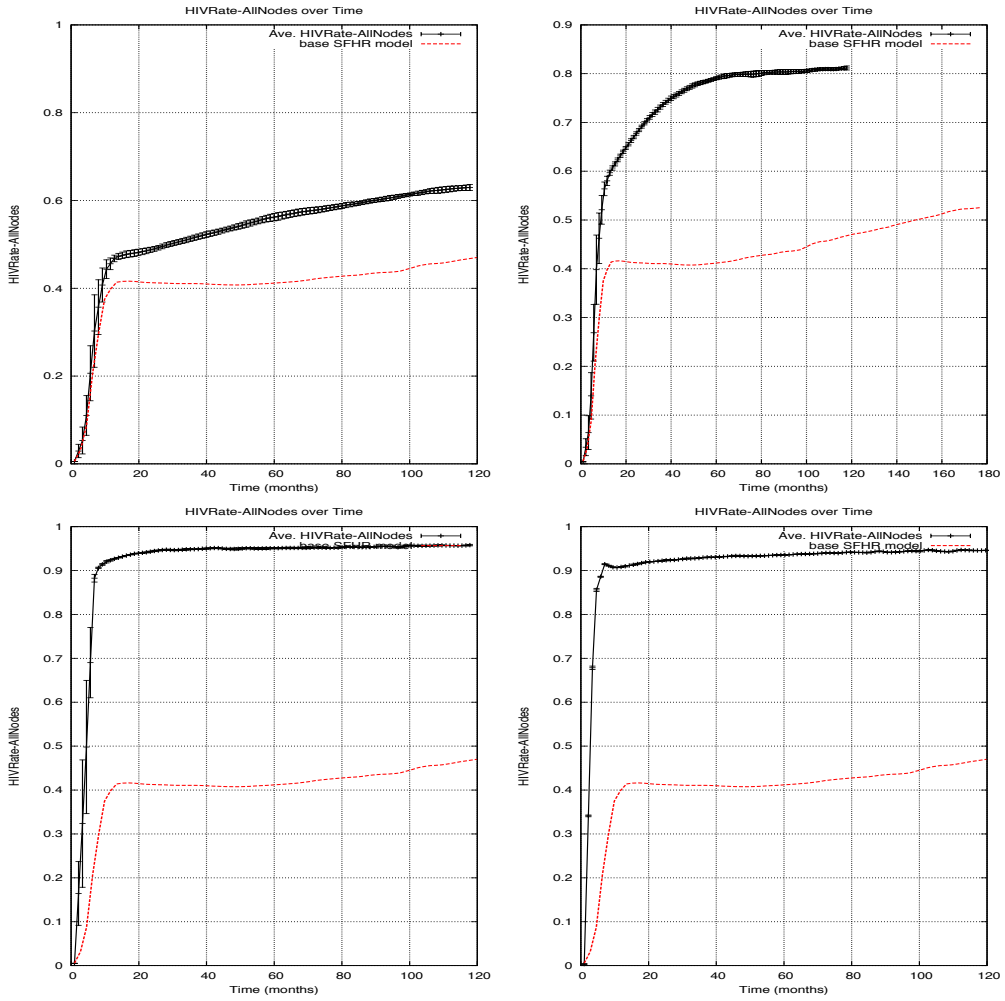

Figure 7.8: HIV prevalence over 10 years, in a risk network of 10,000 nodes with 0% (top left), 2% (top right), 5% (bottom left), and 10% transients (bottom right).

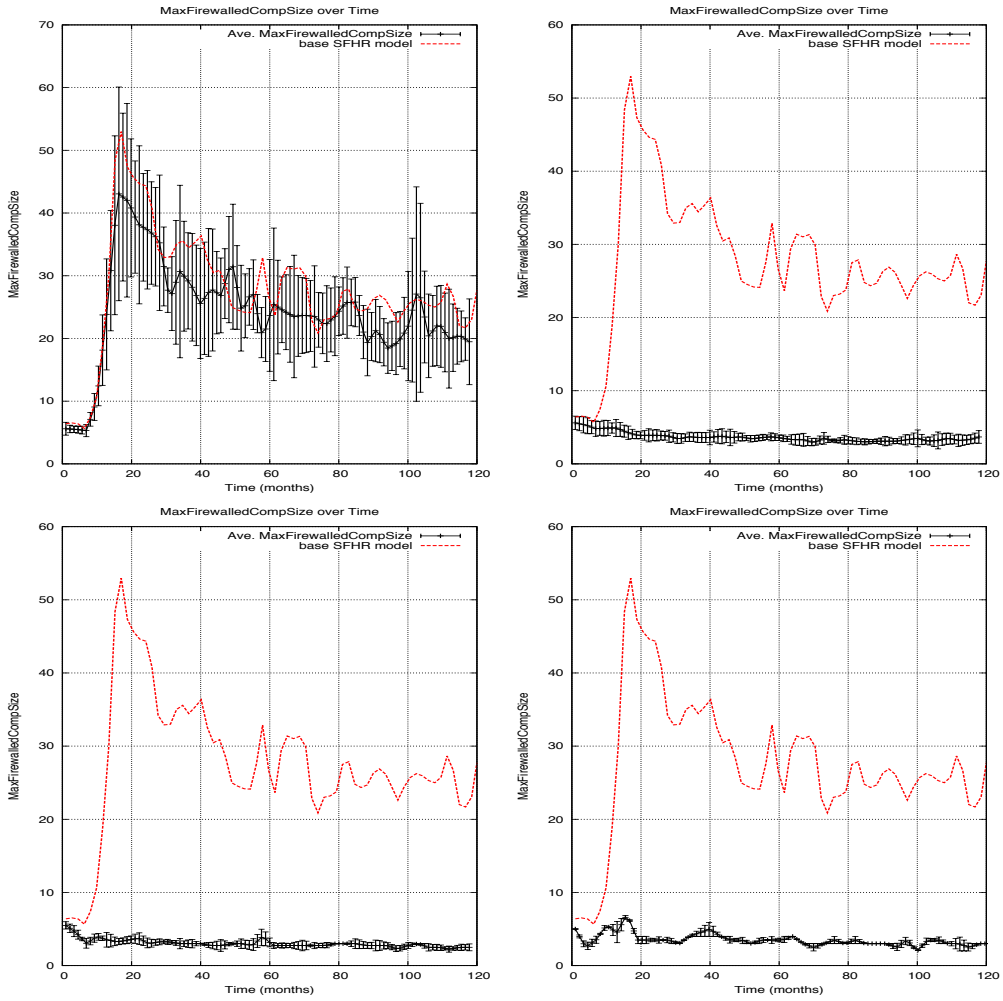

Figure 7.9: Maximum firewalled component size over 10 years, in a risk network of 10,000 nodes with 0% (top left), 2% (top right), 5% (bottom left), and 10% transients (bottom right).

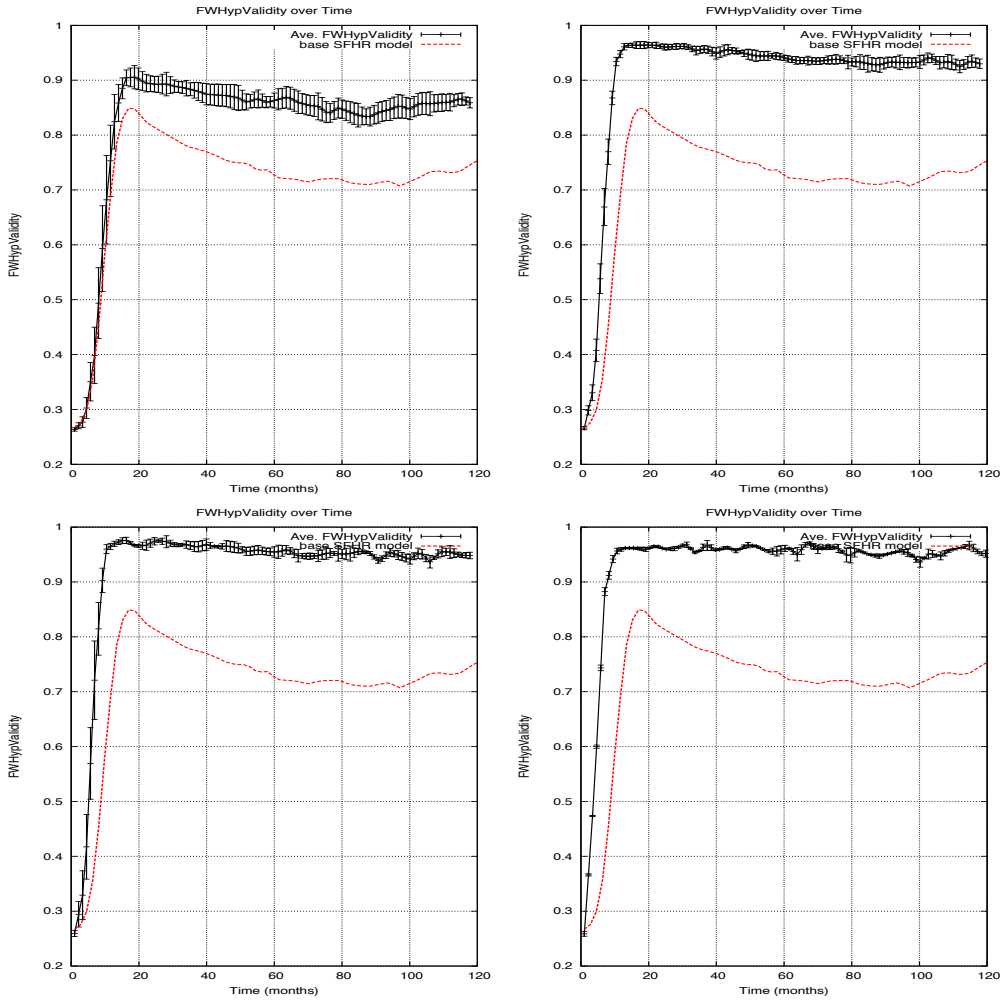

Figure 7.10: Firewall hypothesis validity over 10 years, in a risk network of 10,000 nodes with 0% (top left), 2% (top right), 5% (bottom left), and 10% transients (bottom right).

As with high levels of infectiousness demonstrated in the previous chapter, it is clear that transient participation in the network greatly increases the apparent validity of the firewall hypothesis. Here too, however, this is mainly a result of the fact that HIV infection rates approach near saturation, rather than demonstrating the topological features discussed in Chapter 4. Where so few nodes remain uninfected, the likelihood that these nodes represent very low degree nodes (degree 1 or even, at the time of measurement, 0)

would necessarily place their solitary neighbor in the position of a "firewall", though in fact what is being demonstrated is that infection failing to reach only the furthest margins of the graph.

Apart from the issue of how transients affect IDU network HIV rates, the question of how transient participation in the network affected the surrounding population can also be examined. As above, the particular HIV dynamics of sub-saturation stabilization have been shown to produce a steady rate of new infections which, while though does not move rapidly through the IDU network, nevertheless serves as potential sources of infection for short-term, transient participants who then may serve to transmit the virus to other communities.

This turned out to be the case. Over the course of 10 trials of 10 years for each scenario, the month-by-month average of the following were found:

Scen.	f_{tr}	Steady Pop.	Steady Avg. Hot Rate	%	Trans. Pop.	Trans. Avg. Hot Rate	%
1	10^{-3}	9,990	371	3.7%	10	2.0	20%
2	0.01	9,900	482	4.9%	100	12.3	12%
3	0.05	9,500	544	5.7%	500	180	36%
4	0.1	9,000	515	5.7%	1000	392	39%

Two remarks regarding this table: one can see here, as in Figure 7.8 that the effect of greater proportion of transients causes an increase in HIV rates, and here in the mean number of recent (highly infectious) nodes. In addition, among the bearers of recent infection, the proportion of transients versus steady participants is weighted heavily toward the transients. From the perspective of the surrounding population, the fact that transients who spend 3 days or fewer in the network become infected at such high proportions points to a critical concern for public health officials.

7.2.2 The impact of in-network lifetimes

The following parameters of the population process (see Section 2.2.2 on p. 64) are of interest:

- μ_{st}: Mean duration of steadies' lifetimes (in months).
- σ_{st}: Standard deviation of steadies' lifetimes (in months).
- f_{tr}: Fraction of individuals that are "transient" (between 0 and 1). Fixed in these experiments, at 0.
- μ_{tr}: Mean duration of transients' lifetimes (in months). Irrelevant in these experiments, since $f_{tr} = 0$.
- σ_{tr}: Standard deviation of transients' lifetimes (in months). Irrelevant in these experiments, since $f_{tr} = 0$.

Of these, the following parameters were varied in the experiments that follow.

Scenario	μ_{st}	σ_{st}
1	10	8
2	30	24
standard	60	48
3	120	96
4	240	192

Taken together, the following graphs show the effect of varying the amount of time individual nodes spend in the risk network (from their first appearance in the network to their self-initiated removal). In the standard experiments of

Chapters 4 and 5, the average amount of time a node spends in the network is 60 months, with a standard deviation of 48 months. This implies (in the standard model) that roughly 80% of the nodes are in the network for a period of 1-9 years, with the vast majority having a network life-expectancy of 4-8 years. As discussed above, the standard parameter was set to mimic the amount of turnover in IDU communities caused by any number of real world factors. The remaining distributions were taken from the SFHR structural model (see p. 84), extended by the standard dynamism model parameters (Section 3.5, p. 90). In what follows, the mean time-in-network is altered above and below the standard level, to simulate networks where participant turnover is both well-above and well-below the level seen in the SFHR network.

As seen in Figure 7.11, the alteration of participants' time-in-network has important effects on the overall network HIV rate. Where average participation time is lowered considerably, the overall HIV rate does not stabilize at the same level as when participation is prolonged. In fact, it is both higher and in relative terms far less stable. In graphs of scenarios where the participation times were 10 months and 30 months, the overall HIV rate begins to stabilize to the standard level, but then begins to again climb more quickly than in does in the standard settings. Interestingly, however, longer mean time-in-network settings also produce slightly higher overall HIV rates, though here the "dip" following the spike in initial infections is minimal, and the plateau of sub-saturation is arrived at directly, and holds very steady over the remaining 9 years of simulation time. We may, from these graphs, observe that long-term participation in the network creates very stable rates of infection, despite the fact that individuals within the network continue to "churn" their connections to one another, and that the high turn over of network participants, even where new participants enter the network in an uninfected state, necessarily produces both higher and continuously rising HIV rates.

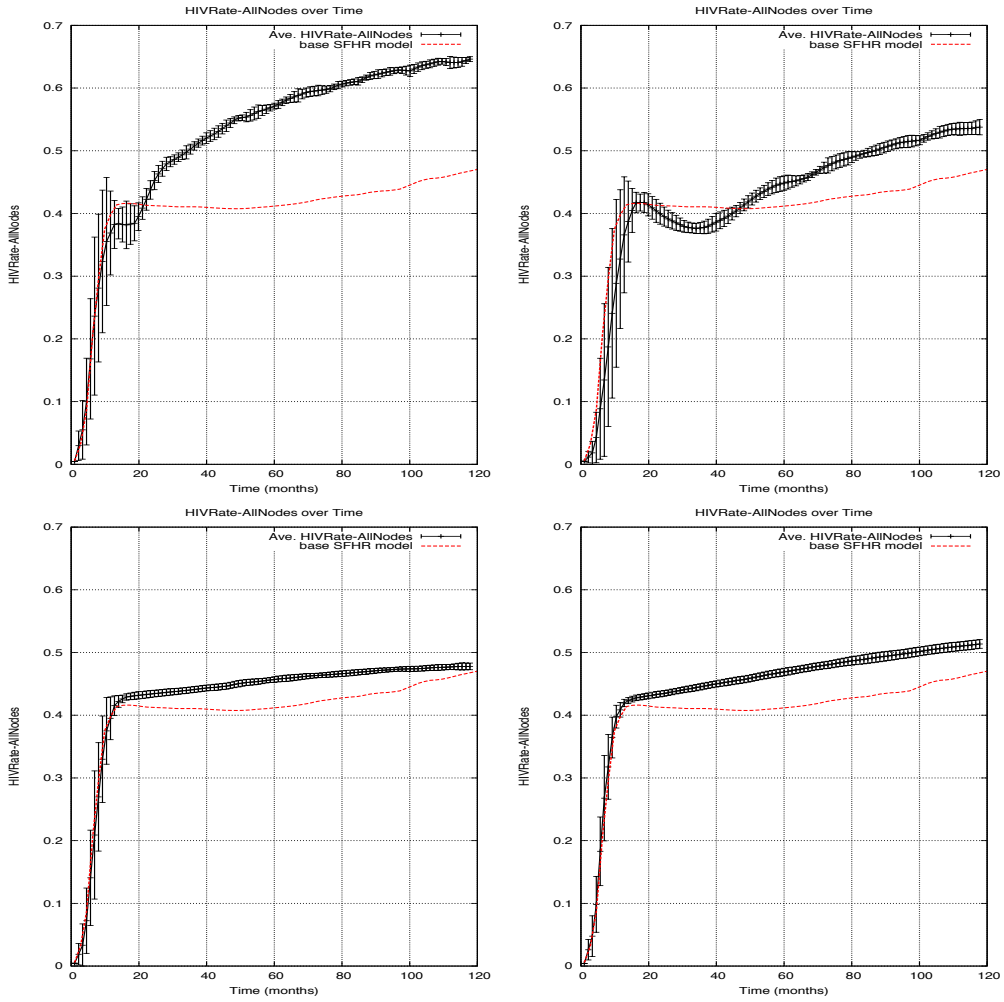

Figure 7.11: HIV prevalence over 10 years, in a risk network of 10,000 nodes with steady node lifetimes of 10 months (top left), 30 months (top right), 120 months (bottom left), and 240 months (bottom right).

The number of new infections in networks whose participation time varies show marked difference from the standard simulations. In situations of low average participation duration (top left and top right), the characteristic "hot spike" is either absent or less pronounced, while the production of new infections over time significantly exceeds that of the standard network (indicated by the dotted line). As with the overall network-wide HIV rate, the high turnover networks feature greater risk of infection transmission, due to the

higher proportion of new infections as a percentage of the total population (between 5-20% of the total population at any given time). On the other hand, long-term mean participation settings continue to produce a steady number of new infections over time, but at a rate lower than the standard settings. And while the number of new infections in the standard settings shows a tendency to increase gradually over the 10 years of simulation time, the long-term participation networks apparently do not.

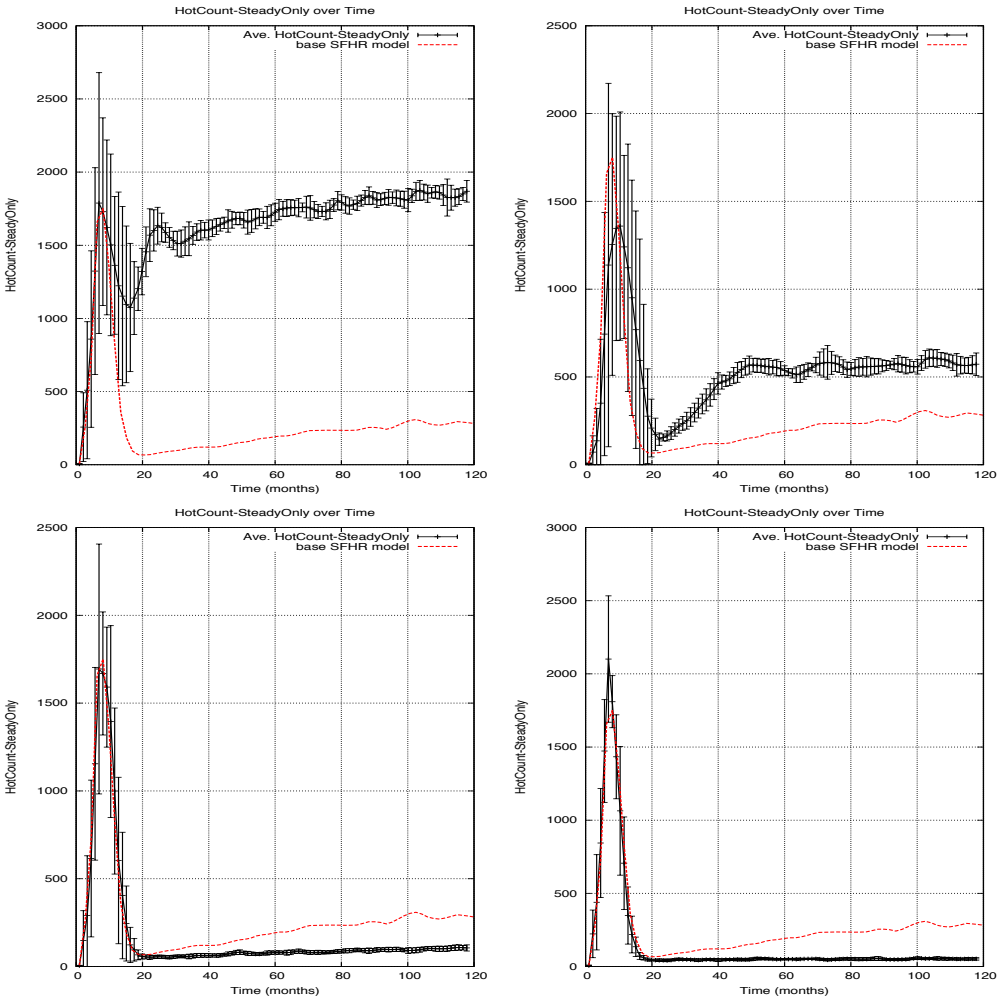

Figure 7.12: Highly infectious steady nodes over 10 years, in a risk network of 10,000 nodes with steady node lifetimes of 10 months (top left), 30 months (top right), 120 months (bottom left), and 240 months (bottom right).

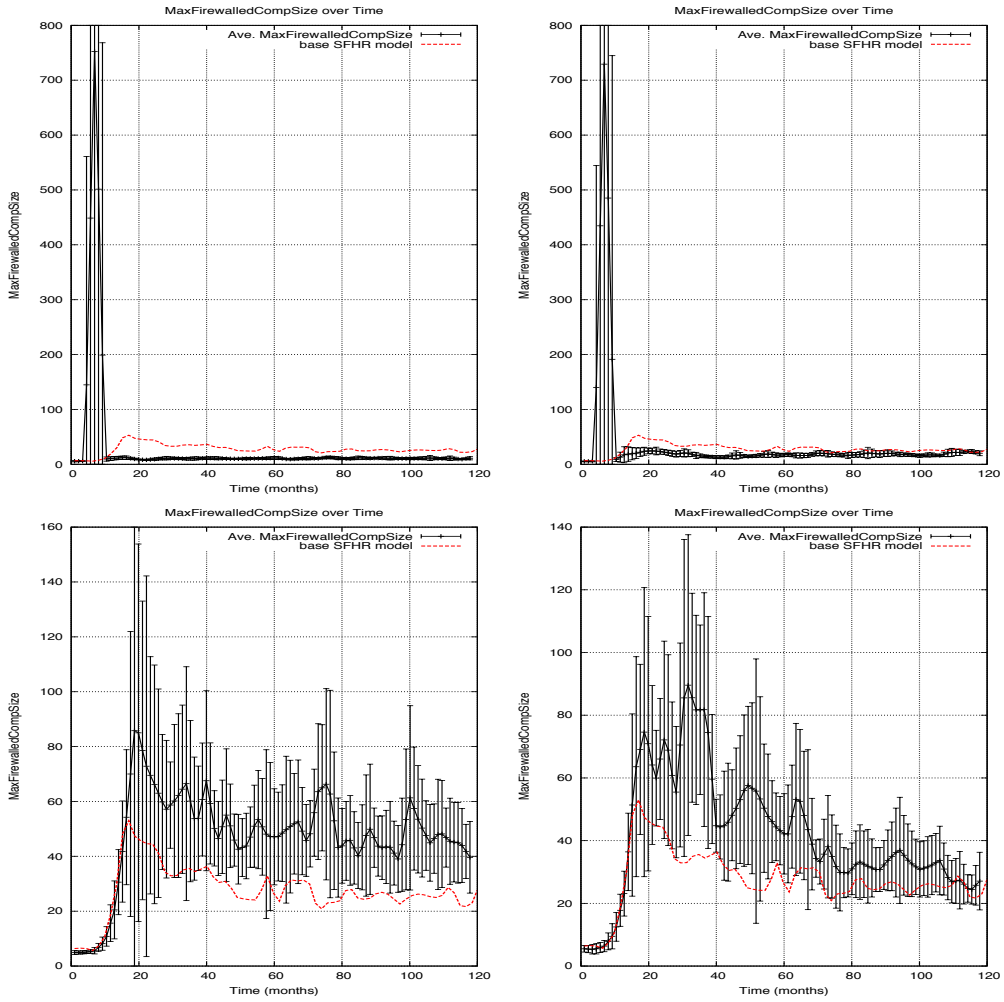

Figure 7.13: Maximum firewalled component size over 10 years, in a risk network of 10,000 nodes with steady node lifetimes of 10 months (top left), 30 months (top right), 120 months (bottom left), and 240 months (bottom right).

Figure 7.13 shows the size of the largest component of interconnected uninfected nodes following the deletion of those nodes in a state of low infectiousness. The effects of participation duration are apparent here as well: in situations where participation length is longest, the presence of large blocks of uninfected nodes separated from paths of infection by individuals with

older, less infectious status are clear. Those graphs showing short term participation demonstrate uninfected components of half or even smaller size.

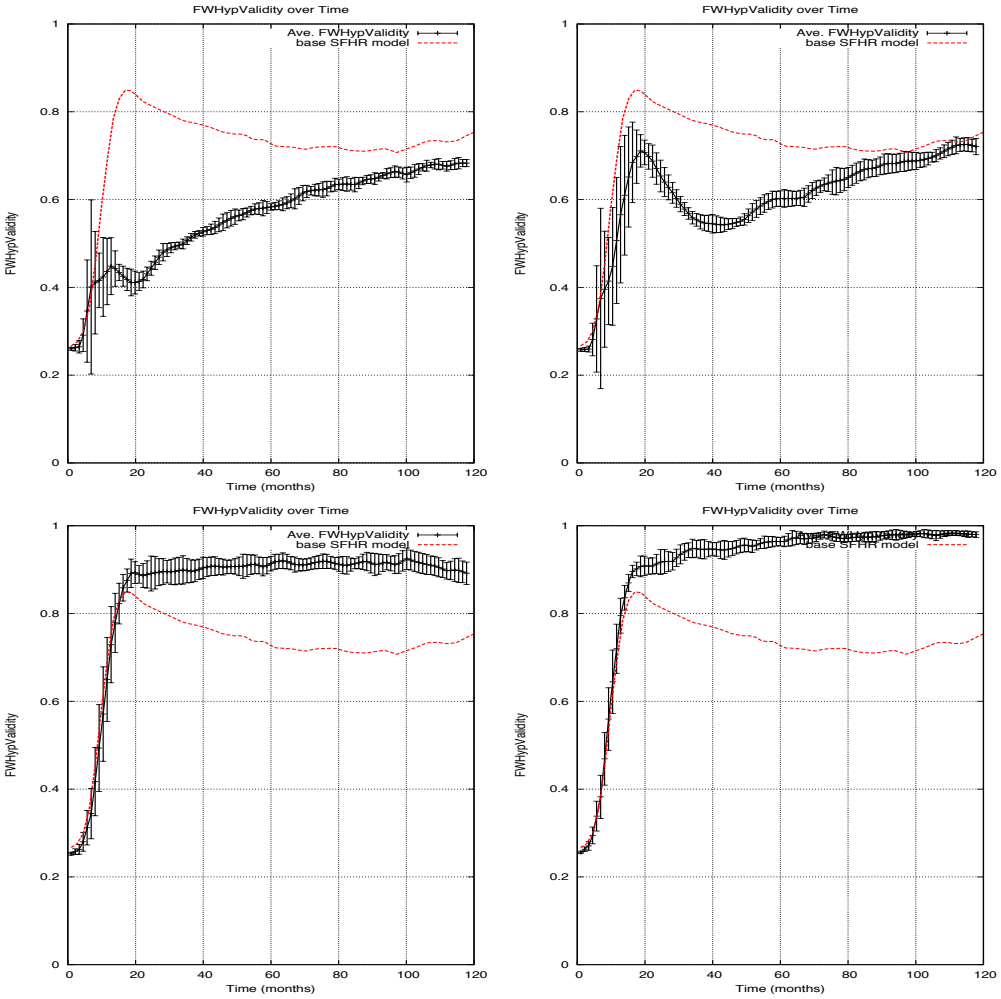

Figure 7.14: Firewall hypothesis validity over 10 years, in a risk network of 10,000 nodes with steady node lifetimes of 10 months (top left), 30 months (top right), 120 months (bottom left), and 240 months (bottom right).

Perhaps not surprisingly, the frequent coming and going of network participants tends to create bridges of infection to uninfected pockets of the network where such bridges would not exist if participation were long-term. These

results are similar to those discovered for the effects of transient participants in the network, though here the model is focused on network-wide behavioral characteristics rather than on the inclusion of a distinct group of radically different participants.

In Figure 7.14, we see the extent to which the test of the firewall hypothesis described in Chapter 5 holds true under a range of participation durations of network nodes. The effects are clear. In those graphs where overall participation is shortest (top left, top right), the firewall effect seems to account for a relatively low percentage of uninfected nodes. In the remaining graphs, where participation is longer than the standard settings, the firewall hypothesis approaches 90-100% validity. Indeed, looking only at the graph showing longest mean participation (bottom right), where very few nodes ever leave the network, and very few new nodes enter, the firewall effect accounts for nearly 100% of the non-spreading of HIV, even while new infections continue to appear (Figure 7.12) and where the total number of uninfected nodes in the network is nearly 60% (Figure 7.11. Again, this holds true despite the fact that individual nodes continue to exercise network dynamism, choosing new risk partners and eliminating old ones, and engage in risk events at rates equal to those in the standard model (where the firewall effect accounted for roughly 75% of HIV negative statuses). It would seem clear from this that the firewall effect is most apparent in networks showing long-term participation, and that in these circumstances, network topological features can largely account for the "non-spreading" of HIV.

7.3 Mapping churn process influence

Finally, we conclude by considering variations in the churn process and their impact on network dynamics exhibited. The churn process and its parameterization was described at length in Section 2.2.2 (p. 60). We shall focus on the effects of changes in three parameters: intensity of the churn process the degree stability of individuals, and the network bias towards triadic closure.

7.3.1 The impact of churn process intensity

The following parameters of the churn process (see Section 2.2.2 on p. 60) are of interest:

- μ_j^C: Mean inter churn impulse interval in layer j (in months) normalized by the individual's layer j ego network size.
- σ_j^C:Inter churn impulse interval standard deviation in layer j (in months) normalized by the individual's layer j ego network size.
- w_j^S: Degree stability bias in layer j. Fixed in these experiments, at 2.9
- w_j^Δ: Triangle bias in layer j. Fixed in these experiments, at 3.

Since we only consider one layer in our network for these simulations, we will drop the j subscript, taking μ^C, σ^C, w^S, and w^Δ as our parameters. Of these, the following parameters were varied in the experiments that follow.

Scenario	μ^C	σ^C
1	10	8
2	30	24
standard	60	48
3	120	96
4	240	192

In varying the churn parameter in this way, we test the robustness of the conclusions regarding HIV stabilization rates in the overall network and the validity of the firewall hypothesis as one varies the rate at which individual nodes change their network connections—considering both setting when very rapid changes are being made, to ones which enjoy extended network structural stability. The remaining distributions were taken from the SFHR structural model (see p. 84) extended by the standard dynamism model parameters (Section 3.5, p. 90).

In the standard simulation settings of Chapter 4, the churn parameter is set for 60 months, with a standard deviation of 48 months. This means that (in the standard simulation) a node will, on average, delete and add a number of connections equal to its total ideal degree over 60 months. As discussed above, each node draw their particular churn rate from a distribution described by the mean and standard deviation, a rate which the node then retains for its entire time in the network. As a result, while the overall average of 60 months is maintained network-wide, some nodes will change partners much more rapidly, and some much more slowly. By varying the churn parameter mean, we alter the distribution from which individual nodes select their churn rates. Yet throughout, a diversity of churn rates (as reflected in σ^C) is maintained across individuals.

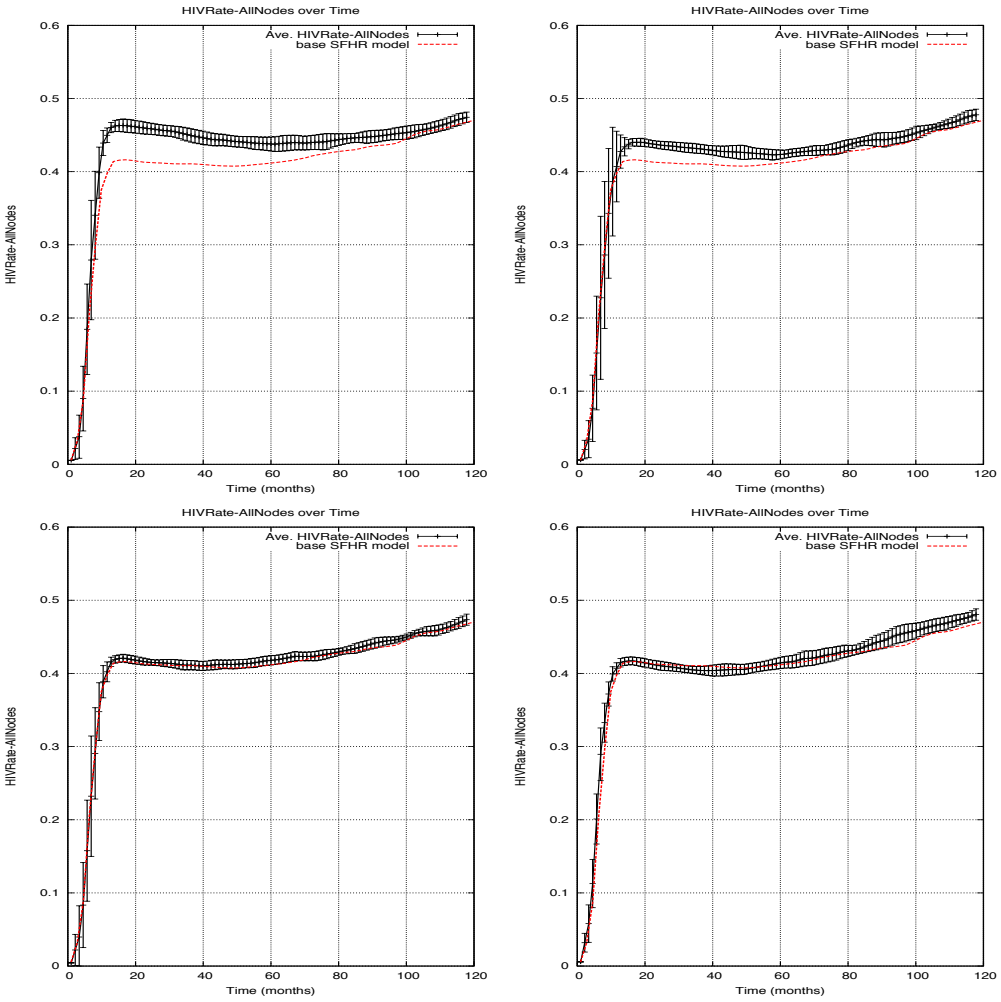

Figure 7.15: HIV prevalence over 10 years, in a risk network of size 10,000 nodes with mean normalized churn interval 10 (top left), 30 (top right), 120 (bottom left), and 240 (bottom right) months.

In contrast to the majority of the parameter setting discussed thus far, Figure 7.15 demonstrates that the network-wide HIV infection rate remains largely impervious to even large changes in the rate at which nodes change risk partners. This held true regardless of whether the churn rate was set at 1/6th the standard setting, or at 6 times the standard setting. In each of the graphs above, the standard model (dotted, red) line remains at or close to the mean results of the 10 trials performed for each exploratory churn setting.

The closest to an exception to this rule is where the churn parameter was set to a period of 10 months. Here, a node will, on average, change a number of its connections equal to its degree every 10 months. In a network of 10k nodes such as this, with a mean of 3.4 connections per node, we can estimate that a total of approximately 400,000 connections were added and deleted over the course of the 10 year simulation. Regardless, the HIV rate stabilizes at roughly 5% above the standard initially, and is equivalent after 10 years.

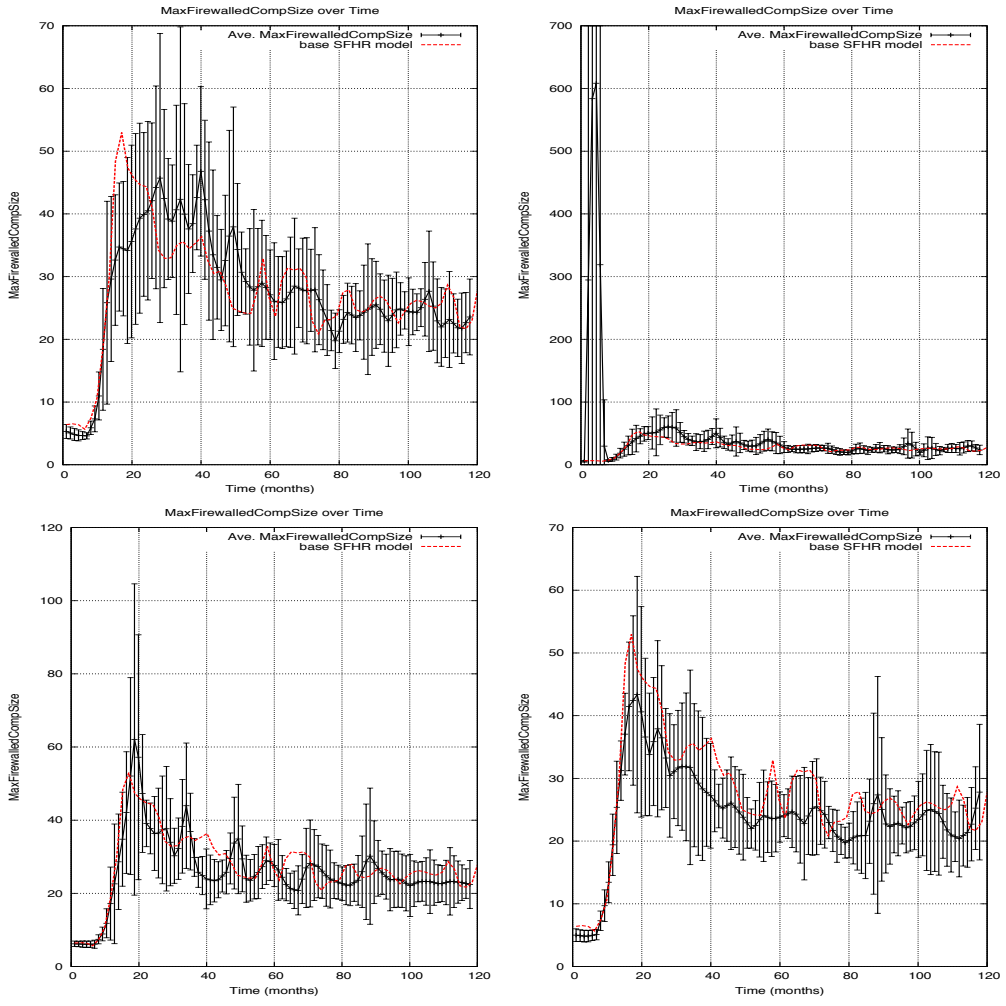

Figure 7.16: Maximum firewalled component size over 10 years, in a risk network of size 10,000 nodes with mean normalized churn interval 10 (top left), 30 (top right), 120 (bottom left), and 240 (bottom right) months.

The graphs in Figure 7.16 reveal dynamics similar to those for overall HIV rates. Here too the overall graph dynamics seem relatively unchanged by large changes in the churn rate. In each of these cases the largest island in the virus-centric view of the network—that interconnected HIV negative nodes that are not connected to a highly infectious node (after the deletion of low infectiousness nodes)—declines steadily in size for roughly the first five years of the simulation, stabilizing at roughly 25 nodes. This result remains consistent whether nodes are changing their risk partners within the network rapidly, or sluggishly.

And finally, Figure 7.17 shows the effect of increasing/decreasing rates of average churn on the validity of the Firewall Hypothesis. More so than the other graphs in this section, these results seem to reflect the parameter changes. At churn rates that are faster than the standard, the Firewall Hypothesis is able to account for a greater number of HIV negative nodes, while at rates of churn that are slower than the standard, the Firewall Hypothesis accounts for fewer of the HIV negative nodes. This is true despite the fact that churn rates seem to have little effect on the overall rates of HIV. Interestingly, however, and perhaps counterintuitively, it is in those networks with the highest churn rate where network structural factors appear to account for the non-spreading of HIV. Such results would seem to contradict results discussed above that showed that turnover in network participants would result in the Firewall Hypothesis accounting for fewer HIV negative statuses. It would appear that, at least at the levels tested here, high turn over in network connections would have quite different long-term network dynamics than high turn over in network participants.

At first, this phenomenon puzzled us. We propose the following explanation: given that, in the trials shown here, much like those discussed for the standard case, network HIV infection takes place rapidly—mainly through an initial spike in highly infectious nodes—in what appears as an epidemic phase. Under these conditions, new infections are likely to quickly infect network cores and highly connected individuals (hubs). After this initial phase, individual nodes who have become HIV positive and passed into a phase of low infectiousness are likely to be connected to others whose status and rate of infectiousness is the same as their own. This is particularly true of hubs, who are likely, post-epidemic, to have a high proportion of risk partners who status is also HIV+ and low infectiousness.

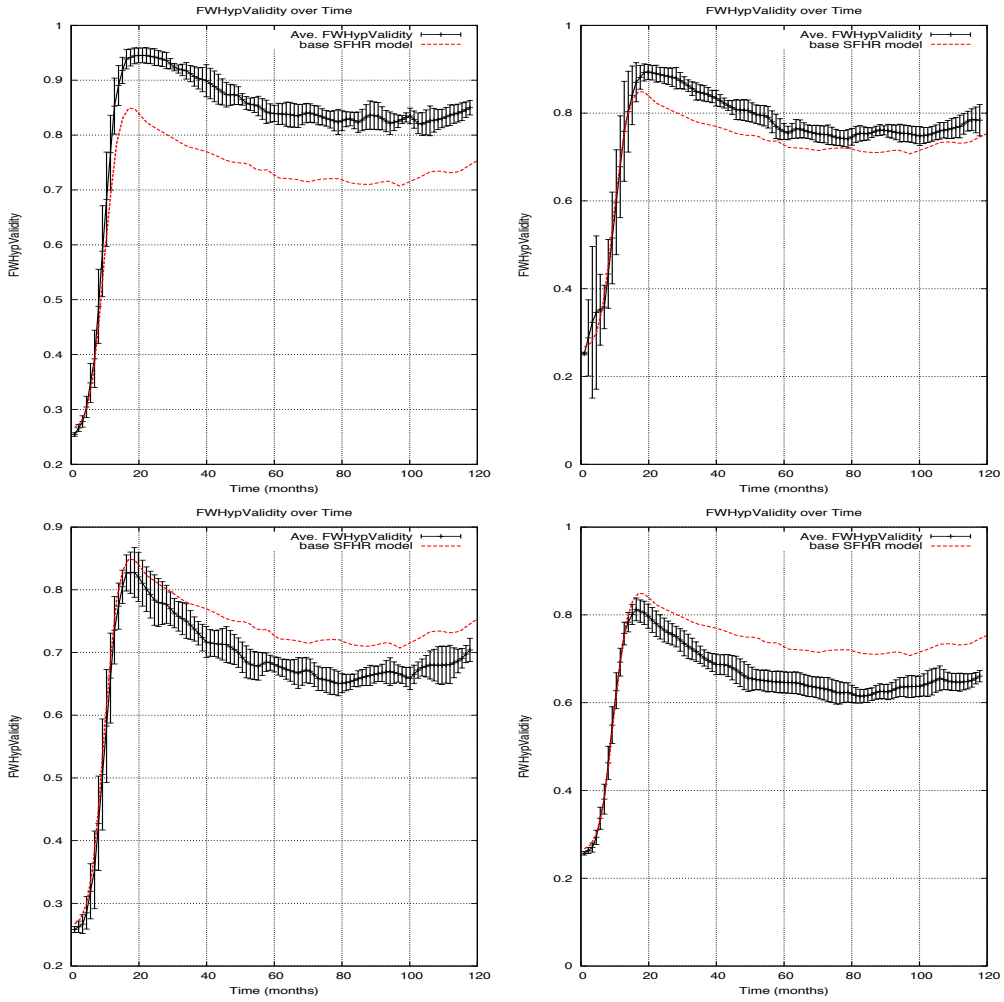

Figure 7.17: Firewall hypothesis validity over 10 years, in a risk network of size 10,000 nodes with mean normalized churn interval 10 (top left), 30 (top right), 120 (bottom left), and 240 (bottom right) months.

Where churn rates remain low, these core clusters of HIV+ low infectiousness individuals remain as such, minimizing their potential firewall effect by isolating older, low infectiousness nodes in a highly interconnected core where for each member, a high proportion of their connections to others already HIV+. The firewall effect in such a configuration is low, despite the fact that a low churn scenario reflects a relatively steady topology.

Where churn rates are high, core connections are more likely to be broken, inducing hubs to eliminate and replace quickly a large number of their connections. While there is no reason to suspect core members seek out HIV negative partners (and indeed it plays no role in the simulation), stochastic factors will likely create at least some connections outside the core. To the extent that low infectious, network core members make connections to network margins, the firewall effect of these nodes will increase.

7.3.2 The impact of degree stability

The following parameters of the churn process (see Section 2.2.2 on p. 60) are of interest:

- w_j^S: Degree stability bias in layer j.
- μ_j^C: Mean inter churn impulse interval in layer j (in months). Fixed in these experiments, at 5 years.
- σ_j^C:Inter churn impulse interval standard deviation in layer j (in months). . Fixed in these experiments, at 4 years.
- w_j^Δ: Triangle bias in layer j. Fixed in these experiments, at 3.

Since we only consider one layer in our network for these simulations, we will drop the j subscript, taking μ^C, σ^C, w^S, and w^Δ as our parameters. Of these, the following parameters were varied in the experiments that follow.

Scenario	w_j^S
1	0.5
2	1.5
standard	2.9
3	6.0
4	12.0

As above, the parameter of particular interest in this section is the degree stability parameter. This parameter determines how widely the number of partners for a given actor may vary before the actor takes steps to correct his/her number of partners towards his/her ideal degree. The standard setting of 2.90 ensured that a degree difference of 1 is corrected 50% of the time, while a difference of 2 is corrected approximately 85% of the time; higher divergences yield increasing likelihoods of actor-initiated correction.

Here we vary the strictness with which each actor adheres to the recommendations implicit in their ideal degree, and examine whether variations of this parameter affect the phenomena of interest—HIV rate stabilization and the firewall effect. When the stabilization parameter is set below 2.90, actors are more prone to let their current degree vary from their ideal degree. When set above 2.90, actors react sooner to correct their degree. The remaining distributions and parameters were taken from the SFHR structural model (see p. 84) extended by the standard dynamism model parameters (Section 3.5, p. 90).

Figure 7.18 shows the mean (over all nodes) of the absolute value of the deviation from ideal degree, plotted over the 10 year simulation. The results of the standard run (degree stability=2.90) is shown as a red dotted line. The graph shows that in the course of the standard simulation runs of 10k nodes, the average node was within 1.2 connections of his/her ideal degree. When the degree stability parameter is lower than 2.90, (top left and top right), the mean deviation from ideal degree approaches 2 and 1.5, respectively. When the parameter is set above 2.90, the mean deviation magnitude drops below the standard level, even going below 1 in the most constrictive setting (see bottom right, degree stability=12.0, approximately 4 times greater than the standard setting).

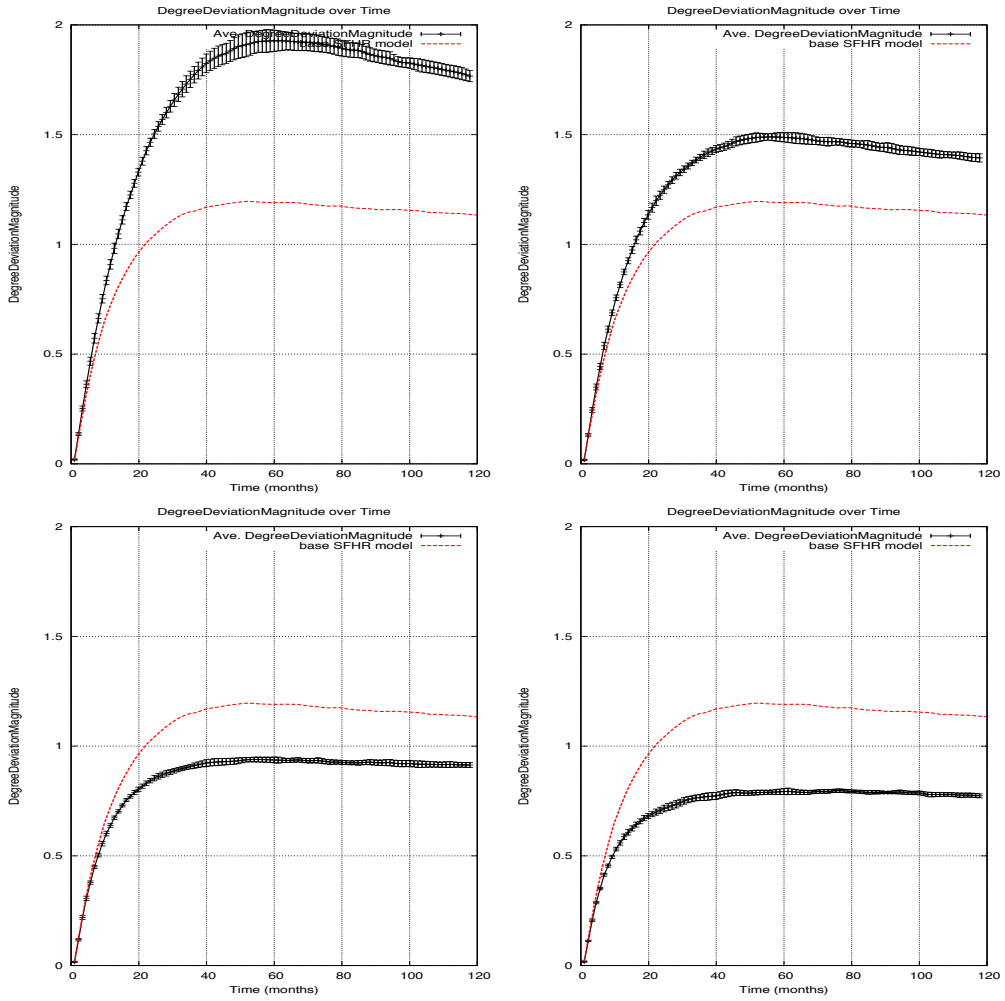

Figure 7.18: Average degree deviation magnitude over 10 years, in a risk network of size 10,000 nodes with degree stability 0.5 (top left), 1.5 (top right), 6.0 (bottom left), and 12.0 (bottom right).

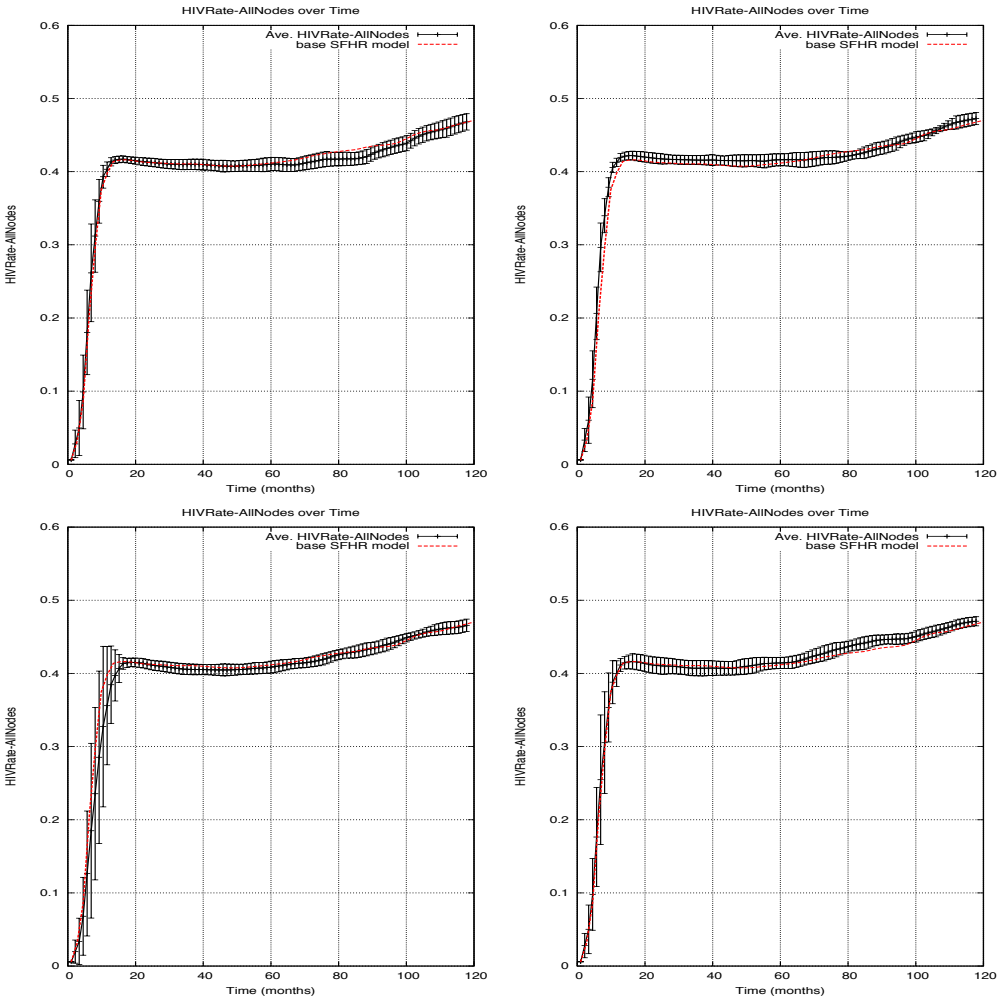

Figure 7.19: HIV prevalence over 10 years, in a risk network of size 10,000 nodes with degree stability 0.5 (top left), 1.5 (top right), 6.0 (bottom left), and 12.0 (bottom right).

Figure 7.19 shows the effect of varying the degree parameter on the overall HIV rate. From these graphs it is clear that varying the adherence to ideal degree has little effect on HIV rates over the course of the simulations. Indeed, in each case, despite the low variance in trajectories across trials, the standard case falls close to the mean trajectory, regardless of how far individuals allowed their to drift from its ideal value.

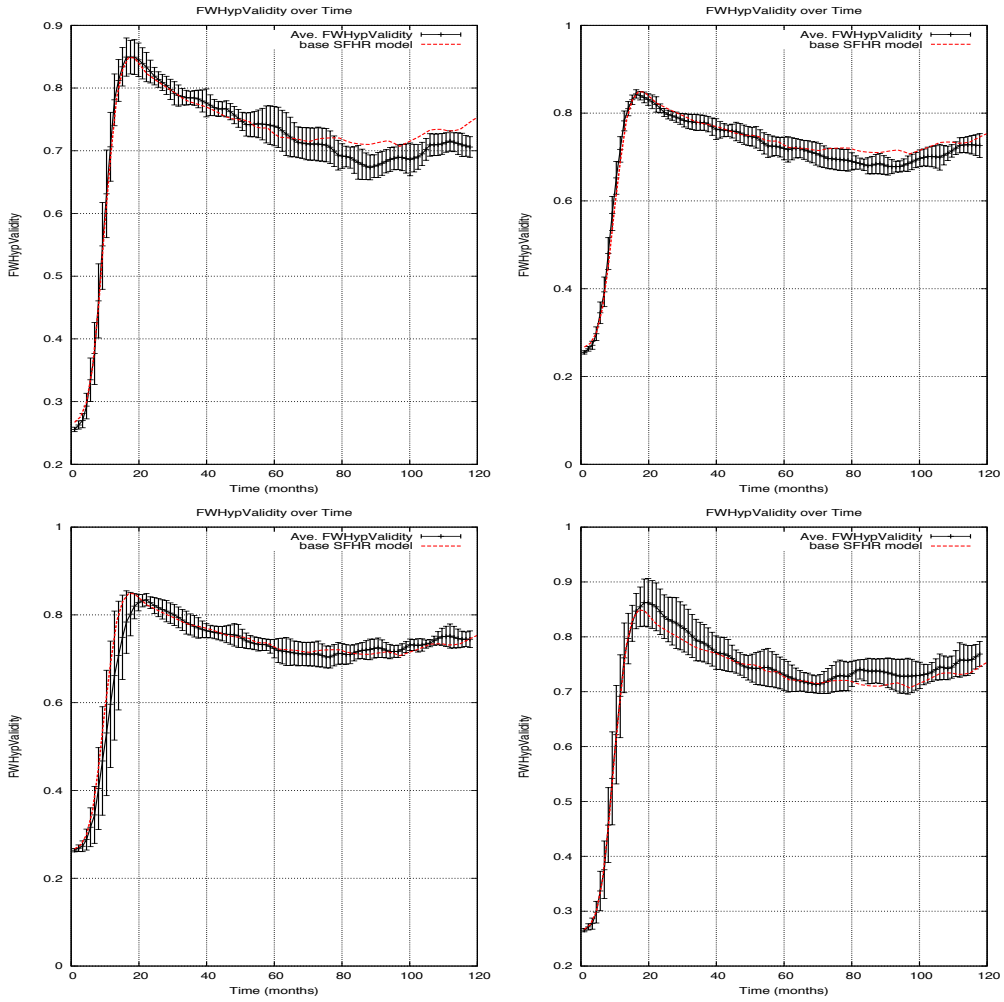

Figure 7.20: Firewall hypothesis validity over 10 years, in a risk network of size 10,000 nodes with degree stability 0.5 (top left), 1.5 (top right), 6.0 (bottom left), and 12.0 (bottom right).

The same conclusions reached for HIV rate seem to hold true for the results of the Firewall Hypothesis tests. In Figure 7.20, as in Figure 7.19, variations in the parameter had no noticeable effect. From this we can conclude that, unlike many of the parameters discussed above, either degree stability plays little role in HIV rates and the firewall effect, or that visible effects lie at parameter settings well outside those tested here.

7.3.3 The impact of triadic closure bias

The following parameters of the churn process (see Section 2.2.2 on p. 60) are of interest:

- w_j^{Δ}: Triangle bias in layer j.
- μ_j^C: Mean inter churn impulse interval in layer j (in months). Fixed in these experiments, at 5 years.
- σ_j^C:Inter churn impulse interval standard deviation in layer j (in months). . Fixed in these experiments, at 4 years.
- w_j^S: Degree stability bias in layer j. Fixed in these experiments, at 2.9 years.

Since we only consider one layer in our network for these simulations, we will drop the j subscript, taking μ^C, σ^C, w^S, and w^{Δ} as our parameters. Of these, the following parameters were varied in the experiments that follow.

Scenario	w^{Δ}
1	0.5
2	1
standard	3
3	10
4	30

Here, a final element of the dynamic model is tested to examine the nature of the effects of the parameter setting on overall HIV rate and the firewall effect. In this case, we test the extent to which variations in our weighting of the influence of transitive closure (in relation to homophily in gender, race/ethnicity, age, and ideal degree) influences experimental outcomes.

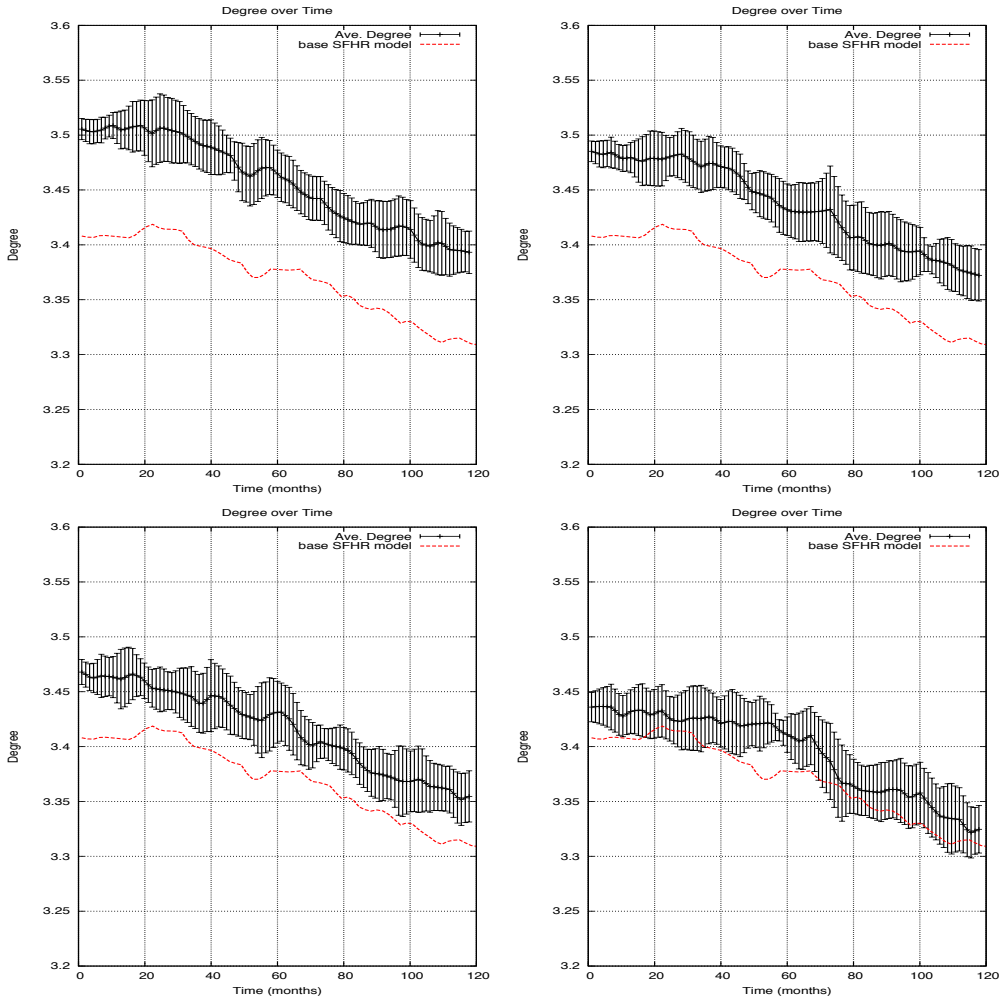

Figure 7.21: Average degree over 10 years, in a risk network of size 10,000 nodes with triangle bias 0.5 (top left), 1.0 (top right), 10.0 (bottom left), and 30.0 (bottom right).

As the reader will recall from above, the standard setting for triadic bias was set at 3, meaning that the likelihood of a connection was increased threefold over the effects of attribute-based homophily if the edge involved making a connection to an existing connection of an existing risk partner. In the experiments that follow, we alter the settings from a state of very low triadic biases to a very high triadic bias (indeed, the lowest setting, triadic bias=0.5, actually means that those connections which would cause the completion of

a triangle will actually be less likely). The remaining distributions were taken from the SFHR structural model (see p. 84) extended by the standard dynamism model parameters (Section 3.5, p. 90).

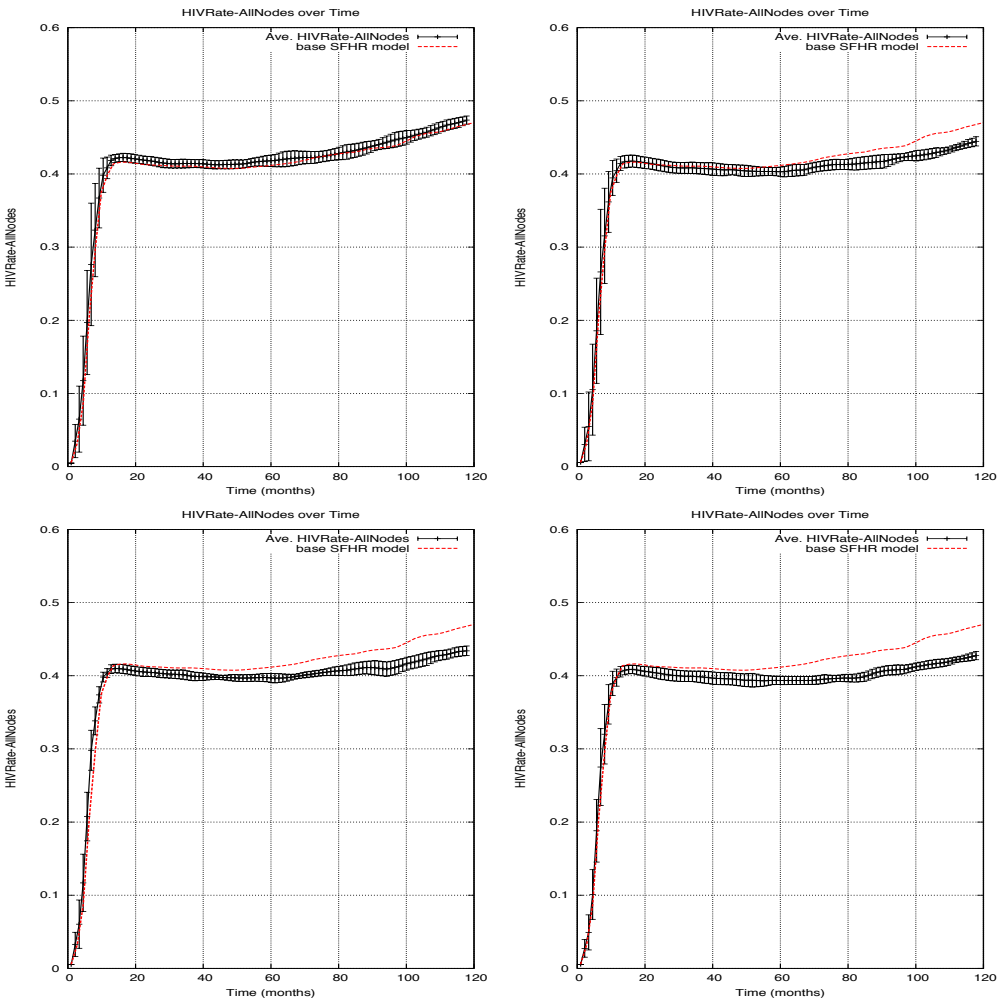

Figure 7.22: HIV prevalence over 10 years, in a risk network of size 10,000 nodes with triangle bias 0.5 (top left), 1.0 (top right), 10.0 (bottom left), and 30.0 (bottom right).

Taken together, Figures 7.21 and 7.22 show that, while changing the triadic emphasis had an influence on overall average degree, it had little effect on HIV rates. Like several of the churn parameters, wide variation of this setting seems to affect overall network topology, but not in ways that affect HIV transmission.

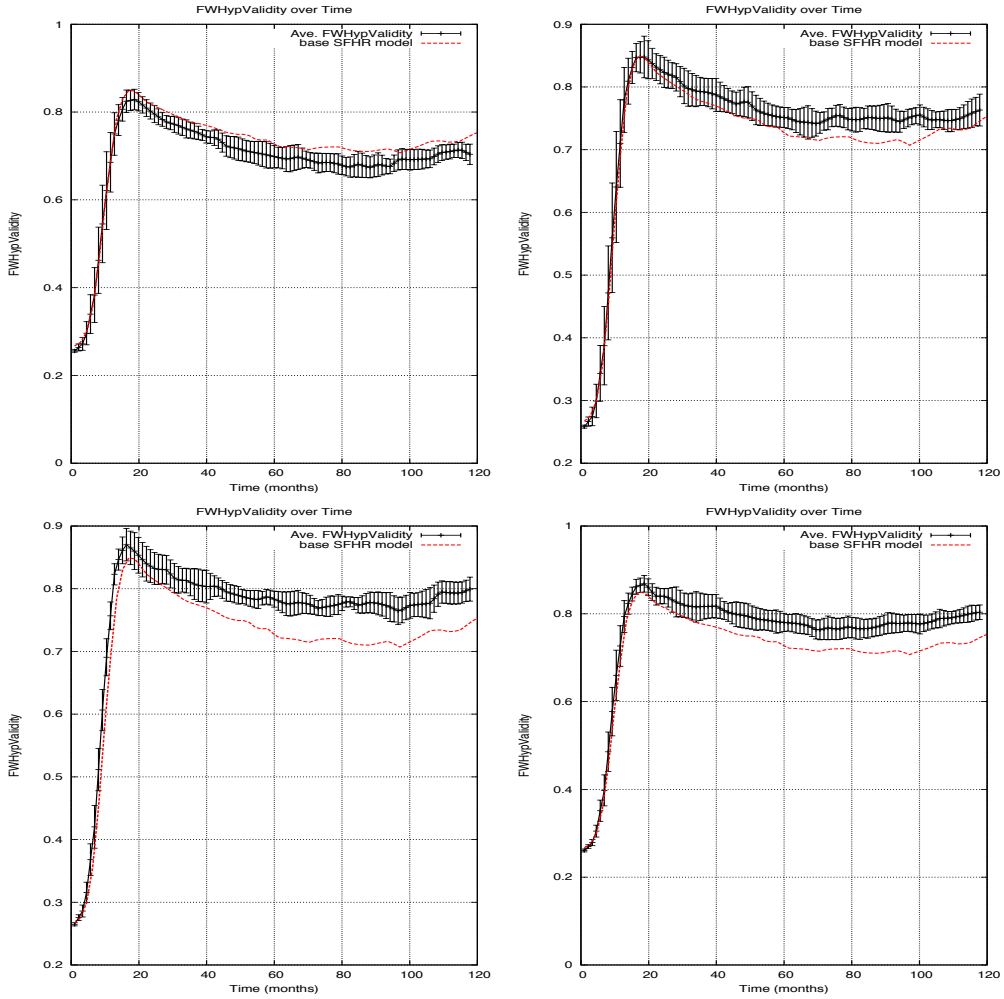

Figure 7.23: Firewall hypothesis validity over 10 years, in a risk network of size 10,000 nodes with triangle bias 1.5 (top left), 1.0 (top right), 10.0 (bottom left), and 30.0 (bottom right).

On the other hand, as can be seen in Figure 7.23, triadic closure bias does seem to have some measure of impact on the Firewall Hypothesis results. Here, as the triadic bias is increased, the firewall effect seems to rise, meaning that the presence of old infections in key structural positions potentially accounts for a greater proportion of HIV negative statuses. Like the churn parameter discussed at the beginning of this section, we find that the triadic bias parameter influences topology in a way that alters not the overall HIV prevalence, but in how that rate is achieved. Such results are novel and would seem to suggest new lines of research on the effects of internal structures on HIV disease dynamics in IDU networks.

Chapter 8

The multi-actor-based universal simulation engine

In this chapter, we describe the Multi-Actor-Based Universal Simulation Engine, or MABUSE[1] (pronounced "mah-BOO-zah"). The exposition is divided into

- **Software usage** is presented in Section 8.1. Here we discuss the structure of information flows through the functional components of MABUSE. We also provide a description of the top-level command-line program that are used by researchers in conducting experiments.

- **Software design** is presented in Section 8.2. Here we discuss the layered architecture of the MABUSE software.

- **Software implementation** is presented in Section 8.4. Here we provide a very brief description of the code implementing the MABUSE software.

[1]For possible etymology, see Lang (1922, 1933, 1960).

8.1 Software usage

We begin by considering the information flow through the various functional modules of MABUSE, which are depicted in Figure 8.1. The functional decomposition of MABUSE (from the user's vantage point) consists of the following:

1. **MABUSE Utilities**: Used to generate XML files which specify the structural model and the dynamism model. They are also used to specify simulation configuration—i.e., which node, edge, and graph behaviors are enabled, which node and graph metrics are to be computed, and what the model degeneracy criteria are for pruning the simulation.

2. **MABUSE Network Generator**: Used to take the structural model and generate an initial risk network. In practice, two steps are required. First, the nodes are made using the structural model. Then, to make the edges, we run a simulation for 1 unit of time. During this time, nodes attach to each other in an attempt to reach their target degree. This process is formally described in Section 2.1.4. At the end of this process, nodes and edges are checkpointed as part of the risk network specification. This checkpoint is used as the initial risk network of the simulation.

3. **MABUSE Simulator**: Used to simulate the evolution of a risk network, as specified by the dynamism and structural model parameters. Periodically, the simulator writes a checkpoint of the risk network. The checkpoint consists of XML files describing the instantaneous state of its nodes and edges, as well as any dynamic simulation parameters. The MABUSE Simulator is extensible through a "plugin" architecture which allows external specifications of node, edge, and graph behaviors. This design of "growth through extension" (Fishwick, 1994) is a strategy we adopted so as to enable 3rd parties to develop their own risk network simulations without requiring modifications to the core MABUSE system.

4. **MABUSE Analyzer**: Used to analyze each of the risk network checkpoints generated by the MABUSE Simulator. The MABUSE Analyzer

is extensible through external specifications of node and graph metrics, as well as model degeneracy testers. Once again, "growth through extension" (Fishwick, 1994) enables 3rd parties to develop their own analyses without requiring modifications to the core MABUSE system.

5. **MABUSE Aggregator**: Used to collect analyses generated by the MABUSE Analyzer, and renders from these graphs which depict trajectories of the metrics of interest.

6. **MABUSE Visualizer**: Used to inspect and collate generated graphs, producing images quite similar to those found in this report.

8.1.1 Command-line interface

The previous section described the 6 principal process elements (functional data transformers) which comprise the MABUSE system. At the level of user interactions, the functionality of these process elements is partitioned and organized into a set of command line scripts/programs described below:

- `testlist`
  Lists all the tests, by name. A test is an experiment: it constitutes a structural mode, a dynamism model, a population size, a duration, and the number of independent simulation trials to be executed.

- `showtest testName`
  Displays the structural and dynamism model for a specific test.

- `newtest oldtestName newtestName`
  `numTrials numNodes durationMonths concurrency`
  Creates a new test scenario, using the structural and dynamism models from an existing "old" test. Specify the number of nodes, trials, and duration of the new test (which may be different from the values in the "old" test).

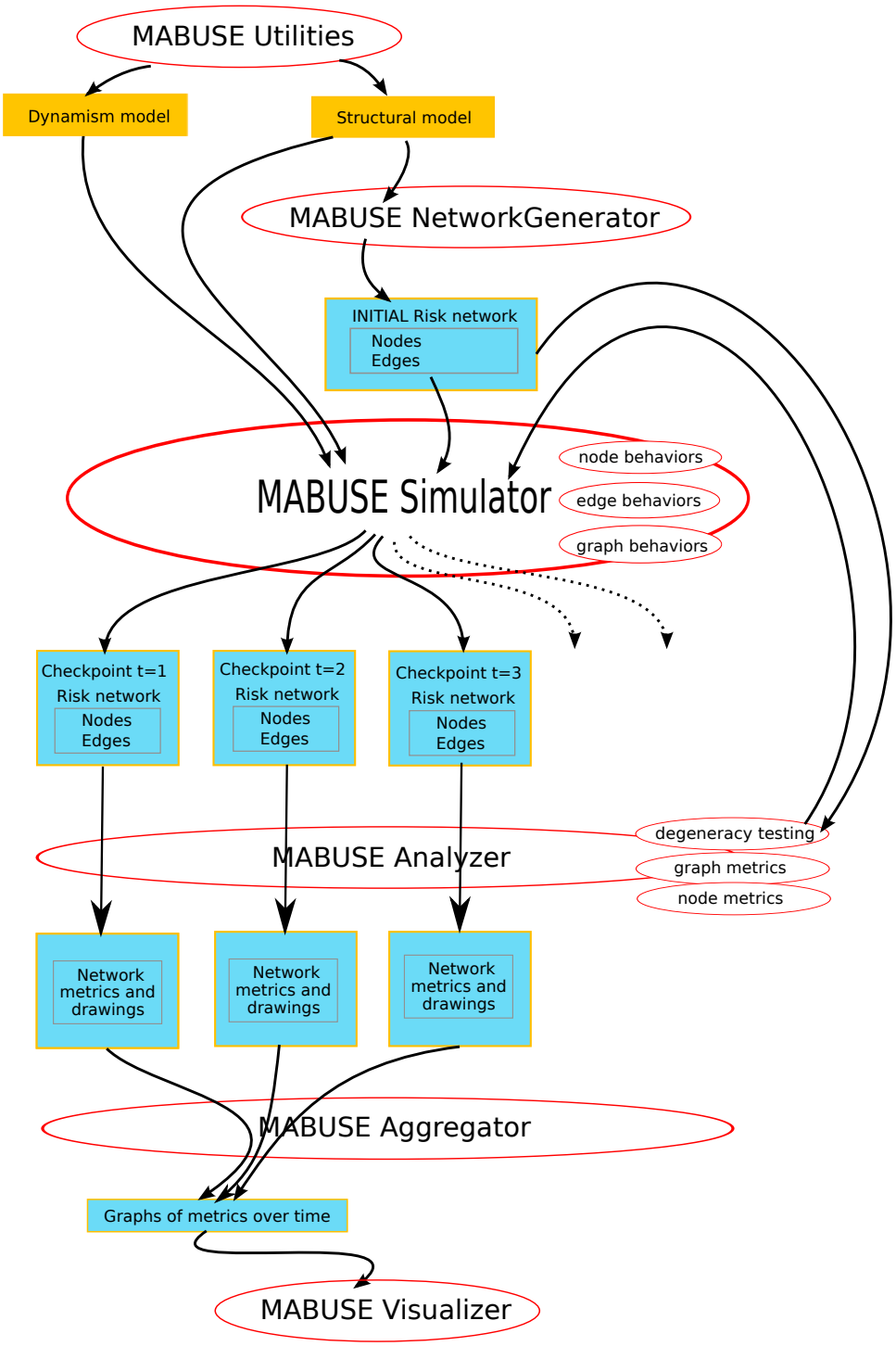

Figure 8.1: Information flow within MABUSE

- `edittest testName parameter-name`
  Permits the user to edit a particular parameter of the structural model or the dynamism model associated with a test.
- `runtest testName`
  Runs the simulation trials mandated by the specified test.
- `progress testName trialNumber`
  Reports on the progress of a specified trial of a given test.
- `check testName time1 time2`
  Checks the model divergence between the network at two specified temporal markers: time1 and time2.
- `shoot`
  Kills all running MABUSE simulations.
- `aggregate-results testName trialList`
  Generate a collated LaTeXreport describing the structural and dynamism models, together with the graphs of metrics collected during the simulation.

8.2 Network simulator design

The design of MABUSE draws freely upon its predecessors, particularly on the simulation platforms below, as well as on the general theory of modeling and discrete event simulation. A good introduction to the latter may be found in Sokolowski (2009); a specialized treatment to network simulation is to be found in Guizani, Rayes, Khan, and Al-Fuqaha (2010); Fujimoto, Perumalla, and Riley (2007); for a treatment of the topic in the context of medicine see Sokolowski and Banks (2011), and for an exposition specific to public health we recommend Salerno, Yang, Nau, and Chai (2011); Witten and Vincent (1996).

- **REAL** is a simulator for studying the dynamic behavior of flow and congestion in packet switch data networks. Network topology, protocols, data and control parameters are represented by scenarios, which

are described using NetLanguage, a simple ASCII representation of the network. About 30 modules are provided which can exactly emulate the actions of several well-known flow control protocols (Keshav, 1988).

- **INSANE** is a network simulator designed to test computer network simulations derived from empirical traffic measurements (Mah, 1998). A Tk-based graphical simulation monitor can provide an easy way to check the progress of multiple running simulation processes.

- **NetSim** is intended to offer a very detailed simulation computer networks, including realistic modeling of signal propagation, the effect of the relative geographic positions of stations on events in the network, transmission collision detection and handling (Penoff, Wagner, Tüxen, & Rüngeler, 2009).

- **Maisie** is a C-based language for hierarchical simulation, providing a specification language for parallel discrete event simulation (R. L. Bagrodia & Liao, 1994). A logical process is used to model one or more physical processes; the events in the physical system are modeled by message exchanges among the corresponding logical processes in the model. **Parsec** are parallel extension of Maisie (R. Bagrodia, Takai, Chen, Zeng, & Martin, 1998) with recent operating system level support (Sharma & Thazhuthaveetil, 2001). In addition, several object-orient extensions to Maisie, e.g. **MOOSE**, (Cubert, Goktekin, & Fishwick, 1997) are available.

- **OPNET** (Optimized Network Engineering Tool) is an object-oriented simulation environment, and is one of the most powerful general-purpose network simulator available today (OPNET Technologies, 2011). OPNET's comprehensive analysis tools are able to interpret simulation outputs, and its built-in Proto-C language support makes it capable of realizing almost any functions and protocols. OPNET provides a comprehensive development environment for the specification, simulation and performance analysis of dynamic networks (Ahmad et al., 2009).

- **SimJava** is a discrete event, process oriented network simulation package (McNab & Howell, 1998), one of several Java-based platforms available (Helsgaun, 2000; Howell & Mcnab, 1996). The original SimJava was based on the HASE++ simulation library (Robertson & Ibbett,

1994; Ibbett, Heywood, & Howell, 1995), which was in turn based on SIM++ (Lomow & Baezner, 1991). A SimJava simulation is a collection of entities each running in its own thread. Entities are connected together by ports and can communicate with each other by sending and receiving event objects. A central system class controls all the threads, advances the simulation time, and delivers the events. The progress of the simulation is recorded through trace messages produced by the entities and saved in a file. Using a programming language to build models (rather than building them graphically) has the advantage that complex regular interconnections are straightforward to specify, which is crucial for some of the networks we are interested in simulating. It also allows the inclusion of existing libraries of code to build simulations. The SimJava package has been designed for simulating fairly static networks of active entities which communicate by sending passive event objects via ports.

- **Network Simulator 2 (ns-2)** is an object-oriented, discrete event simulator targeted to be used in research in networking (Mccanne, Floyd, & Fall, n.d.; Issariyakul & Hossain, 2008). Developed at UC Berkeley and written in C++ and OTcl, ns is primarily useful for simulating local and wide area computer networks[2]. One of the main advantages of ns-2 is its Open Source availability and many extensions, e.g. (Baldo, Maguolo, Miozzo, Rossi, & Zorzi, 2007).

- **Simulink** is a platform for multi-domain model-based simulation of dynamic systems, with wide ranging applications–see Altmann and Hatnik (2004); Binh (2009). It provides an interactive graphical environment and a customizable set of block libraries, that let one accurately design, simulate, implement, and test control, signal processing, communications, and other time-varying systems. Simulink is an extension to MATLAB which uses an icon-driven interface for the construction of a block diagram representation of a process. Simulink is integrated with MATLAB, providing immediate access to an extensive range of tools for algorithm development, data visualization, data analysis access, and numerical computation.

[2]The related fast ns-2 simulator is the modification of the network simulator (ns-2). Fast ns-2 is developed at the Laboratory for Software Technologies at ETH Zurich to enable simulation of large scale ad hoc wireless networks.

- **CASiNO** is a framework for designing visualizable object oriented network simulations (Battou, Khan, et al., 2002), supporting distribution and parallelization (Bhutani, Khan, & Roy, 2002; Bhutani & Khan, 2002). CASiNO is the foundation of several large scale complex network simulations. Among the most prominent of these, the Signaling Entity for ATM Networks (**SEAN**), developed Battou, Marsh, et al. (2002), and The PNNI Routing and Simulation Toolkit (**PRouST**), developed by Battou, Khan, and Mountcastle (1999).

The above simulation platforms have been reviewed and compared extensively in the literature, including for example by Wehrle and Gross (2010); Brakmo and Peterson (1996); Aguilar and Castilla (2009), and others.

8.3 Tiered architecture

The architecture of MABUSE follows scalable software design patterns for enterprise-class software (Fowler, 2002). MABUSE is structured as a multi-tier system in which the presentation, application processing, and data management functions are logically separated (Eckerson, 1995). The business and logic tiers are built using a framework base layer which provides support for logging, serialization, probabilistic computations, discrete event simulation, and optimized memory-resident data structures. The overall layered architecture and its constituent components are depicted in Figure 8.2. By breaking up the MABUSE application into distinct tiers, the process of augmenting the system to provide major new functionalities requires only the modification of an isolated specific layer, rather than rewriting the entire application over.

At the implementation level, MABUSE's main C# solution is named "DNA" — Dynamic Network Analyzer.

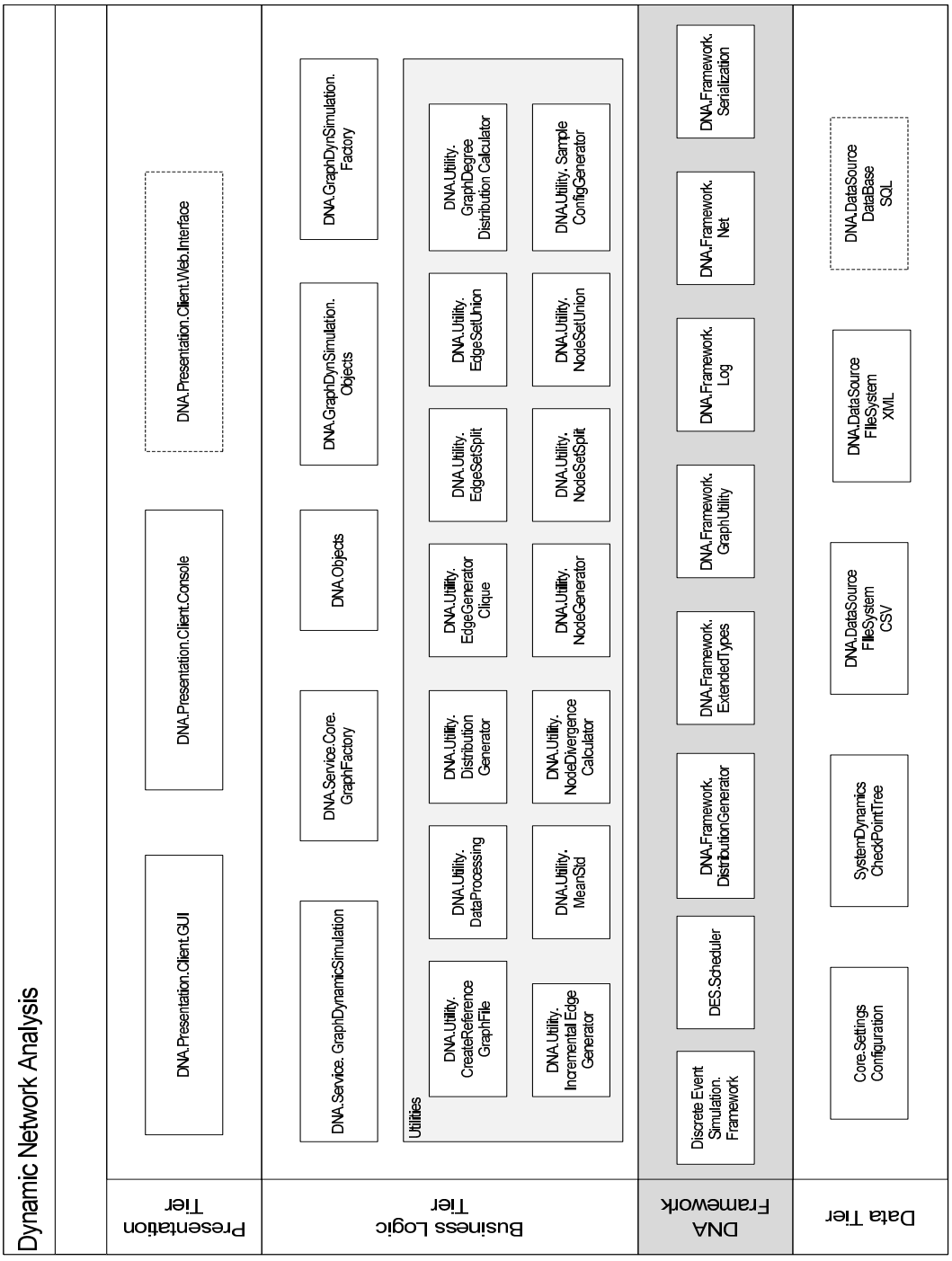

Figure 8.2: The multi-tier architecture of MABUSE.

8.3.1 Presentation Tier

The presentation tier is the topmost level of the application. This tier displays the graph and simulation attributes to the user, and embodies direct interactions with the user.

DNA.Presentation.Client.Console is the command line interface between the user and the DNA application. For users who are terminal and command line oriented this module provides for them full interactive capabilities with the executing service processes, simulation checkpoints and simulation parameters.

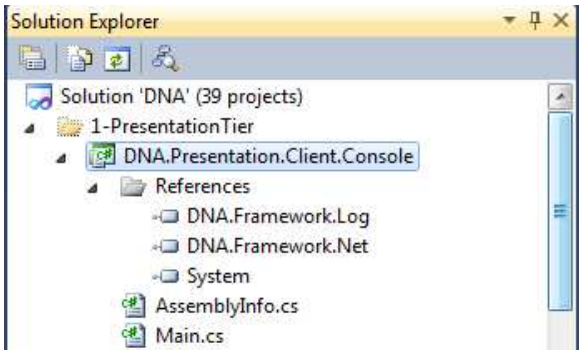

Figure 8.3: DNA.Presentation.Client.Console

Main.cs is a class that has been designed to facilitate execution as a client application on Linux, Windows and Mac, connecting the user to the DNA server and core service functionalities. The user can submit serialized commands and arguments to a set of utilities on the server to allow graph generation and initialization, and calibrating graph evolution simulation process.

DNA.Presentation.Client.Drawing is the Graphical User Interface, representing one of the top level modules, through which the user may observe the graph dynamics, and be presented with graphical diagrams and charts for the simulation process.

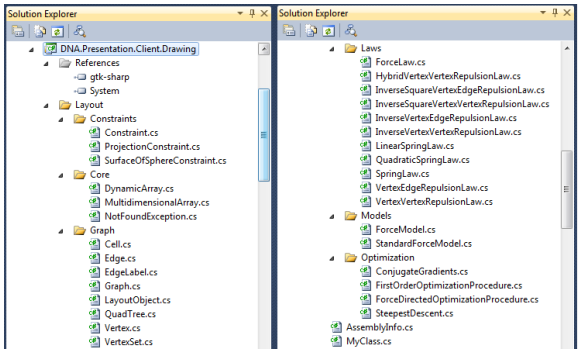

Figure 8.4: DNA.Presentation.Client.Drawing

8.3.2 Business Logic Tier

The Business Logic Tier represents the layer that coordinates the application execution, processes client requests, processes initialization and simulation tasks. This layer makes the logical decisions based on predicates and simulation distributions, and evaluates the various probability distribution functions. It also dispatches, moves and distributes data and events between other layers and modules in the system.

Application layer

DNA.Service.Core.Console is one of the key and core modules that is responsible of loading graph nodes and edges and binding instances of them based on global unique identifiers (GUIDs). This module loads various configuration files (via the Data tier) as needed to initialize the graph factories (Gamma, Helm, Johnson, & Vlissides, 1994) which will create node and edge instances that need to be created dynamically at run-time. This process loads the application layers and configures them based on the system attributes and passed parameters and arguments.

DNAConsole.cs is an essential process that needs to be running on the DNA server. Any configuration errors that may exist in the distribution and simulation configuration files (via the Data tier), repre-

sented in syntax errors or inconsistencies, are handled by this process. The system exception handling conducts a graph file validation process to make sure that the graph nodes are valid and all graph edges are correctly attached to the nodes, without any orphan objects (edges instances with any node attachments). It also verifies application instances follow the application logic semantics, guards and constraints.

DNA.Service.GraphDynamicSimulation has ownership of the static graph instances, together with their constituent nodes and edges. It is responsible for loading the graph manager and the dynamic business logic. This core process manages time-related process, and the logic by which the graph evolves: including the birth/death process, i.e. the introduction of new nodes to the graph, and the removal of existing nodes. The edges addition and removal process follows the probabilistic processes specified by the dynamic edge churn model. The node and edge factories are the configured modules responsible for constructing node and edge instances in accordance with the model and the provided distributions and parameters.

GraphDynSimDaemon.cs is a continuously listening process that coordinates between the client user application interaction and the service respond, as well as managing the evolving checkpoints of the graph simulation. It also handles serialization and deserialization to the data tier. The core process starts by loading configuration files (via the Data tier), and proceeds to construct the application core layers. What follows is the construction and initialization of business logic instances. Following the initialization of business logic components, logger observers are enabled, allowing each layer, component and module in the system to log information, debugging data, warnings and fatal exceptions.

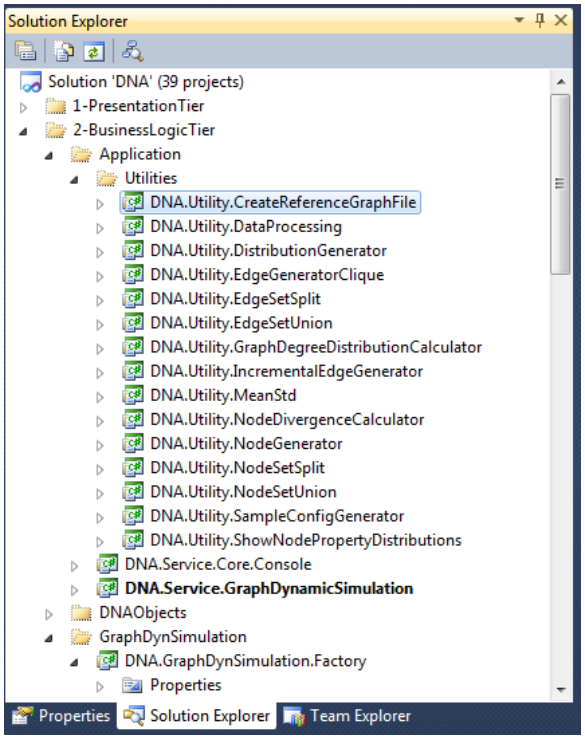

Figure 8.5: DNA.Utilities

Utility programs

The DNA server provides a set of stand alone utilities to facilitate end user manipulation of configuration and distribution files (via the Data tier). In addition, the utilities serve to provide the data processing and graph generation functions necessary for preparing and executing dynamic simulations. The utilities are essential for the system user to set the server's initial state, and to produce analytical metrics and results.

DNA.Utility.CreateReferenceGraphFile executes the process of loading serialized graph nodes from the file system, and populating each node with the associated property values. The utility validates the correctness of the graph nodes file before loading nodes into memory. Next, the serialized edges file is loaded and validated. The graph edges

go through 2 validation steps: in the first step univariate and bivariate properties are added, and edge instances are constructed in memory; second, the edges are validated against the graph node instances in memory, and vertex-edge attachments are made. The full validated graph instance is loaded into memory, and the utility creates a reference file representing this validated graph bundle.

DNA.Utility.DataProcessing is the utility which prepares and validates files (through the Data tier) and conducts pre-processing for the DNA service.

DNA.Utility.DistributionGenerator is the utility which enables the user to compute attribute distributions from risk networks. The utility takes as input a set of nodes and edges, and produces univariate and bivariate distributions from these, for use in the structural model of the provided network.

DNA.Utility.IncrementalEdgeGenerator is a utility that generates a risk network incrementally, based on an inductive process in which new nodes join an existing stable graph. The utility takes as input a graph reference file which includes a pointer to an XML file containing a list of N nodes (wherein each node has a list of node attribute values), and a second pointer to an XML file containing a list of E edges (wherein each edge has a list of edge attribute values). In addition, it requires an edge generation configuration file containing a list of D nodes, in which each node has a list of attribute values. These D nodes are attached sequentially to the network of N nodes and E edges. Another input required by the utility is the distribution file specifying ideal node degrees, that is the probability that a node, upon arrival, will attach to a given number of preexisting nodes.

The utility main process executes the following logic: Consider each of the D nodes in turn. For each node, determine its ideal degree by randomly sampling from the degree distribution file. Consider a star of edges between the new node and all existing nodes. For each edge, construct a vector of weights (one per node attribute), where each entry in the vector is determined using the bivariate frequency files and other constituents as per the model framework. Collapse this vector to a single scalar propensity, as specified by the aggregation type. Interpret

this scalar as a relative likelihood for the edge. Sample edges from the star (with replacement) until the desired degree is attained. For each edge selected, select attributes by random sampling of the univariate distributions of edge attributes.

DNA.Utility.EdgeGeneratorClique is a utility which takes as input an edge generation configuration file. In this configuration file, we specify the properties and attributes of each generated edge instance, provide a path to an existing file of nodes, and specify which node attributes influence edge formation likelihoods. The user also specifies a tag to represent the "edge type" of the edges that will be generated. This allows the user to superimposing multiple graphs onto the same set of graph nodes, thereby supporting multiple layers in the risk network. Finally, the user specifies an aggregator configuration file that specifies the aggregation function that is used to coalesce together the bivariate attribute distributions for each influential node attribute.

Note: Both the **DNA.Utility.IncrementalEdgeGenerator** and the **DNA.Utility.EdgeGeneratorClique** make use of node and edges factories. The factory design pattern requires configuration files (via the Data tier) which specify the node and edge attributes and their corresponding distributions. The node and edge factories retrieve these distribution files (via the Data tier) as needed, and perform random assignment of node attributes based on the specified distributions. The probabilistic attribute selection is conducted by constructing a Probability Distribution Function object for each node and edge property. From this Probability Distribution Function object a Commutative Distribution Function object is constructed, whose inverse is then used to convert uniform sampling into sampling over the categorical set of values for the variable. Model degeneracy is also estimated by computing the Shannon-Jenson divergence of the node and edges properties against the original user specified distributions. The output of this utility serves as the initial risk network for the DNA server simulation processes, together with divergence measures between the population and the attribute distributions.

DNA.Utility.EdgeSetSplit is a utility that can be invoked by the user in order to split a set of edges into two parts. The utility takes as input

an XML file containing a list of edges, and can be run in deterministic or probabilistic mode. In deterministic mode, the input file is split into two pieces, with a specified number of edges falling in each of the two output files (via the Data tier). In probabilistic mode, a probability is provided, and the utility randomly assigns each edge in the input file to one or the other of the two output files (written via the Data tier), with the specified probability. The utility outputs two XML files (written via the Data tier) embodying the requested split of the input edge set. For safety, the utility conducts output validity checks, ensuring that GUIDs are preserved, the two output files are disjoint, and their union is precisely equal to the input file.

DNA.Utility.EdgeSetUnion is a utility that can be invoked by the user to merge sets of edges. It takes as input a series of XML files with the specified probability. The utility outputs two XML files (read via the Data tier) each containing a list of edges, with each edge having list of attribute values. The output of the utility is an XML file containing the union of all edges. The utility conducts output validity checks to ensure that all edge GUIDs are preserved, and appear without duplication.

DNA.Utility.GraphDegreeDistributionCalculator is a utility is invoked by the user to compute a degree distribution from a set of nodes and edges. It takes as input a graph reference file which includes a pointer to an XML file containing a list of N nodes (wherein each node has a list of node attribute values), and a second pointer to an XML file containing a list of E edges (wherein each edge has a list of edge attribute values). For each edge type the utility compute the graph nodes degree distribution and serialize the resulting distribution to an XML output file. The utility also computes a cumulative degree distribution over all edge types.

DNA.Utility.NodeDivergenceCalculator is a utility is invoked by the user to compute the divergence between a set of nodes and a set of distributions. It takes as input an XML file containing a list of nodes (wherein each node has a list of attribute values), a configuration file containing a list of node attributes names (and a univariate distribution file for each of these attributes). The utility computes the Shannon-Jensen divergence between the sample distribution of the attribute exhibited by the set of nodes, and the authoritative univariate distribution

of the same attribute—for each node attribute. The utility serialize the output of this calculations to serialized XML file.

DNA.Utility.NodeGenerator is a utility that may be invoked by the user to create nodes. It takes as input, a configuration file containing a list of node attributes names, and specifications of the univariate distribution files (read via the Data tier) for each of the node attributes. In addition to the configuration file the utility takes the number of nodes to be created, and a random seed as additional arguments. The utility produce an XML file containing a list of nodes, where each node has a list of node attribute values. Each node's attribute values are generated by independent random selection using the specified univariate distributions.

DNA.Utility.NodeSetSplit is a utility which takes an input of an XML file containing a list of nodes (wherein each node has a list of attribute values). , and can be run in deterministic or probabilistic mode. In deterministic mode, the input file is split into two pieces, with a specified number of nodes falling in each of the two output files. In probabilistic mode, a probability is provided, and the utility randomly assigns each node in the input file to one or the other of the two output files, with the specified probability. The utility outputs two XML files embodying the requested split of the input node set. For safety, the utility conducts output validity checks, ensuring that GUIDs are preserved, the two output files are disjoint, and their union is precisely equal to the input file.

DNA.Utility.NodeSetUnion is a utility that can be invoked by the user to merge sets of nodes. It takes as input a series of XML files each containing a list of nodes, with each node having list of attribute values. The output of the utility is an XML file containing the union of all nodes. The utility conducts output validity checks to ensure that all edge GUIDs are preserved, and appear without duplication.

DNA.Utility.SampleConfigGenerator is a utility which assists the user in building configuration file to the DNA service. The utility generates templates and samples for the XML simulation configuration file, the node generation configuration file, the edge generation configuration

file, the attributes aggregation configuration files and a full set of probability distribution files.

DNA.Utility.ShowNodePropertyDistributions is a utility which computes the univariate distribution of attributes manifested in a set of nodes, nodes file, for each property listed in the Configuration file. Then the computed distribution is serialized into standard XML format of a distribution.

DNA.Utility.MeanStd is a utility which analyze simulation outputs across multiple trials, showing the mean and standard deviation as a function of time, across multiple trials.

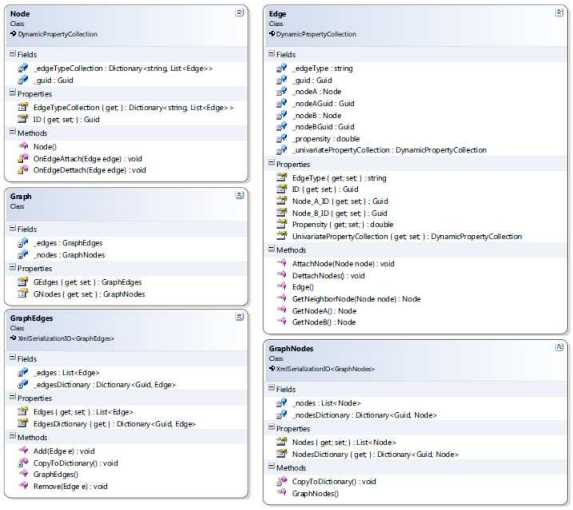

Figure 8.7: DNA.Objects

DNA objects and assemblies

DNA.Objects is a base common assembly that defines core objects like the Node class which hold the node attributes and properties, the Edge class which bind nodes in directional and unidirectional graph setting,

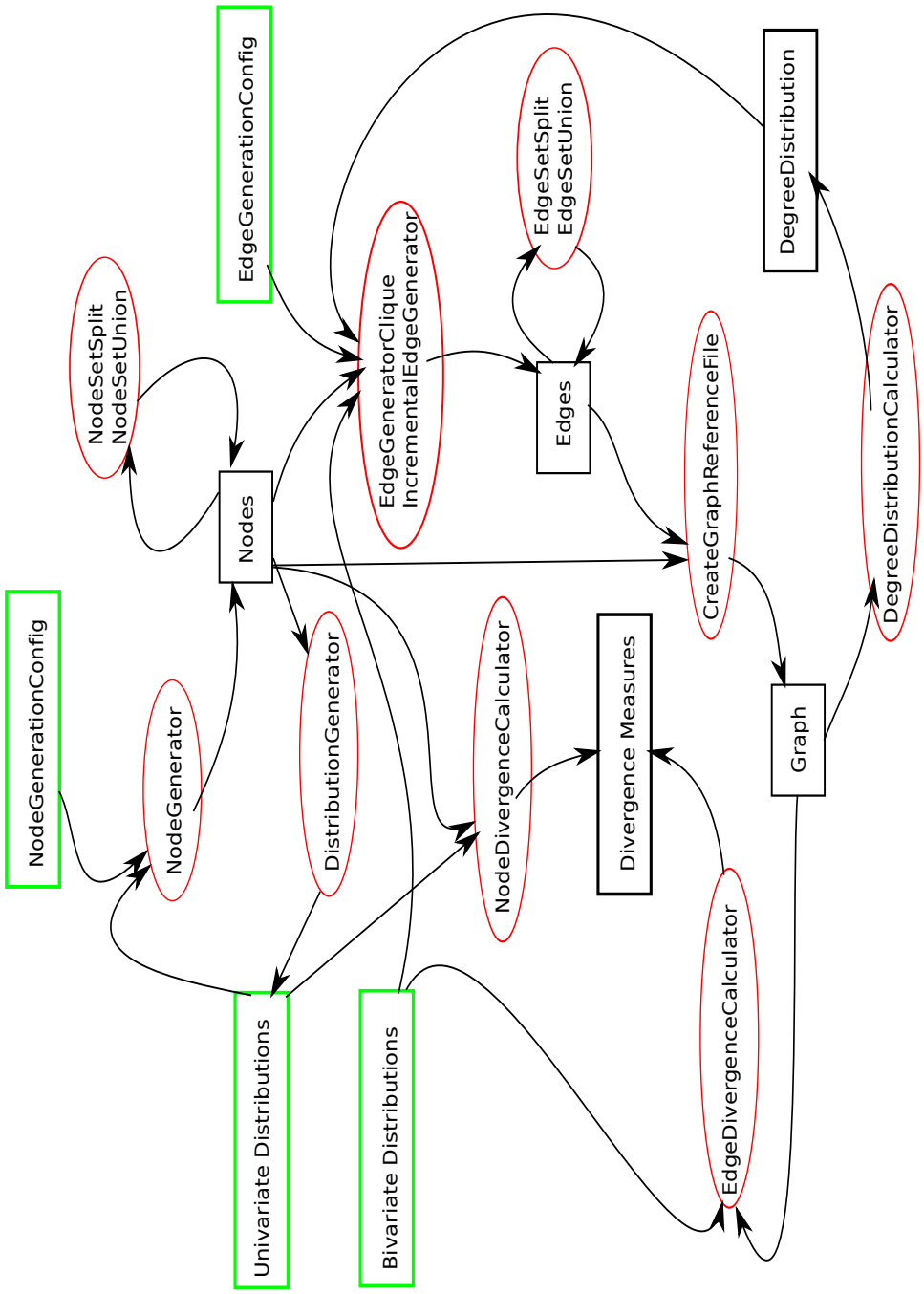

Figure 8.6: The producer-consumer relationships between DNA utilities.

with support for univariate and bivariate distributions. In addition to the node and edge classes, the assembly defines the collections and dictionaries for graph nodes and graph edges dynamic structures, through which formatting, serialization and de-serialization to the Data tier is conducted.

DNA.Service.Core.Settings is the common assembly for graph simulation configuration objects. It defines the dynamic property rules and both the node generation and the edge generation configuration objects. The utility also define the attributes aggregation configuration objects, and holds the application settings caching instance. The utility provides serialization and de-serialization functionality to the system configuration objects, via the Data tier.

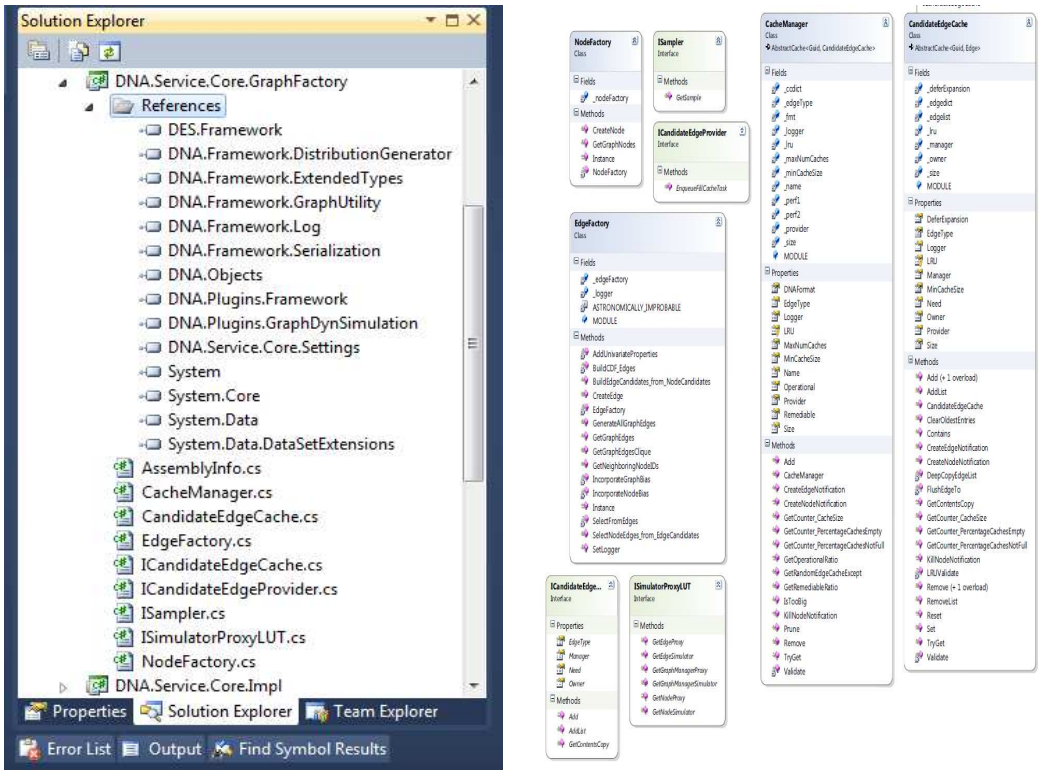

Figure 8.8: DNA.Service.Core.GraphFactory

DNA.Service.Core.GraphFactory is a creational assembly implementing the factory design pattern. This pattern models an interface for creating DNA graph objects which at creation time defer to its subclasses the decision of which graph object or class to instantiate. The DNA core service makes use of this Factory Pattern since it is responsible for "manufacturing" nodes and edges, but the precise types of these may change based on Business Logic plugins. The Factory Pattern thus facilitates a loose coupling, by eliminating the need to bind application-specific classes into the code.

DNA.Service.Core.SystemDynamics is a utility assembly which maintains historical information as the graph simulation evolves. As the simulation proceeds, a sequence of snapshots and checkpoints are generated, allowing the system to track the divergence of the risk network from its starting point and detecting possible onset of model degeneracy. The serialized checkpoints are milestones to which user can "roll back" if model degeneracy arises. This assembly provides the ability to move backward along a tree of simulation checkpoints. The checkpoint hierarchy is stored in serialized XML file (via the Data tier). This allows the system user to conduct multiple trials, measure divergences, and reconfigure and calibrate system to the particular simulation domain.

Plugin architecture

The **DNA.Business-Logic.GraphDynSimulation** is a business logic extension, to which all the DNA framework and functionalities are provided via a mediator. In effect, it is a "plugin" to the Business Logic layer. The mediator provides the plugin with discrete event simulation functionalities, as well as proxies to edge and node instances. This provides the plugin with access to graph properties and node attributes. The plugin, in turn must specify node, edge, and simulator behaviors or "simulators", through its own custom code. It does this using a set of finite state machine primitives which are provided to plugin developers. This helps maintain correct, event-triggered behavior implementations, and consistency in plugin designs.

Simulation objects and assemblies

DNA.GraphDynSimulation.Objects is the assembly which contains the base classes and implementation for finite state machine instances, as well as the base implementation of the mediated graph objects and node and edge proxies.

DNA.GraphDynSimulation.Factory is a base creational assembly implementing the factory design pattern. This pattern models an interface for creating the dynamic simulator objects, which represents the plugin instances constructed from the extended business logic module. The dynamic simulation modules call this factory assembly for "manufacturing" node, edge and graph simulators (i.e. behavioral specification objects).

8.3.3 Data tier

The Data tier isolates all components from direct access to the file system and database servers. Through this tier all information is stored and retrieved. This tier keeps data storage neutral and independent from the application modules or business logic. This tier also abstracts the data source which improves scalability and performance.

DNA.DataSource is a project module contains all of the file system, database and instance objects used by the application. It provides a single unit for authoring, deploying, and managing the data-tier objects instead of having to manage them separately. The abstractions in the data source allow the application to work effectively with various data base system like Oracle, MySql and Microsoft SQL as well as the file system, all without direct impact on the application code and business logic. Currently, the data tier is configured to retrieve and store data to an XML based file system. The implementation support data storage and retrieval from Linux, Windows and Mac OS X based systems. If at a later stage, we migrate to a SQL based data base, this will be achieved without recompilation of the server code or impact on the design and implementation of the higher tiers.

8.3.4 Framework tier

In the Framework layer, reusability is the key feature in all of the code segments in this layer modules. The Framework provides common functionalities to the other application layers and modules. The Framework's reusable modules and classes reduce implementation time, increase the likelihood that prior testing and use has eliminated bugs and localizes code modifications when a change in implementation is required.

Key common functionalities are the mathematical computation of distribution functions as well as the random number generation modules. Other functionalities provided to the application components and layers are logging for purposes of debugging, as well as reporting normal process information and warnings. In addition, the Framework tier provides common graph related data types.

DNA.Framework.Log is a framework project module is based on Singleton Logger class through which a single instance consolidate all logging events in the system and dispatch them to a set of observers. The module allows the application components to control which log statements are output by assigning each output a severity level, with arbitrary granularity. Its verbosity is fully configurable at runtime using external configuration files. The logger assembly supports a set of logging event observers, file observers, database observers and console observers, each can be individually configured to filter and categorize log events.

Inserting log statements within the code is an effective method for debugging it, as debuggers are not always available or applicable when switching between different operating systems and environments that the application support. Moreover, once the MABUSE application has been distributed to researchers and users, the development team can use effective logs and traces from systems process execution to diagnose and fix issues, since the logs provides precise context about the execution of the application. Once inserted into the code, the generation of logging output requires no additional intervention.

DNA.Framework.DistributionGenerator is a framework assembly that provide shared computational functionalities for handling Probability

Distribution Functions, Cumulative Distribution Functions, Discrete Distribution Tables and Shannon Jensen Divergence computations, as well as a common multi-purpose random number generator.

DNA.Framework.Serialization is a common assembly which facilitate serializing instances and objects to the file system in standard XML file formats.

DES.Framework is an assembly which maintains the base implementation for the discrete event simulator (described in the next section), related objects and interfaces, like the simulation event, the scheduler, the event handler.

DNA.Framework.GraphUtility defines the edge and node propensity aggregation instances.

8.3.5 Framework for Discrete Event Simulation

A Discrete Event Simulation (DES) framework controls events in time, through a queue of events sorted by the simulation time when they should occur. The simulator processes each event in the queue sequentially, and possibly triggering new events when existing events are handled. The following are the main components of almost every DES framework:

Event queue A list that contains all the events waiting to happen, sorted by time.

Simulation Clock A global variable that represents the present simulation time.

State variables Variables that, together, completely describe the state of the system.

Event routines Routines that handle the occurrence of events. If an event occurs, its corresponding event routines are executed to update the state variables and the event queue appropriately.

Input routines The routine that gets the input parameters from the user and supplies them to the model.

Report generation routine The routine responsible for calculating and analyzing results and exporting them out to the end user.

Initialization routine The routine responsible for initializing the values of the various state variables, global variables, and statistical variables at the beginning of the simulation program.

The **SimEnt** is an abstract class, which defines the characteristics of a simulation entity. The base class can not represent a functional simulation entity, as it is not a concrete implementation. To fully define the functionality of a simulation entity (thereby making it concrete and instantiable), one needs to specify how the particular SimEnt will respond to the arrival of events.

The **SimEvent** represents a simulation event, and is an interface in the DES framework. Application level events are concrete classes which implement the SimEnt interface. SimEvents happen at SimEnts. SimEnts respond to the arrival of SimEvents by changing their own state, and by scheduling more SimEvents to be sent to other SimEnts (or to themselves) in the future. This is the essence of a discrete event simulation. .

The **Scheduler** is a C# implementation based on the java based DES presented by (Guizani et al., 2010). The scheduler represents the core component of the simulator. Since the scheduler is the focal point of the simulator, we allow one and only one instance of the scheduler to be constructed. We achieve this by coding the scheduler class as a Singleton class. The scheduler maintains a list of SimEvents, ordered by the time at which the SimEvent is to be delivered to a specified SimEnt. The receiving SimEnt can interrogate the arriving SimEvent to determine its nature, as well as determine who the SimEvent was sent by. These factors go into the determination of how the SimEnt will respond.

8.4 Software implementation

As of September 2011, the MABUSE platform is implemented as roughly 50,000 lines of code written in the C# programming language (ECMA International, 2006) over the Mono[3] runtime environment. Using C# makes the MABUSE simulations execute almost as fast as if they were written in native C. At the same time, using the Mono runtime allows us to maintain easy binary portability across Windows, Macintosh, and Linux platforms—indeed, the same executable file runs on all platforms.

[3]Mono is a free and open source project led by Xamarin, and seeks to create an ECMA-standard compliant .NET-compatible set of software development tools including, among others, a C# compiler and a Common Language Runtime.

Chapter 9

Conclusions and the road ahead

The central purpose of this project has been an exploration of well-known but until now unaccounted for HIV-1 infection patterns among injecting populations. To accomplish this, we have modeled the actor interactions within a risk network, an evolving approach in HIV research. Because IDU communities remain reservoirs of potential HIV infection for the larger communities in which they live and with whom they interact, understanding the short and long term dynamics of infection transmission represents an important public health priority for both the IDU community itself, and the general population that surrounds them.

The project began with three interrelated hypotheses:

- **Hypothesis 1.** Firewall phenomenon will consist of individual agents with mature infections which partition the overall risk network into a series of clusters, in which uninfected clusters remain relatively stable (over simulation time).
- **Hypothesis 2.** Local (neighborhood-level) social network structures within IDU networks will combine with varying rates of individual HIV-1 infectiousness over the course of time to stabilize infection rates—contributing to the proposed firewall effect that allows IDU communities to remain at relatively stable infection levels below saturation.

- **Hypothesis 3.** IDU networks with stable, sub-saturation levels of HIV-1 infection, will continue to produce new infections over the course of time that fail to propagate fully throughout the network, but will instead function as reservoir of overall network infectiousness.

All three hypotheses were shown to be true—with varied levels of effectiveness—based on simulations set according to network parameters drawn from the SFHR data set, from Bushwick New York in the early 1990s. Throughout a variety of simulation scenarios, the "firewall effect" appears to form an important barrier to HIV infection in risk networks. Small, component level pockets of uninfected nodes separated from the rest of the network by mature, low infectious nodes, co-exist alongside a low but steady number of new infections which nevertheless fail to propagate across the topology. From this we can say with increasing confidence that, as originally proposed by Friedman et al. (2000), the presence of highly infectious individuals engaging in risk activities within a network does not, alone, ensure that HIV infection spreads throughout a risk network.

Taken together, these findings represent a step forward in an approach that sees networks and communities—social bodies rather than single individuals—as carriers and transmitters of disease, without ignoring the fact that such collective bodies are composed of actors whose individual actions and decisions give networks and communities their form. By approaching networks as emergent phenomena—as entities whose characteristics derive from the aggregate behavior of multiplex actors, none of whom alone determine the overall dynamism of the whole—we advocate a complex systems approach.

In the course of this research, several corollary findings emerged that demonstrate the establishment of our three main hypotheses. Included among these is the fact that sub-saturation stabilization of HIV rates in IDU networks was a robust phenomenon, which appeared across a wide variety of parameter settings. As importantly, we note that this stabilization-across-settings took place despite the fact that no behavioral changes were induced among network actors. The same behavioral profile—and the same network forming actor preferences—that created the initial rapid infection within the simulation networks also produced long, steady periods of near constant HIV infection rates. These findings do not rule out the effects of individual be-

havior change, but do show that network-structural factors can account for observed infection dynamics. While subsequent declines in the HIV rate among injecting drug users in New York are not explained here (and very likely owe their dynamic to interventions aimed at altering individual behaviors, user-education, and the like (Des Jarlais, Arasteh, & Friedman, 2011), no such explanations are required to understand the early dynamics of infection spreading—and non-spreading.

Past researchers have also drawn attention to structural factors (Adimora et al., 2006; Neaigus et al., 1996; Kottiri et al., 2002; Fernando et al., 2003; Gore-Felton et al., 2003) though in most cases this refers to macro-social features such as gender, race/ethnicity, or age rather than local topologies (though see Potterat et al., 1999, 2002; Friedman et al., 1997; Friedman, 1999). One of the key findings here—discovered in the preliminary steps of fitting model parameters—is that local structural factors, in the form of network transitivity, must also be accounted for in our discussions of the effects of social structure. Too few projects gather the necessary structural data to determine whether this is the case more broadly.

An important feature of an approach based on simulation of complex systems is that it allows us to examine multiple instances of phenomena for which on-the-ground empirical research would prove difficult or impossible, such as the growth and shrinking of networks through time. While simulation remains a less desirable approach that empirical research, where such research is not possible, simulation allows a view of long-term dynamics that can point us toward (or away) from explanations that might otherwise appeal to mistaken "common" sense.

Tests of parameter settings also provide a number of observations. We were surprised to find that significant growth and shrinkage of networks had little effect on HIV infection dynamics or on the network structural factors that influenced its spreading. This is, as far as we know, a new finding—suggesting that interventions aimed at lowering drug use/drug network participation alone may not lower infection rates or the ongoing production of new infections in IDU networks. Where HIV rates have fallen in shrinking networks, our findings would suggest that it is factors other than the shrinking of the network itself that have led to the decline.

Our research also suggests that overall network size plays a key role in HIV dynamics among injecting drug user networks. Consistently, networks of size 5,000 through 25,000 behaved within a narrow (and therefore predictable) range of overall characteristics. Networks of 1000 nodes or fewer, on the other hand, showed high variability in their network-wide behavior. This latter finding bears serious consideration for those concerned with interventions aimed at influencing the overall rate of HIV among injecting drug user networks. If smaller networks show high variability in their dynamics—leading to the idea that they are more subject to stochastic events than networks of large size—then understanding where and how particular interventions will succeed or fail becomes very difficult.

What such variability in outcomes indicates is that stochastic factors may outweigh node level dynamics in determining network-wide outcomes through time in small networks. Put another way, the outcome of interventions in small-scale networks may not serve as good indicators of likely outcomes of the same intervention in other small networks, nor in the same networks at a different time, nor in large networks. In each case, the effects of random events may render the otherwise most successful interventions moot, or the most ill-adapted interventions successful—this without a change in the underlying set of network attributes or dynamics. We recognize that this finding represents a difficult challenge to policies advocating "Demonstrated Evidence-Based Interventions", or DEBIs (Galbraith et al., 2011). Regardless of whether the precise findings regarding scale seen here hold up under further investigation, it is clear that factors of scale ought to be an important criterion for evaluating what constitutes "demonstration" in evaluating intervention success or failure.

Not surprisingly, varying the overall levels of risk behavior of network actors shows high impact on overall network HIV rates. Indeed, even small changes in this setting affected viral prevalence. Yet such changes did not seem to affect overall infection-spreading dynamics. All but the lowest risk behavior settings continued to produce an initial "hot spike" in infections, followed by a long period of stabilization.

In much the same way, changes in the likelihood that a risk event would result in infection across serodiscordant risk partners showed a consistent impact on both the overall rate of network infection, and on the stabilization

potential of the network. At levels well below (1/50th) the standard SFHR level of transfer risk, the virus fails to spread at all; while at a level twice the standard risk, the network-wide rate stabilizes more quickly and to a higher level.

Likewise, the dynamics of high levels of infectiousness deserve comment. High rates of infectiousness regularly produced a higher "hot spike" and higher overall HIV rates, though they do not produce a greater number of highly infectious nodes in the mature network than trials using a lower infectiousness value. As in simulations of lower levels of infectiousness, the rate at which new infections were generated after the period of initial rapid spread, is relatively constant. If new (and thus highly infectious) cases of HIV are seen as the most persistent threat to surrounding communities, the level of this threat would seem to be robust against changes in the level of infectiousness of the virus itself.

Along these lines, testing the effects of transient network members showed that even low numbers of short term participants in an IDU network can have a serious impact on the overall HIV rate. While HIV stabilization was manifested, transient participation increased HIV rates to levels approaching saturation. It has long been believed that transient visitors pose a risk of infection from IDU communities to the general public. What seems equally clear is that transient users play a role in increasing rates of HIV infection within IDU networks.

Similarly, simulations which varied participants' time-in-network showed important effects on the overall network HIV prevalence. Where average participation time is lowered considerably, the overall HIV rate does not stabilize at the same level (or to the same extent) as when participation is prolonged. We observe that long-term participation in the network creates very stable rates of infection, despite the fact that individuals within the network continue to "churn" their connections among one another, and that high turn over of network participants, even where new participants enter the network in an uninfected state, necessarily produce both higher and continuously rising HIV rates. Given that many law-enforcement-based interventions produce high turn-over of network participants who subsequently reenter the network at a later time, such interventions would seem likely to have important negative consequences for HIV infection rates.

The number of new infections in networks whose actor participation time varies also showed marked differences from the standard SFHR simulation. In situations of low average participation duration, the characteristic "hot spike" is either absent or less pronounced, while the production of new infections over time significantly exceeds that of the standard network. As with the overall network-wide HIV rate, the high turnover networks feature greater risk of infection transmission, due to the higher proportion of new infections as a percentage of the total population. On the other hand, long-term mean participation settings continue to produce a steady number of new infections over time, but at a rate lower than the standard settings.

Again, these results point to the fact that interventions based around stabilizing social participation (such as New York City's HIV+ housing programs) can maximize structural barriers to HIV spreading, or minimize them when they move people from place to place over short periods of time. Other examples of injection drug user geographic mobility, include those induced by limited access to methadone treatment, and residential mobility associated with living in decarceration facilities such as half-way houses or shelters.

Somewhat in contrast to the above observations, variation in the rate at which network actors change their risk partners produced little effect on overall HIV rates. At churn rates that are faster than the standard, the firewall effect is able to account for a greater number of HIV negative nodes, while at rates of churn that are slower than the standard, it accounts for fewer of the HIV negative nodes.

We also note that, despite the fact that network transitivity/triadic closure were shown to be important structural elements in predicting the pattern of ties shown by the SFHR topology, varying the relative importance of triadic closure bias in network churn events had little effect on HIV rates. Like several of the churn parameters, wide variation of this setting seems to affect overall network topology, but not in ways that affect HIV transmission.

Together, these results serve as observations from a vantage point not available to empirical research. All should be viewed as testable hypotheses, and not accorded the weight of actual historical findings. In this light, they point to one of the key strengths of simulation based research: the ability to view currently-accepted ideas and theories from an new perspective which can, in

turn, raise new questions, suggestions, and points of critique. As an adjunct to both research and intervention planning, the potential contributions of such an approach are, as we see it, many.

The Road Ahead

Possible future plans for this research includes the following:

- **Interventions.** The MABUSE simulation platform can be extended so as to enable us to model proposed intervention strategies that are designed to control the spread of HIV in risk networks. In retrospective application, using MABUSE to fit dynamic network models of prior interventions would provide an understanding of the network-centric mechanisms underlying the relative merits of different approaches that have been considered historically in IDU communities, such as the one found in Bushwick on which our simulation was based. Applied prospectively, such a platform represents the first viable promise of a data-driven stance toward public health policies and their optimized design *based on network structural dynamics*. Simulations could also be used to provide a measure of sensitivity to model parameters, which in turn would yield a better understanding of which aspects of the environment are most critical to ensuring the anticipated outcomes. Simulation of proposed interventions—potentially at the scale of small cities and over multiple decades—would enable one to determine reliable local predictors as to where (in the network) and when (in time) the policies were anticipated to be most/least effective in meeting their intended objective. These insights would then be used to adjust and augment the proposed intervention, in what we anticipate would be a cyclic design-simulate-design process.

- **Fidelity.** The network simulations here entail 3 potential dimensions of real world fidelity: the risk network, the risk event, and the pathogen. In each case, these were treated here singularly. That is, we considered a risk network largely in isolation from the ambient social network in which it is embedded (except in the case of transients, which quickly

pointed to the centrality of extra-network interactions). At the level of the event, again we chose to amalgamate a variety of actual behavioral means for infection transmission into a single risk act type. And in the case of the pathogen, we considered HIV in isolation from other factors of co-infection. The MABUSE platform is capable of incorporating multiplicity in each of these dimensions.

- **Scale.** One strength of the MABUSE platform is its ability to simulate large networks. The simulations of 25k nodes described here can be expanded to networks of 100-250k nodes. One avenue for this is the implementation of parallel processing. While this scale likely dwarfs the majority of risk networks outside of very large cities, it would allow for the full modeling of risk networks as they interact with the larger social networks in which they are embedded. Simulations of this sort move further away from closed-network assumptions and toward still more accurate, real world, epidemiological trajectories. This would also allow us to move away from coarse prevalence estimates and toward questions of viral distributions in the general population.
- **Co-infection** The modeling co-infection dynamics (such as co-infection with Hepatitis C) represent a second step in achieving greater fidelity with real world epidemiology. Toward this end, we have begun collaborating with Dr. Holly Hagan at the Center for Drug and HIV Research (NYU School of Nursing) and Sam Friedman (NDRI) on co-infection models that affect HIV rates in IDU networks. We are currently developing a joint research proposal with the Center for Drug and HIV Research, to be submitted in the next 6 months.
- **Multiple Relational Framework** The ways in which HIV is transmitted within IDU networks (and between IDU networks and the surrounding population) is likewise far from singular. Indeed research today points to sexual transmission as the key method of virus spreading even among injecting drug users (Des Jarlais, Arasteh, & Friedman, 2011). Here too, the MABUSE platform can be extended to incorporate multiple forms risk of interaction among network actors, maintaining multiple distinct pathways of infection that interact at the level of network-wide infection rates,

but emerge from distinct social dynamics. Like increases in scale and the incorporation of co-infection dynamics, a multi-relational framework would add greater fidelity to the simulations themselves, and with that, higher confidence in the simulator's ability to model complex real-world infection dynamics.

- **Neutral Networks.** A continuing question from the current set of findings is the extent to which the phenomenon of interest here—HIV stabilization and the firewall effect are specific to the topology of the SFHR network. While simulations of the IDU core of the P90 data showed similar results, we plan to test the effect of more neutral topologies, such as random networks or ERGM produced networks.

References

Adimora, A. A., Schoenbach, V. J., & Doherty, I. A. (2006, July). HIV and african americans in the southern united states: sexual networks and social context. *Sexually Transmitted Diseases*, *33*(7 Suppl), S39–45. Available from http://www.ncbi.nlm.nih.gov/pubmed/16794554 (PMID: 16794554)

Aguilar, R. M., & Castilla, I. (2009). Java for parallel discrete event simulation: a survey. *21st European Modeling Simulation Symposium proceedings*, 72–79.

Ahlgren, D. J., Gorny, M. K., & Stein, A. C. (1990). Model-based optimization of infectivity parameters: a study of the early epidemic in san francisco. *Journal of Acquired Immune Deficiency Syndromes*, *3*(6), 631–643. Available from http://www.ncbi.nlm.nih.gov/pubmed/2338619 (PMID: 2338619)

Ahmad, M., Akbas, M., Turgut, D., Palaniappan, R., Goldiez, B., & Dere, T. (2009, March). Design and development of a simulation environment in opnet using high performance computing. In *Proceedings of 2009 spring simulation interoperability workshop (siw)* (p. 426-434).

Altmann, S., & Hatnik. (2004). Using ModelSim, Matlab/Simulink and NS for simulation of distributed systems. *Parallel Computing in Electrical Engineering International Conference on*, *49*, 114–119.

Amadora-Nolasco, F., Alburo, R. E., Aguilar, E. J. T., & Trevathan, W. R. (2002, June). Knowledge and perception of risk for HIV and condom use among male injecting drug users in cebu city, philippines. *Drug and Alcohol Review*, *21*(2), 137–143. Available from http://www.ncbi.nlm.nih.gov/pubmed/12188992 (PMID: 12188992)

Bachanas, P. J., Morris, M. K., Lewis-Gess, J. K., Sarett-Cuasay, E. J., Sirl, K., Ries, J. K., et al. (2002). Predictors of risky sexual behavior in african american adolescent girls: Implications for prevention interventions. *Journal of Pediatric Psychology*, *27*(6), 519-530. Available from http://jpepsy.oxfordjournals.org/content/27/6/519.abstract

Baeten, J. M., & Overbaugh, J. (2003, January). Measuring the infectiousness of persons with HIV-1: opportunities for preventing sexual HIV-1 transmission. *Current HIV Research*, *1*(1), 69–86. Available from http://www.ncbi.nlm.nih.gov/pubmed/15043213 (PMID:

15043213)

Bagrodia, R., Takai, M., Chen, Y. an, Zeng, X., & Martin, J. (1998). Parsec: A parallel simulation environment for complex systems. *IEEE Computer*, *31*, 77–85.

Bagrodia, R. L., & Liao, W.-T. (1994, April). Maisie: A language for the design of efficient discrete-event simulations. *IEEE Trans. Softw. Eng.*, *20*, 225–238. Available from http://dl.acm.org/citation.cfm?id=630806.631113

Baldo, N., Maguolo, F., Miozzo, M., Rossi, M., & Zorzi, M. (2007). ns2-miracle: a modular framework for multi-technology and cross-layer support in network simulator 2. In *Proceedings of the 2nd international conference on performance evaluation methodologies and tools* (pp. 16:1–16:8). ICST, Brussels, Belgium, Belgium: ICST (Institute for Computer Sciences, Social-Informatics and Telecommunications Engineering). Available from http://dl.acm.org/citation.cfm?id=1345263.1345284

Barla, A., Odone, F., & Verri, A. (2003). Histogram intersection kernel for image classification. In *Image processing, 2003. ICIP 2003. proceedings. 2003 international conference on* (Vol. 3, pp. III–513-16 vol.2). Available from http://dx.doi.org/10.1109/ICIP.2003.1247294

Battou, A., Khan, B., Lee, D. C., Marsh, S., Mountcastle, S., & Talmadge, D. (2002). Casino: component architecture for simulating network objects. *Softw., Pract. Exper.*, *32*(11), 1099-1128.

Battou, A., Khan, B., & Mountcastle, S. (1999). Pnni and the optimal design of high-speed atm networks. *Informatica (Slovenia)*, *23*(3).

Battou, A., Marsh, S., Khan, B., Mountcastle, S., Talmadge, D., & Lee, D. C. (2002). Sean for modeling and simulating atm signaling. *Simulation*, *78*(4), 231-238.

Bearman, P. S., Moody, J., & Stovel, K. (2004, July). Chains of affection: The structure of adolescent romantic and sexual networks. *American Journal of Sociology*, *110*(1), 44–91. Available from http://www.jstor.org/stable/10.1086/386272 (ArticleType: research-article / Full publication date: July 2004 / Copyright 2004 The University of Chicago Press)

Bell, D. C., Montoya, I. D., Atkinson, J. S., & Yang, S. (2002, October). Social networks and forecasting the spread of HIV infection. *Journal of Acquired Immune Deficiency Syndromes (1999)*, *31*(2), 218–229. Available from http://www.ncbi.nlm.nih.gov/pubmed/

12394801 (PMID: 12394801)

Bhutani, K. R., & Khan, B. (2002). Minimizing communication costs in hierarchical multi-agent systems. In H. J. Caulfield et al. (Eds.), *Jcis* (p. 1435-1442). JCIS / Association for Intelligent Machinery, Inc.

Bhutani, K. R., Khan, B., & Roy, B. (2002). Minimizing computational load and communication costs in multi-agent systems. In S. G. Akl & T. F. Gonzalez (Eds.), *Iasted pdcs* (p. 363-368). IASTED/ACTA Press.

Binh, L. N. (2009). MATLAB simulink simulation platform for photonic transmission systems. *Intl J of Communications Network and System Sciences*, *02*(02), 97–117.

Blower, S., Hartel, D., Dowlatabadi, H., Anderson, R. M., & May, R. M. (1991, February). Drugs, sex and HIV: a mathematical model for new york city. *Philosophical Transactions of the Royal Society of London. Series B, Biological Sciences*, *331*(1260), 171–187. Available from http://www.ncbi.nlm.nih.gov/pubmed/1674152 (PMID: 1674152)

Brakmo, L. S., & Peterson, L. L. (1996, May). Experiences with network simulation. *SIGMETRICS Perform. Eval. Rev.*, *24*, 80–90. Available from http://doi.acm.org/10.1145/233008.233027

Brenner, B. G., Roger, M., Routy, J., Moisi, D., Ntemgwa, M., Matte, C., et al. (2007, April). High rates of forward transmission events after acute/early HIV-1 infection. *The Journal of Infectious Diseases*, *195*(7), 951–959. Available from http://www.ncbi.nlm.nih.gov/pubmed/17330784 (PMID: 17330784)

Brown, B. S., & Needle, R. H. (1994, November). Modifying the process of treatment to meet the threat of AIDS. *The International Journal of the Addictions*, *29*(13), 1739–1752. Available from http://www.ncbi.nlm.nih.gov/pubmed/7852000 (PMID: 7852000)

Burt, R. D., Hagan, H., Garfein, R. S., Sabin, K., Weinbaum, C., & Thiede, H. (2007, May). Trends in hepatitis b virus, hepatitis c virus, and human immunodeficiency virus prevalence, risk behaviors, and preventive measures among seattle injection drug users aged 18-30 years, 1994-2004. *Journal of Urban Health: Bulletin of the New York Academy of Medicine*, *84*(3), 436–454. Available from http://www.ncbi.nlm.nih.gov/pubmed/17356901 (PMID: 17356901)

Cates, W., Chesney, M. A., & Cohen, M. S. (1997, December). Primary HIV infection–a public health opportunity. *American Journal of Public Health*, *87*(12), 1928–1930. (PMID: 9431278 PMCID: 1381231)

Cubert, R., Goktekin, T., & Fishwick, P. A. (1997). Moose: architecture of an object-oriented multimodeling simulation system. In *Proceedings of enabling technology for simulation science, part of spie aerosense '97 conference* (pp. 22–24).

Curtis, R., Friedman, S. R., Neaigus, A., Jose, B., Goldstein, M., & Ildefonso, G. (1995). Street-level drug markets: Network structure and hiv risk. *Social Networks*, *17*(3-4), 229 - 249. Available from http://www.sciencedirect.com/science/article/pii/0378873395002640 (Social networks and infectious disease: HIV/AIDS)

Daar, E. S., Moudgil, T., Meyer, R. D., & Ho, D. D. (1991, April). Transient high levels of viremia in patients with primary human immunodeficiency virus type 1 infection. *The New England Journal of Medicine*, *324*(14), 961–964. Available from http://www.ncbi.nlm.nih.gov/pubmed/1823118 (PMID: 1823118)

Danon, L., Ford, A. P., House, T., Jewell, C. P., Keeling, M. J., Roberts, G. O., et al. (2011). Networks and the epidemiology of infectious disease. *Interdisciplinary Perspectives on Infectious Diseases*, *2011*, 284909. Available from http://www.ncbi.nlm.nih.gov/pubmed/21437001 (PMID: 21437001)

Des Jarlais, D. C., Arasteh, K., & Friedman, S. R. (2011). HIV among drug users at beth israel medical center, new york city, the first 25 years. *Substance Use & Misuse*, *46*(2-3), 131–139. Available from http://www.ncbi.nlm.nih.gov/pubmed/21303233 (PMID: 21303233)

Des Jarlais, D. C., Arasteh, K., McKnight, C., Hagan, H., Perlman, D. C., & Semaan, S. (2011, July). Associations between herpes simplex virus type 2 and HCV with HIV among injecting drug users in new york city: the current importance of sexual transmission of HIV. *American Journal of Public Health*, *101*(7), 1277–1283. Available from http://www.ncbi.nlm.nih.gov/pubmed/21566021 (PMID: 21566021)

Des Jarlais, D. C., Arasteh, K., Perlis, T., Hagan, H., Abdul-Quader, A., Heckathorn, D. D., et al. (2007, January). Convergence of HIV seroprevalence among injecting and non-injecting drug users in new york city. *AIDS (London, England)*, *21*(2), 231–235. Available from http://www.ncbi.nlm.nih.gov/pubmed/17197815 (PMID: 17197815)

Des Jarlais, D. C., Friedman, S. R., Novick, D. M., Sotheran, J. L., Thomas, P., Yancovitz, S. R., et al. (1989, February). HIV-1 infection among

intravenous drug users in manhattan, new york city, from 1977 through 1987. *JAMA: The Journal of the American Medical Association*, *261*(7), 1008 –1012. Available from http://jama.ama-assn.org/content/261/7/1008.abstract

Des Jarlais, D. C., Hagan, H., Arasteh, K., McKnight, C., Perlman, D., & Friedman, S. R. (2007, November). Herpes simplex virus-2 and HIV among noninjecting drug users in new york city. *Sexually Transmitted Diseases*, *34*(11), 923–927. Available from http://content.wkhealth.com/linkback/openurl?sid=WKPTLP:landingpage&an=00007435-200711000-00017

Des Jarlais, D. C., Perlis, T., Arasteh, K., Hagan, H., Milliken, J., Braine, N., et al. (2004, February). "Informed altruism" and "partner restriction" in the reduction of HIV infection in injecting drug users entering detoxification treatment in new york city, 1990-2001. *Journal of Acquired Immune Deficiency Syndromes (1999)*, *35*(2), 158–166. Available from http://www.ncbi.nlm.nih.gov/pubmed/14722449 (PMID: 14722449)

Des Jarlais, D. C., Perlis, T., Arasteh, K., Torian, L. V., Beatrice, S., Milliken, J., et al. (2005). Hiv incidence among injection drug users in new york city, 1990 to 2002: Use of serologic test algorithm to assess expansion of hiv prevention services. *Am J Public Health*, *95*(8), 1439-1444. Available from http://ajph.aphapublications.org/cgi/content/abstract/95/8/1439

Des Jarlais, D. C., Perlis, T., Friedman, S. R., Deren, S., Chapman, T., Sotheran, J. L., et al. (1998, December). Declining seroprevalence in a very large HIV epidemic: injecting drug users in new york city, 1991 to 1996. *American Journal of Public Health*, *88*(12), 1801–1806. Available from http://www.ncbi.nlm.nih.gov/pubmed/9842377 (PMID: 9842377)

Doherty, I. A., Padian, N. S., Marlow, C., & Aral, S. O. (2005, February). Determinants and consequences of sexual networks as they affect the spread of sexually transmitted infections. *The Journal of Infectious Diseases*, *191 Suppl 1*, S42–54. Available from http://www.ncbi.nlm.nih.gov/pubmed/15627230 (PMID: 15627230)

Duan, S., Shen, S., Bulterys, M., Jia, Y., Yang, Y., Xiang, L., et al. (2010). Estimation of HIV-1 incidence among five focal populations in dehong, yunnan: a hard hit area along a major drug trafficking route. *BMC Public Health*, *10*, 180. Available from http://www.ncbi.nlm.nih

.gov/pubmed/20374618 (PMID: 20374618)

Eckerson, W. W. (1995). Three tier client/server architecture: Achieving scalability, performance, and efficiency in client server applications. *Open Information Systems*, *10*(1).

ECMA International. (2006). *Standard ecma-334 - c# language specification* (4th ed.). Available from http://www.ecma-international.org/publications/standards/Ecma-334.htm

Endres, D. M., & Schindelin, J. E. (2003, July). A new metric for probability distributions. *IEEE Transactions on Information Theory*, *49*(7), 1858–1860.

Fennema, J. S., Van Ameijden, E. J., Van Den Hoek, A., & Coutinho, R. A. (1997, November). Young and recent-onset injecting drug users are at higher risk for HIV. *Addiction (Abingdon, England)*, *92*(11), 1457–1465. Available from http://www.ncbi.nlm.nih.gov/pubmed/9519489 (PMID: 9519489)

Fernando, D., Schilling, R. F., Fontdevila, J., & El-Bassel, N. (2003, June). Predictors of sharing drugs among injection drug users in the south bronx: implications for HIV transmission. *Journal of Psychoactive Drugs*, *35*(2), 227–236. Available from http://www.ncbi.nlm.nih.gov/pubmed/12924745 (PMID: 12924745)

Fishwick, P. (1994). Computer simulation: Growth through extension. In *Society for computer simulation* (pp. 3–20).

Fowler, M. (2002). *Patterns of enterprise application architecture* (1st ed.). Addison-Wesley Professional.

Frajzyngier, V., Neaigus, A., Gyarmathy, V. A., Miller, M., & Friedman, S. R. (2007, July). Gender differences in injection risk behaviors at the first injection episode. *Drug and Alcohol Dependence*, *89*(2-3), 145–152. Available from http://www.ncbi.nlm.nih.gov/pubmed/17276623 (PMID: 17276623)

Frank, O., & Strauss, D. (1986). Markov graphs. *Journal of the American Statistical Association*, *81*(395), 832–842. Available from http://www.jstor.org/stable/2289017 (ArticleType: research-article / Full publication date: Sep., 1986 / Copyright 1986 American Statistical Association)

Friedman, S. R. (1999). *Social networks, drug injectors' lives, and HIV/AIDS*. Springer.

Friedman, S. R., Curtis, R., Neaigus, A., Jose, B., & Jarlais, D. C. D. (2010). *Social networks, drug injectors' lives, and HIV/AIDS* (1st ed. Softcover

of orig. ed. 1999 ed.). Springer.

Friedman, S. R., Flom, P. L., Kottiri, B. J., Zenilman, J., Curtis, R., Neaigus, A., et al. (2003, February). Drug use patterns and infection with sexually transmissible agents among young adults in a high-risk neighbourhood in new york city. *Addiction (Abingdon, England)*, *98*(2), 159–169. Available from http://www.ncbi.nlm.nih.gov/pubmed/12534420 (PMID: 12534420)

Friedman, S. R., Furst, R. T., Jose, B., Curtis, R., Neaigus, A., Des Jarlais, D. C., et al. (1998, September). Drug scene roles and HIV risk. *Addiction (Abingdon, England)*, *93*(9), 1403–1416. Available from http://www.ncbi.nlm.nih.gov/pubmed/9926546 (PMID: 9926546)

Friedman, S. R., Kottiri, B. J., Neaigus, A., Curtis, R., Vermund, S. H., & Des Jarlais, D. C. (2000, November). Network-related mechanisms may help explain long-term HIV-1 seroprevalence levels that remain high but do not approach population-group saturation. *American Journal of Epidemiology*, *152*(10), 913–922. Available from http://www.ncbi.nlm.nih.gov/pubmed/11092433 (PMID: 11092433)

Friedman, S. R., Mateu-Gelabert, P., Curtis, R., Maslow, C., Bolyard, M., Sandoval, M., et al. (2007, June). Social capital or networks, negotiations, and norms? a neighborhood case study. *American Journal of Preventive Medicine*, *32*(6 Suppl), S160–170. Available from http://www.ncbi.nlm.nih.gov/pubmed/17543707 (PMID: 17543707)

Friedman, S. R., Neaigus, A., Jose, B., Curtis, R., Goldstein, M., Ildefonso, G., et al. (1997, August). Sociometric risk networks and risk for HIV infection. *American Journal of Public Health*, *87*(8), 1289–1296. Available from http://www.ncbi.nlm.nih.gov/pubmed/9279263 (PMID: 9279263)

Fujimoto, R. M., Perumalla, K. S., & Riley, G. F. (2007). *Network simulation*. Morgan & Claypool Publishers.

Galbraith, J. S., Herbst, J. H., Whittier, D. K., Jones, P. L., Smith, B. D., Uhl, G., et al. (2011, May). Taxonomy for strengthening the identification of core elements for evidence-based behavioral interventions for HIV/AIDS prevention. *Health Education Research*. Available from http://www.ncbi.nlm.nih.gov/pubmed/21536712 (PMID: 21536712)

Gamma, E., Helm, R., Johnson, R., & Vlissides, J. (1994). *Design patterns: Elements of reusable Object-Oriented software* (1st ed.). Addison-Wesley Professional.

Ghani, A. C., & Garnett, G. P. (2000, November). Risks of acquiring and transmitting sexually transmitted diseases in sexual partner networks. *Sexually Transmitted Diseases*, *27*(10), 579–587. Available from `http://www.ncbi.nlm.nih.gov/pubmed/11099073` (PMID: 11099073)

Goldstein, M., Friedman, S. R., Neaigus, A., Jose, B., Ildefonso, G., & Curtis, R. (1995, August). Self-reports of HIV risk behavior by injecting drug users: are they reliable? *Addiction (Abingdon, England)*, *90*(8), 1097–1104. Available from `http://www.ncbi.nlm.nih.gov/pubmed/7549778` (PMID: 7549778)

Goodreau, S. M. (2006a). Assessing the effects of human mixing patterns on human immunodeficiency virus-1 interhost phylogenetics through social network simulation. *Genetics*, *172*(4), 2033.

Goodreau, S. M. (2006b, April). Assessing the effects of human mixing patterns on human immunodeficiency virus-1 interhost phylogenetics through social network simulation. *Genetics*, *172*(4), 2033–2045. (PMID: 16636112 PMCID: 1456410)

Goodreau, S. M. (2007, May). Advances in exponential random graph (p*) models applied to a large social network. *Social Networks*, *29*(2), 231–248. Available from `http://www.sciencedirect.com/science/article/pii/S0378873306000402`

Goodreau, S. M. (2011). A decade of modelling research yields considerable evidence for the importance of concurrency: a response to sawers and stillwaggon. *Journal of the International AIDS Society*, *14*, 12–12. (PMID: 21406079 PMCID: 3065394)

Goodreau, S. M., Kitts, J. A., & Morris, M. (2009). Birds of a feather, or friend of a friend? using exponential random graph models to investigate adolescent social networks*. *Demography*, *46*(1), 103125.

Gore-Felton, C., Somlai, A. M., Benotsch, E. G., Kelly, J. A., Ostrovski, D., & Kozlov, A. (2003). The influence of gender on factors associated with HIV transmission risk among young russian injection drug users. *The American Journal of Drug and Alcohol Abuse*, *29*(4), 881–894. Available from `http://www.ncbi.nlm.nih.gov/pubmed/14713145` (PMID: 14713145)

Guizani, M., Rayes, A., Khan, B., & Al-Fuqaha, A. (2010). *Network modeling and simulation: A practical perspective* (1st ed.). Wiley-Interscience.

Hacker, M. A., Friedman, S. R., Telles, P. R., Teixeira, S. L., Bongertz, V., Morgado, M. G., et al. (2005). The role of "long-term" and "new"

injectors in a declining HIV/AIDS epidemic in rio de janeiro, brazil. *Substance Use & Misuse*, *40*(1), 99–123. Available from http://www.ncbi.nlm.nih.gov/pubmed/15702651 (PMID: 15702651)

Hammett, T. M., Kling, R., Johnston, P., Liu, W., Ngu, D., Friedmann, P., et al. (2006, April). Patterns of HIV prevalence and HIV risk behaviors among injection drug users prior to and 24 months following implementation of cross-border HIV prevention interventions in northern vietnam and southern china. *AIDS Education and Prevention: Official Publication of the International Society for AIDS Education*, *18*(2), 97–115. Available from http://www.ncbi.nlm.nih.gov/pubmed/16649956 (PMID: 16649956)

Handcock, M. S., & Jones, J. H. (2004, June). Likelihood-based inference for stochastic models of sexual network formation. *Theoretical Population Biology*, *65*(4), 413–422. Available from http://www.ncbi.nlm.nih.gov/pubmed/15136015 (PMID: 15136015)

Helsgaun, K. (2000). Discrete event simulation in java. *Citeseer*.

Hendriks, J. C., Satten, G. A., Ameijden, E. J. van, Druten, H. A. van, Coutinho, R. A., & Griensven, G. J. van. (1998, August). The incubation period to AIDS in injecting drug users estimated from prevalent cohort data, accounting for death prior to an AIDS diagnosis. *AIDS (London, England)*, *12*(12), 1537–1544. Available from http://www.ncbi.nlm.nih.gov/pubmed/9727576 (PMID: 9727576)

Holland, P. W., & Leinhardt, S. (1981, March). An exponential family of probability distributions for directed graphs. *Journal of the American Statistical Association*, *76*(373), 33–50. Available from http://www.jstor.org/stable/2287037 (ArticleType: research-article / Full publication date: Mar., 1981 / Copyright 1981 American Statistical Association)

Howell, F. W., & Mcnab. (1996). Using java for discrete event simulation. *Proceedings of the 12th UK Computer and Telecommunications Performance Engineering Workshop UKPEW*, 219228.

Hunter, D. R., Handcock, M., Butts, C. T., Goodreau, S. M., & Morris, M. (2008, May). ergm: A package to fit, simulate and diagnose Exponential-Family models for networks. *Journal of statistical software*, *24*(3), nihpa54860–nihpa54860. (PMID: 19756229 PMCID: 2743438)

Iannelli, M., Milner, F. A., Pugliese, A., & Gonzo, M. (1997, January). The HIV/AIDS epidemics among drug injectors: A study of contact struc-

ture through a mathematical model. *Mathematical Biosciences*, *139*(1), 25–58. Available from http://www.sciencedirect.com/science/article/pii/S002555649600137X

Ibbett, R. N., Heywood, P. E., & Howell, F. W. (1995). Hase: A flexible toolset for computer architects. *Comput. J.*, *38*(10), 755-764.

Issariyakul, T., & Hossain, E. (2008). *Introduction to network simulator NS2*. Springer.

Jacquez, J. A., Koopman, J. S., Simon, C. P., & Longini, J., I M. (1994, November). Role of the primary infection in epidemics of HIV infection in gay cohorts. *Journal of Acquired Immune Deficiency Syndromes*, *7*(11), 1169–1184. Available from http://www.ncbi.nlm.nih.gov/pubmed/7932084 (PMID: 7932084)

Jones, J. H., & Handcock, M. S. (2003, June). Social networks: Sexual contacts and epidemic thresholds. *Nature*, *423*(6940), 605–606; discussion 606. Available from http://www.ncbi.nlm.nih.gov/pubmed/12789329 (PMID: 12789329)

Jose, B., Friedman, S. R., Neaigus, A., Curtis, R., Grund, J. P., Goldstein, M., et al. (1993, December). Syringe-mediated drug-sharing (backloading): a new risk factor for HIV among injecting drug users. *AIDS (London, England)*, *7*(12), 1653–1660. Available from http://www.ncbi.nlm.nih.gov/pubmed/8286076 (PMID: 8286076)

Kahn, J. O., & Walker, B. D. (1998). Acute human immunodeficiency virus type 1 infection. *New England Journal of Medicine*, *339*(1), 33-39. Available from http://www.nejm.org/doi/full/10.1056/NEJM199807023390107

Kellerman, S., Begley, E., Boyett, B., Clark, H., & Schulden, J. (2004a). Changes in hiv and aid in the united states: Entering the third decade. *Current HIV/AIDS Reports*, *1*, 153-158. Available from http://dx.doi.org/10.1007/s11904-004-0024-9 (10.1007/s11904-004-0024-9)

Kellerman, S., Begley, E., Boyett, B., Clark, H., & Schulden, J. (2004b, December). Changes in HIV and AIDS in the united states: entering the third decade. *Current HIV/AIDS Reports*, *1*(4), 153–158. Available from http://www.ncbi.nlm.nih.gov/pubmed/16091236 (PMID: 16091236)

Keshav, S. (1988). *Real: A network simulator* (Tech. Rep.). Berkeley, CA, USA.

Khan, A. A., Awan, A. B., Qureshi, S. U., Razaque, A., & Zafar, S. T.

(2009). Large sharing networks and unusual injection practices explain the rapid rise in HIV among IDUs in sargodha, pakistan. *Harm Reduction Journal*, *6*, 13. Available from http://www.ncbi.nlm.nih.gov/pubmed/19558668 (PMID: 19558668)

Klovdahl, A., Potterat, J. J., Woodhouse, D., Muth, J. B., Muth, S. Q., & Darrow, W. (1994, January). Social networks and infectious disease: The colorado springs study. *Social Science & Medicine*, *38*(1), 79–88. Available from http://www.sciencedirect.com/science/article/pii/0277953694903026

Kolaczyk, E. D. (2010). *Statistical analysis of network data: Methods and models* (Softcover reprint of hardcover 1st ed. 2009 ed.). Springer.

Kolari, B., Stajduhar, D., Gajnik, D., Rukavina, T., & Wiessing, L. (2010, June). Seroprevalence of blood-borne infections and population sizes estimates in a population of injecting drug users in croatia. *Central European Journal of Public Health*, *18*(2), 104–109. Available from http://www.ncbi.nlm.nih.gov/pubmed/20939261 (PMID: 20939261)

Koopman, J. (2004). Modeling infection transmission. *Annu. Rev. Public Health*, *25*, 303326.

Koopman, J. S., Jacquez, J. A., Welch, G. W., Simon, C. P., Foxman, B., Pollock, S. M., et al. (1997, March). The role of early HIV infection in the spread of HIV through populations. *Journal of Acquired Immune Deficiency Syndromes and Human Retrovirology: Official Publication of the International Retrovirology Association*, *14*(3), 249–258. Available from http://www.ncbi.nlm.nih.gov/pubmed/9117458 (PMID: 9117458)

Kottiri, B. J., Friedman, S. R., Neaigus, A., Curtis, R., & Des Jarlais, D. C. (2002, May). Risk networks and racial/ethnic differences in the prevalence of HIV infection among injection drug users. *Journal of Acquired Immune Deficiency Syndromes (1999)*, *30*(1), 95–104. Available from http://www.ncbi.nlm.nih.gov/pubmed/12048369 (PMID: 12048369)

Kretzschmar, M., & Wiessing, L. (2008, August). New challenges for mathematical and statistical modeling of HIV and hepatitis c virus in injecting drug users. *AIDS (London, England)*, *22*(13), 1527–1537. Available from http://www.ncbi.nlm.nih.gov/pubmed/18670211 (PMID: 18670211)

Kretzschmar, M., & Wiessing, L. G. (1998, May). Modelling the spread of HIV in social networks of injecting drug users. *AIDS (London,*

England), *12*(7), 801–811. Available from http://www.ncbi.nlm.nih.gov/pubmed/9619813 (PMID: 9619813)

Kretzschmar, M., Zhang, W., Mikolajczyk, R., Wang, L., Sun, X., Kraemer, A., et al. (2008). Regional differences in HIV prevalence among drug users in china: potential for future spread of HIV? *BMC Infectious Diseases*, *8*(1), 108. Available from http://www.biomedcentral.com/1471-2334/8/108

Kullback, S., & Leibler, R. A. (1951, March). On information and sufficiency. *The Annals of Mathematical Statistics*, *22*(1), 79–86. Available from http://projecteuclid.org/DPubS?service=UI&version=1.0&verb=Display&handle=euclid.aoms/1177729694

Lang, F. (1922). *Dr. Mabuse, der Spieler*. Berlin: Nero-Film AG. Film.

Lang, F. (1933). *The Testament of Dr. Mabuse [film]*. Berlin: Nero-Film AG. Film.

Lang, F. (1960). *Die Tausend Augen des Dr. Mabuse*. Berlin: Nero-Film AG. Film.

Latkin, C. A., Kuramoto, S. J., Davey-Rothwell, M. A., & Tobin, K. E. (2010, October). Social norms, social networks, and HIV risk behavior among injection drug users. *AIDS and Behavior*, *14*(5), 1159–1168. Available from http://www.ncbi.nlm.nih.gov/pubmed/19466537 (PMID: 19466537)

Liljeros, F., Edling, C. R., Amaral, L. A. N., Stanley, H. E., & Aberg, Y. (2001, June). The web of human sexual contacts. *Nature*, *411*(6840), 907–908. Available from http://dx.doi.org/10.1038/35082140

Liljeros, F., Edling, C. R., & Nunes Amaral, L. A. (2003, February). Sexual networks: implications for the transmission of sexually transmitted infections. *Microbes and Infection / Institut Pasteur*, *5*(2), 189–196. Available from http://www.ncbi.nlm.nih.gov/pubmed/12650777 (PMID: 12650777)

Lin, J. (1991). Divergence measures based on the shannon entropy. *IEEE Transactions on Information theory*, *37*, 145–151.

Lomow, G., & Baezner, D. (1991). A tutorial introduction to object-oriented simulation and sim++. In *Proceedings of the 23rd conference on winter simulation* (pp. 157–163). Washington, DC, USA: IEEE Computer Society. Available from http://dl.acm.org/citation.cfm?id=304238.304275

Lyles, C. M., Kay, L. S., Crepaz, N., Herbst, J. H., Passin, W. F., Kim, A. S., et al. (2007, January). Best-Evidence interventions: Findings from a

systematic review of HIV behavioral interventions for US populations at high risk, 2000-2004. *Am J Public Health*, *97*(1), 133–143. Available from http://ajph.aphapublications.org/cgi/content/abstract/97/1/133

Mah, B. A. (1998). Insane users manual.

Mathei, C., Shkedy, Z., Denis, B., Kabali, C., Aerts, M., Molenberghs, G., et al. (2006, August). Evidence for a substantial role of sharing of injecting paraphernalia other than syringes/needles to the spread of hepatitis c among injecting drug users. *Journal of Viral Hepatitis*, *13*(8), 560–570. Available from http://www.ncbi.nlm.nih.gov/pubmed/16901287 (PMID: 16901287)

Mccanne, S., Floyd, S., & Fall, K. (n.d.). *ns2 (network simulator 2).* Available from http://www-nrg.ee.lbl.gov/ns

McNab, R., & Howell. (1998). SimJava: a discrete event simulation package for java with applications in computer systems modelling.

Morris, M. (1997). Sexual networks and HIV. *AIDS-LONDON-CURRENT SCIENCE THEN RAPID SCIENCE PUBLISHERS THEN LIPPINCOTT RAVEN-*, *11*, 209216.

Morris, M., Handcock, M., & Hunter, D. R. (2008). Specification of exponential-family random graph models: Terms and computational aspects. *Journal of statistical software*, *24*(4), 1548.

Morris, M., & Kretzschmar, M. (1997). Concurrent partnerships and the spread of HIV. *Aids*, *11*(5), 641.

Morris, M., & Kretzschmar, M. (2000). A microsimulation study of the effect of concurrent partnerships on the spread of HIV in uganda. *Mathematical Population Studies*, *8*(2), 109133.

Morris, M., Kurth, A. E., Hamilton, D. T., Moody, J., & Wakefield, S. (2009). Concurrent partnerships and HIV prevalence disparities by race: linking science and public health practice. *American journal of public health*, *99*(6), 1023.

Muga, R., Sanvisens, A., Egea, J. M., Tor, J., & Rey-Joly, C. (2003, December). Trends in human immunodeficiency virus infection among drug users in a detoxification unit. *Clinical Infectious Diseases: An Official Publication of the Infectious Diseases Society of America*, *37 Suppl 5*, S404–409. Available from http://www.ncbi.nlm.nih.gov/pubmed/14648455 (PMID: 14648455)

Nasir, A., Todd, C. S., Stanekzai, M. R., Bautista, C. T., Botros, B. A., Scott, P. T., et al. (2011, March). Prevalence of HIV, hepatitis b

and hepatitis c and associated risk behaviours amongst injecting drug users in three afghan cities. *The International Journal on Drug Policy*, *22*(2), 145–152. Available from http://www.ncbi.nlm.nih.gov/pubmed/21146392 (PMID: 21146392)

Neaigus, A., Friedman, S. R., Curtis, R., Des Jarlais, D. C., Furst, R. T., Jose, B., et al. (1994, January). The relevance of drug injectors' social and risk networks for understanding and preventing HIV infection. *Social Science & Medicine (1982)*, *38*(1), 67–78. Available from http://www.ncbi.nlm.nih.gov/pubmed/8146717 (PMID: 8146717)

Neaigus, A., Friedman, S. R., Goldstein, M., Ildefonso, G., Curtis, R., & Jose, B. (1995). Using dyadic data for a network analysis of HIV infection and risk behaviors among injecting drug users. *NIDA Research Monograph*, *151*, 20–37. Available from http://www.ncbi.nlm.nih.gov/pubmed/8742759 (PMID: 8742759)

Neaigus, A., Friedman, S. R., Jose, B., Goldstein, M., Curtis, R., Ildefonso, G., et al. (1996, April). High-risk personal networks and syringe sharing as risk factors for HIV infection among new drug injectors. *Journal of Acquired Immune Deficiency Syndromes and Human Retrovirology: Official Publication of the International Retrovirology Association*, *11*(5), 499–509. Available from http://www.ncbi.nlm.nih.gov/pubmed/8605596 (PMID: 8605596)

Newman, M. E. J. (2002, April). The spread of epidemic disease on networks. *cond-mat/0205009*. Available from http://arxiv.org/abs/cond-mat/0205009 (Phys. Rev. E 66, 016128 (2002))

OPNET Technologies. (2011). *User manual*. Available from http://www.mil3.com

Penoff, B., Wagner, A., Tüxen, M., & Rüngeler, I. (2009). Mpi-netsim: A network simulation module for mpi. In *Icpads* (p. 464-471).

Peterson, D., Willard, K., Altmann, M., Gatewood, L., & Davidson, G. (1990). Monte carlo simulation of HIV infection in an intravenous drug user community. *Journal of Acquired Immune Deficiency Syndromes*, *3*(11), 1086–1095. Available from http://www.ncbi.nlm.nih.gov/pubmed/2213509 (PMID: 2213509)

Philipson, T. (1995). Modeling the aids epidemic: Planning, policy, and prediction, edited by edward h. kaplan and margaret l. brandeau. new york: Raven press, 1994, 624 pp. *Journal of Policy Analysis and Management*, *14*(3), 493–495. Available from http://dx.doi.org/10.2307/3325040

Potterat, J. J., Phillips-Plummer, L., Muth, S. Q., Rothenberg, R. B., Woodhouse, D., Maldonado-Long, T. S., et al. (2002, April). Risk network structure in the early epidemic phase of HIV transmission in colorado springs. *Sexually Transmitted Infections*, *78 Suppl 1*, i159–163. Available from http://www.ncbi.nlm.nih.gov/pubmed/12083437 (PMID: 12083437)

Potterat, J. J., Rothenberg, R. B., & Muth, S. Q. (1999, March). Network structural dynamics and infectious disease propagation. *International Journal of STD & AIDS*, *10*(3), 182–185. Available from http://www.ncbi.nlm.nih.gov/pubmed/10340199 (PMID: 10340199)

Potterat, J. J., Woodhouse, D., Muth, J. B., Muth, S. Q., Darrow, W., & Klovdahl, A. (1994). Social networks and infectious disease: the colorado springs study. *Social science medicine*, *38*(1), 79–88.

Potterat, J. J., Woodhouse, D., Rothenberg, R. B., Muth, S. Q., Darrow, W., Muth, J. B., et al. (1993, November). AIDS in colorado springs: is there an epidemic? *AIDS (London, England)*, *7*(11), 1517–1521. Available from http://www.ncbi.nlm.nih.gov/pubmed/8280420 (PMID: 8280420)

Prejean, J., Song, R., Hernandez, A., Ziebell, R., Green, T., Walker, F., et al. (2011, 08). Estimated hiv incidence in the united states, 20062009. *PLoS ONE*, *6*(8), e17502. Available from http://dx.doi.org/10.1371%2Fjournal.pone.0017502

Read, C. B. (1993, November 09). Freeman–tukey chi-squared goodness-of-fit statistics. *Statistics & Probability Letters*, *18*(4), 271–278. Available from http://www.sciencedirect.com/science/article/B6V1D-45D9T97-H/1/0157a1c70c493176f5cce78b3e4448df

Remis, R. S. (2002, April). HIV incidence among injection drug users in vancouver. *CMAJ: Canadian Medical Association Journal = Journal De l'Association Medicale Canadienne*, *166*(7), 908–909. Available from http://www.ncbi.nlm.nih.gov/pubmed/11949988 (PMID: 11949988)

Rhodes, T., Lowndes, C., Judd, A., Mikhailova, L. A., Sarang, A., Rylkov, A., et al. (2002, September). Explosive spread and high prevalence of HIV infection among injecting drug users in togliatti city, russia. *AIDS (London, England)*, *16*(13), F25–31. Available from http://www.ncbi.nlm.nih.gov/pubmed/12218407 (PMID: 12218407)

Robert, C. P. (1995). Simulation of truncated normal variables. *Statistics and Computing*, *5*, 121-125. Available from http://dx.doi.org/10.1007/

BF00143942 (10.1007/BF00143942)

Robertson, A. R., & Ibbett, R. N. (1994). Hase: A flexible high performance architecture simulator. In *Hicss (1)* (p. 261-270).

Robins, G., Snijders, T. A., Wang, P., Handcock, M., & Pattison, P. (2007). Recent developments in exponential random graph (p*) models for social networks. *Social Networks*, *29*(2), 192215.

Rothenberg, R. B., Potterat, J. J., & Woodhouse, D. (1996, October). Personal risk taking and the spread of disease: beyond core groups. *The Journal of Infectious Diseases*, *174 Suppl 2*, S144–149. Available from http://www.ncbi.nlm.nih.gov/pubmed/8843244 (PMID: 8843244)

Salerno, J., Yang, S. J., Nau, D., & Chai, S. (2011). *Social computing, Behavioral-Cultural modeling and prediction: 4th international conference, SBP 2011, college park, MD, USA, march 29-31, 2011. ... applications, incl. Internet/Web, and HCI)* (1st Edition. ed.). Springer.

Schneeberger, A., Mercer, C. H., Gregson, S. A. J., Ferguson, N. M., Nyamukapa, C. A., Anderson, R. M., et al. (2004, June). Scale-free networks and sexually transmitted diseases: a description of observed patterns of sexual contacts in britain and zimbabwe. *Sexually Transmitted Diseases*, *31*(6), 380–387. Available from http://www.ncbi.nlm.nih.gov/pubmed/15167650 (PMID: 15167650)

Sharma, S., & Thazhuthaveetil, M. (2001). Twlinux: Operating system support for optimistic parallel discrete event simulation. In *Proceedings of the 8th international conference on high performance computing* (pp. 262–271). London, UK: Springer-Verlag. Available from http://dl.acm.org/citation.cfm?id=645447.757612

Smyth, B. P., O'Connor, J. J., Barry, J., & Keenan, E. (2003, April). Retrospective cohort study examining incidence of HIV and hepatitis c infection among injecting drug users in dublin. *Journal of Epidemiology and Community Health*, *57*(4), 310–311. Available from http://www.ncbi.nlm.nih.gov/pubmed/12646549 (PMID: 12646549)

Snijders, T. A., Bunt, G. G. Van de, & Steglich, C. E. (2010). Introduction to stochastic actor-based models for network dynamics. *Social Networks*, *32*(1), 4460.

Snijders, T. A., Pattison, P., Robins, G., & Handcock, M. (2006a). New specifications for exponential random graph models. *Sociological Methodology*, *36*(1), 99–153. Available from http://dx.doi.org/10.1111/j.1467-9531.2006.00176.x

Snijders, T. A., Pattison, P., Robins, G., & Handcock, M. (2006b, January).

New specifications for exponential random graph models. *Sociological Methodology*, *36*, 99–153. Available from http://www.jstor.org/stable/25046693 (ArticleType: research-article / Full publication date: 2006 / Copyright 2006 American Sociological Association)

Sokolowski, J. A. (2009). *Principles of modeling and simulation: A multidisciplinary approach* (1st ed.). Wiley.

Sokolowski, J. A., & Banks, C. M. (2011). *Modeling and simulation in the medical and health sciences* (1st ed.). Wiley.

Solomon, S. S., Celentano, D. D., Srikrishnan, A. K., Vasudevan, C. K., Murugavel, K. G., Iqbal, S. H., et al. (2010, October). Low incidences of human immunodeficiency virus and hepatitis c virus infection and declining risk behaviors in a cohort of injection drug users in chennai, india. *American Journal of Epidemiology*. Available from http://aje.oxfordjournals.org/content/early/2010/10/21/aje.kwq288.abstract

Stephens, M. A. (1974). EDF statistics for goodness of fit and some comparisons. *Journal of American Statistical Association*, *69*(347), 730–737.

Van Den Berg, C., Smit, C., Van Brussel, G., Coutinho, R., & Prins, M. (2007, September). Full participation in harm reduction programmes is associated with decreased risk for human immunodeficiency virus and hepatitis c virus: evidence from the amsterdam cohort studies among drug users. *Addiction (Abingdon, England)*, *102*(9), 1454–1462. Available from http://www.ncbi.nlm.nih.gov/pubmed/17697278 (PMID: 17697278)

Wehrle, K., & Gross, J. (2010). *Modeling and tools for network simulation*. Springer.

Weissenbacher, M., Rossi, D., Radulich, G., Sosa-Estni, S., Vila, M., Vivas, E., et al. (2003, December). High seroprevalence of bloodborne viruses among street-recruited injection drug users from buenos aires, argentina. *Clinical Infectious Diseases: An Official Publication of the Infectious Diseases Society of America*, *37 Suppl 5*, S348–352. Available from http://www.ncbi.nlm.nih.gov/pubmed/14648445 (PMID: 14648445)

Witten, M., & Vincent, D. J. (Eds.). (1996). *Computational medicine, public health and biotechnology - building a man in the machine: Proceedings of the first world congress*. World Scientific Pub Co Inc.

Woodhouse, D., Potterat, J. J., Muth, S. Q., Darrow, W., Klovdahl, A., & Rothenberg, R. B. (1995). Social networks in disease transmission: the

colorado springs study. *NIDA Research Monograph*, *151*, 3–19.

Woodhouse, D., Rothenberg, R. B., Potterat, J. J., Darrow, W., Muth, S. Q., Klovdahl, A., et al. (1994, September). Mapping a social network of heterosexuals at high risk for HIV infection. *AIDS (London, England)*, *8*(9), 1331–1336. Available from `http://www.ncbi.nlm.nih.gov/pubmed/7802989` (PMID: 7802989)

sterreicher, F., & Vajda, I. (2003, September). A new class of metric divergences on probability spaces and its applicability in statistics. *Annals of the Institute of Statistical Mathematics*, *55*(3), 639–653. Available from `http://www.springerlink.com/content/32170n2w82618777/`

Author Index

Index